NOVEL COMBINATION STRATEGIES WITH AURORA KINASE INHIBITORS: USING PRE-CLINICAL DATA TO GUIDE CLINICAL TRIAL DESIGN

JENNIFER HARRINGTON

PETERHOUSE

This dissertation is submitted for the degree of Doctor of Philosophy

April 2018

CANCER RESEARCH UK | CAMBRIDGE INSTITUTE

DECLARATION

This dissertation is the result of my own work and includes nothing which is the outcome of work done in collaboration, except where specifically indicated in the text.

It is not substantially the same as any that I have submitted, or, is being concurrently submitted for a degree or diploma or other qualification at the University of Cambridge or at any other University or similar institution. I further state that no substantial part of my dissertation has already been submitted, or is being concurrently submitted for any such degree, diploma or other qualification at the University of Cambridge or any other University or similar institution.

This dissertation is within the prescribed word limit (60,000 words) for the Degree Committee.

SUMMARY

Anti-mitotic drugs such as paclitaxel are successful chemotherapeutics, but their utility is limited by toxicity and resistance. My research aimed to identify novel therapeutic strategies combining current drugs with aurora kinase inhibitors (AKI) in pre-clinical models and then to design a clinical trial to assess these in patients with bladder cancer. Particular interest was stimulated by the correlation between over-expression of aurora kinases (AKs) with aggressive clinical behaviour in many cancers and the network of interactions which AKs have with other key proteins. Pre-clinical studies suggested that the use of AKIs in combination with other drugs, particularly other anti-mitotic agents, might increase efficacy but this had not been studied in bladder cancer.

As over-expression of AK-A can induce resistance to paclitaxel, I hypothesised that an AK-A inhibitor would synergistically enhance the cytotoxicity of paclitaxel. Human bladder cancer cell lines were used in cytotoxicity assays to study a range of novel AKIs as single agents and in combination with paclitaxel. Application of mathematical models identified regions of synergy when AK-A specific inhibitors were combined with low concentrations of paclitaxel in T24, RT112 and UM-UC-3 cell lines, with 80-100% growth inhibition. The effects of these combinations on non-cancer cell lines and in neutrophil precursor cells demonstrated differential toxicity, with a reduced risk of myelotoxicity compared with higher dose paclitaxel, suggesting they may provide a better therapeutic window. Mechanistic investigations included live cell imaging, which showed a correlation between the time cells spent in mitosis and cell fate, and an assessment of the potential contribution of AK-A expression in sensitivity to the drug combination. Combinations of MLN8237 (an AK-A inhibitor) with paclitaxel and docetaxel were studied in a T24 bladder cancer xenograft model, and these confirmed tolerability with evidence of efficacy in tumour growth inhibition.

Published clinical trials have now demonstrated the potential efficacy of AK-A inhibitors in combination with taxanes but at the expense of additive toxicity. My work suggests that using AK-A inhibitors with lower concentrations of paclitaxel could reduce toxicity, highlighting the need to explore a range of combinations. Existing early phase clinical data have emerged from trials using traditional rule-based trial designs, where limited dose ranges were explored. Therefore, an alternative novel Bayesian adaptive design should be considered to fully assess the efficacy of the combination of MLN8237 and paclitaxel.

ACKNOWLEDGEMENTS

Firstly I am grateful to my funding bodies: Cancer Research UK and the Cancer Research UK Cambridge Research Institute for giving me the opportunity to undertake laboratory based research. I would also like to acknowledge the gifts of cell lines and constructs received from Professor Stephen Taylor, Dr Ultan McDermott and Dr Masashi Narita, and to thank Astex Pharmaceuticals and Cyclacel for use of their compounds under material transfer agreements.

I know how fortunate I have been to use the facilities at Cancer Research UK Cambridge Institute, and to benefit from the expertise of the staff in the core facilities, in particular the Biological Resources Unit, Microscopy and Histopathology. In addition, I am grateful to Dr Penny Wright for her advice on analysis of mouse bone marrows, and to Dr David Perera for his practical advice and assistance. Professor Ashok Venkitaraman gave valuable feedback, particularly early in my project. Dr Adrian Mander, Dr Mike Sweeting and Dr Graham Wheeler have aided my understanding of Phase 1 clinical trial design.

I would like to thank all the members of the Jodrell lab, both past and present, for their support and friendship during my research. In particular, discussions and collaboration with Dr Siang Boon Koh, Dr Yao Lin and Dr Tashinga Bapiro was much appreciated. I have learned a great deal about mathematical modelling of drug combinations from Dr Ben-Fillippo Krippendorff and Dr Giovanni Di Veroli. I would like to particularly thank Jo Bramhall for her unfailing practical support and advice and her patience in explaining experimental techniques to someone who struggled to even pipette in the early days.

My research has been complicated and prolonged by health issues. The University of Cambridge Disability Resource Centre gave invaluable advice and I would like to thank all the staff at Cancer Research UK Cambridge Institute who made it possible for me to continue, despite my ongoing challenges. Dr Ann Kaminski's support throughout has been much appreciated. The encouragement of my family and friends has been crucial through the most challenging times, particularly from Eric, my husband, and my parents together with lots of hugs from my daughter, Meredith. Above all, I could not have completed this work without the incredible understanding and compassion from my supervisor Professor Duncan Jodrell and my laboratory head, Dr Fran Richards. Their support has meant so much to me and I am extremely grateful to them both.

CONTENTS

LIST OF TABLES

LIST OF FIGURES

1 *INTRODUCTION*

Effective new cancer treatments are urgently required, particularly for cancers such as metastatic bladder cancer where there is a paucity of systemic treatment options. Increasingly combinations of drugs are used, aiming to target cancer cells with differing drug sensitivities and reduce the likelihood of drug resistance (1). In the era of molecularly targeted agents, an understanding of the pre-clinical behaviour of these agents in combination is critical when translating promising *in vitro* and *in vivo* work into successful clinical trials. My research focuses on aurora kinase inhibitors (AKI) and the potential to combine these with other anti-cancer agents targeting mitosis in bladder cancer. It was stimulated by the finding that over-expression of aurora kinase A (AK-A) could lead to resistance to a commonly used anti-mitotic agent, paclitaxel (2), suggesting there could be potential to overcome this in combination with AKI.

Cancer is a disease characterised by a deregulated cell cycle and therefore firstly I will briefly review the cell cycle and process of mitosis. Next I describe the aurora kinase family, their role in mitosis and the evidence that led to interest in them as a therapeutic target in bladder cancer. Based on this, multiple AKI have been developed, targeting either aurora kinase A (AK-A), aurora kinase B (AK-B) or both AK-A and AK-B. The evidence for potential efficacy both pre-clinically and in clinical trials is then summarised, before considering the combination of an AKI with other drugs and how best to design clinical trials to assess drug combinations.

1.1 Cell cycle

The cell cycle consists of four distinct stages: Gap phase 1 (G1), DNA synthesis phase (S) during which DNA replication takes place, Gap phase 2 (G2) and the mitosis (M) phase, during which the cell divides into two daughter cells (Figure 1-1). Phases G1, S and G2 are also collectively known as interphase. Not all cells are continually replicated, and the G0 phase is a period in the cell cycle where cells may be quiescent or senescent. This complex process is carefully regulated with a series of checkpoints. The G1 checkpoint is the first defence in the cell cycle, sensing DNA damage and preventing cells from entering the S phase by inhibiting the initiation of DNA replication. However, it is frequently compromised in cancer due to mutations in tumour suppressor genes such as p53. This makes these cells dependent on the G2 checkpoint to detect cells which have escaped the G1 checkpoint with DNA damage

and prevent mitotic entry. Although the G1/S phase checkpoint is designed to ensure DNA is fully repaired prior to progression, the intra-S checkpoint also exists to respond to damage during S phase (3). It is critical that mitosis, the process of cell division, is performed accurately, and there is an additional checkpoint at metaphase, the spindle assembly checkpoint (SAC). Despite these tight control mechanisms, disruption can occur, leading to genetic instability and aneuploidy, hallmarks of cancer (4).

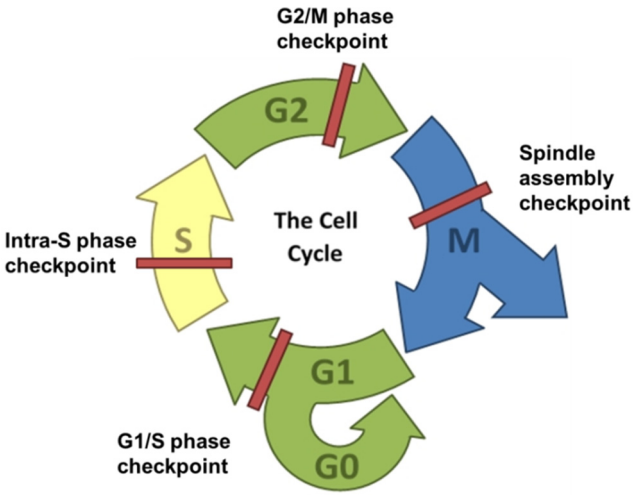

Figure 1-1: The cell cycle.
This illustrates the stages G1 (Gap 1), S (Synthesis), G2 (Gap 2) and M (mitosis) together with the key checkpoints.

Mitosis (M phase) consists of five distinct stages. During prophase, chromosomes condense, the two centrosomes separate to the poles of the cell and the mitotic spindle starts to form, made up of microtubules. Pro-metaphase starts with the breakdown of the nuclear envelope and continues until all sister chromatids are attached to the spindle and have moved to the equator of the cell. When all chromosomes are aligned correctly in metaphase, the cells progress into anaphase, where sister chromatids are separated. Mitosis ends with telophase, where a new nuclear envelope forms around each set of chromosomes, which have begun to de-condense. Finally cytokinesis takes place, during which the cell divides. The SAC delays the metaphase to anaphase transition until all the chromatids have formed correct microtubule attachments (5, 6). Failure to satisfy the SAC leads to mitotic arrest to allow time for correct kinetochore-microtubule attachments to form. A great deal is now known about the SAC and the complex interactions of multiple molecules in its regulation, fully reviewed in (7). These include the important role of the aurora kinases.

1.2 Aurora kinases

This family of three serine-threonine protein kinases, Aurora A, B and C, share a high degree of sequence conservation. Despite this, they have distinct localisations and functions, partly explained by their strict regulation through intricate networks of interactions (8). AK-A and AK-B have been shown to be important for multiple events during mitosis (Figure 1-2).

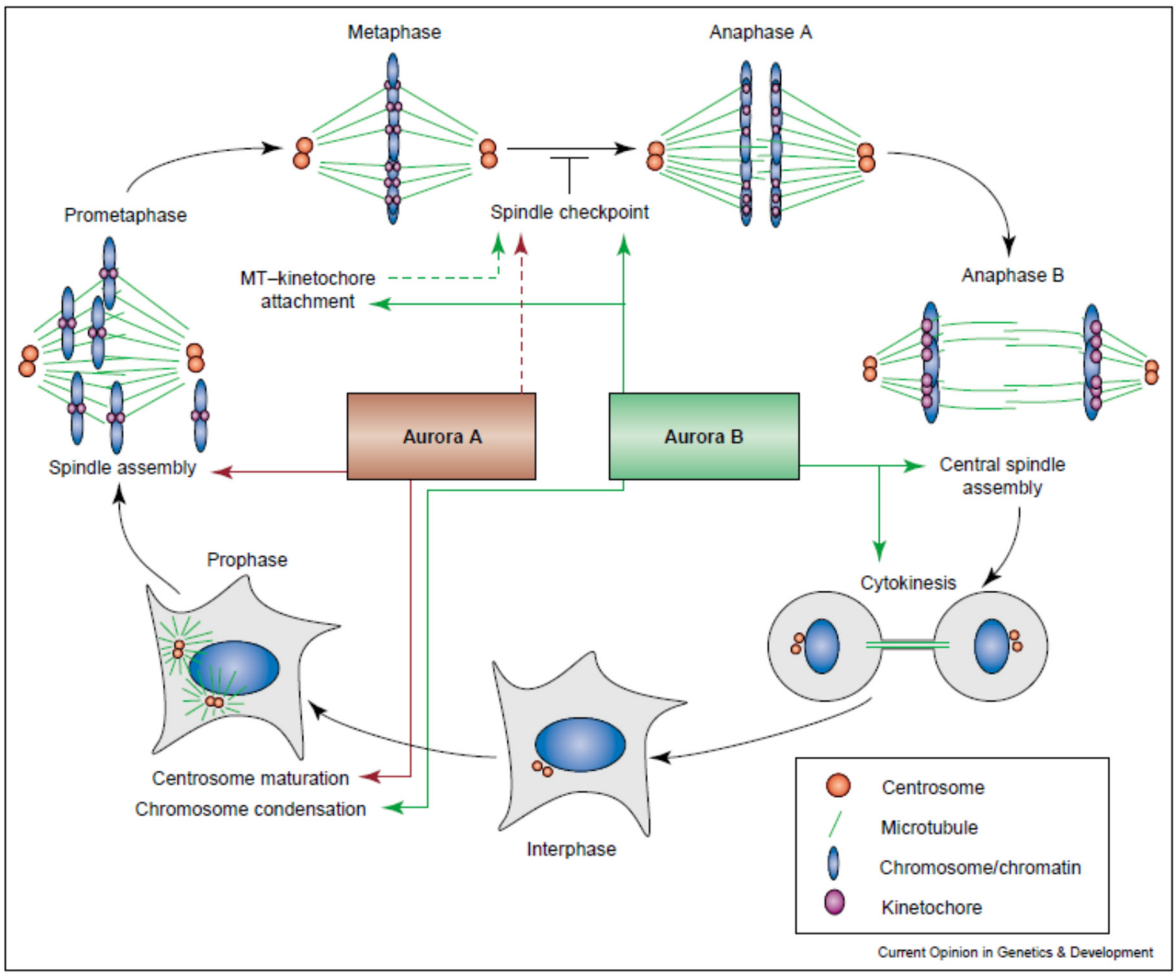

Figure 1-2: The role of Aurora A and Aurora B during mitosis.
Image used from Meraldi et al. (9)

AK-A is encoded by AURKA (Aurora-2/BTAK/STK15**)** on Chromosome 20q13.2. It regulates cell cycle events occurring from late S-phase through M phase, including centrosome maturation, mitotic entry, centrosome separation, bipolar spindle assembly, chromosome alignment, cytokinesis, and mitotic exit (reviewed in (10)). Its expression rises rapidly during G2, peaking in early mitosis (11).

AK-B is encoded by AURKB on Chromosome 17p13.1. It forms the catalytic component of the chromosomal passenger complex. This complex regulates chromosome condensation via direct phosphorylation of histone H3 at Ser^{10} (12) and

Ser^{28} by AK-B (13). Subsequently it directs the proper orientation of the chromosomes, correct assembly of the mitotic spindle and cytokinesis.

Aurora C is largely involved in meiosis, although it does appear to have an overlapping role with AK-B in mitosis and potentially tumour formation when over-expressed (14, 15). It has been less studied and is not discussed further in this review.

Expression of AK-A and AK-B are closely linked to proliferation, with inappropriately high or low levels of AK activity associated with genetic instability. As the AKs are cell-cycle associated genes, they would be expected to be expressed at higher levels in rapidly dividing cells. Thus, elevated expression of AK-A and AK-B could purely reflect this proliferation. However, the AKs are more diffusely expressed in malignant cells rather than just around the nucleus. This is thought to promote aberrant phosphorylation of cytoplasmic proteins (16).

Over-expression, amplification and polymorphisms in both AK-A and AK-B have been found in many tumour types (Table 1-1). A meta-analysis of the prognostic significance of AK-A over-expression showed a significant association with shorter overall survival and progression free survival in solid tumours (17). Several studies have also suggested that gene polymorphisms in AURKA are associated with cancer risk; for example the AURKA (F31I) polymorphism has been identified as a low penetrance cancer susceptibility allele affecting multiple cancer types (18).

Cancer type	Alteration	Aurora Kinase	Correlation
Bladder (19-25)	Over-expression, amplification	A, B	Grade, stage, prognosis, recurrence
Brain (26-30)	Over-expression, amplification	A, B	Grade, outcome, survival
Breast (31-45)	Over-expression, amplification, polymorphisms	A, B, C	Chromosomal instability, high grade, ER/PR negativity, nuclear grade, BRCA2, cancer risk, prognostic
Cervix (46, 47)	Over-expression	A, B	Also increased in cervical intraepithelial neoplasia, no correlation with survival
Colon (48-52)	Over-expression, Amplification	A	Cancer risk, aneuploidy, chromosomal instability, transformation of adenomas
Endometrium (53, 54)	Over-expression, Amplification	A, B	Poor prognosis
Gastric (55-59)	Over-expression, amplification, polymorphisms	A, B	Cancer risk, progression
Head/Neck (60-62)	Over-expression, amplification	A, B	Progression, survival
Hepatocellular (63-67)	Over-expression	A	Grade, stage
Lung (68-76)	Over-expression, polymorphisms	A, B	Poor differentiation, genetic instability
Melanoma (77)	Over-expression, amplification	A	
Oesophagus (78-83)	Over-expression, amplification polymorphisms	A	Also associated with Barrett's, response to treatment
Ovary (84-90)	Over-expression, polymorphisms	A	Survival, cancer risk
Pancreas (91, 92)	Over-expression	A	Over-expression
Prostate (93-95)	Over-expression	A, B	Grade, proliferation, prognosis
Renal (96-98)	Over-expression	A	
Thyroid (99, 100)	Over-expression	B	Grade, proliferation
T-cell lymphoma (101, 102)	Over-expression	A	

Table 1-1: Review of evidence linking aurora kinases with solid tumours

1.3 AK-A and bladder cancer

As seen in Table 1-1, there is evidence of a link between AK-A and bladder cancer. Transitional cell carcinoma (TCC) of the bladder is the tenth most common malignancy in the UK, with approximately 10,000 new cases a year in the UK (103). There are two

distinct types of tumours, arising by different biological pathways (104). The most common are low grade papillary tumours, with a low rate of progression to muscle invasive disease, but high frequency of local recurrence. However, 20-30% of patients have a more aggressive tumour type, marked by aneuploidy and loss of p53 mutations (105), showing high rates of both progression and metastases (106). More recently, comprehensive molecular characterisation of bladder tumours has provided detailed information about the molecular pathways involved (107).

In patients with advanced unresectable or metastatic disease, outcomes even with the most active chemotherapy treatment of cisplatin and gemcitabine chemotherapy are poor. Despite an initial response rate of 50%, median overall survival is only 13-15 months (108). Multiple agents have been tested in the second line setting demonstrating limited activity, with single agent anti-mitotics such as vinflunine, paclitaxel and docetaxel commonly used, despite response rates of only 5-20% (109). Immunotherapy is now showing promise an alternative to chemotherapy (110).

The first observation suggesting a role for AK-A in bladder cancer came from evidence of increased copies of Chromosome 20q, with amplification of the region in invasive bladder cancers with significant aneuploidy (111-113). Once the AURKA gene was identified in this region, analysis of human bladder cancers confirmed that increasing levels of AK-A amplification correlated with aneuploidy (24) and it proved possible to reproduce the chromosome mis-segregation and aneuploidy observed by forced over-expression of AK-A (114). High AK-A over-expression was prevalent in cells showing dysregulation of the DNA damage response genes such as BRCA1 and Chk2 (113) and was also associated with functional suppression of p53 (113, 115, 116).

A comparison of AK-A expression between normal bladder, non-invasive cancers and muscle-invasive bladder cancers found abnormal levels even in the early stages of bladder cancer, with significant upregulation in invasive tumours (21), with evidence that AK-A over-expression could independently predict tumour recurrences in early stage tumours (117). In addition, increased tumour expression of AK-A was a poor prognostic factor (118), strongly associated with risk of recurrence (22, 119), and decreased survival (24). A FISH test for AK-A gene copy number performed on urine samples was shown to have potential as a diagnostic biomarker for bladder cancer with high specificity and sensitivity (114). A census of amplified and over-expressed human cancer genes identified AURKA as a gene important for bladder cancer (120). Together

these studies support the hypothesis that AK-A is functionally important in advanced stage bladder cancer.

At the time my research began, there was no published research exploring AK-A inhibition in bladder cancer. However, subsequent to my experimental work, others have explored the role of AK-A in bladder cancer. Zhou *et al.* confirmed upregulation of genes involved in the spindle assembly checkpoint including AK-A and AK-B in human bladder cancer samples (121). An AK-A specific inhibitor, MLN8237, was tested in two human bladder cancer cell lines (T24 and UM-UC-3) and induced cell cycle arrest and apoptosis. In a mouse T24 bladder cancer xenograft model, MLN8237 induced tumour growth arrest. Their findings will be compared with mine in later chapters. Another recent study has shown that AK-A over-expression enhanced the invasiveness of bladder cancer cells through modulation of the transcription factor Pax-3, causing the downregulation of the nicotinamide N-methyltrasferase (NNMT) gene, resulting in the downstream over-expression of matrix metalloproteinases. Analysis of tissue microarrays of bladder cancer identified a subset of aggressive tumours, characterised by AK-A over-expression and downregulation of NNMT (122), suggesting that AK-A inhibition may be of particular value for this group.

1.4 AK-A and its interactions

Interest in AK-A intensified after its activation resulted in *in vitro* and *in vivo* transformation of rodent fibroblast cells (123). However, over-expression is not generally tumorigenic *in vivo* (124), suggesting dysregulation of other pathways is required for malignant transformation. AK-A has complex interactions with other key molecules implicated in carcinogenesis, including p53, BRCA, Ras and Myc.

Of these, p53 is of particular interest, given the frequency of mutations in p53 in bladder cancer and its important role in the G1 checkpoint. AK-A has been shown to interfere with p53 function by direct phosphorylation at Ser-315, facilitating its MDM-2 mediated degradation (116) and inactivating its transcriptional activity (125). Phosphorylation of p53 at Ser-106 decreases its interaction with MDM2 and actually prolongs the half-life of p53 in contrast to the effect of phosphorylation at Ser-215 and Ser-315 (126). Mechanistic studies have shown that p53 negatively regulates AK-A expression level via both transcriptional and post-translational changes (127). p53 itself binds to AK-A to directly inactivate its kinase function (128).

The P53 family also comprises TP63 and TP73. AK-A has been shown to phosphorylate p73 at Ser-235, facilitating inactivation of the SAC and mitotic exit (129). TP73 has been shown to be important in determining cell fate in p53 deficient cells exposed to AK-A inhibitors (129-132), with p73 potentially able to compensate for lack of p53 function in tumour cells.

There are many other important substrates that interact with AK-A that have now been identified. In particular, AK-A interacts with BRCA1 and BRCA2 (133, 134) and with the Ras signalling pathway (135-138). AK-A over-expression enhanced both the expression level and transcriptional activity of c-Myc (139, 140). These processes are highly regulated and have now been extensively researched, identifying reasons why AK-A over-expression can contribute to cancer development. These are reviewed in detail by Nikonova *et a*l (141), summarised in the schematic in Figure 1-3.

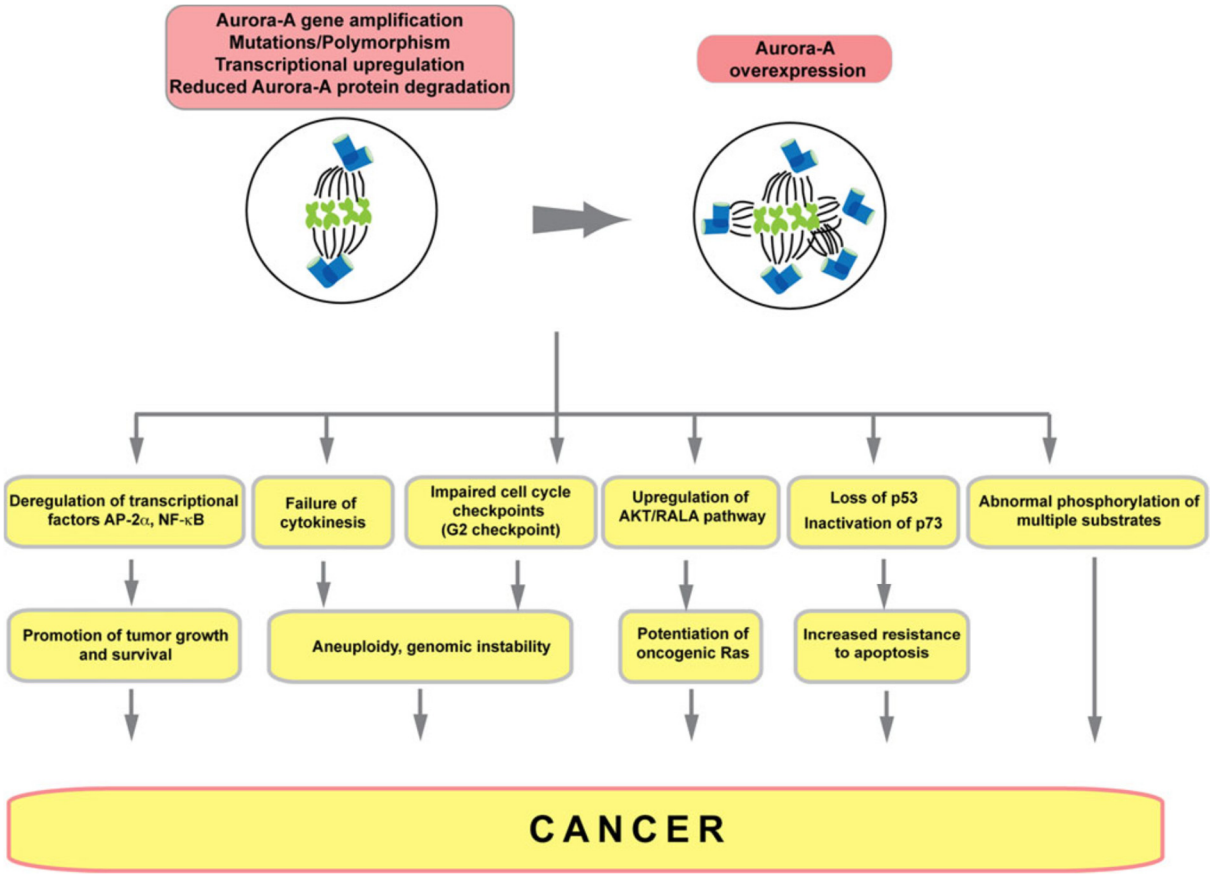

Figure 1-3: The effects of AK-A over-expression in cancer.
Image used from Nikonova *et al.* (141).

1.5 Anti-mitotic cancer drugs

The value of cytotoxic drugs targeting mitosis in cancer has already been demonstrated. The two most common classes of these disrupt microtubule dynamics. The taxanes (paclitaxel and docetaxel) stabilise microtubules inducing multi-polar spindles and the

vinca alkaloids inhibit microtubule assembly. Through SAC activation, cell cycle arrest is triggered at the G2/M checkpoint and cells accumulate in pro-metaphase. Cells may die during mitotic arrest, or slip out of arrest into a tetraploid G1 state from which they may die, arrest in G1 or continue the cell cycle with a variety of subsequent fates (142). This is dictated by two competing but independent networks – one involving activation of cell death pathways, the other dependent on the level of cyclin B1 (which progressively falls during prolonged mitotic arrest) (143). By working in opposite directions, the fate of the cell is dictated by which threshold is reached first (Figure 1-4). If cyclin B1 levels fall below the threshold required to maintain mitotic arrest, slippage occurs, leading to potential cell survival. In contrast, if cyclin B1 levels remain high enough for activation of apoptosis, cells will die in mitosis.

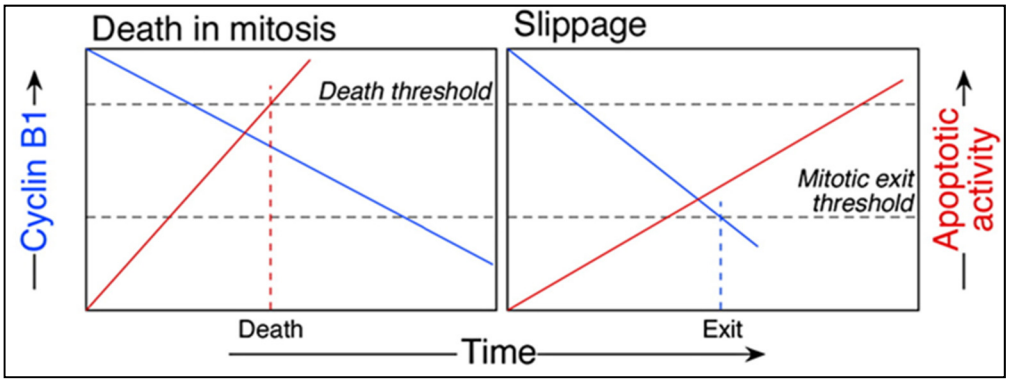

Figure 1-4: The competing networks model.
Image used from Gascoigne KE and Taylor SS (142).

It is now known that multiple proteins are important in determining fate once cells have arrested in mitosis on exposure to drugs such as taxanes (144, 145), with increasing interest in the Bcl-2 family, particularly Mcl-1 and Bcl-xL (146-148).

Anti-mitotic drugs such as taxanes rely on rapid tumour cell cycling to preferentially kill tumour cells and have proved effective with wide clinical use. However, proliferative normal tissues such as the bone marrow are also affected and neurotoxicity is a significant issue (149). Resistance can also develop. Drug development of newer anti-mitotic agents has aimed to design compounds which specifically target protein kinases such as AKs which control cell division. The hope was that these would reduce off-target effects such as neurotoxicity, hence giving a better efficacy-to-toxicity ratio (therapeutic index).

1.6 Effects of AK-A and AK-B inhibition

Pre-clinical experiments have investigated the consequences of interfering with AK function using a range of techniques including RNA interference (RNAi), together with small molecule aurora kinase inhibitors (AKI) as these were developed. AK-A inhibition leads to delayed entry into mitosis, due to arrest at G2/M by SAC activation, and abnormal spindle formation. This can result in defects in chromosome segregation and aneuploidy. In contrast, AK-B inhibition inactivates the SAC, allowing cells to over-ride mitotic arrest despite misaligned chromosomes. Continued suppression leads to further rounds of genome replication without division (endoreduplication), and ultimately cell death (150). Dual AK-A and AK-B inhibition causes a phenotype similar to that of inhibiting AK-B alone (151, 152). These effects together with the range of potential cell fates are summarised in Figure 1-5.

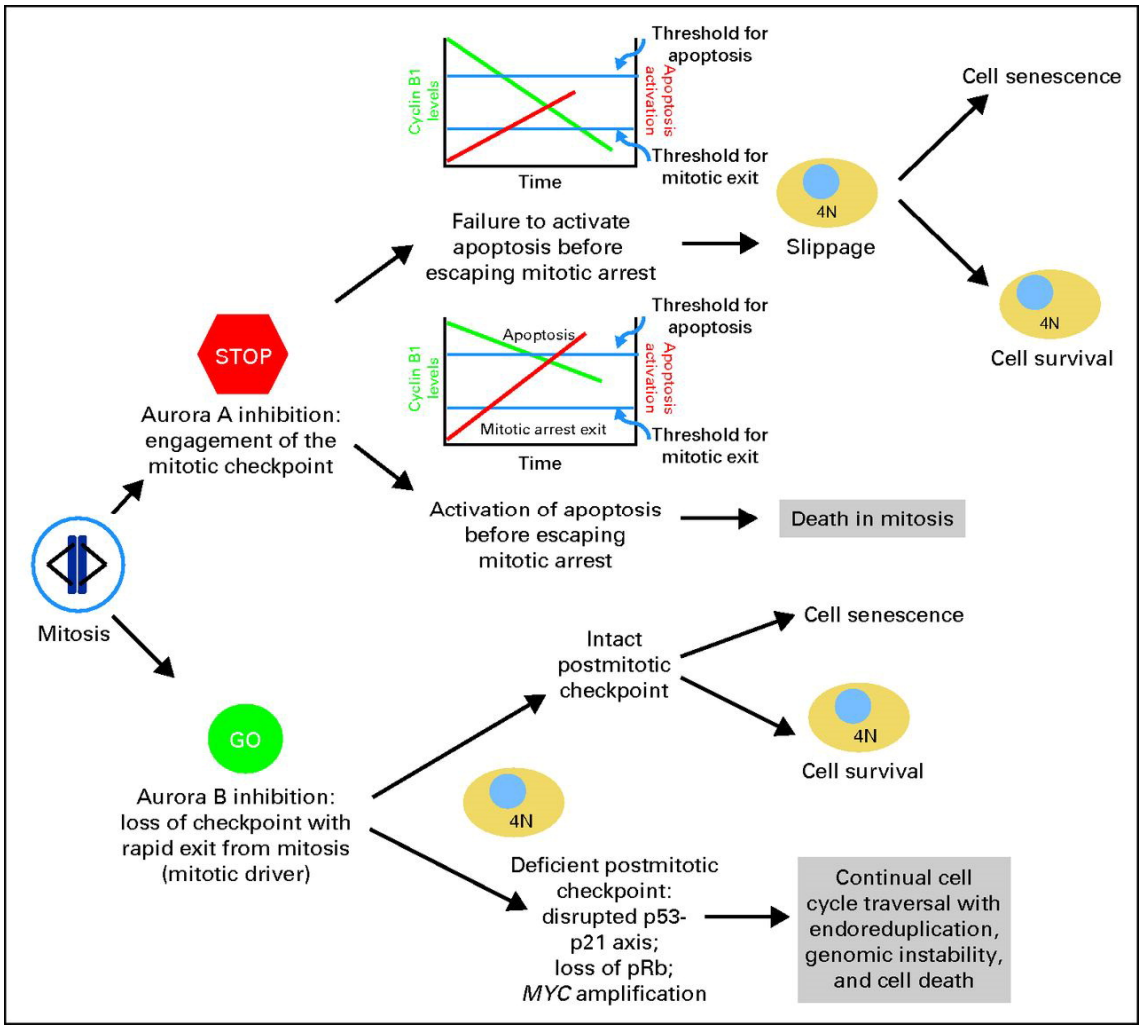

Figure 1-5: Differential effects of AK-A and AK-B inhibition on mitosis.
Image used from Hilton JF and Shapiro GI (153).

Normal cells with intact p53 arrest at the G1 checkpoint, whereas in cells with defective p53, AKI-induced mitotic abnormalities are exacerbated (154). This differential effect

could allow the use of higher doses of chemotherapeutics without significant impact on normal tissues (155, 156), with non-cancer cells (with intact p53) not subject to the effects of AKI. This is of particular interest in bladder cancer, where p53 mutations are linked to the development of muscle invasive disease (105). Myc amplification and loss of Rb can also influence cell fate (153), particularly in response to AK-B inhibition.

There remains debate about whether the best therapeutic target is AK-A or AK-B or in fact the use of a pan-AKI (157, 158). For example, in one study the effects of AK-A and AK-B anti-sense oligonucleotides were compared in pancreatic cancer cells (159). Although induction of apoptosis was faster with AK-A inhibition, both AK-A and AK-B inhibition led to potentially useful therapeutic effects with cell cycle arrest and apoptosis. In colorectal cancer cells, a similar study compared the effects of RNAi and AKI and concluded that the cells were more sensitive to AK-B inhibition (150). Therefore drug development of AKI involved attempts to find both AK-A and AK-B specific inhibitors, together with pan-AKI, with the knowledge that dual AK-A and AK-B inhibition would produce a biological effect and phenotype similar to AK-B inhibition alone.

1.7 Clinical development of AKI

Many of the AKI developed inhibit all three AK, due to a highly conserved catalytic domain between AK-A and AK-B, meaning that higher doses of AK specific inhibitors have a pan-aurora inhibitory effect (160). Therefore, they have been sub-divided into three general classes, those with selectivity for AK- A over AK-B, AK-B over AK-A or both (reviewed in (160-162)), although most show some cross-reactivity with other kinases. Work to develop new AKI has been ongoing using a range of screening techniques (reviewed in (163)), for both pan-AKI (164, 165), selective AK-A inhibitors (166, 167), selective AK-B inhibitors (168) and for multi-targeted agents aiming for therapeutic synergy within a single drug with examples including AK-A and CDK-1 inhibition (169) and pan-AKI with Src (170).

I next review the leading clinical candidates, concentrating on those with AK selectivity, which have shown sufficient pre-clinical efficacy to be tested in clinical trials, together with toxicities reported (161, 171). Phase 1 clinical trials assess the safety of a novel drug or drug combination, allowing both the Maximum Tolerated Dose (MTD) and the Recommended Phase 2 Dose (RP2D) to be identified. Patients are recruited sequentially and based upon the occurrence of dose limiting toxicities (DLTs),

subsequent patients receive a dose equal to or higher than the previous patient until the RP2D is defined (172), with the assumption that the probability of observing DLTs in patients increases with dose. The RP2D can then be evaluated in Phase 2 clinical trials which aim to determine activity against specific cancer types, together with further safety evaluation. Adverse events (AE) are graded in severity from 0-5 according to National Cancer Institute Common Terminology Criteria. Those considered drug related and Grade ≥3 are usually dose limiting, although this depends on pre-specified DLT criteria.

Whilst the AKI have shown promise in non-solid haematological malignancies (reviewed in (173)), my focus is on advanced solid tumours, and only trials in this category are covered in this review. The majority of these have been reported since my research commenced. Single agent studies are reviewed in this section, with combinations with other agents assessed in 1.8. The tables show the IC_{50} for the AK together with other key targets, toxicities seen in trials and evidence of efficacy.

1.7.1 Pan-AKI

Given the differing roles of AK-A and AK-B in cell division, it was hypothesised that a dual AK inhibitor might be the most effective drug in cancer. Pre-clinically these pan-AKI showed a phenotype consistent with AK-B inhibition as expected, and several candidates showed *in vivo* efficacy and therefore proceeded to clinical trials. Table 1-2 summarises the published results of clinical trials with seven different pan-AKI as single agents. The majority of these showed stable disease as the best response, with the main DLTs haematological, particularly neutropenia. Several phase 2 trials were terminated due to toxicity or lack of anti-tumour activity, and the majority of further clinical development of these pan-AKI has been in non-solid haematological malignancies (174, 175).

1.7.2 AK-A specific

Table 1-3 summarises the published clinical trials with four AK-A specific inhibitors as single agents. MLN8054 was the first AKI reported to be selective for AK-A over AK-B, with little cross reactivity with other kinases. However, due to its structural similarity to benzodiazepines, off-target toxicities occurred and it was replaced with MLN8237 (alisertib), with increased AK-A selectivity and reduced benzodiazepine-like effects. Although considered AK-A specific, at concentrations above 250 nM *in vitro*, AK-B inhibition was seen. Multiple clinical trials have been performed with MLN8237 with

evidence of limited clinical activity, with the main toxicity neutropenia. Based on the overall response rate in T cell lymphoma, a phase 3 study in relapsed/refractory T cell lymphoma comparing MLN8237 with investigator's choice of alternative therapy commenced (176). However, this was discontinued following a pre-specified interim analysis, which indicated that the study was unlikely to demonstrate improved progression-free survival (PFS) over the standard-of-care (177).

Although there had been no published pre-clinical data in bladder cancer at the time my research began, a Phase 2 trial of MLN8237 in patients with metastatic bladder cancer, following failure of at least one platinum based chemotherapy regimen has now been performed (178). The primary endpoint was an objective response with the plan to continue to a randomised trial of paclitaxel plus either MLN8237 or placebo. However, although objective responses were seen (partial response in two patients and seven with stable disease), these did not meet the criteria for the planned combination study. Significant toxicity was seen in the twenty patients evaluable for response with two treatment related deaths due to septic shock and Grade 3-4 AE including mucositis (41%), fatigue (36%) and neutropenia (18%) with febrile neutropenia in 14%.

A more recent candidate MK-5108 is a highly specific AK-A inhibitor, which did not show DLT as a single agent. Although ENMD-2076 was initially reported as a selective AK-A inhibitor, it also inhibits multiple other kinases, including VEGFR and FGFR and hence has combined anti-proliferative and anti-angiogenic properties (179), reflected in the additional toxicity of hypertension in the trials.

1.7.3 AK-B specific

The majority of AK-B specific inhibitors were found to be pan-AKI but three compounds have been tested in clinical trials. Table 1-4 summarises the published results of clinical trials with these as single agents. Dose limiting toxicities were similar to those seen with both pan-AKI and AK-A specific inhibitors, with neutropenia the main DLT.

1.7.4 Summary of single agent AKI clinical trials

The AKI were generally well tolerated as single agents with reversible neutropenia the main DLT due to anti-proliferative effects in the bone marrow. Although some activity was seen in solid tumours, the majority have had stable disease as their best response using standard tumour response radiological criteria. Therefore, the potential to combine

AKI with other drugs, including those that depend on the SAC such as taxanes was assessed to see if this could increase anti-tumour activity.

Compound	AKA IC_{50} nM	AKB IC_{50} nM	AKC IC_{50} nM	Other targets, pre-clinical ref	Phase	Patients (tumour type, no.)	Schedule	MTD/RP2D	Dose limiting toxicity	Anti-tumour activity
AMG900 (180, 181)	5	4	1	(182)	1	Dose escalation: Advanced solid Dose expansion: taxane- and platinum-resistant epithelial ovarian cancer, taxane-resistant triple-negative breast cancer, or castration-resistant and taxane- or cisplatin-etoposide-resistant stage IV prostate cancer	Oral od Days 1-4 every 14 days	24 mg od without GCSF, 40 mg od with GCSF	Neutropenia, febrile neutropenia, thrombocytopenia	Dose escalation: 1 PR (ovarian),13 SD Dose expansion: 1 PR (ovarian), 7 PR ovarian by Ca125 Disease control rate ovarian (PR + SD) 83%

Compound	AKA IC_{50} nM	AKB IC_{50} nM	AKC IC_{50} nM	Other targets, pre-clinical ref	Phase	Patients (tumour type, no.)	Schedule	MTD/RP2D	Dose limiting toxicity	Anti-tumour activity
AT9283 (183)	3	3	NA	Include BCR-Abl T315I, JAK2, JAK3, GSK3 β (184)	1	Advanced solid; 40	72 hr continuous iv infusion every 21 days	27 mg/m^2/72 hrs	Febrile neutropenia	4 SD ≥ 6 mo.
AT9283 (185)	3	3	NA	Include BCR-Abl T315I, JAK2, JAK3, GSK3 β	1	Advanced solid or NHL; 35	24 hr continuous iv infusion days 1, 8 of 21 day cycle	47 mg/m^2/day	Febrile neutropenia, neutropenia with Grade 3 infection	1 PR (SCC anus), 4 SD (median 2.6 mo.)
Danusertib (PHA-739358) (186)	13	79	61	Includes VEGF, FLT3, BCR-Abl T315I (187)	1	Advanced solid; 50	3 hr or 6 hr iv infusion Days 1, 8, 15 of 28 day cycle	330 mg/m^2 for 6 hr infusion (3 hr not identified)	Neutropenia (with/without fever), hypertension, fatigue	5 SD ≥ 6 mo. (1 NSCLC for 2 yrs.)

Compound	AKA IC_{50} nM	AKB IC_{50} nM	AKC IC_{50} nM	Other targets, pre-clinical ref	Phase	Patients (tumour type, no.)	Schedule	MTD/RP2D	Dose limiting toxicity	Anti-tumour activity
Danusertib (PHA-739358) (188)	13	79	61	Includes VEGF, FLT3, BCR-abl T315I (187)	1	Advanced solid; 40 in part 1, 16 in part 2	24 hr infusion every 14 days without GCSF (part 1) or with (part 2)	500 mg/m^2 without GCSF, 750 mg/m^2 with GCSF	Neutropenia (part 1, without GCSF), escalation halted due to elevated creatinine (part 2)	1 PR (SCLC), 1 PR with CA125 decline (ovarian), 42% SD with 4 pts prolonged SD (24-52 wks.)
Danusertib (PHA-739358) (189)	13	79	61	Includes VEGF, FLT3, BCR-abl T315I (187)	2	Advanced solid, disease cohorts breast, ovarian, colorectal, pancreatic, SCLC, NSCLC; 219 total	24 hr 500 mg/m^2 iv infusion every 14 days	NA	NA but note Grade 3 neutropenia 83%	PFS at 4 mo 18% breast 12% ovarian 10% pancreas 10% NSCLC, 0% SCLC and colorectal

Compound	AKA IC_{50} nM	AKB IC_{50} nM	AKC IC_{50} nM	Other targets, pre-clinical ref	Phase	Patients (tumour type, no.)	Schedule	MTD/RP2D	Dose limiting toxicity	Anti-tumour activity
Danusertib (PHA-739358) (190)	13	79	61	Includes VEGF, FLT3, BCR-abl T315I (187)	2	Castrate-resistant prostate cancer; 88 total, A (43), B (38)	Two schedules: A - 330 mg/m^2 6 hr iv infusion days 1, 8 and 15 every 4 weeks or B. 24 hr 500 mg/m^2 iv infusion days 1 &15 every 4 wks.	NA	NA but most common Grade 3 or 4 AE neutropenia (A: 37%, B: 16%)	PFS 12 wks. 21 SD including 11 SD ≥ 6 mo.
MSC1992371A (AS703569 R763) (191)	4	4.8	6.8	Include FLT3, BCR-ABL, JAK2 (192)	1	Advanced solid, 92	A. Days 1 and 8 every 21 days B. Days 1-3 every 21 days C. Days 1, 2, 3 and Days 8, 9, 10 every 21 days, oral	Schedules A&B 74 mg/m^2/cycle Schedule C: 60 mg/m^2/cycle	Neutropenia, febrile neutropenia, thrombocytopenia, nausea and vomiting	SD ≥ 3 mo. 11 pts

Compound	AKA IC_{50} nM	AKB IC_{50} nM	AKC IC_{50} nM	Other targets, pre-clinical ref	Phase	Patients (tumour type, no.)	Schedule	MTD/RP2D	Dose limiting toxicity	Anti-tumour activity
PF-03814735 (193)	0.8	5	NA	Flt1, FAK, Met, FGFR1 (194)	1	Advanced solid; 57, 32 schedule A, 25 schedule B	Schedule A: Days 1-5 od of 21 day cycle Schedule B: Days 1-10 od of 21 day cycle, oral	Schedule A: 80 mg od Schedule B: 50 mg od	Febrile neutropenia, increased AST, LV dysfunction	19 SD, 4 SD ≥ 6 mo.
SNS-314 (195)	9	31	3	(196)	1	Advanced solid, 32	3 hr iv infusion Days 1, 8, 15 of 28 day cycle	Not established – Grade 3 neutropenia at 1440 mg/m^2	Not established – Grade 3 neutropenia at 1440 mg/m^2	6 SD
Tozasertib (VX-680, MK-0457) (197)	0.7	18	4.6	FLT3, BCR-Abl T315I, JAK(198)	1	Advanced solid, 27	24 hr infusion every 21 days	64 mg/m^2/hr 24 hr infusion	Neutropenia, herpes zoster	12 SD, 1 SD 11 mo. (ovarian)

Table 1-2: Published clinical trials in pan-AKI.
Abbreviations: GCSF (granulocyte colony stimulating factor), hr (hour), iv (intravenous), LV (left ventricle), mo (months), MTD (maximum tolerated dose), NA (not applicable), NHL (non-Hodgkin's lymphoma), NSCLC (non-small cell lung cancer), od (once daily), PFS (progression free survival), PR (partial response), RP2D (recommended Phase 2 dose), SCC (squamous cell carcinoma), SCLC (small cell lung cancer), SD (stable disease).

Compound	AKA IC_{50} nM	AKB IC_{50} nM	AKC IC_{50} nM	Other targets, pre-clinical ref	Phase	Patients (tumour type, no.)	Schedule	MTD/RP2D	Dose limiting toxicity	Anti-tumour activity
ENMD-2076 (199)	14	350	NA	VEGF2, FGFR1, FGFR2, Src, c-kit, FAK (179)	1	Advanced solid; 67	Continuous oral dosing od	160 mg/m^2	Hypertension, neutropenia	2 PR (platinum refractory/resistant ovarian), SD 49 pts, 26 ≥ 3 mo.
ENMD-2076 (200)	14	350	NA	VEGF2, FGFR1, FGFR2, Src, c-kit, FAK	2	Platinum-resistant ovarian, fallopian tube or peritoneal cancer; 64	325 mg/day reduced to 275 mg/day		NA. Most common Grade 3 or 4 hypertension, fatigue, Note: need for dose reduction in schedule due to toxicity.	PFS 6 mo. 22%, 58% SD or PR with 5 PR
MLN8054 (201)	4	172	NA	(202)	1	Advanced solid, 61	Oral od for 7, 14 or 21 days with 14 day treatment rest period	60 mg daily (as 4 divided doses) Days 1-14 of 28 day cycle	Benzodiazepine-like effects incl. somnolence, confusion	3 SD ≥ 6 mo.

Compound	AKA IC_{50} nM	AKB IC_{50} nM	AKC IC_{50} nM	Other targets, pre-clinical ref	Phase	Patients (tumour type, no.)	Schedule	MTD/RP2D	Dose limiting toxicity	Anti-tumour activity
MLN8054 (203)	4	172	NA		1	Advanced solid, 43	Oral od Days 1-14 of 28 day cycle	70 mg daily (as 4 divided doses) Days 1-14 of 28 day cycle	Somnolence, transaminitis	3 SD ≥ 4 cycles
MLN8237 (alisertib) (204)	61	>200	NA	(205)	1	Advanced solid, 87	Oral od or bd for 7, 14 or 21 days with 14 day treatment rest period	50 mg bd for 7 days in 21 day cycle	Febrile neutropenia, thrombocytopenia, somnolence, confusion, memory impairment	1 PR (ovarian) 2.9 yrs., 20 pts SD ≥ 3 mo.
MLN8237 (alisertib) (206)	61	>200	NA		1	Advanced solid, 59	Oral od or bd for 7, 14 or 21 days with 14 day treatment rest period	50 mg bd for 7 days in 21 day cycle	Neutropenia, thrombocytopenia, stomatitis	22 SD, SD ≥ 6 mo. 6 pts

Compound	AKA IC_{50} nM	AKB IC_{50} nM	AKC IC_{50} nM	Other targets, pre-clinical ref	Phase	Patients (tumour type, no.)	Schedule	MTD/RP2D	Dose limiting toxicity	Anti-tumour activity
MLN8237 (alisertib) (207)	61	>200	NA		1	Multiple myeloma, NHL, CLL, 58	Oral od (then bd) Days 1-14 or Days 1-21 with 14 or 7 day treatment rest period powder-in-capsule formulation, then changed to enteric coat Days 1-14 of 28 day cycle	50 mg bd for Days 1-7 of 21 day cycle, enteric coated formulation	Neutropenia, thrombocytopenia, anaemia, leucopenia	6 PR, 13 SD
MLN8237 (alisertib) (208)	61	>200	NA		1	Advanced solid, 24	Oral bd Days 1-7 of 21 day cycle, new enteric coated formulation	50 mg bd for Days 1-7 of 21 day cycle	Neutropenia, febrile neutropenia	9 SD

Compound	AKA IC_{50} nM	AKB IC_{50} nM	AKC IC_{50} nM	Other targets, pre-clinical ref	Phase	Patients (tumour type, no.)	Schedule	MTD/RP2D	Dose limiting toxicity	Anti-tumour activity
MLN8237 (alisertib) (209)	61	>200	NA		1	Advanced solid, East Asian population, 36	Oral bd Days 1-7 of 21 day cycle, new enteric coated formulation	30 mg bd for Days 1-7 of 21 day cycle	Neutropenia, fatigue	1 PR (lymphoma), 18 SD
MLN8237 (alisertib) (210)	61	>200	NA		2	Epithelial ovarian, fallopian tube, primary peritoneal, 31	MLN8237 50 mg bd for Days 1-7 of 21 day cycle	NA	NA, most common Grade 3 or 4 neutropenia, leucopenia	3 PR, 16 SD
MLN8237 (alisertib) (211)	61	>200	NA		2	Cohorts breast, SCLC, NSCLC, head and neck, gastro-oesophageal adenocarcinoma, 249	MLN8237 50 mg bd for Days 1-7 of 21 day cycle	NA	NA, most common Grade 3 or 4 neutropenia, leucopenia, anaemia. Dose reductions in 28%	Breast 18% PR, 51% SD SCLC 21% PR, 33% SD NSCLC PR 4%, SD 74% Head and neck 9% PR, 49% SD Gastro-oesophageal PR 9%, SD 38%

Compound	AKA IC_{50} nM	AKB IC_{50} nM	AKC IC_{50} nM	Other targets, pre-clinical ref	Phase	Patients (tumour type, no.)	Schedule	MTD/RP2D	Dose limiting toxicity	Anti-tumour activity
MLN8237 (alisertib) (212)	61	>200	NA		2	Sarcoma, 72	MLN8237 50 mg bd for Days 1-7 of 21 day cycle	NA	NA, most common Grade 3 or 4 neutropenia, thrombocytopenia, anaemia, mucositis, leucopenia	PFS 12 wks., 2 pts with prolonged SD
MLN8237 (alisertib) (213)	61	>200	NA		2	Recurrent/metastatic leiomyosarcoma, 21	MLN8237 50 mg bd for Days 1-7 of 21 day cycle	NA	NA, most common Grade 3 or 4 neutropenia, leucopenia, anaemia	SD 38%, PFS 1.7 mo.
MLN8237 (alisertib) (178)	61	>200	NA		2	Recurrent/metastatic bladder cancer, at least 1 prior platinum, 20	MLN8237 50 mg bd for Days 1-7 of 21 day cycle	NA	NA, most common Grade 3 or 4 mucositis, fatigue, neutropenia, febrile neutropenia, 2 deaths due to septic shock. Dose reductions in 18%.	2 PR, 7 SD (2 ≥6 mo.)

Compound	AKA IC_{50} nM	AKB IC_{50} nM	AKC IC_{50} nM	Other targets, pre-clinical ref	Phase	Patients (tumour type, no.)	Schedule	MTD/RP2D	Dose limiting toxicity	Anti-tumour activity
MLN8237 (alisertib) (214)	61	>200	NA		2	B and T cell NHL, 48	MLN8237 50 mg bd for Days 1-7 of 21 day cycle	NA	NA, most common Grade 3 or 4 neutropenia, leucopenia, anaemia, fatigue, diarrhoea. Dose reductions in 52%	Overall RR 27% (10% CR, 17% PR), 33% SD
MLN8237 (alisertib) (215)	61	>200	NA		2	Relapsed/refractory T cell NHL and mycosis fungoides, 37	MLN8237 50 mg bd for Days 1-7 of 21 day cycle	NA	NA, most common Grade 3 or 4 neutropenia, anaemia, thrombocytopenia, febrile neutropenia, mucositis	None in mycosis fungoides Overall RR in T cell NHL 30% (7% CR, 23% PR)
MK-5108/VX-689 (216)	0.064	14	12	(217)	1	Advanced solid, 18	MK-5108 oral bd Day 1-2 in 14-21 day cycles	MTD not determined for monotherapy (no DLT)	None	9 SD

Table 1-3: Published clinical trials in AK-A specific inhibitors.
Abbreviations: bd (twice daily), GCSF (granulocyte colony stimulating factor), hr (hour), iv (intravenous), mo (months), MTD (maximum tolerated dose), NA (not applicable), NHL (non-Hodgkin's lymphoma), NSCLC (non-small cell lung cancer), od (once daily), PFS (progression free survival), PR (partial response), RP2D (recommended Phase 2 dose), SCC (squamous cell carcinoma), SCLC (small cell lung cancer), SD (stable disease).

Compound	AKA IC_{50} nM	AKB IC_{50} nM	AKC IC_{50} nM	Other targets/pre-clinical ref	Phase	Patients (tumour type, no.)	Schedule	MTD/RP2D	Dose limiting toxicity	Anti-tumour activity
Barasertib (AZD1152) (218)	1369	0.36	17	(219)	1	Advanced solid; 59, 19 schedule A, 40 schedule B	Two schedules: A 2 hr infusion every 7 days or B. 2 hr infusion every 14 days	200 mg in 2 hr infusion every 7 days or 450 mg every 14 days	Neutropenia with or without fever	SD 15 pts, 2 SD ≥6 mo. (adenoid cystic carcinoma and adenocarcinoma unknown primary)
BI811283 (220)	NA	9	NA	(221)	1	Advanced solid, 121, 63 (schedule A), 58 (schedule B)	24 h**r** infusion on Days 1 and 15 of a 4-week cycle (schedule A) or Day 1 of a 3-week cycle (schedule B)	Schedule A: 125 mg Schedule B: 230 mg	Neutropenia, febrile neutropenia	SD 38 pts, 10 ≥10 cycles
BI811283 (222)	NA	9	NA	(221)	1	Advanced solid, 25	24 hr infusion Days 1 and 15 of 4 week cycle	Not reached	1 febrile neutropenia Terminated prior to further escalation.	1 PR (cervical), 4 SD
GSK1070916A (223)	490	0.38	1.5		1	Advanced solid, 32	1 hour iv infusion days 1 – 5, every 21 days	85 mg/m^2/day	Neutropenia, febrile neutropenia	1 PR (ovarian), 19 SD

Table 1-4: Published clinical trials with AK-B specific inhibitors.
Abbreviations: hr (hour), iv (intravenous), mo (months), MTD (maximum tolerated dose), PR (partial response), RP2D (recommended Phase 2 dose), SD (stable disease).

1.8 Combination studies with AKI

1.8.1 Techniques to assess combinations

Traditionally three types of drug interactions are described - additive, antagonistic or synergistic. The total effect may be lower than expected –antagonistic, or greater than expected - synergistic (224). A synergistic combination may target tumour cells with differing drug susceptibilities, achieve a higher intensity of dose with non-overlapping toxicities and reduce the likelihood of drug resistance (1). To determine the extent of interaction between two drugs, the simplistic combination index (CI) defines a value of either CI<1 (synergy), CI=1 (additive) or CI>1 (antagonism) (225). However, a combination could produce different results according to the ratios of each drug used. Various mathematical models have been developed (reviewed in detail in (226)), with the most commonly used the Bliss and Loewe models (227). The Bliss model assumes that drugs act independently with different modes of action, but each contributes to a common result. In contrast, Loewe additivity assumes an additive behaviour of the two drugs, with similar modes of action and requires parallel dose-response curves with identical slopes. Because of this, the resulting effect can be described by different equipotent dose ratios.

1.8.2 Pre-clinical studies combining AKI with other drugs

To increase the anti-tumour activity of AKI, combination therapy with cytotoxic anti-cancer agents, radiotherapy, and other targeted agents has shown potential, but my focus here is on the evidence for combinations with other cytotoxics. At the time I started my research, two early pre-clinical studies demonstrated the potential of AK-A inhibitors in combination with other drugs. Nocodazole destabilises microtubules and should lead to activation of the SAC. However AK-A over-expression led to a failure of nocodazole-exposed cells to arrest at the metaphase–anaphase transition despite improper attachments of kinetochore to microtubules, allowing them to override the SAC. Propidium iodide staining and flow cytometry showed an increased 4N population (due to polyploidy) and a reduced sub G1 population (<2N DNA content) regarded as apoptotic, suggesting cell death was also reduced (228). This report was consistent with another study, using cells over-expressing AK-A up to five times higher than endogenous levels, within a range seen in cancer cells with AURKA gene amplifications (123). When mock transfected and AK-A over-expressing cells were

treated with paclitaxel, there was a significant reduction in the percentage of apoptotic cells (again measured using flow cytometry to identify the sub G1 population), indicating resistance to paclitaxel (2), as seen in Figure 1-6. Others report that ectopic expression of AK-A is associated with resistance to paclitaxel, together with two other commonly used chemotherapeutics etoposide and cisplatin (229).

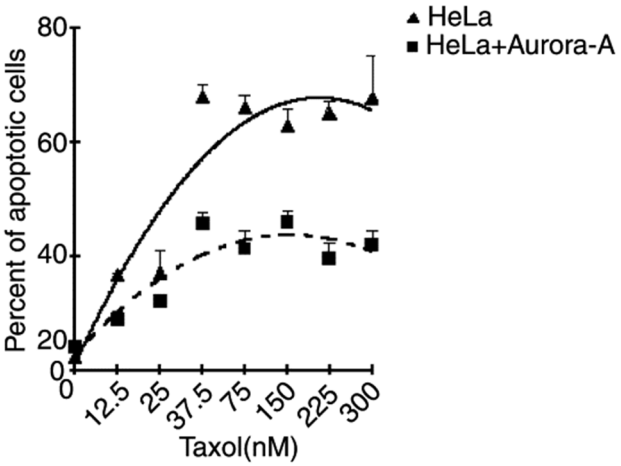

Figure 1-6: The effects of paclitaxel on the percentage of apoptotic cells in mock transfected HeLa cells against those transfected with AK-A.
From Anand et al. (2).

Therefore this work suggested that AK-A inhibition could potentially sensitise cells to the effects of taxanes. Indeed RNAi knockdown of AK-A synergistically enhanced the cytotoxic effects of both paclitaxel and docetaxel in pancreatic cancer cell lines (230). In mantle cell lymphoma models, low dose combinations of MLN8237 and docetaxel increased the percentage of apoptotic cells (sub G1 population) three to four fold compared to single agents. Whilst single agent MLN8237 showed limited anti-tumour effects *in vivo*, the combination showed significantly greater tumour growth inhibition, associated with improved survival (231). When MK-5108 was combined with docetaxel, increased growth inhibition and apoptosis was seen across a range of cancer cell lines and in docetaxel-resistant xenograft models, the combination showed increased efficacy without excess toxicity (217). Subsequent work which also used flow cytometry and quantification of the sub-G1 population showed synergy with low concentrations of docetaxel and MLN8237 in upper gastrointestinal tumour models (232), consistent with other reports (233).

The majority of AKI are pan-AKIs and these have also been investigated in combination with anti-mitotic drugs such as paclitaxel and docetaxel. For example, in ovarian cancer models, pre-treatment of cells with MK-0457 followed by docetaxel led to enhanced cytotoxicity and increased apoptosis, and efficacy in taxanes and platinum-

resistant xenograft models (234). AMG900 inhibited proliferation in cell lines including those resistant to paclitaxel and to other AKI, with anti-tumour activity in paclitaxel and docetaxel resistant xenograft models (182). In a triple negative breast cancer model, paclitaxel or ixabepilone administered 24 hours prior to AMG900 for 48 hours showed synergistic growth inhibition and *in vivo* the combination of docetaxel followed by AMG900 showed increased efficacy (235). At low doses of VE-465 (reported as specific for AK-A inhibition) synergy was seen in combination with paclitaxel, with increased apoptosis, even in paclitaxel-resistant cell lines (236).

The mechanism for the enhanced cytotoxicity between AKI and taxanes is not yet fully understood. It is likely to be influenced by the length of mitotic arrest. For example, the fate of cells exposed to concurrent treatment with ZM447439 (pan-AKI) and paclitaxel or nocodazole was critically influenced by their mitotic age, linking to the competing networks model discussed in 1.5. When cells were pre-treated with paclitaxel, adding ZM447439 drove all cells out of mitosis within 0.5-2 hours. However, whilst cells that were blocked for ≥15 hours died shortly after being driven out of mitosis, cells blocked for <15 hours showed variable fates (237). AK-A inhibition using either MLN8054 or by RNAi AK-A knockdown in cells treated with paclitaxel or nocodazole accelerated mitotic slippage, and induced polyploidy, a phenotype similar to that seen with AK-B inhibition (although they demonstrated that AK-B was not inhibited at the concentration of MLN8054 used) (233).

1.8.3 Combination clinical trials with AKI

The *in vitro* results combining both AK-A specific AKI and pan-AKI suggested it could be effective at overcoming paclitaxel and docetaxel resistance but also indicate that the scheduling of the combination may be important. Whilst there were no clinical trials of combinations reported at the time my research commenced, there were concerns about synergistic toxicity, particularly neutropenia based on the single agent data available. Since then, combination clinical trials have been performed, with published results summarised in Table 1-5.

Other current studies include the combination of MLN8237 with fulvestrant in patients with hormone receptor positive locally advanced or metastatic breast cancer (NCT02219789), the combination of MLN8237 with vorinostat in patients with Hodgkin, B-cell non-Hodgkin or peripheral T cell lymphomas (NCT01567709) and the combination of MLN8237 with romidepsin in patients with relapsed or refractory B or T cell lymphomas (NCT01897012). In addition, a range of targeted agents are now

being tested in combination with MLN8237, including the combination of a pan-RAF kinase inhibitor plus either a TORC1/2 inhibitor, MLN8237, paclitaxel, cetuximab or irinotecan NCT02327169 (238). A Phase 1b study combining MLN8237 with MLN0128 (dual TORC1/2 inhibitor) is also active, with a planned expansion cohort in metastatic triple-negative breast cancer (NCT02719691). The potential for MLN8237 to act as a radiosensitiser is also being investigated, with one study studying the effects of MLN8237 combined with stereotactic radiosurgery in patients with recurrent high-grade gliomas (NCT02186509) and another the combination with cetuximab and definitive radiation in patients with head and neck cancer (NCT01540682).

As seen in Table 1-5, the majority have tested AK-A specific inhibitors (mainly MLN8237) in combination with taxanes (paclitaxel and docetaxel). Whilst there have been encouraging tumour responses, overlapping toxicities, particularly neutropenia have prevented dose escalation when administering the taxanes at full dose and dose reductions have been required, usually in the AK-A inhibitor as investigators have been reluctant to reduce the taxane dose. Thus the combination with MK-5108 was terminated early due to DLT below the pharmacokinetic (PK) target (216).

In the published phase 2 trial of MLN8237 in combination with paclitaxel, despite reducing both drug starting doses, increased AE have been seen, with patients coming off trial due to toxicity (239). Another phase 2 trial of MLN8237 in combination with paclitaxel is ongoing in patients with metastatic or locally recurrent breast cancer, with patients randomised to either paclitaxel 90 mg/m^2 (a higher than normal single agent dose) on days 1, 8 and 15 of a 28-day cycle or paclitaxel 60 mg/m^2 on days 1, 8 and 15 of a 28-day cycle together with MLN8237 40 mg bd on days 1-3, 8-10, and 15-17 of a 28-day cycle (NCT02187991).

Compound	Phase	Patients (tumour type, no.)	Schedule	MTD/RP2D	Dose limiting toxicity	Anti-tumour activity
MSC1992371A (AS703569 R763) (240)	1	Advanced solid, 66	Schedule 1: 1000 mg/m^2 gemcitabine days 1 & 8 and MSC1992371A on days 2 and 9 of 21 day cycle Schedule 2: MSC1992371A on days 1 and 8, 1000 mg/m^2 gemcitabine days 2 and 9 of 21 day cycle	MSC1992371A 37 mg/m^2	Neutropenia	2 confirmed PR (HCC, NSCLC), 1 unconfirmed PR (spindocellular skin ca), 5 SD ≥ 6 mo.
MK-5108/VX-689 (216)	1	Advanced solid, 17	MK5108 oral bd Days 1-2 in combination with docetaxel 60 mg/m^2 iv Day 1 every 21 days	MK-5108 150 mg bd Days 1-2 in combination with docetaxel 60 mg/m^2 Day 1 iv in 21 day cycle	Febrile neutropenia, Grade 3 infection. Terminated early as DLT below PK exposure target	1 PR, 7 SD

Compound	Phase	Patients (tumour type, no.)	Schedule	MTD/RP2D	Dose limiting toxicity	Anti-tumour activity
MLN8237 (alisertib) (241)	1/2	Ovarian, fallopian tube, primary peritoneal and breast, 49	Paclitaxel 80 mg/m^2 iv Days 1, 8 and 15, oral MLN8237 bd days 1-3, 8-10, 15-17 in 28 day cycles	MLN8237 10 mg bd with paclitaxel 80 mg/m^2 AND MLN8237 40 mg bd with paclitaxel 60 mg/m^2 but RP2D MLN8237 40 mg bd with paclitaxel 60 mg/m^2 based on biological activity	Neutropenia with or without fever, diarrhoea, stomatitis	Ovarian 1 CR, 9 PR, 11 SD Breast 6 PR, 3 SD
MLN8237 (alisertib) (242)	1	Castrate refractory prostate cancer, amended to all advanced solid, 41	Docetaxel 75 mg/m^2 iv Day 1 and MLN8237 bd Days 1-7 of 21 day cycle	Docetaxel 75 mg/m^2 Day 1 with MLN8237 20 mg bd Days 1-7 without GCSF *Due to toxicity, range of dosing tried including MLN8237 days 1-5 only, reduction in docetaxel dose and use of GCSF	Febrile neutropenia, neutropenia, stomatitis	7 PR, 11 SD
MLN8237 (alisertib) (243)	1	Advanced solid (part 1), 17 pts pancreatic or neuroendocrine (part 2), 16 pts	Nab-paclitaxel 100 mg/m^2 iv Days 1, 8, 15 and MLN8237 oral bd Days 1-3, 8-10, 15-17 of 28 day cycle	Nab-paclitaxel 100 mg/m^2 with MLN8237 40 mg bd Days 1-3, 8-10, 15-17	Febrile neutropenia, neutropenia	1 PR (SCLC), 9 SD

Compound	Phase	Patients (tumour type, no.)	Schedule	MTD/RP2D	Dose limiting toxicity	Anti-tumour activity
MLN8237 (alisertib) (244)	1	Advanced solid, 21 Pre-planned expansion into pancreatic cancer ongoing	Gemcitabine 1000 mg/m^2 iv Days 1, 8 and 15 and MLN8237 bd Days 1-3, 8-10 and 15-17 of 28 day cycle	Gemcitabine 1000 mg/m^2 iv Days 1, 8 and 15 and MLN8237 50 mg bd Days 1-3, 8-10 and 15-17 of 28 day cycle	Neutropenia, mucositis, infection	10 SD
MLN8237 (alisertib) (245)	1/2	Castrate refractory prostate cancer, progressing on abiraterone, only 9 enrolled	Abiraterone 1 g od and prednisone and MLN8237 days 1-7 of 21 day cycle	Terminated due to toxicity and lack of clinical benefit	Fatigue with memory impairment, febrile neutropenia, diarrhoea	
MLN8237 (alisertib) (246)	1	Relapsed or refractory neuroblastoma, 22	MLN8237 oral od Days 1-7, irinotecan 50 mg/m2 iv and temozolamide 100 mg/m2 oral od Days 1-5 of 21 day cycle	MLN8237 60 mg/m^2 oral od Days 1-7, irinotecan 50 mg/m^2 iv and temozolamide 100 mg/m^2 oral od Days 1-5 of 21 day cycle – but with mandatory GCSF and cephalosporin prophylaxis for diarrhoea	Neutropenia, diarrhoea, nausea	Overall response rate 32%, PFS 52% NB patients irinotecan naive

Compound	Phase	Patients (tumour type, no.)	Schedule	MTD/RP2D	Dose limiting toxicity	Anti-tumour activity
MLN8237 (alisertib) (247)	1	Metastatic gastrointestinal tumours, 13	MLN8237 oral bd Days 1-3, leucovorin and oxaliplatin 85 mg/m^2 Day 2, continuous 5-flurouracil 2400 mg/m^2 Days 2-14 in 14 day cycles	MLN8237 10 mg bd, Days 1-3, leucovorin and oxaliplatin 85 mg/m^2 Day 2, continuous 5-flurouracil 2400 mg/m^2 Days 2-14 in 14 day cycles	Fatigue, nausea and vomiting	1 PR, 6 SD NB eligible patients could be FOLFOX naïve and FOLFOX active treatment
MLN8237 (alisertib) (248)	1	Advanced solid, 27	MLN8237 oral bd Days 1-7, pazopanib od Days 1-21 of 21 day cycle	MLN8237 20 mg bd, pazopanib 600 mg od	Grade 3 colonic obstruction, rise in liver enzymes, thrombocytopenia, mucositis	2 PR, 14 SD
MLN8237 (alisertib) (249)	1	Advanced NSCLC, 18	MLN8237 oral bd Days 1-7, erlotinib od Days 1-21 of 21 day cycle	MLN8237 40 mg bd, erlotinib 150 mg od	Febrile neutropenia, neutropenia	1 PR, 5 SD
MLN8237 (alisertib) (239)	2	Ovarian, fallopian tube or primary peritoneal, 149	Randomised to MLN8237 40 mg bd Days 1-3, 8-10, 15-17 with paclitaxel 60 mg/m^2 iv Days 1, 8 and 15 vs paclitaxel 80 mg/m^2 iv Days 1, 8 and 15 of 21 day cycle		NA, at time of interim report increased toxicity with combination including ≥Grade 3 neutropenia 64% vs 9%, with 14% vs 1% discontinued due to toxicity	Median PFS increased with combination 7 mo. vs 4.4 mo. (p=0.021)

Compound	Phase	Patients (tumour type, no.)	Schedule	MTD/RP2D	Dose limiting toxicity	Anti-tumour activity
MLN8237 (alisertib) (250)	2	Small cell lung cancer, 178	Randomised to MLN8237 40 mg orally bd on days 1-3, 8-10, 15-17 and paclitaxel 60 mg/m^2 iv on days 1, 8, 15 (Arm A) or matched placebo + paclitaxel 80 mg/m^2 (Arm B) in 28-day cycles.		NA, Drug related ≥ grade 3 AE 67% combination vs 25%; neutropenia (all grades) in 49% combination	median PFS 101 days in combination vs 66 days, HR 0.71 (0.51, 0.99, p=0.038); median OS 186 vs 165 days HR 0.79 (0.55, 1.10, p=0.20); disease control rate 58% vs 46%

Table 1-5: Published clinical trials of AKI in combination with other drugs.
Abbreviations: GCSF (granulocyte colony stimulating factor), hr (hour), HR (hazard ratio), iv (intravenous), mo (months), MTD (maximum tolerated dose), NA (not applicable), NHL (non-Hodgkin's lymphoma), NSCLC (non-small cell lung cancer), od (once daily), PFS (progression free survival), PR (partial response), RP2D (recommended Phase 2 dose), SD (stable disease).

1.9 Aims and objectives

Based on the evidence presented, the aims of my research were to study AKI in bladder cancer, particularly in combination with paclitaxel as a potential therapeutic option.

Aim 1 (Chapter 3) was to assess a range of novel AKI in the human bladder cancer cell line T24, in order to determine whether the cells were most sensitive to specific AKI (AK-A or AK-B) or pan-AKI. Having established single agent activity and selected the AKI of most interest, I then characterised the effects of combining the AKI with paclitaxel *in vitro*, using response-surface modelling to determine the combined drug action over the full concentration-combination ranges of both drugs (226). Synergistic combinations were explored further, with findings expanded to a wider panel of bladder cancer cell lines.

Aim 2 (Chapter 4) was to investigate the therapeutic window for the combination of AKI and paclitaxel, specifically to determine *in vitro* whether non-cancer cells were less sensitive than tumour cells.

Aim 3 (Chapter 5) was to explore whether the extent of AK-A expression in cell lines may contribute to synergy with the combination of AKI with paclitaxel and identify whether AK-A expression level could be used as a predictive biomarker in clinical trials.

Aim 4 (Chapter 6) was to assess the efficacy of the AKI and taxane combination in bladder cancer xenografts *in vivo*, with a particular focus on the effects of the combination on the bone marrow. Potential pharmacodynamic endpoints were assessed.

Aim 5 (Chapter 7) was to design an early phase clinical trial of the combination of AKI with taxanes, using Bayesian adaptive design with the choice of strategy informed from my pre-clinical response surfaces and *in vivo* work.

2 *MATERIALS AND METHODS*

2.1 Materials

2.1.1 Manufacturers

Company	Headquarters
Abcam	Cambridge, UK
Abnova	Taipei City, Taiwan
Alfa Aesar	Massachusetts, USA
Aperio (Leica Biosystems)	Nussloch, Germany
Applied Biosystems	California, USA
America Type Culture Collection (ATCC)	Virginia, USA
Astex Pharmaceuticals	Cambridge, UK
BD Bioscience	California, USA
Beckman Coulter	California, USA
Bethyl Laboratories	Texas, USA
BioRad	Hemel Hempstead, UK
BioTek Instruments, Inc	Vermont, USA
BMG LabTech	Ortenberg, USA
Cayman Chemicals	Michigan, USA
Cell Signaling Technology	Massachusetts, USA
Charles River Laboratories	Kent, UK
Cell Lines Service (CLS)	Eppelheim, Germany
CTC Analytics AG	Zwingen, Switzerland
Corning Life Sciences	Massachusetts, USA
Cyclacel Pharmaceuticals, Inc	New Jersey, USA
Dako	Glostrup, Denmark
Dechra Vetinerary Products	Northwich, UK
European Collection of Cell Cultures	Salisbury, UK
Essen Bioscience	Michigan, USA
Fisher Scientific UK Ltd	Loughborough, UK
FlowJo	Oregon, USA
GE Healthcare	Buckinghamshire, UK
Gibco™ (now part of Thermo Fisher Scientific)	Massachusetts, USA
Horizon Discovery Ltd	Cambridge, UK
Ibidi	Munich, Germany
Indica Labs	New Mexico, USA
Invitrogen	California, USA
InvivoGen	California, USA
Leica Microsystems GmbH	Wetzler, Germany
LI-COR Biosciences	Nebraska, USA
MEDIpoint inc	New York, USA
Merck Millipore	Massachusetts, USA
Nikon	New York, USA
Ontario Chemicals	Ontario, Canada
Oxford Optronix	Oxfordshire, UK

Company	Headquarters
Peviva via BIOAXXESS	Gloucestershire, UK
Precellys	Versailles, France
Promega	Wisconsin, USA
QMX Laboratories	Essex, UK
Scantibodies Laboratory Ltd	California, USA
Scientifc Laboratory Supplies	Yorkshire, UK
Selleck Chemicals	Texas, USA
Sigma-Aldrich	Missouri, USA
Stem Cell Technologies	British Columbia, Canada
Thermo Fisher	Massachusetts, USA
Tocris	Bristol, UK
Vector Laboratories	California, USA
Woodley Equipment	Lancashire, UK

Table 2-1 List of manufacturers of materials used in this research, together with headquarters

2.1.2 Buffers

- Phosphate-Buffered Saline (PBS 1x): 11.9mM phosphate, 137mM Sodium Chloride, 2.7mM Potassium Chloride, pH7.4
- Tris-Buffered Saline (TBS 1x): 137mM Sodium Chloride, 2.7mM Potassium Chloride, 25mM Tris, pH7.4
- RIPA buffer: 25 mM Tris-HCl pH 7.6, 150mM NaCl, 1% Igepal (Nonidet), 1% sodium deoxycholate, 0.1% SDS

2.1.3 Cell lines

Cell lines were obtained from commercial sources or as kind gifts from Dr Ultan McDermott, Wellcome Trust Sanger Institute (WTSI) or Dr Masashi Narita's group at CRUK Cambridge Institute (CRUK-CI) as indicated in Table 2-2. Each cell line was grown in media obtained from Gibco® as listed in Table 2-2. Cells were incubated at 37ºC and 5% CO_2/air (apart from IMR-90 which are grown in hypoxic conditions at 5% O_2 and 5% CO_2) and passaged before confluence in the usual manner. Cells were counted using Vi-CELL XR™ 2.03. Cell lines were authenticated by the CRUK-CI Biorepository core facility, by genetic profiling of polymorphic short tandem repeat (STR) loci using either Promega GenePrint® 10 System or Promega PowerPlex® 16HS kit together with Applied Biosystems Gene Mapper® software (version 3.2.1 or 4.0) for fragment analysis. All cell lines were grown up to a maximum of 20 passages and for fewer than six months following resuscitation. They were routinely verified to be mycoplasma-free by the CRUK-CI Biorepository core facility, using the MycoProbe® Mycoplasma Detection Kit (R&D Systems, Cat. CUL001B).

Cell line	Tissue of origin	Source	Media
ARPE-19	Human retinal pigment epithelial cells	ATCC	DMEM/F12 (1:1) + 10% FBS
HeLa Aur A	Modified HeLa cells with over-expression of Aur A	Created in house (see section 2.2.10)	DMEM+10% FBS + 4 µg/ml blasticidin +200 µg/ml hygromycin
HT1197	Human bladder cell carcinoma	WTSI	DMEM/F12 (1:1) + 10% FBS
IMR90	Human primary fibroblasts	Narita Group, CRUK CRI	DMEM + 10% FBS.
J82	Human bladder cell carcinoma	WTSI	DMEM/F12 (1:1) + 10% FBS
MIA PaCa-2	Human pancreatic carcinoma	ECACC	DMEM + 10%FBS
RT4	Human bladder cell carcinoma	WTSI	DMEM/F12 (1:1) + 10% FBS
RT112	Human bladder cell carcinoma	WTSI	RMPI-1640 + 10% FBS
SW780	Human bladder cell carcinoma	WTSI	DMEM/F12 (1:1) + 10% FBS
T24	Human bladder carcinoma	CLS	DMEM/F12 (1:1) + 5% FBS
UM-UC-3	Human bladder cell carcinoma	WTSI	DMEM/F12 (1:1) + 10% FBS

Table 2-2: List of cell lines used in research.
Cell lines used together with tissue of origin, source and media used for culture (WTSI: Wellcome Trust Sanger Institute, CRUK CI: Cancer Research UK Cambridge Institute, ECACC (European Collection of Cell Cultures), CLS (Cell lines service).

2.2 Methods

2.2.1 Sulforhodamine B Assay (SRB)

The SRB assay was used for *in vitro* cytotoxicity testing (251). Cells were seeded in 96-well assay plates (Corning® 96 well flat clear bottom black wall polystyrene TC-Treated microplates, Cat. 3603, Corning) at an appropriate seeding density (detailed in Table 2-3) for each cell line and incubated at 37°C in 5% CO_2/air (apart from IMR-90 incubated at 5% O_2 and 5% CO_2).

Cell line	Seeding density (cells/well)
ARPE-19	2500
HeLa and HeLa Aur A	2500
HT1197	2500
IMR-90	5000
J82	2500
MIA PaCa-2	2500
RT4	5000
RT112	2500
SW780	4000
T24	2500
UM-UC-3	2000

Table 2-3: Cell line seeding densities/well in 96 well plates for SRB assay.

Twenty-four hours later, cells were treated with serial dilutions of the relevant drug or drug combinations and incubated for the appropriate time period. Three wells were treated with DMSO alone at the same concentration used for drug dilution as a solvent control. A positive control was also added to the plate layout using a concentration expected to suppress growth by at least 90%, typically gemcitabine.

At the end of the experimental time (typically 72 hours), the media was removed from cells and they were washed with pre-warmed PBS. Cells were then fixed by the addition of 100 µl of ice cold 3% Trichloracetic acid (TCA) (Sigma Aldrich, Cat. 91228) and incubated at 4ºC for 90 minutes. After fixation, the TCA was removed and the plate was rinsed once with ice-cold water manually and dried overnight. Wells were then stained with 50 µl of Sulforhodamine B solution (Sigma Aldrich, Cat. S1402) (0.057% in 1% acetic acid (in deionised water) (Sigma Aldrich, Cat. 27221)) for 30 minutes. The plate was then rinsed four times with 1% acetic acid (either manually or using a plate washer (Biotek ELx405™ Microplate Washer Select CW, Biotek Instruments) to remove the unbound dye and left to dry. On the day of analysis, 200 µl of 10 mM Tris base solution pH 10.5 (Tris-Base from Fisher Scientific, Cat. BP152) was added to each well and the plate shaken on a gyratory shaker to solubilise the protein bound dye. Fluorescence was then quantified using a Tecan Infinite M200 plate-reader at excitation and emission wavelengths of 488 and 585 nm, respectively.

2.2.1.1 Single agent SRB assay data analysis

Further data and statistical analysis was performed using GraphPad Prism software Versions 5.03 or 6. Data sets were transformed with the formula: x=log(x) and a non-linear regression curve fitted to the data. The concentration of drug that resulted in 50% of the cell growth of the solvent control was designated as the GI_{50} concentration. The

IC_{50} was calculated by the software, defined as the concentration of compound that provokes a response halfway between the minimum and maximum response to the drug. At least three biological replicates were performed for each assay.

2.2.1.2 Combination SRB assay data analysis

After SRB staining to obtain the growth inhibition data, we used software developed by Dr Giovanni Di Veroli (CRUK-CI Jodrell lab) to identify synergistic drug combinations – Combenefit (252). The single agent inhibition values are used to calculate a drug combination surface under the assumption of an additive effect. To obtain this additive surface, two different models were applied – Bliss and Loewe as described in 1.8. Regions of synergy are then detected by comparing obtained data from a combination with the calculated additive effect. This is done by subtracting the calculated additive inhibition values from the measured inhibition to obtain the final difference values. In the final synergy surface, positive values indicate synergy, whereas negative values identify antagonism.

I initially analysed the data with the Bliss and Loewe models to examine differences in results. As discussed in 1.8, each model makes different assumptions. Loewe additivity assumes that two inhibitors act through a similar mechanism on the same biological site, differing only in potency. This leads to the concept of dose substitution in which the effects of each inhibitor and the inhibitor combination are related through consistent equipotent dose ratios, requiring similar dose-response curves. As this was not seen across the different AKI, the Bliss independence model, which can be used regardless of the shape of the single-agent dose-response curves, was considered the most appropriate to allow consistent analysis and comparisons across multiple drug combinations and therefore the combination data is only shown for this model.

An example is shown in Figure 2-1 where the Bliss model has been applied to data with the combination of AT9283 and paclitaxel in T24 cells. The mean and standard deviation (SD) of growth relative to solvent control from at least three replicates is shown in Plot (A), with the first column and last row treated with the single agent AT9283 and paclitaxel respectively. All other wells have varying concentrations of the two agents in combination. Plot (B) shows the predictions made by the Bliss additivity model and Plot (C) shows the difference between the model prediction and experimental data. Areas with positive values indicate growth inhibition greater than predicted i.e. synergy, with blue areas showing the strongest regions. Areas with negative values indicating growth inhibition less than predicted i.e. antagonism are represented in red.

As I aimed to identify combinations which showed synergistic effects, I considered combinations with a difference value (synergy score (SS)) of ≥25 potentially significant. The model also tested for the statistical significance of findings (with significant areas marked with a *). Of note, areas of synergy or antagonism at points where the SD was ≥10 are not shown in blue or red by the automated software, for example the combination of AT9283 30 nM with paclitaxel 0.3 nM where the synergy score is 16±11.

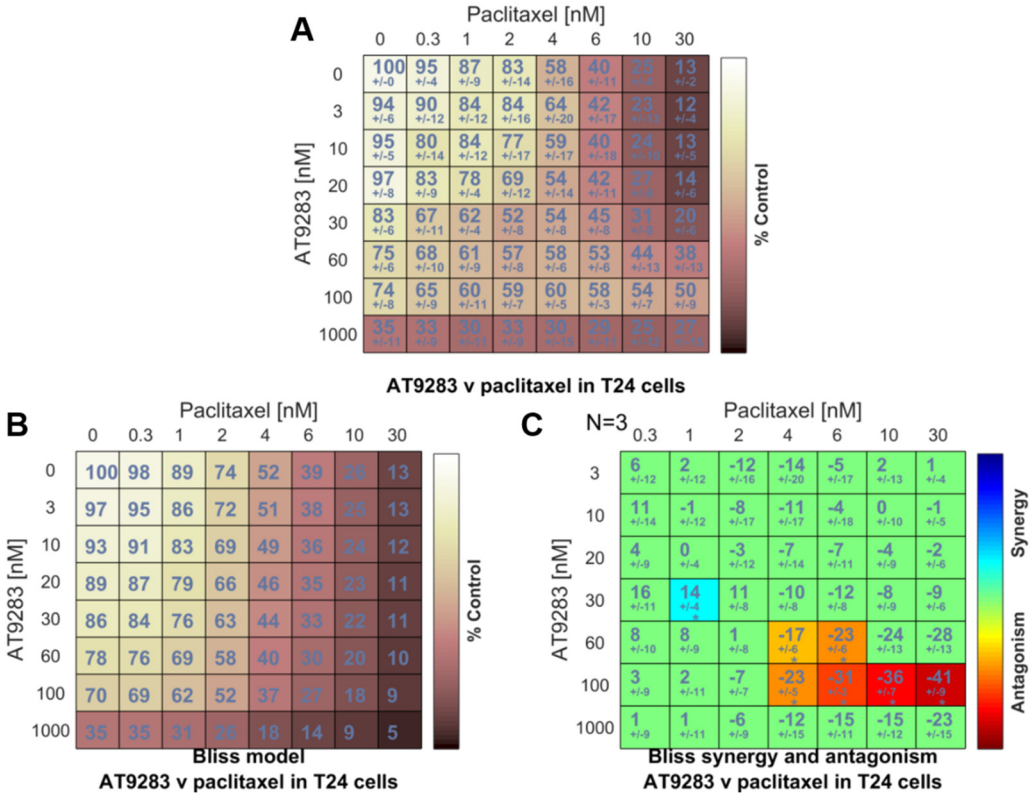

Figure 2-1: Combination of AT9283 and paclitaxel in T24 cells.
T24 cells were seeded in 96-well plates and treated with combinations of paclitaxel and AT9283 for 72 hours. The experimental data (mean of 3 replicates) is shown in (A). The Bliss model was then applied to the experimental data (B) and the tabulated difference values between the model and experimental data are presented in (C). Synergy spots are in blue and antagonism in orange/red in these "Data-additivity" tables.

2.2.2 Drug formulation for in vitro studies

The AT9283 and Cylacel compounds were supplied under material transfer agreements.

Drug	Supplier	Catalogue number
AT9283	Astex Pharmaceuticals	N/A
CYC1	Cyclacel Pharmaceuticals, Inc	N/A
CYC116	Cyclacel Pharmaceuticals, Inc	N/A
CYC3	Cyclacel Pharmaceuticals, Inc	N/A
Docetaxel	Sigma Aldrich	O1885
Gemcitabine hydrochloride	TOCRIS Bioscience	3259
MLN8237(alisertib)	Stratech Scientific	S1133
Paclitaxel	Sigma Aldrich	T7191
Paclitaxel	TOCRIS Bioscience	1097

Table 2-4: Cytotoxic drugs used in research together with supplier and catalogue number. Note two different suppliers of paclitaxel were used during the project.

For all compounds, "master" stock solutions were prepared in Dimethyl Sulfoxide (DMSO) (Sigma Aldrich, D2348) and stored in aliquots at -20ºC for a maximum of three months. These were diluted further in appropriate media to create "working" solutions for dosing. Final DMSO concentrations (0.2%) were kept constant in all experiments.

2.2.3 Live cell imaging with IncuCyte™

Images were acquired with the IncuCyte™ Live Cell Imaging systems either IncuCyte™ FLR 10x or IncuCyte Zoom® (Essen Bioscience) every three hours under cell culture conditions. Averaged bright field cell confluence was calculated from three random fields of view per well using the IncuCyte™ in-built algorithm. Relative confluence values were obtained by normalizing each value to the time zero value in each sample.

2.2.4 Propidium Iodide (PI) staining and flow cytometry

Cells were plated in Petri dishes in an appropriate volume of media and incubated for 24 hours. The medium was then removed, drug was added with fresh media and the dish incubated for the necessary time before harvesting. Controls of untreated cells and solvent control were also analysed. Cells were harvested with 0.05% trypsin, retaining the culture media containing floating cells. They were then washed twice with PBS and fixed with 70% ice-cold ethanol for at least 30 minutes and kept at 4ºC until analysed. On the day of analysis, the Flow Stain solution was prepared as follows: 10 ml PBST (PBS + 0.1% (v/v) Triton-X-100 (Sigma Aldrich, Cat, T9287)), 200 µL of 1 mg/mL Propidium Iodide (PI) Solution (Sigma Aldrich, Cat. D4864) and 40 µL of 50 mg/mL

ribonuclease A dissolved in water (Sigma Aldrich, Cat. R6513). This was kept in the dark on ice.

Samples were re-suspended in this solution to a concentration of $1x10^6$ cells/ml. The solution was then transferred to the cell strainer lid of a Falcon tube (Corning Life Sciences, Cat: 352235 tube) and allowed to flow through. The cell samples were kept in the dark on ice until required for flow cytometry analysis. Each sample was vortexed before being analysed and 20000 cells were read for each cell cycle profile. A BD™ Biosciences FACS-Calibur flow cytometer was used in analysis, with an FL-2 detector (564-606 nM) for PI and a 488 nM excitation laser. The cell cycle distribution of the samples was determined using FlowJo version 7.6.1. Pseudocolour dot plots were generated from the raw data, and manually gated to exclude outliers and capture the subset of cells of interest. From this subset, the plots depicting the cell cycle profiles were created and the percentage of cells in each stage of the cell cycle was determined.

On these plots, the *y* axis is the cell count and the *x* axis shows the intensity of fluorescence in the FL2-H channel, propidium iodide; a measure of DNA content (sample plot shown in Figure 2-2).

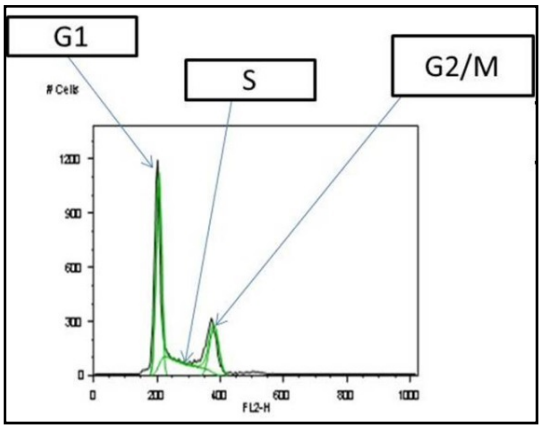

Figure 2-2: Sample histogram plot of flow cytometry data.
The y axis is the cell count and the x axis shows the intensity of fluorescence in the FL2-H channel, propidium iodide. The peaks representing G1, S and G2/M phase are marked.

The Watson pragmatic cell cycle model was applied to these data to quantify changes in cell cycle profiles.

2.2.5 Western blotting

2.2.5.1 Western blot technique

Proteins were extracted from cell pellets using RIPA buffer. Protein quantification was calculated using either the Bio-RAD DC Protein Assay Kit I Bradford assay reagent (Biorad, Cat. 500–011) or the Direct Detect™ Spectrometer (Merck Millipore). Equal

amounts were then loaded on Nu PAGE™ Novex™ Bris-Tris 4-12% gels (ThermoFisher Scientific, Cat. NP0336BOX, NP0329BOX, WG1403BOX) in NuPAGE® MOPS SDS running buffer (ThermoFisher Scientific, Cat. NP001) and separated by SDS-PAGE. They were then transferred to nitrocellulose membranes using the iBlot® system (iBlot™ Transfer Stack, nitrocellulose, regular size, Cat. IB301001, ThermoFisher Scientific). After blocking with Odyssey blocking buffer (LI-COR Biosciences, Cat. 927-50000), the membrane was stained with the appropriate primary antibody diluted in Odyssey block buffer with 0.1% Ultra Pure Tween 20 (Scientific Laboratory Supplies, Cat. EC-607) and rocked overnight at 4ºC. The following day, the membrane was washed four times on a rotary shaker with either Tris-buffered saline or phosphate-buffered saline with 0.1 % Tween (TBS-T or PBS-T). It was then incubated with fluorescently-labelled secondary antibody in Odyssey block buffer with 0.1% Tween for 1 hr at room temperature on a rocker platform before being washed three times with either TBS-T or PBS-T for five minutes and a final wash with TBS/PBS to remove residual Tween. The blots were imaged using the Odyssey® CLx Infrared Imaging System (LI-COR Biosciences). Quantification of Western blots was then performed using LI-COR® Odyssey® software and results normalised to DMSO treated controls.

2.2.5.2 Primary antibodies

Table 2-5 shows the primary antibodies used for Western blotting.

Target	Description	Supplier	Cat. No.	Dilution
Anti-Myc tag, clone 4A6	Mouse monoclonal	Millipore	05-724	1:5000
Aurora A	Rabbit monoclonal	Cell Signaling	4718	1:500
Aurora B	Rabbit polyclonal	Cell Signaling	3094	1:1000
β-Actin	Mouse monoclonal	Abcam	Ab6276	1:5000
β-Actin	Rabbit polyclonal	Abcam	Ab1801	1:5000
Cleaved caspase 3 (Asp 175)	Rabbit polyclonal	Cell Signaling	9661	1:1000
Cleaved caspase 9 (Asp 330)	Rabbit monoclonal	Cell Signaling	7237	1:1000
Cleaved PARP (Asp 14)	Rabbit monoclonal	Cell Signaling	5625	1:1000
Phospho-Aur A (Thr288)	Rabbit monoclonal	Cell Signaling	3079	1:500
Phospho-Aur A (Thr288)/Aur B (Thr232)/Aur C (Thr198)	Rabbit monoclonal	Cell Signaling	2914	1:500
Phospho-histone H3 (Ser10)	Rabbit monoclonal	Cell Signaling	3377	1:1000
Total Aur A	Rabbit polyclonal	Cell Signaling	3092	1:500

Table 2-5: List of primary antibodies used for Western blotting.
Primary antibodies are listed together with supplier, catalogue number (Cat. No.) and dilution.

2.2.5.3 Secondary antibodies

Secondary antibodies used for Western blots were IRDye 680- or 800CW conjugated goat anti-mouse or anti-rabbit IgGs (LiCOR, Cat. 926–32210, 926–32211, 926–32220, 926–32221) at 1:5000 dilution.

2.2.6 Colony forming assay

Cells were plated 24 hours prior to treatment in six-well plates (Falcon® 6 well culture plates, Corning Life Sciences, Cat. 351146) at a density of 50000 cells/well. After 24 hours, the cells were treated with drugs for the designated length of time. Following treatment, cells were harvested using trypsin and counted using Vi-CELL XR™ 2.03. Equal numbers of viable cells (500 and 1000 cells) from each sample were seeded in

triplicate in their usual medium into six-well plates and incubated. Seven days later, cells were fixed with 70% methanol and stained with 5% Giemsa (Sigma-Aldrich, Cat. 48900). Colonies were imaged using GelCount colony counter (Oxford Optronix) and quantified using the ImageQuant TL software (GE Healthcare).

2.2.7 Live cell imaging with time-lapse microscopy

The work in this section was performed with assistance from the staff of CRUK-CI Microscopy core. These experiments were designed together with Dr Yao Lin (T24 and ARPE-19 cell lines) and Dr Siang Boon Koh (HeLa Aur A cell line) and performed by them with my assistance.

Cells were seeded in eight-well chamber slides (Ibidi, Cat. 80826) at a density of 5000 cells/well. After 24 hours incubation, cells were treated with drugs and sent for 72h live-cell imaging detection. They were kept in a humidified chamber under cell culture conditions (37°C, 5% CO_2). Images were taken from three or more fields of view per well, every five minutes, using a Nikon Eclipse TE2000-E microscope with a 20X long-working distance air objective, equipped with a sCMOS Andor Neo camera acquiring 2048x2048 images with a binning factor of two. After acquisition, the data were analysed in NIS-Elements manually. Mitotic duration was defined as the time between cell rounding (i.e. prophase) and either cell separation, cell flattening without separation (i.e. failed mitosis) or cell death. One daughter cell was chosen at random from a successful mitotic division and tracked for its fate over the following 72 hours.

2.2.8 Immunofluorescence and immunostaining

These experiments were designed in collaboration with Dr Yao Lin (T24 and ARPE-19 cell lines) and Dr Siang Boon Koh (HeLa Aur A cell line) and performed by them with my assistance.

For HeLa Aur A experiments, 2500 cells were seeded in normal growth medium either with or without 1 μg/ml doxycycline in 8-well chamber slides (Ibidi, Cat. 80826) for 24 hours. After that, cells were fixed with 4% paraformaldehyde in PBS, permeabilised with 0.3% Triton-X-100 in PBS, stained with antibodies and counterstained with DAPI. The primary antibodies used were anti-Myc tag at 1:250 dilution (Cat. 4A6, Merck Millipore) and total Aur A (Cat.3092, Cell Signaling) at 1:500 dilution. Secondary antibodies used were anti-rabbit IgG Alexa 647 (Cat. 4414, Cell Signaling Technologies) and anti-mouse IgG Alexa 488 (Cat. 4408, Cell Signaling Technologies) used at 1:1000 dilution. The confocal images were taken using a Leica IR Laser

microscope. The images were then merged to determine localisation of Myc-tagged AK-A.

For T24 and ARPE-19 cell lines, a total of 5000 cells were seeded in 8-well chamber slides (Ibidi, Cat. 80826) and treated with drugs 24 h later. After treatment, cells were fixed with 4% paraformaldehyde in PBS, permeabilised with 0.3% Triton X-100 in PBS, then stained with antibodies and counterstained with DAPI. The primary antibodies were anti-α-tubulin at 1:1000 dilution (Cat. T5168, Sigma) and anti-CDK5RAP2 at 1:1000 dilution (Cat. A300-554A, Bethyl Laboratories); secondary antibodies were anti-rabbit IgG Alexa 647 (Cat. 4414, Cell SignalingTechnologies) and anti-mouse IgG Alexa 488 (Cat. 4408, Cell SignalingTechnologies). CompuCyte Icys® imaging cytometer was used for calculations.

2.2.9 Human CFU-GM colony forming assay

Methylcellulose-based culture medium (Stem Cell Technologies, Cat. MethoCult H4035 Optimum without EPO) was thawed overnight at 4ºC. Frozen human bone marrow mononuclear cells (Stem Cell Technologies, Cat. ABM007 F) were thawed at 37ºC and then re-suspended in Iscove's MDM with 2% FBS (Stem Cell Technologies, Cat. 07700) and counted with a haemocytometer. A cell suspension between 1-2 x 10^5 was prepared (depending on the experiment). Four mls of MethoCult medium was dispensed into 15ml sterile tubes and 0.4 ml of cells was added to allow triplicate samples. The tubes were then vortexed and left to stand for five minutes at room temperature to allow bubbles to dissipate. The mixture was drawn up using a 16 gauge blunt end needle and 1.1ml dispensed per 35 mm dish giving a total of 1-2x10^4 cells. They were then cultured for 14 days at 37ºC as described in the manufacturer's manual (Stem Cell Technologies, Cat. 28404). Colonies (aggregates with more than 30 cells) were then counted manually using a Nikon TS100 microscope. The experimental part of this assay was performed jointly with Dr Yao Lin. Colonies were counted by both myself and Dr Yao Lin, blinded to the treatment group.

2.2.10 Generation of tetracycline inducible HeLa over-expressing Aur A cell line

This cell line was generated with Dr David Perera at the Medical Research Council Cancer Unit, Cambridge, using the Flp-In T-REx system from Invitrogen as described before (253). The parental HeLa LacZeo/TO line, and pOG44 and pcDNA5/FRT/TO plasmids, were kindly provided by Professor Stephen Taylor, University of Manchester.

The parental line grows under selection with 50 µg/ml Zeocin™ (InvivoGen, Cat. Ant-zn-1) and 4 µg/ml Blasticidin (Invitrogen, Cat. B21001).

Cells were plated in a six-well dish at a concentration of $1.5x10^5$ cells/well in triplicate. The following day, they were co-transfected with the following plasmids: pOG44, which encodes the Flp recombinase, and pcDNA5/FRT/TO/Myc-Aur-A (kind gift from Dr David Perera), a modified pcDNA5/FRT/TO vector encoding full-length Aurora-A tagged with a single amino-terminal Myc tag. Transfection was performed using jetPRIME® (Polyplus- transfection S.A, Cat. 114-01) as recommended in the manufacturer protocol and the Flp-In™ T-REx™ Core Kit (Invitrogen, Cat. K6500-01). The media was changed after four hours and the cells split at a 1:10 ratio after 24 hours. The following day the media was changed to media containing 200 µg/ml Hygromycin (Invitrogen, Cat. 10687-010) and 4 µg/ml Blasticidin, and the cells were grown with fresh media changes every three days until colonies appeared. Individual colonies were then selected using cloning cylinders (Sigma, Cat. C7983). Nine clones and one pooled sample were then grown individually and banked at -80ºC. Transgene expression was achieved by treatment with 1 µg/ml tetracycline (Sigma Aldrich, Cat. T7660), and then Western blots were performed with antibodies specific for Aurora A and anti-Myc tag.

2.2.11 Analysis of paclitaxel, CYC3 and MLN8237 by Liquid chromatography-mass spectrometry (LC-MS/MS)

The work in this section was performed with the assistance of Dr Tashinga Bapiro, who performed the LC-MS/MS.

2.2.11.1 Instrumentation

A CTC PAL HTS-xt autosampler (CTC Analytics AG) was used for sample injection. Chromatography was performed on an Accela pump (Thermo Fisher Scientific, USA). LC-MS/MS used a TSQ Vantage triple stage quadrupole mass spectrometer (Thermo Scientific) fitted with a heated electrospray ionisation (HESI-II) probe operated in positive mode at a spray of 5000, capillary temperature of 350ºC, vaporizer temperature of 400 ºC, sheath gas pressure of 50 (arbitrary units) and Aux gas pressure set at 20 (arbitrary units). Quantitative data acquisition was done using LC-Quan 2.5.6 (Thermo Fisher Scientific).

2.2.11.2 Preparation of samples

Sample preparation for cells and tumours was performed by me as detailed below.

2.2.11.2.1 *Cells*

Cells were harvested by trypsinisation, an aliquot was counted using Vi-CELL XR™ 2.03 and the remaining cells were washed with ice-cold PBS and centrifuged. After removing PBS, the cell pellet was re-suspended in ice-cold methanol (70% v/v) and vortexed vigorously. The suspension was sonicated for 10 min in an ice bath and an aliquot (50 µl) was processed for LC-MS/MS analysis.

2.2.11.2.2 *Tumour*

Tumour samples, stored at -80ºC, were transferred onto dry ice. A piece was cut and weighed in Precellys 24 homogeniser tubes (Precellys, Cat. KT03961-1-002.2). The tumour pieces were homogenised in ice-cold acetonitrile (200 µl, 50% v/v) (Fisher Scientific, Cat. A955-1) in a Precellys 24 homogeniser (Precellys) for 2 x 50 seconds at 5700 rpm and more acetonitrile was added to give a final concentration of 0.05 mg/µl of tumour. An aliquot (50 µl) of the tumour homogenate was processed for LC-MS/MS analysis.

2.2.11.3 Analysis of paclitaxel and CYC3

Sample analysis was performed by Dr Tashinga Bapiro. An aliquot of either cell lysate, tumour homogenate or plasma was added to 200 µl of ice-cold acetonitrile (100 %) containing the internal standards $^{2}H_5$-paclitaxel (QMX Laboratories, Cat. 158112/0001) or CYC1 (25 ng/ml) (Cyclacel Pharmaceuticals, Inc). After vortex-mixing, the mixture was centrifuged for 20 min at 20000 xg. The supernatant was transferred to a clean tube and evaporated to dryness under air. The residue was reconstituted in 100 µl of 0.1% acetic acid: [Acetonitrile:methanol, (1:1)] 70:30 and 15 µl was injected into the mass spectrometer. The analytes were separated on an Acquity T3 column (Waters) (50 x 2 mm, 1.8 µm, column temperature 30ºC) with A. 0.1 % acetic acid: [Acetonitrile:Methanol, (1:1) 70:30] and B. 0.1 % acetic acid: [Acetonitrile:Methanol, (1:1)]10:90 as mobile phases. The gradient, at a flow rate of 300 µl/min, was 100% A for 0.6 mins, then 100% B from 0.8-3 mins, then 100% A from 3 to 4.5 mins. The mass spectrometry parameters were optimised for the analytes by Dr Tashinga Bapiro, with multiple-reaction monitoring of the transition 881-308 mass to charge ratio (m/z) for Paclitaxel-$^{2}H_5$, 876-308 m/z for paclitaxel, 454-390 m/z for CYC3 and 438-112 m/z for CYC1.

2.2.11.4 Analysis of MLN8237

Sample analysis was performed by Dr Tashinga Bapiro. An aliquot of the samples was added to 200 µl ice-cold acetonitrile containing the internal standard stable labelled MLN8054 (kind gift from Dr Hiroyoshi Hattori (Medical Research Council Cancer Unit, Cambridge)). After vortex-mixing, the mixture was centrifuged for 20 min at 20000 xg. The supernatant was transferred to a clean tube and 15 µl was injected into the mass spectrometer set an ion spray voltage of 2500 V with the rest of the parameters the same as stated above. The analytes were separated on an Acquity T3 column (Waters) (50 x 2 mm, 1.8 µm, column temperature 30ºC) with A. 0.1% formic acid in water and B. 0.1% formic acid in acetonitrile as mobile phases. The gradient, at a flow rate of 250 µl/min, was 80% A and 20% B for 0.5 mins, then 10% A and 90% B from 0.7-4.2 minutes and then 80% A, 20% B from 4.2 to 5.5 minutes. The mass spectrometry parameters were optimised for the analytes by Dr Tashinga Bapiro, with multiple-reaction monitoring of the transition 519-328 m/z for MLN8237 and 478 to 316 for MLN8054 m/z.

2.2.11.5 Analysis of tumour PK results

The concentrations in tumour homogenate in ng/ml obtained from the LC-MS/MS analysis were converted to ng/mg tissue and then µg/g tissue. The assumption was made that tissue density is 1 g/ml to give a value in mg/litre of tissue. This was then divided by the molecular weight of each drug to give a millimolar concentration. These figures are shown for the PK experiments.

2.3 Animal studies

The work in this section was performed with assistance from the staff of CRUK-CI Biological Resources Unit (including drug dosing) and Dr Frances Richards (drug formulation and performing mouse necropsies). All mouse studies were performed in accordance with UK Animals (Scientific Procedures) Act 1986, under project licence number 80/2346, with approval from the CRUK-CI animal ethics committee and following the 2010 guidelines from the United Kingdom Coordinating Committee on Cancer Research (254). Balb/c nude mice were obtained from Charles River Laboratories and enrolled on studies between six to twelve weeks old. Female mice were used for each protocol apart from the first study which used male mice. Mice were housed in groups in individually ventilated cages.

2.3.1 Xenograft model

Balb/c nude mice were injected subcutaneously with either $2x10^6$ T24 cells (in 0.1 ml 1:1 Matrigel (BD Bioscience, Cat: 354234): PBS) or $5x10^6$ cells MIA PaCa-2 cells (in 0.1 ml 1:1 matrigel: PBS) into one flank. Long (L) and short (S) axes of each tumour were measured with calipers approximately twice a week. Tumour volume (V) measurements were calculated in mm^3 using the formula: $V= \pi/6 \times S^2 \times L$. Once the tumour was >100 mm^3, mice were dosed with drug according to the specific study protocol. For studies with more than one potential drug treatment option, mice were randomised to different treatment groups using the spiral randomisation method (255), recommended by Hazel Jones at Cancer Research Technology. Their health was assessed daily and they were weighed twice a week. Animals were killed humanely either at pre-specified time points as per study protocol, if tumours approached 10% of body weight or if clinical signs of toxicity approached the limit of moderate severity.

2.3.2 Mid-term bleeds

Mid-term bleeds were performed in some studies. The preference was for tail vein bleeds. The mouse was restrained, the tail nicked with a scalpel and a drop of blood (approximately 50 µl) collected into an EDTA (Invitrogen, Cat: 15575020)-treated glass capillary tube. The capillary tube was then put into an open 0.5 ml Eppendorf tube containing 17.5 µl 100mg/ml EDTA on ice and the blood expelled using a 200 µl pipette tip. Blood was mixed thoroughly before counting on the Mythic 18 Vet Haematology Analyser (Woodley Equipment Company Limited). Due to difficulties with obtaining sufficient blood, live submandibular vein bleeds were performed in some mice. The mouse was restrained and a lancet (MediPoint Inc, Cat. Goldenrod 4 mm) used to nick the vein. Approximately 40-100 µl of blood was collected directly into a 0.5 ml Eppendorf tube containing 17.5 µl 100 mg/ml EDTA on ice.

2.3.3 Necropsy

Animals were killed using standard home office humane methods. Mice were weighed and tumours measured at the endpoint. Cardiac puncture was performed under terminal anaesthesia to collect blood using a 26G needle with a 1 mL syringe. Kill was completed by cervical dislocation.

The blood sample was collected into a micro-centrifuge tube containing K_2 EDTA. The tube was stored on wet ice for no more than 30 minutes. A Mythic 18 Vet Haematology Analyser (Woodley Equipment Company Limited, UK) was used to determine the full

blood count using 50 µl of this blood sample, with duplicate or triplicate samples measured if possible. The remaining blood sample was then centrifuged at 14000 rpm at 4ºC for 5 minutes. The plasma was then carefully removed from the blood cell pellet using a pipette and snap frozen in liquid nitrogen.

Following the blood draw, a piece of skin was dissected from the back of the mouse (approximately 1-2 cm in diameter), placed wet side down onto a piece of Invitrolon™ Polyvinylidene difluoride (PVDF) filter paper (Invitrogen, Cat. LC2005) and then fixed for 24 hours at room temperature in 10% neutral buffered formalin solution (NBF) (Sigma Aldrich, Cat. HT501128). The tumour was excised (and weighed in some studies). If possible, half the tumour was fixed in formalin for histology and immunohistochemistry (IHC) with the remaining tumour being snap frozen. Intestines, liver and spleen were also fixed in 10% NBF. Fixative was replaced with 70% ethanol after 24 hours.

Tissue was then cassetted, paraffin embedded, sectioned and stained by the histology core facility at the Cancer Research UK Cambridge Research Institute, as described further in 2.3.4.

In some studies, the femurs were also collected either into PBS (if required for bone marrow aspirate or CFU-GM with methods further detailed in 2.3.7) or into formalin (for histological sections, described below).

2.3.4 Histology methods

The work in this section was performed by the staff of the CRUK-CI Histopathology, particularly Jodi Miller (optimisation of staining), Leigh-Anne McDuffus and Cara Brodie (analysis algorithm optimisation).

2.3.4.1 Tissue preparation

Tissues were fixed in 10% NBF for 24 hours at room temperature, and transferred to 70% ethanol. Tissues were dehydrated in an ascending series of ethanol solutions from 90% to 100%, then into xylenes and paraffin wax using a Leica ASP300S overnight processor. Femurs were demineralised with two changes of 0.5M EDTA over seven days first before being processed as above. Paraffin embedded blocks were then stored until needed.

2.3.4.2 Immunohistochemistry

Wax sections of 3 μm were cut from each block and placed on glass slides. Sections were de-waxed and rehydrated using a Leica/CV5030 autostainer and routine hematoxylin and eosin staining was performed. Additional sections were stained with the antibodies listed in Table 2-6 using Leica's Bond Polymer Refine Detection Kit (Leica, Cat: DS9800) on their automated IHC with DAB Enhancer (Leica, Cat: AR9432), according to manufacturer instructions. Antigen retrieval used either sodium citrate (pH 6) or tris EDTA (pH 9) (Table 2-6) and was performed at 100°C on the Bond™ platform (Leica).

Antibody	Manufacturer	Cat. No.	Antibody Dilution	Antigen Retrieval
Ki67 (hu)	Dako	M7240	1:200	Tris EDTA, 30 minutes
Ki67 (ms)	Bethyl Laboratories	IHC-00375	1:1000	Sodium Citrate, 20 minutes
pH3 (hu/ms)	Merck Millipore	06-570	1:200	Sodium Citrate, 10 minutes
CC3 (hu/ms)	Cell Signaling Technology	9664	1:200	Tris EDTA, 20 minutes
Myeloperoxidase (ms)	Dako	A0398	1:1000	Sodium Citrate, 20 minutes

Table 2-6: Antibodies and antigen retrieval used in immunohistochemistry studies. Abbreviations: hu (human), ms (mouse)

To detect human Ki67 in xenograft samples, a mouse on mouse protocol was required as the antibody is a mouse monoclonal antibody. An additional block with mouse Ig block solution (Vector, Cat: MKB-2213) and an isotype specific secondary antibody was required using rabbit anti-mouse IgG1 diluted 1:1500 (Abcam, Cat: ab125913).

The protocol for myeloperoxidase (MPO) in mouse bone marrows was developed and optimised with Jodi Miller, using spleen and bone marrow. Firstly three retrieval conditions were tested with MPO diluted 1:100 consisting of sodium citrate (pH6) for 20 mins, tris EDTA (pH 9) for 20 mins (both at 100°C) and proteinase K enzyme digestion for ten mins at 37°C. A "no primary" control for each retrieval condition was also run to determine whether any unwanted staining was coming from the primary antibody or the detection system/pre-treatment. The "no primary" controls were clean and specific signal was seen in the red pulp of the spleen with the sodium citrate and tris EDTA treatments. Due to over-staining, both were further investigated with antibody dilutions with sodium citrate selected for antigen retrieval with the primary diluted 1: 1000 determined optimal, with the best signal to noise ratio.

Slides were scanned using a Leica Aperio ScanScope AT2 (Leica) at 20 X magnification (resolution 0.5 µm per pixel). Scanned images were viewed using Aperio Imagescope v12.2 (Aperio Technologies Inc.) and subsequently also using Indica labs HALO software (V2.0.1145.30).

2.3.5 Image analysis

2.3.5.1 Tumour sections

Image analysis algorithms for each stain were developed and optimised by the CRUK-CI histopathology core facility based on positive nuclear staining (Aperio Imagescope Nuclear version 7) apart from CC3 where positive pixel counts were used (Aperio Imagescope Positive Pixel Count version 9), as positive staining was seen both in the nuclei and surrounding cytoplasm and it was difficult for the algorithm to capture the staining. On each slide the "Region of Interest" (the tumour) was individually highlighted manually prior to automated image analysis using the appropriate algorithm. Subsequently algorithms were also developed using Indica labs HALO software (V2.0.1145.30), due to the degree of necrosis seen in T24 tumours. Initially a tissue classifier was applied that was developed to detect viable tumour, areas of necrosis and glass. The appropriate algorithm was then only applied to the remaining viable tumour as illustrated in Figure 2-3.

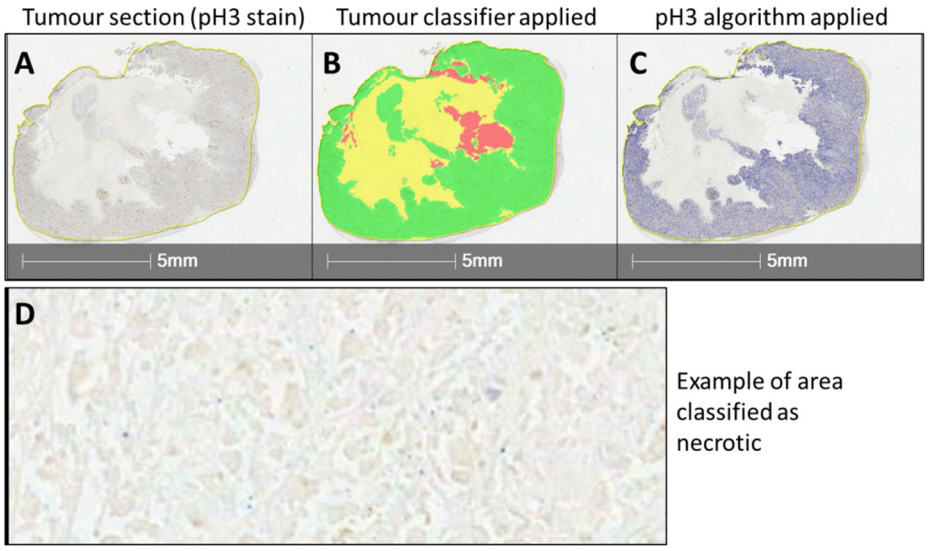

Figure 2-3: Example of tissue classifier algorithm for analysis of T24 xenograft tumours.
In A. a representative tumour section stained with pH3 is seen with the tumour area outlined in yellow. The tumour classified is then applied and B. shows this with viable tumour shown in green, areas of glass in red and areas of necrosis in yellow. C. shows the areas of the tumour which were then analysed for pH3 stain. D. shows an example of an area classified by the algorithm as necrotic.

Due to the nature of serial sections through the tumour and batch staining variability, there was a degree of variability in the percentage of necrosis across the different stains for some individual tumours. After review of all the data with Cara Brodie (Histopathology Core), the pH3 stained slides were the most consistent and hence the data shown for percentage necrosis is from these slides.

For the HALO analysis, the following algorithms were used: Ki67- Multiplex IHC v1.1, CC3–Area quantification v1.0, and pH3– Cytonuclear v1.4. The algorithms scored the tissue for strong, moderate and weak staining. After review, only the strong and moderate staining was scored as positive for Ki67 due to some non-specific staining being classified as weakly positive.

2.3.5.2 Skin sections

For skin samples, three randomly chosen 20 X fields were chosen and the basal epithelial layer in these was highlighted manually prior to automated image analysis using the appropriate algorithm.

2.3.5.3 Femurs

H&E stained femurs were initially scanned at 20X magnification but subsequently also scanned at 40X magnification to aid visualisation of cell types.

The myeloperoxidase (MPO) stain was optimised as described in 2.3.4.2. The HALO™ platform (Indica labs) was then used to specifically identify the areas of bone marrow within the sections of the femur before the MPO algorithm was applied (Halo Cytonuclear version 1). The analysis reported the total number of positive cells, divided into weak, moderate and strong staining as well as the number of negative cells. To ensure cells of monocytic origin were excluded, positive cells were considered those with either strong or moderate staining and those which were weakly positive were counted as negative.

2.3.6 Drug formulation for *in vivo* studies

CYC3 was provided by Cyclacel Pharmaceuticals, Inc. CYC3 was initially dissolved in 100% 1-Methyl-2-pyrrolidinone (NMP) (Sigma Aldrich, 328634) to a concentration of 100 mg/ml. It was then diluted for dosing to a final concentration of 10% 1-Methyl-2-pyrrolidinone (NMP) (Sigma Aldrich, 328634), together with 30 or 40% Polyethylene glycol molecular weight 400 Da (PEG400) (Sigma Aldrich, Cat: 81172), citrate buffer pH3 (Sigma Aldrich, S1804) for oral gavage or 10% NMP, 40% PEG400, 60%

Vetivex™1 (Dechra, Cat. VO1M) saline for intra-peritoneal (IP) dosing. As the IP dosing was not well tolerated (due to the vehicle) for the subsequent experiment with a 50 mg/kg dose of CYC3 IP, the vehicle was changed to 10% NMP, 40% PEG400, 60% citrate buffer pH 3.

Paclitaxel was obtained from Tocris (Cat: 1097) or Cayman Chemicals via Cambridge Bioscience (Cat: CAY10). A concentrated solution was obtained by dissolving 50 mg paclitaxel in 1.25 ml of 1:1 Cremophor EL (Sigma Aldrich, Cat: C5135) and 10ml Ethanol (Sigma Aldrich, Cat: 41322). The mixture was then stirred at room temperature until it had dissolved. If it did not dissolve fully, it was sonicated in cold water at 35 KHz for 2 + 5 + 10 mins. It was then stored at 4ºC for duration of study. On the day of dosing, for lower concentrations of paclitaxel, this stock solution was further diluted to give a final vehicle concentration of 5% Cremophor EL, 5% ethanol, 90% sterile saline (CES vehicle). For 20 mg/kg paclitaxel, the vehicle consisted of 25% Cremophor EL, 25% ethanol, 50% saline. Vehicle only group received 5% Cremophor EL, 5% ethanol, 90% saline.

MLN8237 was obtained from Ontario Chemicals (Cat: M630). It was administered by oral gavage (OG), suspended in 10% hydroxypropyl-beta-cyclodextrin and 1% sodium bicarbonate in water. 1% sodium bicarbonate was made by dissolving 5 g of sodium bicarbonate (Sigma Fluka, Cat: 71631) in 500 ml sterile milli Q water and stored at room temperature. Each week 50 ml of this solution was added to 5 g of 2-hydroxypropyl-beta-cyclodextrin, (Sigma Aldrich, Cat: 332607). The mixture was then stirred vigorously for approximately 30 minutes until dissolved and stored at 4ºC. When this vehicle was added to MLN8237, it was then stirred for several hours and stored at 4ºC between dosing schedules. Prior to administration, it was warmed and mixed well.

Docetaxel (Alfa Aesar, Cat: J60174) was prepared in a vehicle consisting of 5% ethanol, 5% polysorbate 80 and 90% sterile saline (EPS). Firstly the solvent vehicle (EP) was prepared by mixing equal volumes of ethanol (Sigma Aldrich, Cat: 41322) and polysorbate 80 (Sigma Aldrich, Cat: 59924). It was then stored at 4ºC for the duration of the study. A concentrated 40 mg/ml docetaxel solution was made by adding the exact amount of EP solvent and stirring until dissolved. This was then stored at 4ºC. On the day of dosing, this concentrated stock docetaxel was diluted to 4 mg/ml with pre-warmed Vetivex™1 (Dechra, Cat. VO1M) saline and mixed thoroughly. It was kept at room temperature until dosing. Solvent vehicle was also diluted so that both drug and

vehicle had a final concentration of 5% ethanol, 5% polysorbate 80, 90% saline for dosing.

2.3.7 Mouse CFU-GM assay

A pilot study was performed to determine the colony-forming cell ability of the cells in the bone marrow of mice. The method was based on that published by Stem Cell Technologies; Technical Manual 3.1.1 "Mouse Colony-Forming Cell Assays using MethoCult".

To obtain bone marrow cells from mice at necropsy, the abdominal skin was wet with 70% ethanol to decrease the probability of contamination. The femur was dissected and placed in a pre-chilled Bijou tubes filled with 7 mls of D-PBS with 200 U/ml Penicilllin-Streptomycin and 2.5 µg/ml amphotericin (prepared by adding 20 ml of Penicillin-Streptomycin (5,000 U/mL) (Gibco 15070-063) and 5 ml of Amphotericin B (Sigma Aldrich, Cat. A2942-50ml) to a 500 ml bottle of D-PBS). The femur tubes were then placed on ice for no more than 30 minutes before cells were isolated.

Using a 3 cc syringe with a 21 gauge needle, 5 ml of cold Iscove's MDM with 2% FBS (Stem cell technologies, Cat: 07700) was drawn up. The bevel of the needle was inserted into the marrow shaft, twisted and the marrow was flushed into a sterile 15ml culture tube with BD Falcon Cell strainer 70 µm (Fisher Scientific, Cat: 352350) placed on top. A single cell suspension was then made by gently drawing the medium and cells up and down. 20 µl was taken for a cell count and the remaining cells were centrifuged at 300 G for 8 minutes.

A nucleated cell count was performed using Vicell after cells were diluted 1:50 in 3% acetic acid with methylene blue mix (Stem Cell Technologies, Cat: 07060). The value for viable cells/ml was used to re-suspend cells in Iscove's MDM with 2% FBS at 10x final concentration required. The manufacturer recommended seeding 2-3x10^4 cells per 35 mm plate to give an expected number of between 60-100 CFU-GM colonies. However, as we had experienced low numbers of colonies in our experiments with human CFU-GM assays, we decided to use 2x10^5 cells per well.

Four mls of MethoCult medium (Stem Cell Technologies, Cat: 03534) was dispensed into 15ml sterile tubes and 0.4 ml of cells was added to allow triplicate samples. The tubes were then vortexed and left to stand for five minutes at room temperature to allow bubbles to dissipate. The mixture was drawn up using a 16 gauge blunt end needle and 1.1 ml dispensed per 35 mm dish. Three 35 mm dishes (Stem Cell Technologies, Cat: 27100) were placed in a 150 mm petri dish and a fourth uncovered 60 mm dish

containing sterile water added to help maintain humidity. The petri dishes were placed in an incubator at 37°C and 5% CO_2, undisturbed for twelve days. Images of the plates were then taken using GelCount™ (Oxford Optronix) and the number of colonies quantified using an algorithm developed in GelCount™, with results manually checked.

2.3.8 M30/M65 ELISA

M30 and M65 are ELISA assays which detect different circulating forms of the protein cytokeratin 18 (CK18), a marker of epithelial cell death. The M30 antibody recognises a neo-epitope (CK18 Asp^{396}) which is only exposed after caspase cleavage of the protein. In contrast, M65 uses two monoclonal antibodies to detect soluble full length as well as apoptotic fragments of cytokeratin 18 and hence gives a measure of total cell death by any cause (256). The M30 Apoptosense® ELISA (Peviva, Cat. 10011) and M65 EpiDeath® ELISA (Peviva, Cat. 10040) assays specifically detect tumour cell apoptosis and cell death in mice carrying human tumour xenografts (257).

For this pilot study, plasma samples from mice enrolled in the MLN8237 and docetaxel efficacy study were used. Due to limited capacity on the kit, 27 from the efficacy study (selected to represent each treatment group) were chosen. Plasma samples were thawed and then analysed in duplicate with the M30 Apoptosense® ELISA and M65 EpiDeath® ELISA kits according to manufacturer's protocol apart from the following additional step. Previous studies have identified significant levels of background when the M30 and M65 ELISAs were run on mouse or rat plasma, which was reduced by the use of a blocking reagent (257). Therefore, in addition to the normal incubation mixture of 25 µl sample and 75 µl of antibody conjugate, 0.4 µl of heterophilic blocking reagent HBR-Plus purified at concentration 10mg/ml (kind gift from Scantibodies Laboratory, Cat. 3KC545) was used per sample. Absorbance at 450 nM was measured on the PHERAstar microplate reader (BMG LabTech). As per protocol, a standard curve was then plotted using the known standard concentrations versus measured absorbance. This allowed the amount of antigen in each sample to be calculated in units/litre (U/L). I designed this experiment but it was performed by Jo Bramhall under my supervision, and I analysed the results.

3 *DETERMINING THE IN VITRO EFFICACY OF AURORA KINASE INHIBITORS AS SINGLE AGENTS AND IN COMBINATION WITH TAXANES*

3.1 Introduction

Based on the evidence in Chapter 1, I first assessed the effect of a range of aurora kinase inhibitors (AKI), using a panel of inhibitors with different selectivity, together with the effects of other cytotoxic drugs including paclitaxel in the T24 human bladder cancer cell line. Combination studies were then explored to select the optimum schedule, with the findings expanded to a wider panel of bladder cancer cell lines. Subsequently the AK-A inhibitor, MLN8237, was assessed as a specific AK-A inhibitor in combination with paclitaxel.

Contribution of others to this experimental work: All experiments in this chapter were performed by me.

3.2 Comparison of the efficacy *in vitro* of AKI inhibitors with different selectivity in T24 bladder cancer cells

3.2.1 Single agent response to AKI in T24 cells

The data provided by the pharmaceutical companies show that all four provided AKIs are potent inhibitors of AK-A in the low nanomolar range but also target other kinases (Table 3-1).

Compound	**AK-A (nM)**	**AK-B (nM)**	**CDK2/ cyclin E (nM)**	**CDK7/ cyclin H (nM)**	**CDK9/ cyclin T1 (nM)**	**VEGFR2 (nM)**
CYC1	4	4	150	410	100	43
CYC3	6	154	>20000	>20000	>20000	557
CYC116	8	9	380	>10000	480	49
Compound	**AK-A (nM)**	**AK-B (nM)**	**JAK3 (nM)**	**JAK2 (nM)**	**ABL (T315I) (nM)**	
AT9283	3	3	1.1	1.2	4	

Table 3-1 *In vitro* IC_{50} activity of AKI used together with other key kinases targeted. Data provided by Cyclacel and Astex Pharmaceuticals.

The publically available chemical structures of the AKI are shown in Figure 3-1. The structure of CYC1 is confidential.

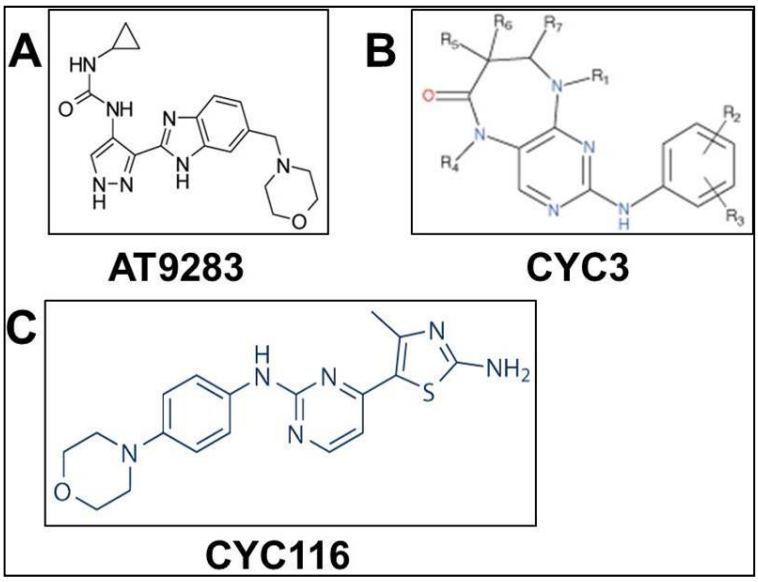

Figure 3-1: Publically available chemical structures of initial AKI used.
A. AT9283, B. CYC3 and C. CYC116

The SRB assay was used to assess the cytotoxicity of these agents in T24 cells treated with varying doses of each drug and incubated for 72 hours. The IC_{50} and GI_{50}s of the relevant compounds were then calculated and the individual dose response curves are shown in Figure 3.2.

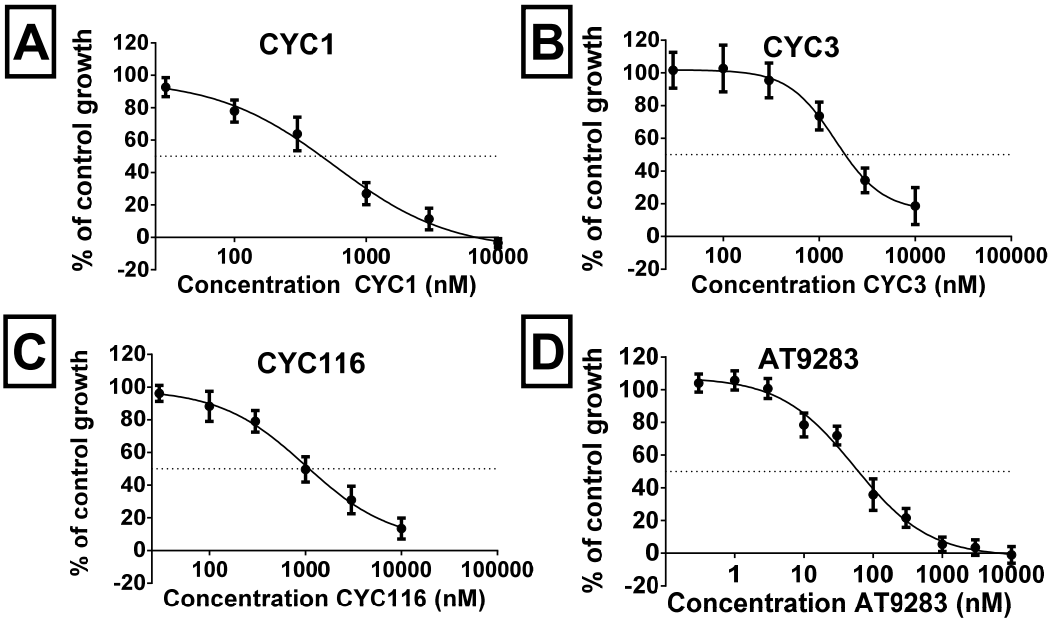

Figure 3-2: Dose response curves for T24 cells exposed to AKI.
Dose response curves for T24 cells treated with A. CYC1 B. CYC3 C. CYC116 D. AT9283. T24 cells were exposed to a range of concentrations of each drug for 72 hours, then analysed using SRB assay. Each graph shows the data for percentage control cell growth at each concentration of three replicates with standard deviation and then a curve fitted to the data using GraphPad Prism to calculate IC_{50}. The dotted line shows 50% cell growth and this was used to identify the GI_{50} from the graph. IC_{50} and GI_{50} are shown in Table 3-2.

Drug	IC_{50} (nM)	GI_{50} (nM)
CYC1	570	480
CYC3	1500	1900
CYC116	1000	1000
AT9283	54	60

Table 3-2: IC_{50} and GI_{50} of AKI tested in T24 cells

Of the AKI tested, AT9283 was the most potent. CYC1, CYC3 and CYC116 all showed potency in the T24 cell line, although with higher IC_{50}s.

Having established the single agent activity of the AKI in T24 cells, I also tested the effects of gemcitabine, which is commonly used in the current management of bladder cancer and the taxanes, both paclitaxel and docetaxel (Figure 3-3 and Table 3-3.)

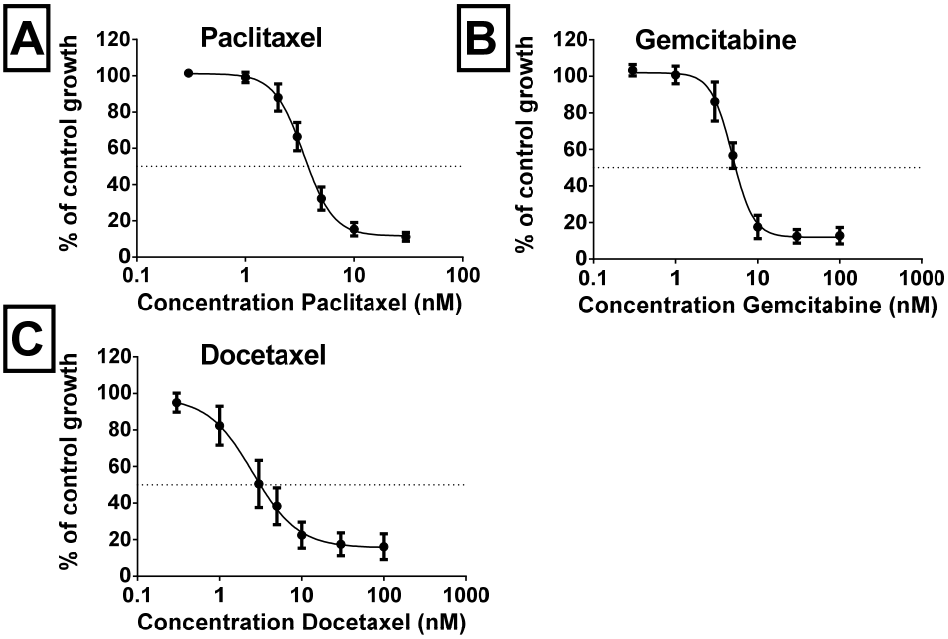

Figure 3-3: Dose response curves for T24 cells exposed to A. Paclitaxel B. Gemcitabine C. Docetaxel.

T24 cells were exposed to a range of concentrations of A. Paclitaxel B. Gemcitabine C. Docetaxel for 72 hours, then analysed using SRB assay. Each graph shows the data for percentage control cell growth at each concentration of at least three replicates with standard deviation and then a curve fitted to the data using GraphPad Prism to calculate IC_{50}. The dotted line shows 50% cell growth and this was used to identify the GI_{50} from the graph. IC_{50} and GI_{50} are shown in Table 3-3.

Drug	IC_{50} (nM)	GI_{50} (nM)
Paclitaxel	3.5	3.8
Gemcitabine	4.9	5.6
Docetaxel	2.6	3.3

Table 3-3: IC_{50} and GI_{50} of paclitaxel, gemcitabine and docetaxel in T24 cells.

Gemcitabine, paclitaxel and docetaxel demonstrated nanomolar potency against T24 cells, consistent with their use in bladder cancer treatment.

3.2.2 Combination of AKI with paclitaxel in T24 cells to select best agent for combinations

As the hypothesis was that AKI would synergistically enhance the cytotoxicity of paclitaxel as over-expression of AK-A can induce resistance to paclitaxel (2), I next investigated the combination of these AKI with paclitaxel. Each AKI was tested in an eight by eight concentration grid to fully explore the interactions between the two drugs, with the concentration range selected to explore synergy in the regions around the IC_{50}s of both drugs and the data analysed with the Bliss model as described in 2.2.1.2.

Figure 3-4 to Figure 3-7 depict the results of SRB assays combining the AKI with paclitaxel, with the actual data (plot A) subtracted from that predicted (plot B) to show differences between the model prediction and experimental data (plot C), as detailed in 2.2.1.2.

When either AT9283 (Figure 3-4) or CYC1 (Figure 3-5) were combined with paclitaxel there was a largely additive picture, with some antagonism at higher concentrations of both drugs.

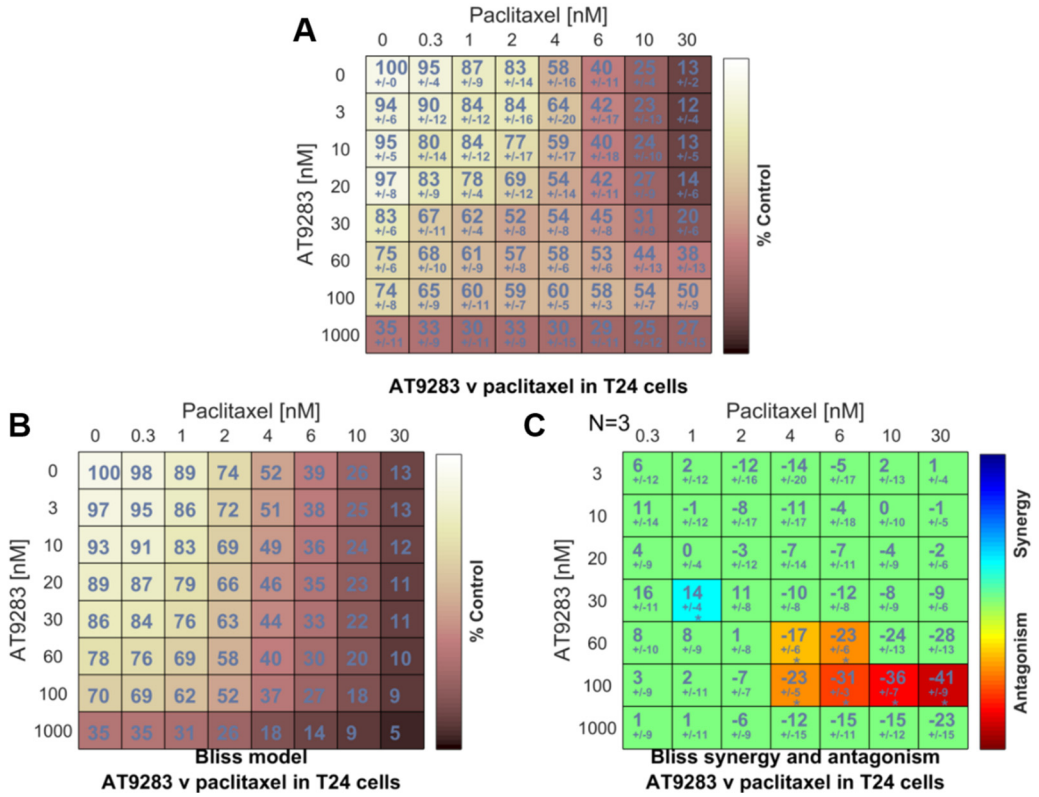

Figure 3-4: Combination of AT9283 and paclitaxel in T24 cells.
T24 cells were seeded in 96-well plates and treated with combinations of paclitaxel and AT9283 for 72 hours.

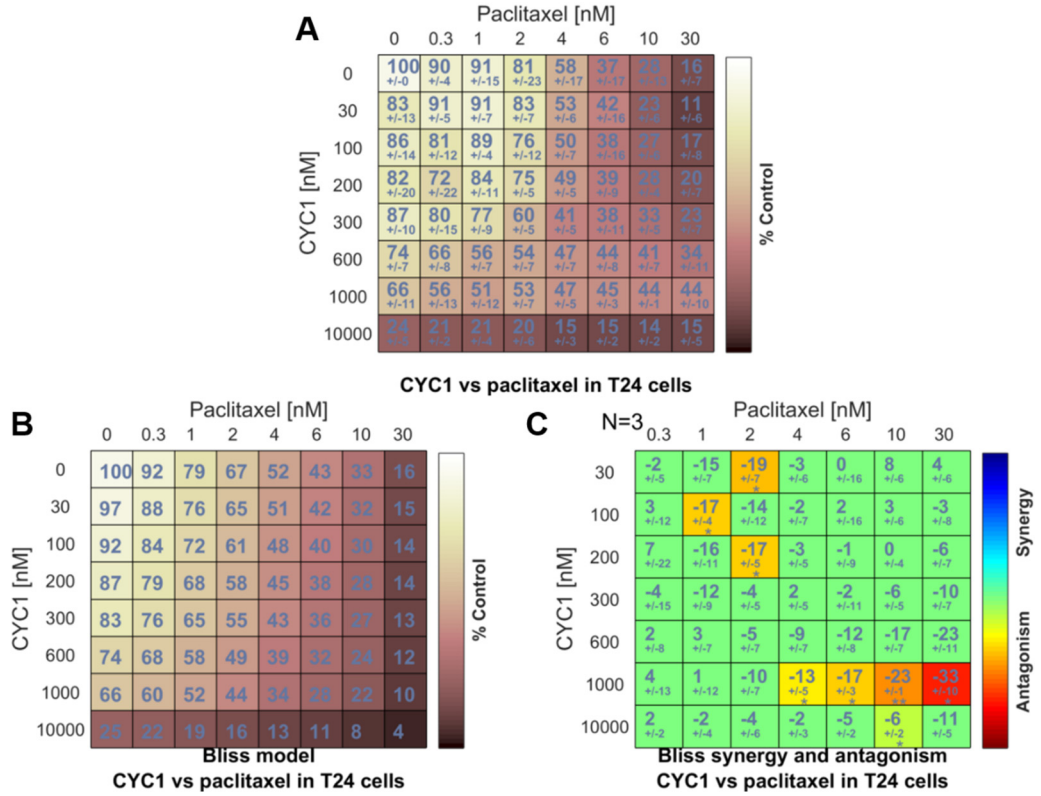

Figure 3-5: Combination CYC1 and paclitaxel in T24 cells.
T24 cells were seeded in 96-well plates and treated with combinations of paclitaxel and CYC1 for 72 hours.

With CYC3 (a more specific AK-A inhibitor) (Figure 3-6), a statistically significant region of synergy was identified between CYC3 500 nM to 1500 nM and paclitaxel 2 nM to 6 nM, with the strongest synergy seen at CYC3 1000 nM and paclitaxel 2 nM, with 52±2% growth compared to control i.e. 48±2% growth inhibition, compared to the additive prediction of 93% of control, giving a synergy score of 41±2. Antagonism was again seen with the higher concentrations of paclitaxel and CYC3.

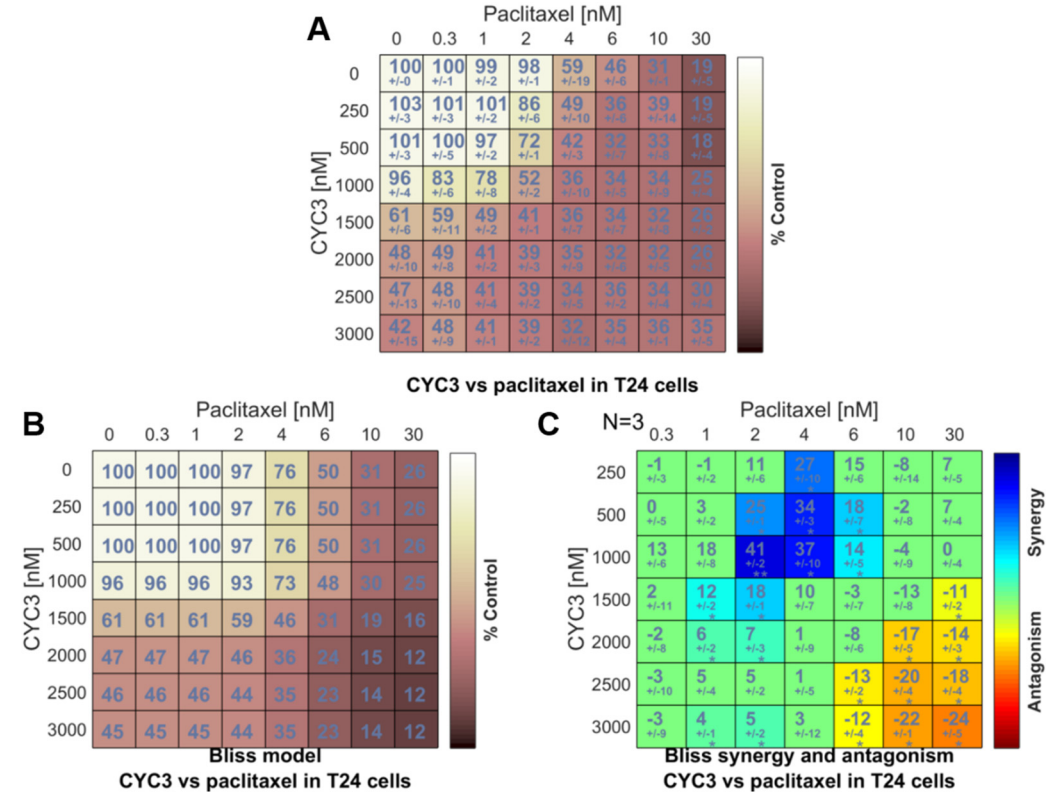

Figure 3-6: Combination of CYC3 and paclitaxel in T24 cells.
T24 cells were seeded in 96-well plates and treated with combinations of paclitaxel and CYC3 for 72 hours.

With CYC116 (Figure 3-7), there were no significant regions of synergy, with areas of antagonism also identified at higher concentrations of both drugs.

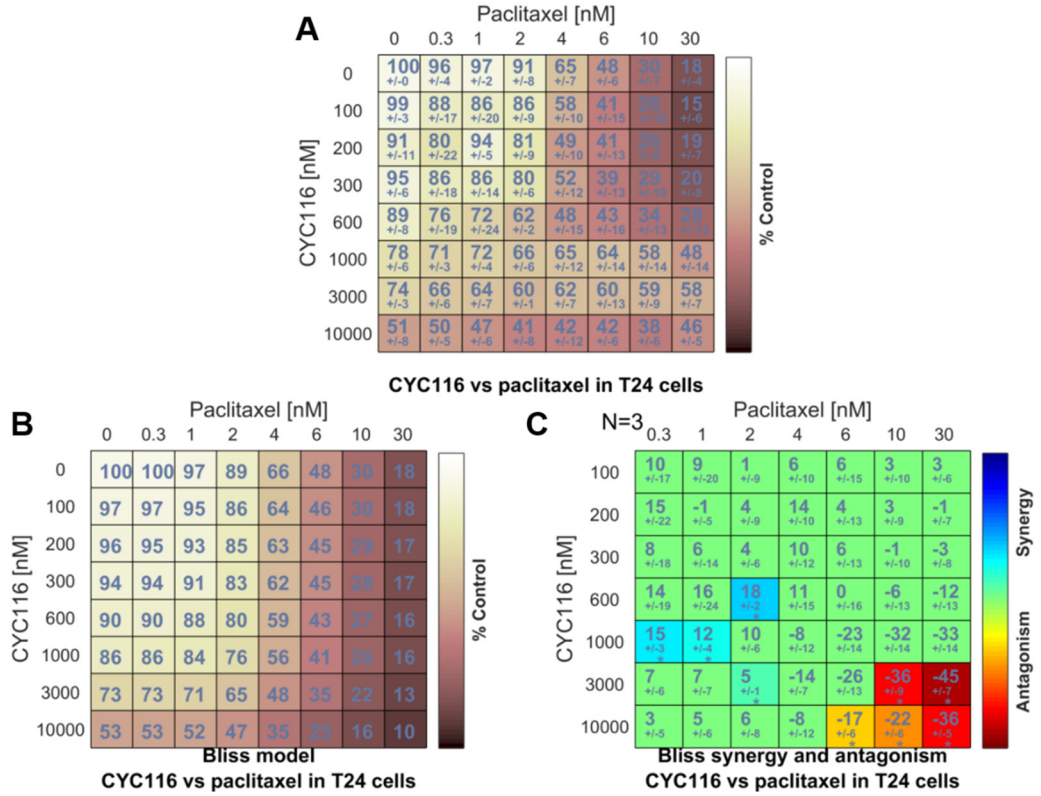

Figure 3-7: Combination CYC116 and paclitaxel in T24 cells.
T24 cells were seeded in 96-well plates and treated with combinations of paclitaxel and CYC116 for 72 hours.

3.2.2.1 Summary of AKI and paclitaxel combinations in T24 cells

There was no therapeutically relevant synergy with paclitaxel and any of the dual AK-A and AK-B inhibitors (AT9238, CYC1 and CYC116). With CYC3, which was the most AK-A-specific compound, with 25-fold selectivity for AK-A over AK-B (Table 3-1), a region of synergy with paclitaxel was seen. Of particular interest was the lack of synergy seen with higher concentrations (10 and 30 nM) of paclitaxel combined with CYC3. This emphasises the utility of investigating a range of concentration-combinations to generate a surface of interaction.

When the same drugs were also studied in pancreatic cancer cell lines, the combination of CYC3 and paclitaxel looked particularly promising, and was explored further together with Dr Yao Lin. I generated the data on combinations of CYC3 with paclitaxel and we jointly performed the CFU-GM colony forming experiments in the paper that we published (Appendix 1 (258)). In the MIA PaCa-2 cell line, maximal synergy was seen with CYC3 1000 nM and paclitaxel 3 nM, with growth inhibition of 89±7%, approaching that of paclitaxel 30 nM as a single agent (99±5%) but with reduced toxicity to the bone marrow.

3.2.3 Validation of synergy seen with combination CYC3 and paclitaxel in T24 cells

I next assessed the effect of the combination of CYC3 and paclitaxel in T24 cells with IncuCyte™ live cell imaging and Western blotting.

3.2.3.1 Incucyte™ live cell imaging in T24 cells with CYC3 and paclitaxel

Incucyte™ time lapse microscopy was used to evaluate the effect of CYC3 and paclitaxel on cell confluency over time, both as single agents and in combination. With CYC3 (Figure 3-8 A), the dose response curve is relatively steep between CYC3 1000 nM and CYC3 1500 nM, but growth inhibition plateaued at concentrations above CYC3 1500 nM, similar to the results seen in the SRB assay (Figure 3-6). With paclitaxel (Figure 3-8 B), the dose response curve was steep between paclitaxel 2 nM and paclitaxel 6 nM. Both combinations (Figure 3-8 C and D) significantly suppressed cell growth with growth inhibition approaching the efficacy of paclitaxel 30 nM.

Figure 3-8: Relative cell confluency over time for CYC3 and paclitaxel as single agents and in combination.
A. CYC3 single agent B. Paclitaxel single agent C. Combination of paclitaxel 2 nM & CYC3 1000 nM and D. Combination of paclitaxel 4 nM & CYC3 1000 nM. T24 cells were seeded in 96-well plates and allowed to grow for 24 hours. They were then dosed with drugs as indicated and imaged using IncuCyte™ for 72 hours. Percentage confluency relative to the start of imaging was then calculated and plotted. Experiments performed in triplicate with mean and standard deviation plotted.

3.2.3.2 Western blotting in T24 cells with CYC3 and paclitaxel

Western blots were performed in order to investigate pharmacodynamic markers of the response to AKI. CYC3 was tested as single agent after 24 and 48 hours exposure to drug, with paclitaxel assessed at 24 hours before the effect of the combination of CYC3 1000 nM and paclitaxel 3 nM was assessed at 24 hours.

After 24 hours (Figure 3-9 A), the total AK-A signal was similar across the CYC3 and paclitaxel samples. A phospho-AK-A signal was barely detectable even in the DMSO sample, despite experimenting with different conditions and amounts of protein loaded and therefore this phosphoprotein is not shown. In many other publications using AKI, Western blots use cells pre-synchronised with nocodazole to amplify p-AK-A to detectable levels, but we preferred not to take this approach as it would be less reflective of the normal state within a tumour when cells would be at different points in the cell cycle.

AK-B phosphorylates phospho-histone H3 (pH3) at serine 10 as cells enter mitosis and pH3 has been widely used as a marker of both AK-A and AK-B inhibition. Phosphorylation rises when cells enter mitosis and therefore in the presence of a drug leading to G2/M arrest (as seen with AK-A inhibitors and paclitaxel), pH3 signal increases. In contrast, with AK-B inhibition, this phosphorylation is prevented and hence pH3 signal falls. With CYC3, there was an increase in pH3 over control at concentrations ≥2000 nM, consistent with the expected effects of an AK-A inhibitor causing G2/M arrest. Similarly paclitaxel showed higher signal than control at all concentrations, but strongly at concentrations ≥3 nM, consistent with arrest of the cells in early mitosis at the SAC. At 24 hours, there was no induction of c-PARP (apoptosis marker) with CYC3. It was only seen with concentrations of paclitaxel of 10 and 30 nM.

As longer exposures would allow more cells in an unsynchronised cell population to enter G2 and be affected by an AK-A inhibitor, CYC3 was assessed after 48 hours. At 48 hours (Figure 3-9 B), increasing levels of c-PARP were evident at concentrations from CYC3 1000 nM, suggesting induction of apoptosis. There was an increase in pH3 compared to control at concentrations ≥1000 nM, supportive of AK-A inhibition after this longer exposure to drug.

Next I assessed the combination of CYC3 1000 nM and paclitaxel 3 nM at 24 hours (Figure 3-9 C). There was induction of p-H3, indicating mitotic arrest with the combination but no significantly detectable c-PARP signal, whereas c-PARP was seen

with paclitaxel 30 nM. This is consistent with the IncuCyte™ data in Figure 3-8 C, where there was little effect of the combination at 24 hours, confirming the Western blot data that significant apoptosis occurs later.

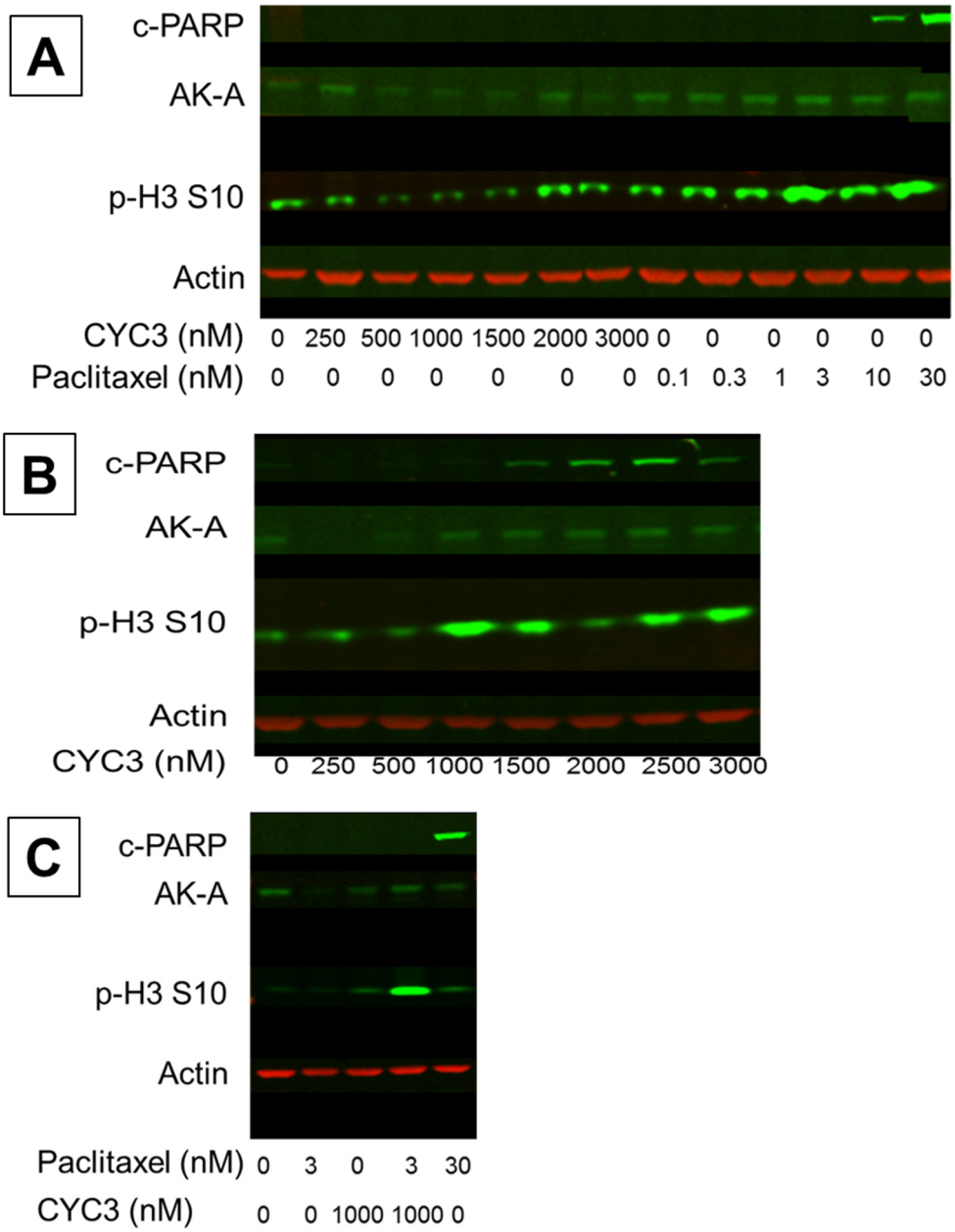

Figure 3-9: Western blots in T24 cells treated with CYC3 and paclitaxel.
Western blots showing the expression of c-PARP, AK-A, p-H3 with drugs as indicated. A. CYC3 and paclitaxel as single agents for 24 hours. B. CYC3 for 48 hours. C. single agent paclitaxel 3 nM and CYC3 1000 nM, the combination of CYC3 1000 nM and paclitaxel 3 nM and paclitaxel 30 nM for 24 hours. Actin used as loading control.

3.2.4 Scheduling of CYC3 and paclitaxel combination in T24 cells

Having observed synergy in T24 cells with the combination of CYC3 and paclitaxel, I wished to investigate the impact of different scheduling. Of particular interest was whether the initial induction of cell cycle arrest with either agent could potentiate the effect of the second agent. The combination of CYC3 1000 nM and paclitaxel 3nM was

selected as the maximum synergy was seen between paclitaxel 2 nM and 4 nM (Figure 3-6). Using the SRB assay, I assessed the effect of either agent given first for a short exposure of six hours or 24 hours, followed by washout and a media change before the second drug was added for the remaining time period to 72 hours, with the end result compared to continuous dosing of both drugs (Table 3-4). In this series of experiments, none of the sequential schedules resulted in more than 40±15% inhibition, whereas continuous concomitant dosing showed maximum inhibition of 72±4% (greater than that seen with CYC3 1000 nM and paclitaxel 2 nM of 48±2).

Treatment	Mean growth inhibition (%) with SD
PTX 3 nM for 72 hours	39±5
CYC3 1000 nM for 72 hours	23±2
PTX 3 nM and CYC3 1000 nM for 72 hours	72±4
PTX 3 nM for 6 hours, then CYC3 1000 nM	31±14
PTX 3 nM for 24 hours, then CYC3 1000 nM	40±15
CYC3 1000 nM for 6 hours, then PTX 3 nM	35±12
CYC3 1000 nM for 24 hours, then PTX 3 nM	27±9

Table 3-4: T24 growth inhibition following different scheduling of CYC3 and paclitaxel.
T24 cells were either dosed continuously or with the schedules indicated for a total time of 72 hours. The end result was then measured using the SRB assay. Growth inhibition calculated from percentage growth compared to control, with mean and standard deviation shown (n=3). Abbreviations: PTX=paclitaxel, SD=standard deviation.

Others have studied sequential versus concurrent administration of AKI with other chemotherapeutics, largely with pan-AKI (reviewed in 1.8.2). With an alternative AK-A specific AKI, MLN8237, the greatest reduction in cell viability was seen when the AKI was given first, followed by gemcitabine or paclitaxel (121) in contrast to my findings. I explored this further with MLN8237 and will discuss the differences in experimental design in 3.4.4.

3.3 Investigating the combination of CYC3 and paclitaxel in a bladder cancer cell line panel

Whilst the combination of CYC3 and paclitaxel looked interesting in T24 bladder cancer cells, it was important to assess its effect in other bladder cancer cell lines. A panel of cell lines with different genotypes (listed in Table 3-5) were selected to assess this drug combination. They were chosen to represent both a range of grades and stages of bladder cancer, with the most commonly seen mutations (259).

Cell line	Grade	Gene	AA mutation	CDS Mutation
T24	3	HRAS	p.G12V	c.35G>T
		TP53	p.Y126*	c.378C>G
J82	3	FGFR3	p.K650E	c.1948A>G
		PIK3CA	p.P124L	c.371C>T
		PTEN	p.N212fs*1	c.635_1212del578
		RB1	p.?	c.2107-2A>G
		TP53	p.K320N	c.960G>C
		TP53	p.?	c.783_919del137
UM-UC-3	3	CDKN2A	p.0?	c.1_471del471
		CDKN2a(p14)	p.0?	c.1_522del522
		KRAS	p.G12C	c.34G>T
		PTEN	p.0?	c.1_1212del1212
		TP53	p.F113C	c.338T>G
RT4	1	CDKN2A	p.0?	c.1_471del471
		CDKN2a(p14)	p.0?	c.1_522del522
		TSC1	p.L557fs*72	c.1669delC
RT112	2	CDKN2A	p.0?	c.1_471del471
		CDKN2a(p14)	p.0?	c.1_522del522
		TP53	p.R248Q	c.743G>A
		TP53	p.S183*	c.548C>G
HT1197	4	NRAS	p.Q61R	c.182A>G
		PIK3CA	p.E545K	c.1633G>A
SW780	1	CDKN2A	p.0?	c.1_471del471
		CDKN2a(p14)	p.0?	c.1_522del522

Table 3-5: Mutation status of bladder cancer cell lines tested.
Data from COSMIC database (260). *RT4 described as Grade 1 but also as transitional cell papilloma. Abbreviations: AA=amino acid, CDS=coding DNA sequence.

3.3.1 Single agent response to CYC3 in bladder cancer cell line panel

GI_{50} was not reached when any of these cell lines were treated with CYC3 (Figure 3-10). They were proliferating, with T0 subtracted from the final SRB value, so do appear to be resistant to CYC3. The percentage of growth inhibition compared to control achieved with CYC3 10 μM was less than 30% in all these cell lines, in contrast to T24 where 81±11% growth inhibition was seen (Table 3-6).

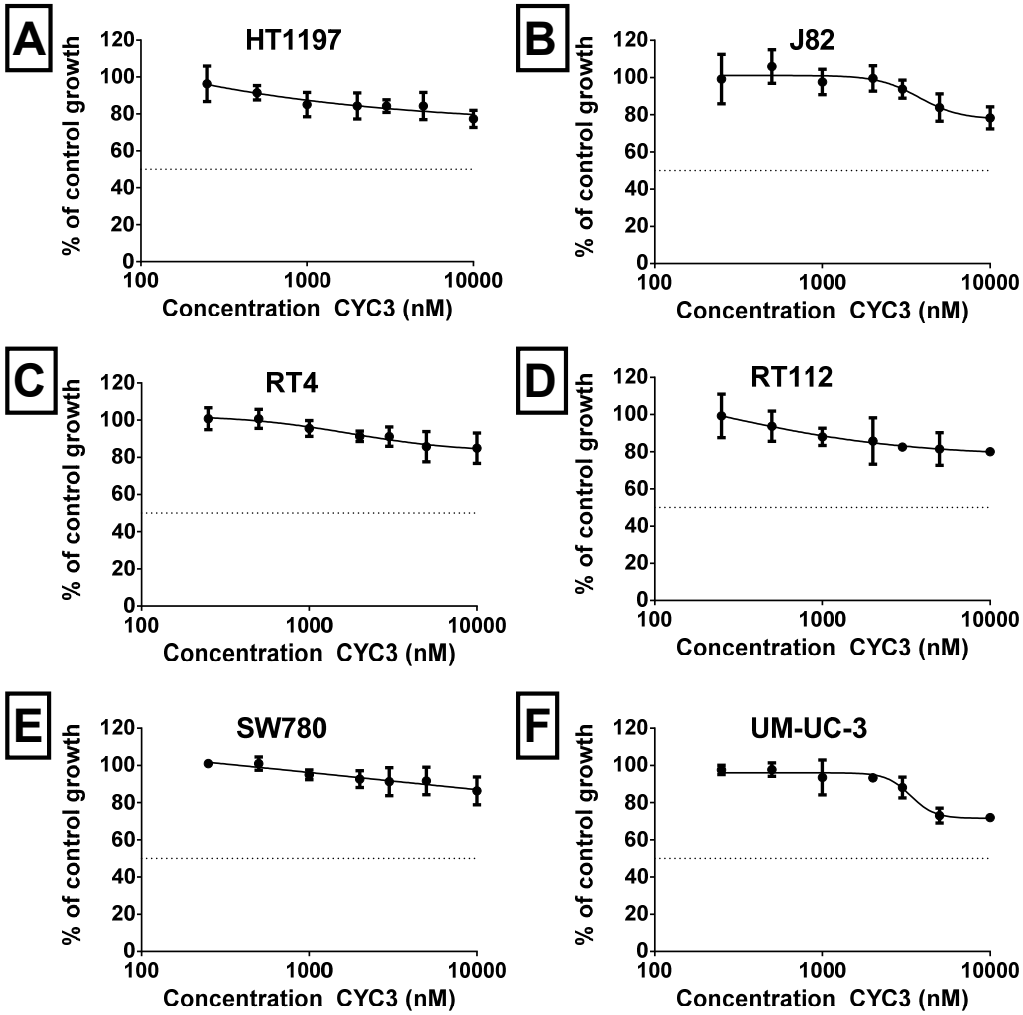

Figure 3-10: Dose response curves for bladder cancer cell line panel exposed to CYC3.
Each cell line was exposed to a range of concentrations of CYC3 for 72 hours, then analysed using SRB assay. A. HT1197 B. J82 C. RT4 D. RT112 E. SW780 F. UM-UC-3. Each graph shows the data for percentage control cell growth at each concentration of at least three replicates with SD and then a curve fitted to the data using GraphPad Prism to calculate IC_{50}. The dotted line shows 50% cell growth.

Cell line	Mean growth inhibition (%) with SD
HT1197	23±5
J82	22±6
RT4	15±8
RT112	20±1
SW780	14±8
UM-UC-3	28±1
T24	81±11

Table 3-6: Growth inhibition seen in bladder cancer cell lines exposed to CYC3 10μM.
Growth inhibition calculated from percentage growth compared to control with mean and standard deviation shown (n=3). Data from Figure 3-2 C reproduced here for comparison. Abbreviation: SD=standard deviation

3.3.2 Testing of other cytotoxic drugs in bladder cancer cell line panel

Given the limited growth inhibition with CYC3 in these cell lines, prior to testing any combinations, I assessed the sensitivity of each cell line to paclitaxel and docetaxel in addition to gemcitabine. The GI_{50} for all the cell lines for each drug together with the maximum growth inhibition seen is summarised in Table 3-7, with T24 shown for comparison.

Cell line		Paclitaxel (nM)	Docetaxel (nM)	Gemcitabine (nM)
HT1197	GI_{50}	NR	NR	NR
	Maximum GI (%)	46±8	42±5	36±7
J82	GI_{50}	234	12	12.6
	Maximum GI (%)	61±17	61±4	73±17
RT4	GI_{50}	19	4.2	7.7
	Maximum GI (%)	53±7	59±8	87±2
RT112	GI_{50}	3.7	9.8	1.2
	Maximum GI (%)	81±9	91±1	73±4
SW780	GI_{50}	47	NR	10
	Maximum GI (%)	56±7	64±9	43±7
T24	GI_{50}	3.8	3.3	5.6
	Maximum GI (%)	89±2	84±6	87±5
UM-UC-3	GI_{50}	3.4	14	1.1
	Maximum GI (%)	74±4	83±1	84±6

Table 3-7: GI_{50} and maximum growth inhibition seen for bladder cancer cell lines exposed to paclitaxel, gemcitabine and docetaxel.
Calculations made using dose response curves for each cell line exposed to range of concentrations of each drug, with GI_{50} identified from the point on curve at 50% control growth. Growth inhibition calculated from percentage growth compared to control with mean and standard deviation shown (n=3). Data for T24 cells from Figure 3-3 included for comparison. Abbreviations: GI= growth inhibition, NR=not reached.

The dose response curves for each cell line for paclitaxel and docetaxel are shown individually in Figure 3-11 and Figure 3-12. As can be seen from Table 3-7 and these figures, each cell line had a different profile of sensitivity to these drugs. For example, HT1197 was relatively resistant to all three drugs. Compared to other cell lines, J82 cells were relatively resistant to paclitaxel with a GI_{50} of 234 nM but they were sensitive to an alternative taxane, docetaxel with a GI_{50} of 12 nM. The response seen in RT4 was of particular interest given that they represent the lowest grade of bladder cancer so may be a closer guide to the effect of drugs on normal bladder cells. The GI_{50} with

gemcitabine was similar to that seen with T24 but the cells seemed more resistant to the effects of paclitaxel and docetaxel, although not as resistant as J82 cells. The RT112 cell line showed a relatively similar profile to T24 cells, although it was more sensitive to docetaxel. The SW780 cell line showed sensitivity to both taxanes but the GI_{50} was not reached with gemcitabine. UM-UC-3 cells were particularly sensitive to docetaxel and paclitaxel with a steep dose response.

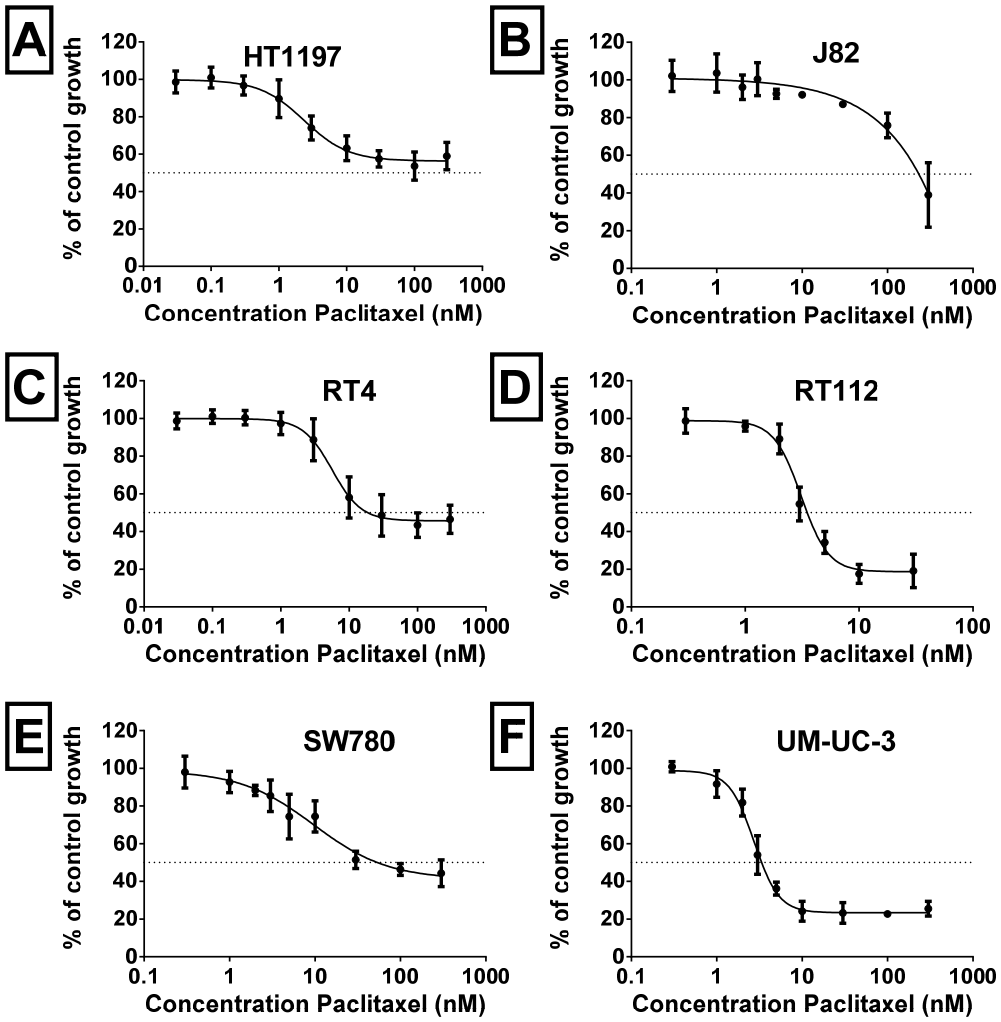

Figure 3-11: Dose response curves for bladder cancer cell line panel exposed to paclitaxel.
Each cell line was exposed to a range of concentrations of paclitaxel for 72 hours, then analysed using SRB assay. A. HT1197 B. J82 C. RT4 D. RT112 E. SW780 F. UM-UC-3. Each graph shows the data for % control cell growth at each concentration of at least three replicates with SD and then a curve fitted to the data using GraphPad Prism. The dotted line shows 50% cell growth.

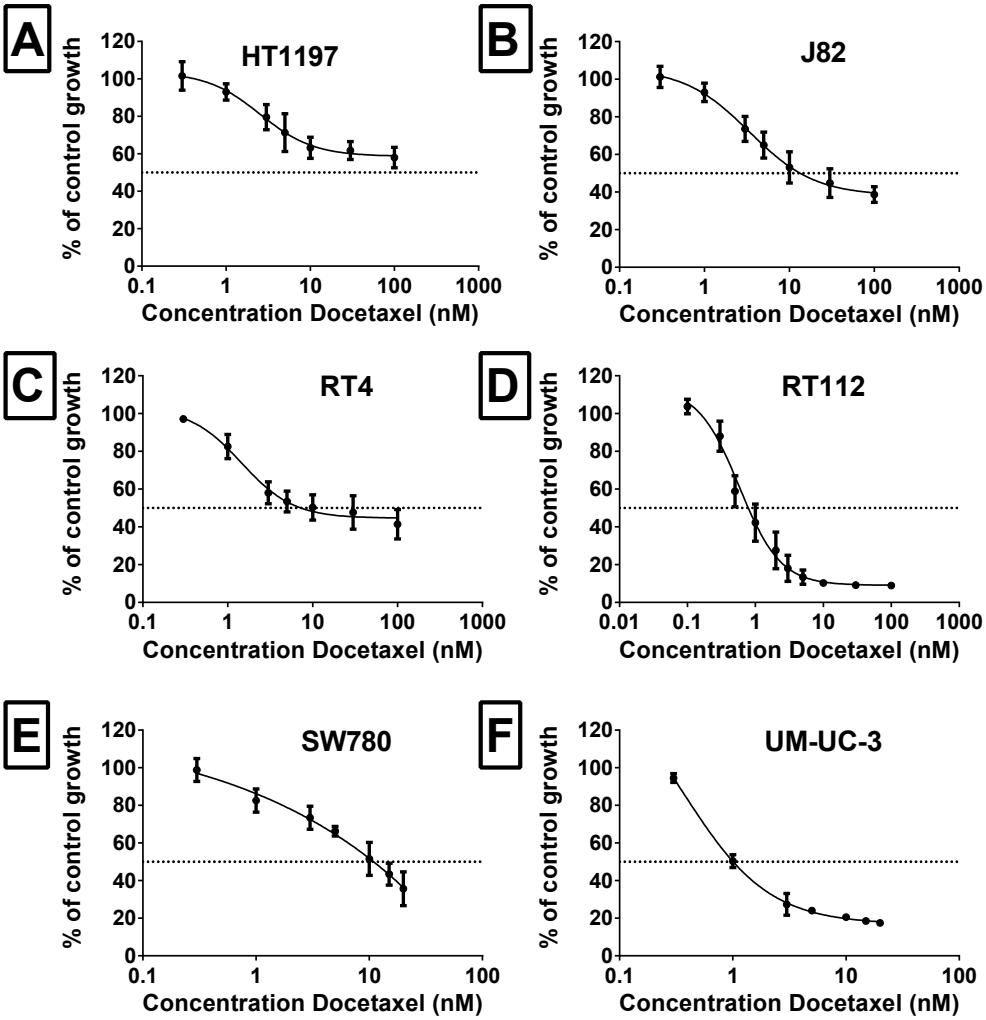

Figure 3-12: Dose response curves for bladder cancer cell line panel exposed to docetaxel.
Each cell line was exposed to a range of concentrations of docetaxel for 72 hours, then analysed using SRB assay A. HT1197 B. J82 C. RT4 D. RT112 E. SW780 F. UM-UC-3. Each graph shows the data for % control cell growth at each concentration of at least three replicates with SD and then a curve fitted to the data using GraphPad Prism. The dotted line shows 50% cell growth.

3.3.3 Combination of CYC3 and paclitaxel in bladder cancer cell line panel

Each cell line was then tested with the combination of CYC3 and paclitaxel. Concentrations of up to paclitaxel up to 300 nM were tested. The results are summarised in Table 3-8, where the Synergy Score (SS) is the point where maximum synergy seen and the maximum growth inhibition at this point is also given. As can be seen, a SS>25 was only identified in T24 (Figure 3-6) and UM-UC-3 cells (with similar maximum growth inhibition of 46±9%). The grids showed largely additive effects in the other cell lines. The detailed experimental combination grids for UM-UC-3 and for RT4 as a comparator are shown in Figure 3-13 and Figure 3-14.

Cell line	SS	GI at maximum SS point (%)	[CYC3] at this point (nM)	[Paclitaxel] at this point (nM)
HT1197	None	n/a	n/a	n/a
J82	14+/-12	36+/-12	2000	10
RT4	9+/-14	19+/-14	3000	0.3
RT112	16±9	37+/-9	10000	0.3
SW780	6±5	10±10	5000	1
T24	41±2	48±2	1000	2
UM-UC-3	33+/-9	46±9	1000	1

Table 3-8: Summary of SRB assay data for bladder cell lines with CYC3 together with paclitaxel. The highest synergy score is shown, together with the extent of growth inhibition at this point and the relevant CYC3 and paclitaxel concentrations. Growth inhibition calculated from percentage growth compared to control with mean and standard deviation shown (n=3). Abbreviations: SS=synergy score, GI=growth inhibition.

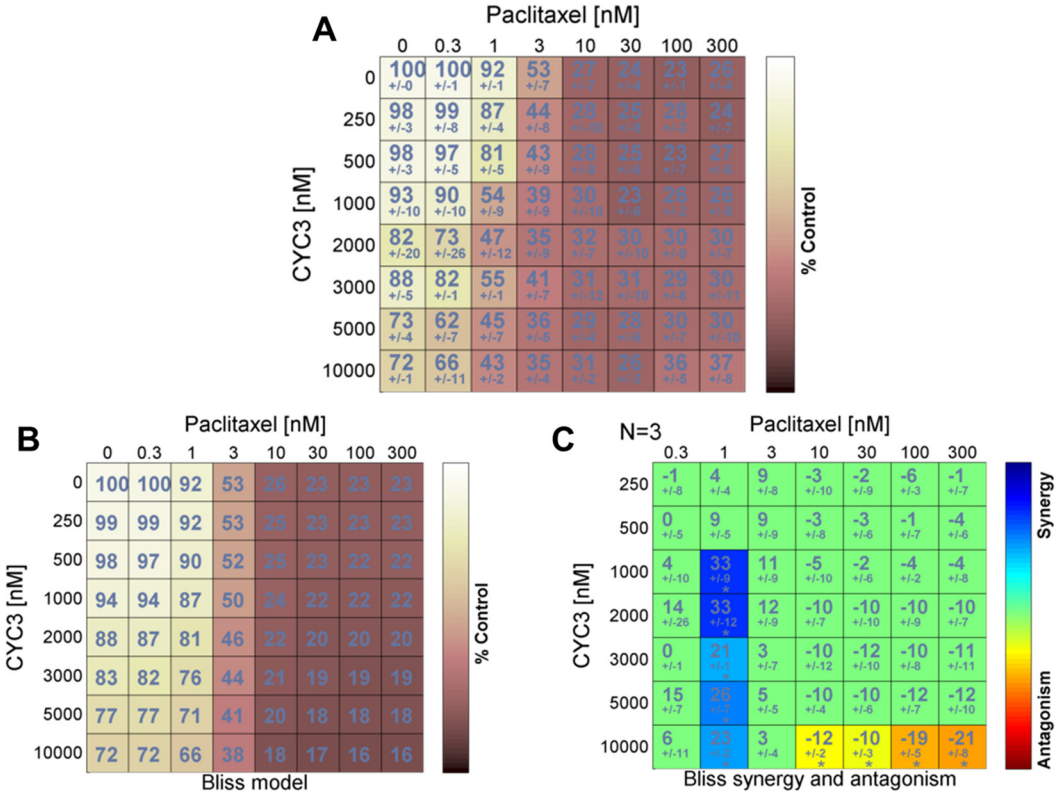

Figure 3-13: Combination of CYC3 and paclitaxel in UM-UC-3 cells.
UM-UC-3 cells were seeded in 96-well plates and treated with 8 x 8 combinations of paclitaxel and CYC3 for 72 hours.

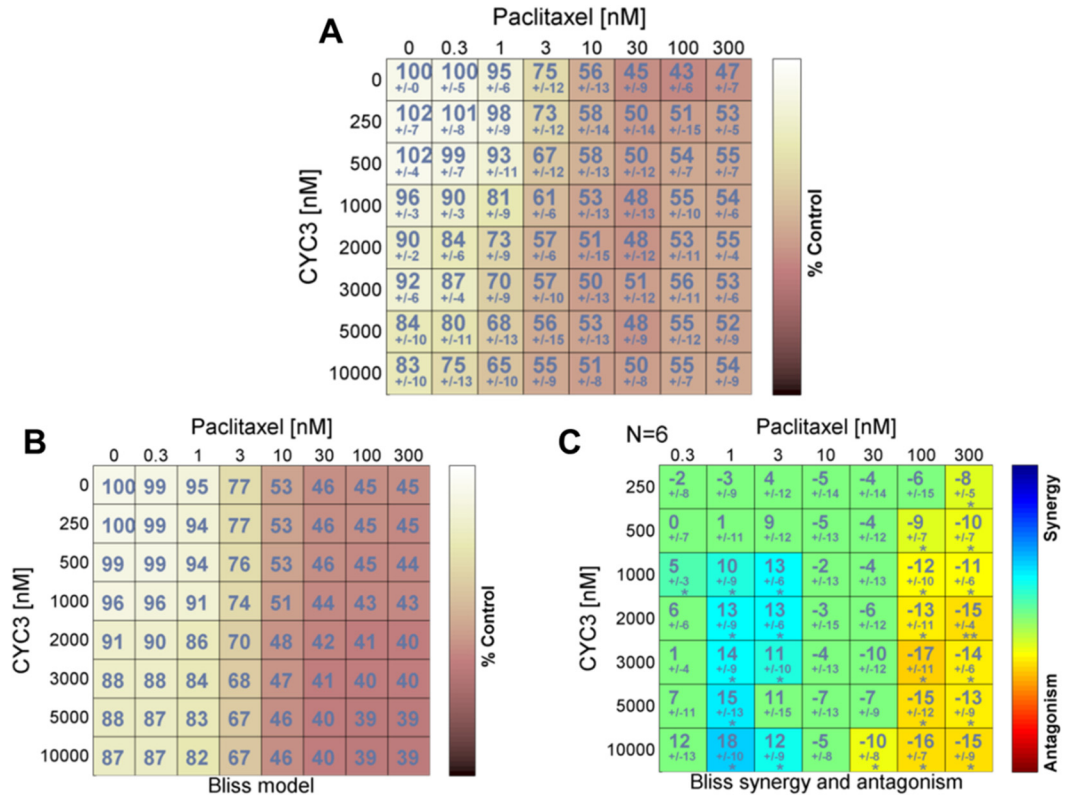

Figure 3-14: Combination of CYC3 and paclitaxel in RT4 cells.
RT4 cells were seeded in 96-well plates and treated with 8 x 8 combinations of paclitaxel and CYC3 for 72 hours.

3.3.4 Summary of CYC3 experimental data in bladder cancer cell lines

These investigations indicated that an AK-A specific inhibitor would be preferable to a pan-AKI, and confirmed that an AK-A inhibitor combined with paclitaxel could show synergy in bladder cancer cell lines, although only in T24 and UM-UC-3. This is consistent with multiple reports in the literature of enhanced cytotoxicity when concentrations of paclitaxel ≤ 10 nM were combined with either siRNA knockdown of AK-A or with AK-A specific inhibitors in a range of cancer cell lines (217, 230, 231, 234, 236). At the time of my findings, there were no reports of the assessment of the combination in bladder cancer. However, there was increasing evidence of the effectiveness of an alternative AK-A inhibitor which was already being tested in clinical trials – MLN8237 (alisertib). Although CYC3 was a pre-clinical candidate, since the aim of my research was to identify a promising combination to take forward into clinical trials, I therefore decided to assess MLN8237 in future experiments.

3.4 Assessment of MLN8237 in bladder cancer cell lines

MLN8237 (alisertib) was developed as an AK-A specific inhibitor. In enzymatic assays the IC_{50} against recombinant AK-A and AK-B was 1.2 nM vs 400 nM, with this

selectivity confirmed in HeLa cell based assays where the IC_{50} for AK-A was 6.7 nM vs 1500 nM for AK-B (205). Its structure is shown in Figure 3-15.

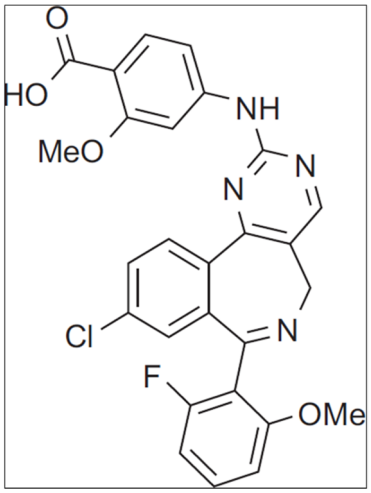

Figure 3-15: Chemical structure of MLN8237

I initially assessed it as a single agent and then in combination in T24 bladder cancer cells, before expanding its assessment in the same bladder cancer cell line panel previously used with CYC3. A subsequent publication from a competitor laboratory explored MLN8237 in T24, UM-UC-3 and RT4 cells (121) and comparisons are made to their data.

3.4.1 Effect of MLN8237 in T24 cells

A consistent biphasic dose-response effect was seen with MLN8237 (Figure 3-16 A). This led to problems with curve fitting so the data was re-plotted without the higher concentrations (above 300 nM), giving an IC_{50} of 20 nM and a GI_{50} of 30 nM (Figure 3-16 B). These are similar to the data subsequently reported in T24 cells using the MTS assay and 96 hours exposure with an IC_{50} of 31 nM (121). The biphasic effect may be a reflection of the SRB assay giving a measure of total protein content – at higher concentrations, MLN8237 can act as an AK-B inhibitor which would lead to polyploidy and larger cells with more protein per cell.

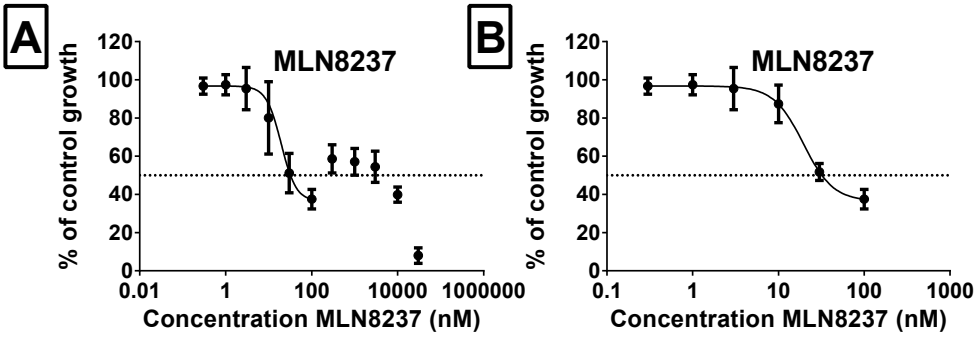

Figure 3-16: Dose response curves for T24 cells exposed to MLN8237
T24 cells were exposed to a range of concentrations of MLN8237 for 72 hours, then analysed using SRB assay with A. Concentrations up to 30 µM. B. Concentrations up to 100 nM. Each graph shows the data for percentage control cell growth at each concentration of three replicates with SD and then a curve fitted to the data using GraphPad Prism to calculate IC_{50}. The dotted line shows 50% cell growth and this was used to identify the GI_{50} from the graph.

Next MLN237 was combined with paclitaxel to compare the response with that seen with CYC3. The data were encouraging, with a region of strong statistically significant synergy seen between concentrations of paclitaxel 1-3 nM and MLN8237 30-100 nM, (Figure 3-17). Maximal synergy of 35±1 was seen with the combination of paclitaxel 2 nM and MLN8237 50 nM, with percentage growth compared to control of only 19±1%, similar to that seen with paclitaxel 30 nM (11±2%). Antagonism was seen with concentrations of paclitaxel ≥ 5 nM and MLN8237 ≥ 100 nM.

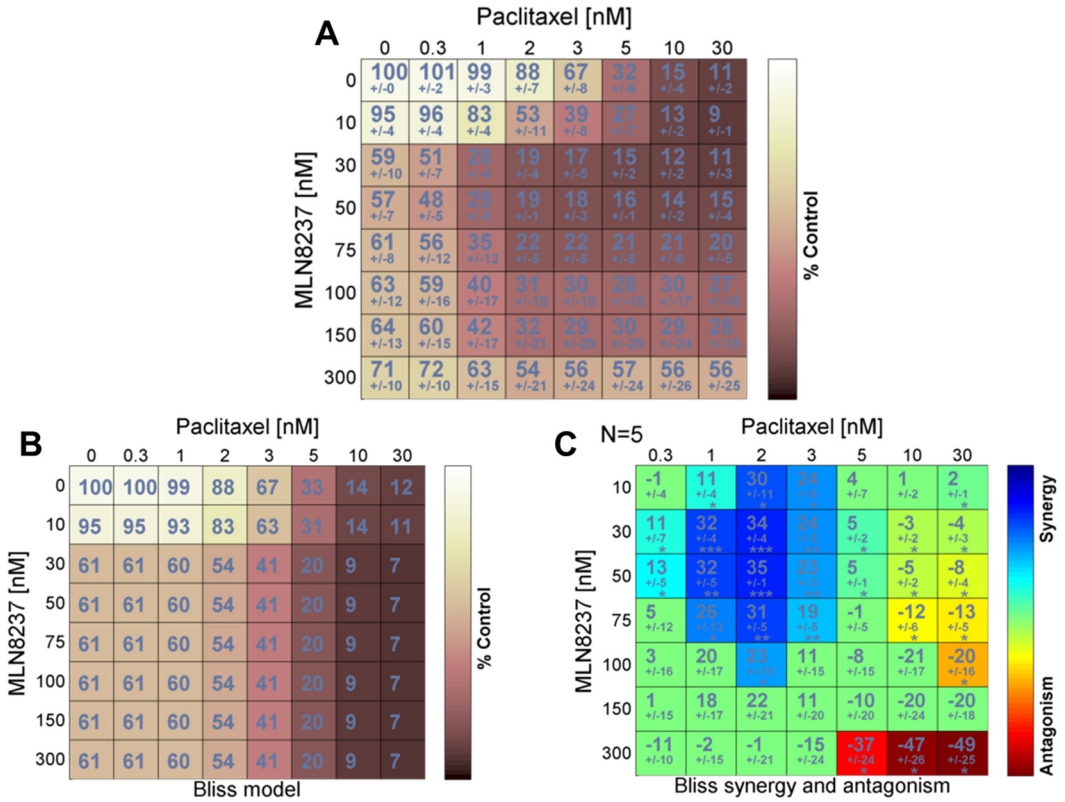

Figure 3-17: Combination of MLN8237 and paclitaxel in T24 cells.
T24 cells were seeded in 96-well plates and treated with combinations of paclitaxel and MLN8237 for 72 hours.

3.4.2 Effect of MLN8237 in bladder cancer cell line panel

With MLN8237 as a single agent, GI_{50} was only reached in RT112 cells at 105 nM (Figure 3-18 D), which contrasts with a reported IC_{50} in UM-UC-3 cells of 45 nM and of RT4 cells of 120 nM (121). These published experiments were done after 96 hours rather than 72 hours but the main difference was that they used the MTS assay. This provides a quantification of viable cells' metabolic activity versus the SRB assay which provides a measure of cellular protein content.

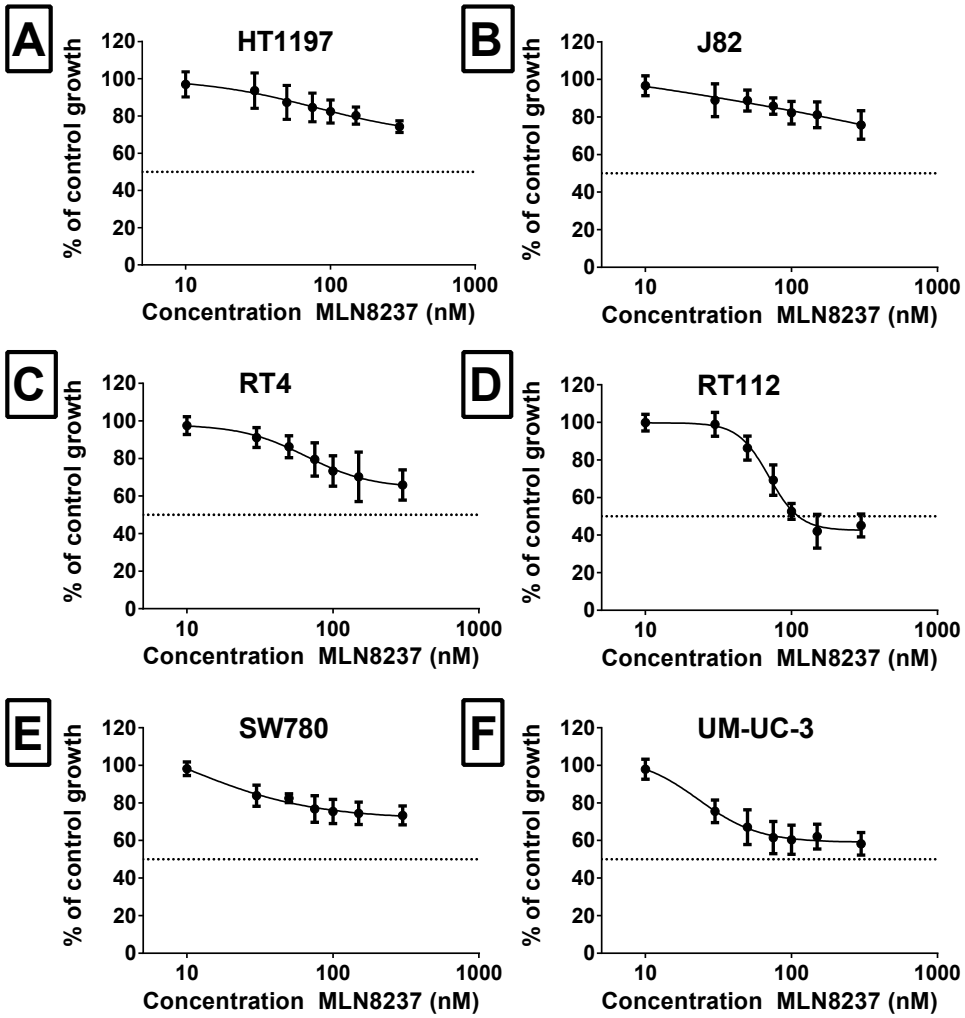

Figure 3-18: Dose response curves for bladder cancer cell line panel exposed to MLN8237.
Each cell line was exposed to a range of concentrations of MLN8237 for 72 hours, then analysed using SRB assay. A. HT1197 B. J82 C. RT4 D. RT112 E. SW780 F. UM-UC-3. Each graph shows the data for % control cell growth at each concentration of at least 3 replicates with SD and then a curve fitted to the data using GraphPad Prism. The dotted line shows 50% cell growth and this was used to identify the GI_{50} from the graph.

The maximum growth inhibition achieved with MLN8237 300 nM is shown in Table 3-9, with the greatest seen in RT112 cells (55±6%) and UM-UC-3 cells (42±6%).

Cell line	Maximum growth inhibition (%) with SD
HT1197	26±3
J82	24±8
RT4	34±8
RT112	55±6
SW780	27±5
UM-UC-3	42±6

Table 3-9: Maximum growth inhibition seen in bladder cancer cell lines exposed to MLN8237 300 nM.

Each cell line was then tested with the combination of MLN8237 and paclitaxel. As Table 3-10 demonstrates, no significant synergy was seen in HT1197, SW780 or RT4 cells. Although two combinations in J82 cells showed synergy, there was no consistent region and it was only seen with MLN8237 300 nM. However, in RT112 (Figure 3-19) and UM-UC-3 (Figure 3-20) cells, a region of synergy was seen between paclitaxel 1-3 nM and MLN8237 30-100 nM similar to T24 (Figure 3-17). Antagonism was also seen with higher concentrations of MLN8237 (≥150 nM) and paclitaxel (≥5 nM).

Cell line	SS	GI at max SS point (%)	[MLN8237] at this point (nM)	[Paclitaxel] at this point (nM)
T24	35±1	81±1	50	2
UM-UC-3	31±12	59±12	30	2
RT112	28±7	67±7	75	2
J82	31±5	53±5	300	1
RT4	9.1±14	17±14	50	2
HT1197	9.4±12	12±12	75	1
SW780	3.3±4	19±4	30	1

Table 3-10: Summary of SRB assay data for bladder cell lines with the combination of MLN8237 and paclitaxel.
The highest synergy score is shown, together with the extent of growth inhibition at this point and the relevant MLN8237 and paclitaxel concentrations. Growth inhibition calculated from percentage growth compared to control with mean and standard deviation shown (n=3). Abbreviations: SS=synergy score, GI=growth inhibition.

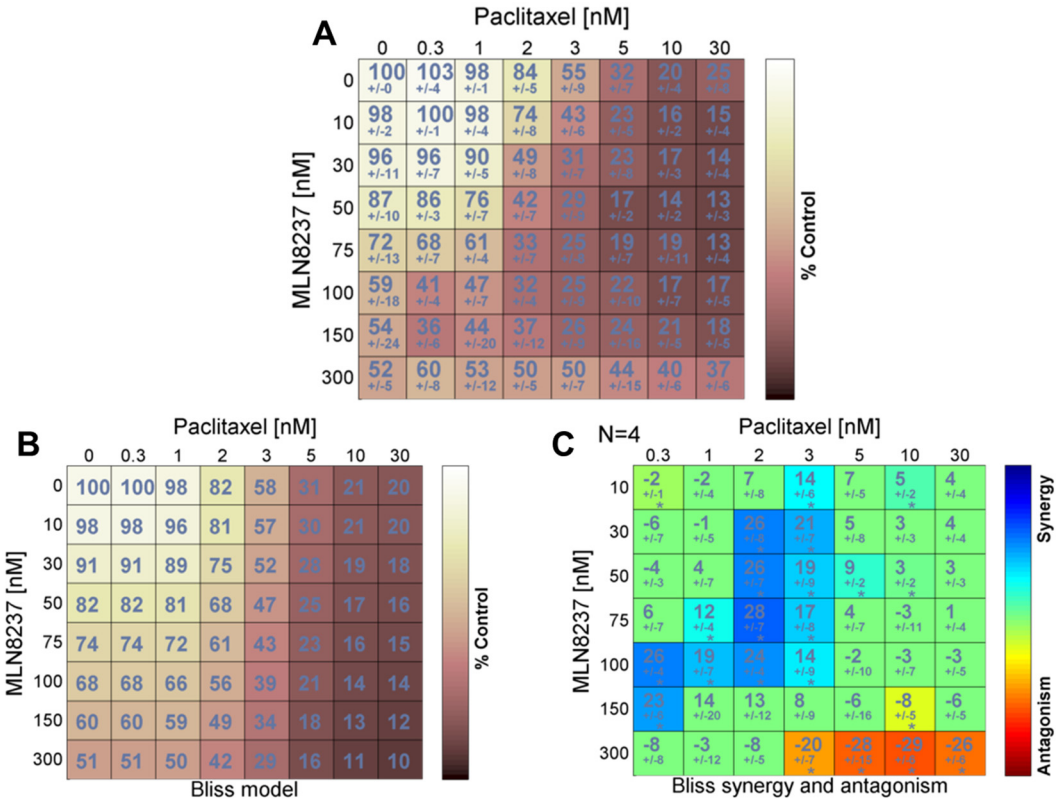

Figure 3-19: Combination of MLN8237 and paclitaxel in RT112 cells.
RT112 cells were seeded in 96-well plates and treated with 8 x 8 combinations of paclitaxel and MLN8237 for 72 hours.

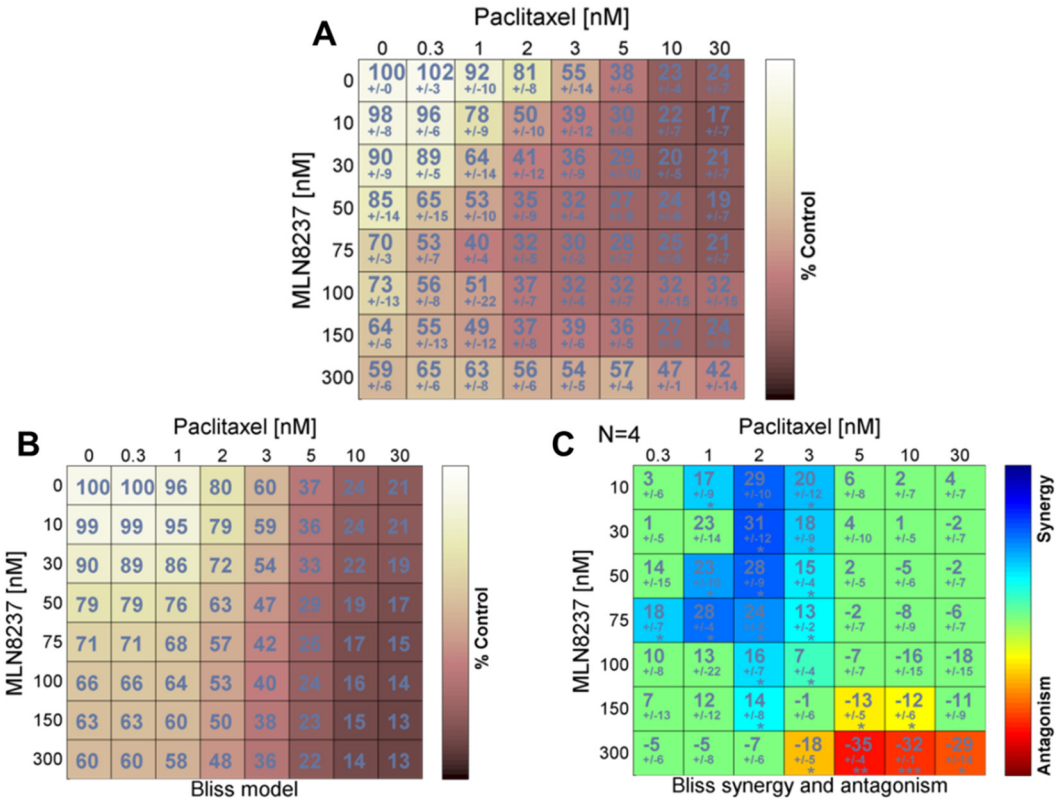

Figure 3-20: Combination of MLN8237 and paclitaxel in UM-UC-3 cells.
UM-UC-3 cells were seeded in 96-well plates and treated with 8 x 8 combinations of paclitaxel and MLN8237 for 72 hours.

Having seen a significant region of synergy in T24, RT112 and UM-UC-3 cells, I next explored this further with other experimental techniques, with the focus on the combination of MLN8237 50 nM with paclitaxel 2 nM where growth compared to control was 19±1% in T24 cells, 42±7% in RT112 cells and 35±8% in UM-UC-3 cells.

3.4.3 Validation of synergy seen with MLN8237 and paclitaxel in bladder cancer cell lines

3.4.3.1 Flow cytometry with combination of MLN8237 and paclitaxel

3.4.3.1.1 *T24 cells*

The characteristic reported features of treatment with both paclitaxel and an AK-A specific inhibitor are an increase in G2/M population due to cell cycle arrest. With MLN8237 as a single agent, there was an increase in G2/M population at both 12 and 24 hours at concentrations of MLN8237 ≥30 nM at both 12 and 24 hours, consistent with its reported role as an AK-A inhibitor (Figure 3-21). Zhou *et al.* observed cell cycle arrest at increasing concentrations of MLN8237 but also commented on aneuploidy (DNA content >4N) at 48 hours (54% with MLN837 1 μM), which I did not observe (121). This may be due to the longer exposure of cells to MLN8237 in their experiment, or a difference in gating strategies. My methods (2.2.4) mean that both debris and doublets were gated out and hence a significant sub G1 population is not shown, which others have reported as a surrogate for cell death (2).

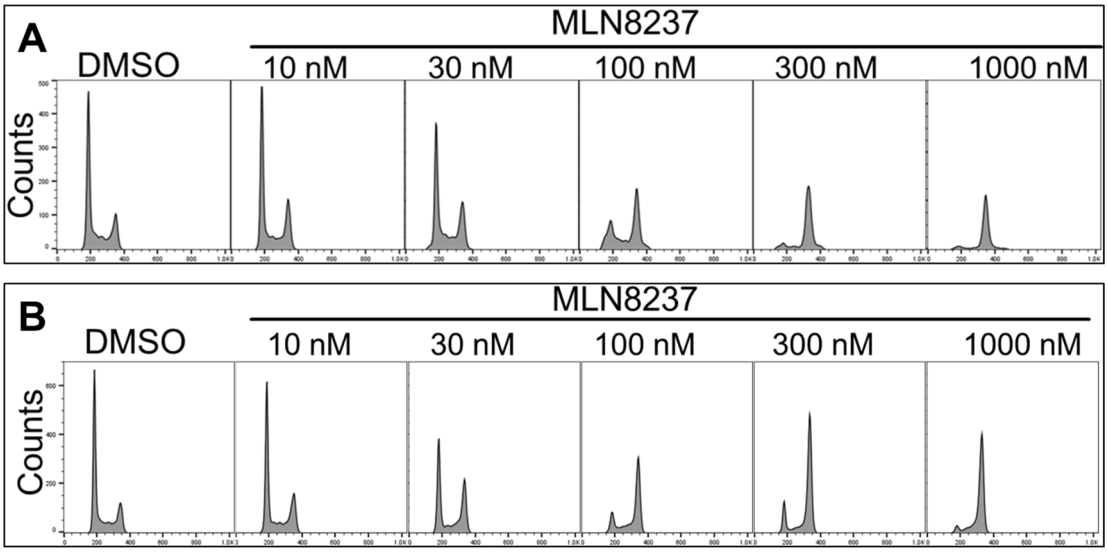

Figure 3-21: Flow cytometry analysis of the cell cycle profiles of T24 cells after treatment with MLN8237.
Cells treated with MLN8237 at concentrations indicated for either A. 12 hours or B. 24 hours. Cell count is shown on the y axis plotted as a histogram to FL2-H (propidium iodide) on the x axis.

When paclitaxel was assessed as a single agent, a shift in the cell cycle profile was seen after just six hours exposure to the drug (Figure 3-22). The G2/M population increased from 13% in the control cell population to 18% with paclitaxel 3 nM, 33% with paclitaxel 10 nM and 46% with paclitaxel 30 nM.

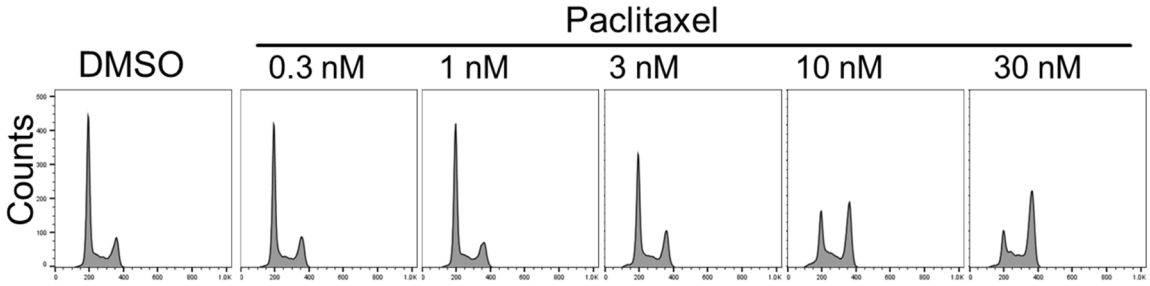

Figure 3-22: Flow cytometry analysis of the cell cycle profiles of T24 cells after treatment with paclitaxel for six hours.
Cells treated with paclitaxel at concentrations indicated for six hours. Cell count is shown on the y axis plotted as a histogram to FL2-H (propidium iodide) on the x axis.

A range of combinations of paclitaxel 1-3 nM and MLN8237 30-100 nM were then examined (Figure 3-23). For the single agent paclitaxel, the cell cycle profile remains very similar to control at concentrations 1-3 nM but the percentage of cells in G2/M with paclitaxel 30 nM increased from 46% at six hours (Figure 3-22) to 84% at 24 hours. The data for single agent MLN8237 was similar to that seen in Figure 3-21, with the G2/M population increasing at concentrations ≥30 nM. Whilst I might have expected the combination of MLN8237 and paclitaxel to lead to an increase in G2/M population, with all of these combinations few cells survived and therefore the model was unable to calculate a percentage of cells in G2/M.

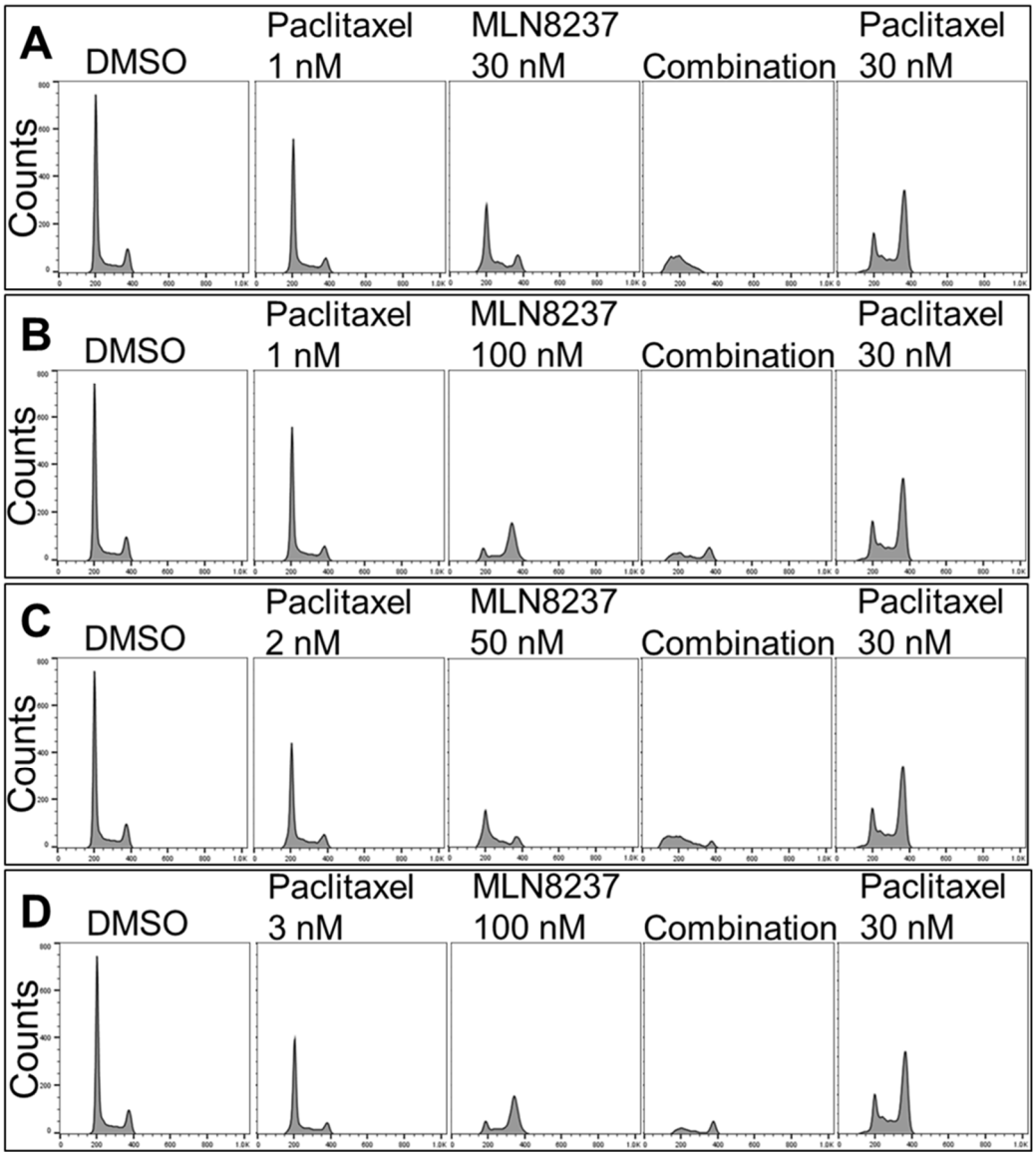

Figure 3-23: Flow cytometry analysis of the cell cycle profiles of T24 cells exposed to a range of paclitaxel and MLN8237 concentrations as single agent and in combination for 24 hours.
Cells exposed to paclitaxel and MLN8237 as indicated. Cell count is shown on the y axis plotted as a histogram to FL2-H (propidium iodide) on the x axis.

3.4.3.1.2 *UM-UC-3 and RT112 cells*

The results for the combination of MLN8237 50 nM and paclitaxel 2 nM in T24 cells were compared in UM-UC-3 and RT112 cells (Figure 3-24). In both cell lines, the cell cycle profile was similar to control with paclitaxel 2 nM. With MLN8237, the G2/M population increased from 13% in DMSO to 39% in the UM-UC-3 cells (Figure 3-24 A), whereas in the RT112 cells the G2/M population did not increase to the same extent (Figure 3-24 B). With the combination, very few cells survived in either cell line.

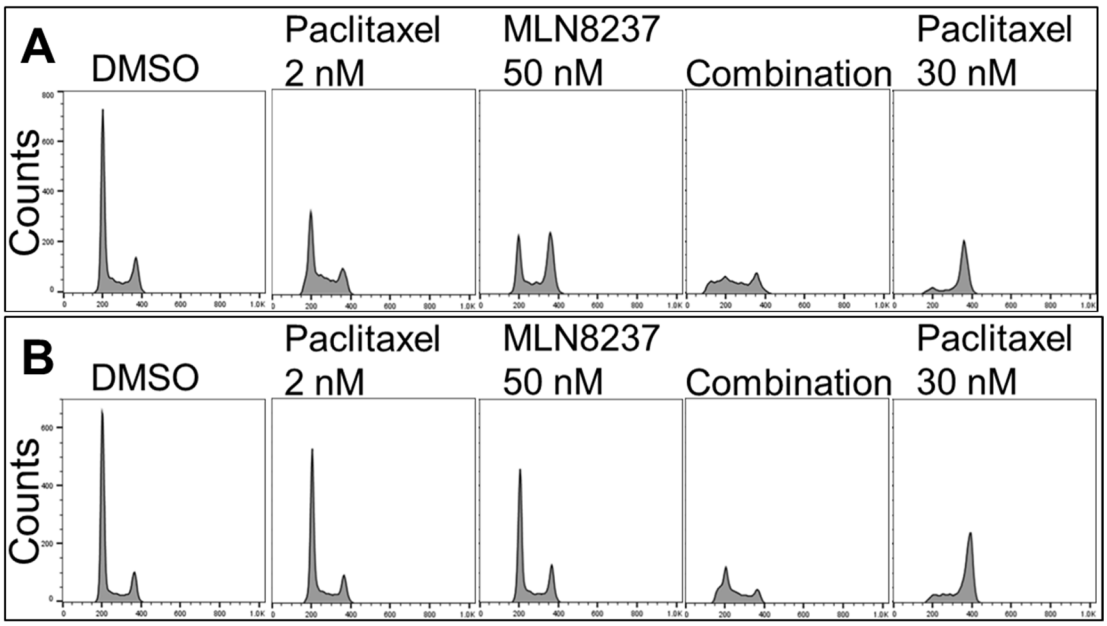

Figure 3-24: Flow cytometry analysis of the cell cycle profiles of UM-UC-3 and RT112 exposed to paclitaxel and MLN8237 as single agents and in combination.
Cell cycle profiles of A. UM-UC-3 and B. RT112 cells exposed to either paclitaxel 2 nM, MLN8237, paclitaxel 30 nM or the combination of MLN8237 50 nM and paclitaxel 2 nM for 24 hours. Cell count is shown on the y axis plotted as a histogram to FL2-H (propidium iodide) on the x axis.

Therefore in all three cell lines where synergy was seen using the SRB assay, the combination of paclitaxel 2 nM and MLN8237 50 nM is associated with a loss of normal cell cycle profile.

3.4.3.2 IncuCyte™ live cell imaging with combination MLN8237 and paclitaxel

To further validate the synergy seen with MLN8237 and paclitaxel in the SRB assay, time lapse microscopy was used to evaluate the effect of the single agents and combination over time in the cell lines where synergy had been seen – T24, RT112 and UM-UC-3. Figure 3-25 shows the changes in relative cell confluency compared to T=0 over the 72 hours of the experiment. The final cell confluencies are summarised in Table 3-11.

For the T24 cells (Figure 3-25 A), growth with the combination was suppressed from the start of imaging, suggesting an early and sustained response in the presence of the combination. Similar to the result seen in the SRB assay (Figure 3-17) where the combination achieved comparable growth inhibition (81±1%) to paclitaxel 30 nM (89±2%), the actual cell confluency at endpoint with paclitaxel 30 nM was similar to the combination (Table 3-11).

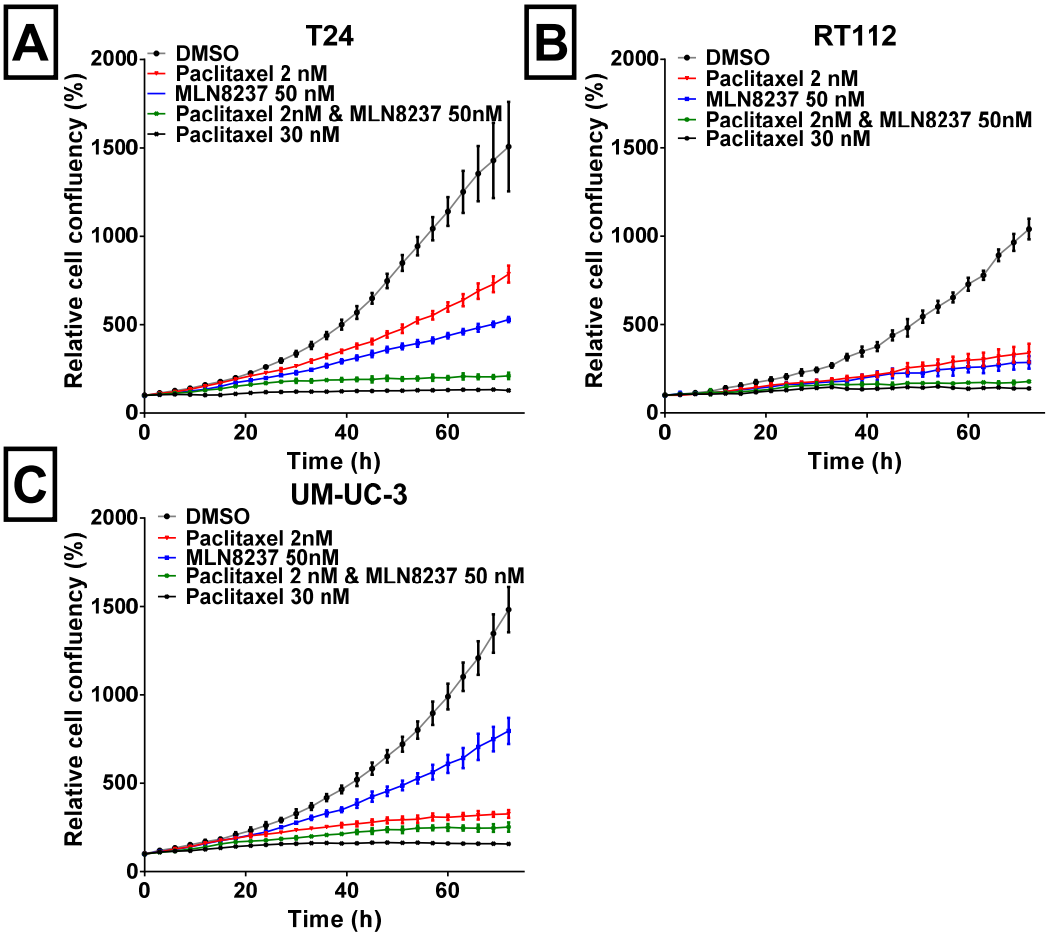

Figure 3-25: Relative cell confluency over time for T24, RT112 and UM-UC-3 exposed to paclitaxel and MLN8237.
Cells were seeded in 96-well plates and allowed to grow for 24 hours. They were then dosed with drugs as indicated and imaged using IncuCyte™ for 72 hours. Percentage confluency relative to the start of imaging was calculated and plotted. These data are the mean of six replicates with SD for T24 and five replicates with SD for RT112 and UM-UC-3.

Drug	T24	RT112	UM-UC-3
Paclitaxel 2 nM	63±15 %	28±4%	15±1%
MLN8237 50 nM	45 ± 4 %	25±2%	51±3%
Combination	15±1 %	10±2 %	11±1%
Paclitaxel 30 nM	9±1%	6±2%	8 ±1%.

Table 3-11: Final cell confluency relative to DMSO at 72 hours for T24, RT112 and UM-UC-3 cells. T24, RT112 and UM-UC-3 cells treated with paclitaxel 2 nM, MLN8237 50 nM, the combination of MLN8237 50 nM and paclitaxel 2 nM or paclitaxel 30 nM.

With the RT112 cells (Figure 3-25 B), the growth inhibitory effect of both paclitaxel and MLN8237 as single agents (<30% of control growth) was greater than might have been anticipated by the SRB assay, where little growth inhibition had been seen (16±5% with paclitaxel 2 nM and 13±10% with MLN8237 (Figure 3-19). With the combination, cell growth was almost completely suppressed from the start of imaging similar to paclitaxel 30 nM, again greater than predicted from the SRB assay where 42±7% growth had been seen.

In the UM-UC-3 cells, the combination final cell confluency was also similar to that achieved with paclitaxel 30 nM and greater than that predicted from the SRB assays where 35±8% growth was shown (Figure 3-25 C). Notably the effect of paclitaxel 2 nM was greater than anticipated from the SRB assays (where only 19±8% growth inhibition was seen, Figure 3-20)). The dose response curve of UM-UC-3 with paclitaxel is steep between paclitaxel 1 to 3 nM (a separate experiment showed final confluency of 64±10% with paclitaxel 1 nM at 69 hours compared to 18±3% with paclitaxel 2 nM), so this may be the reason for the difference seen, particularly as different stock batches of paclitaxel were used.

Taken together these IncuCyte™ experiments confirm the SRB data that MLN8237 in combination with low concentrations of paclitaxel is at least as effective as paclitaxel 30 nM in these three cell lines.

3.4.3.3 Western blotting with combination MLN8237 and paclitaxel

Next Western blotting was used to assess the effect of MLN8237 and paclitaxel as single agents and in combination, analysing total AK-A, phospho-AK-A, c-PARP and pH3.

3.4.3.3.1 *T24 cells*

The total AK-A signal was similar across the samples, other than an increase in the paclitaxel 30 nM (seven times that of DMSO), potentially consistent with G2/M arrest (Figure 3-26). As in previous experiments, a phospho-AK-A signal was barely detectable even in the DMSO sample despite experimenting with different conditions and amounts of protein loaded and therefore this phosphoprotein is not shown. Although there was a small increase in cPARP with single agent MLN8237, it was induced strongly with the combinations, particularly paclitaxel 2 nM and MLN8237 50 nM, together with paclitaxel 30 nM. Consistent with mitotic arrest (and AK-A inhibition), pH3 signal was increased compared to DMSO with MLN8237 30 nM and 50 nM, and with the combinations of paclitaxel 1 or 2 nM with MLN8237 30 or 50 nM. It was strongly induced with paclitaxel 30 nM, consistent with the mitotic arrest observed with flow cytometry (Figure 3-23). However, pH3 signal fell to 20% of the DMSO sample with MLN8237 100 nM and with the combination of paclitaxel 1 nM and MLN8237 100 nM suggesting that in the T24 cell line, AK-B may start to be inhibited by MLN8237 at 100 nM concentration, although this contrasts with the other report where p-H3 signal was constant at concentrations up to 1 μM (121).

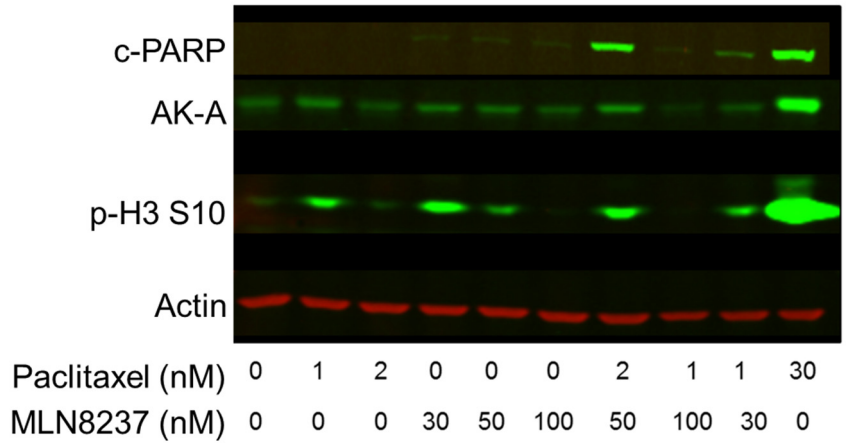

Figure 3-26: Western blots of T24 cell pellets following exposure to drugs as indicated for 24 hours. Actin was used as a loading control.

3.4.3.3.2 *UM-UC-3 cells*

In UM-UC-3 cells (Figure 3-27) the levels of total, phospho-AK-A and c-PARP were all higher in the paclitaxel 30 nM sample at 24 hours. There was no cPARP induction with the combination, potentially because induction of apoptosis is occuring later. pH3 appeared to be strongly induced in the MLN8237 50 nM sample (over 1000 times stronger than DMSO) and stronger than in the combination and paclitaxel 30 nM samples. This is consistent with the mitotic accumulation seen in Figure 3-24A but contrasts with a report that pH3 levels remained constant in UM-UC-3 cells (121).

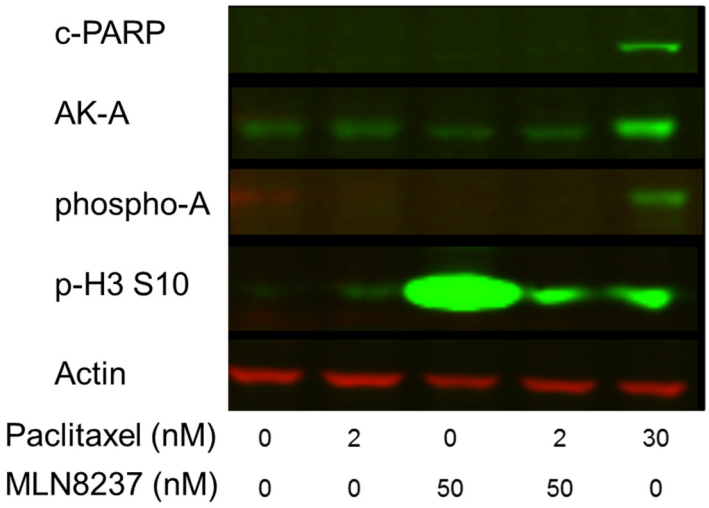

Figure 3-27: Western blots of UM-UC-3 cell pellets following exposure to drugs as indicated for 24 hours.
Actin was used as a loading control.

3.4.3.3.3 *RT112 cells*

In RT112 cells (Figure 3-28) the level of both total AK-A and phospho-AK-A only increased with paclitaxel 30 nM. Whilst there was a small increase in c-PARP signal with single agent paclitaxel 2 nM and MLN8237 50 nM, in the combination this was

thirty times greater, indicating significant induction of apoptosis, and close to that of paclitaxel 30 nM. The lack of induction of pH3 signal with the single agents was consistent with lack of mitotic accumulation in flow cytometry (Figure 3-24 B) but signal was increased with the combination, suggestive of G2/M arrest, even though this was difficult to identify by flow cytometry due to the low numbers of surviving cells. As expected, pH3 was significantly induced with paclitaxel 30 nM.

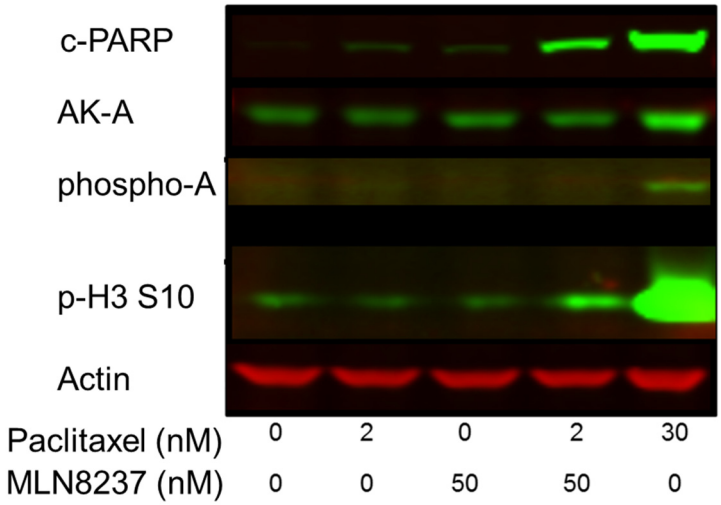

Figure 3-28: Western blots of RT112 cell pellets following exposure to drugs as indicated for 24 hours.
Actin was used as a loading control.

3.4.3.3.4 *Summary of Western blot data*

In T24 cells, the increase in pH3 was consistent with AK-A inhibition with MLN8237 50 nM. With the combination of MLN8237 50 nM and paclitaxel 2 nM, cPARP was induced consistent with apoptosis with the combination (similar to that seen with paclitaxel 30 nM). Whilst cPARP signal was not significantly enhanced with the combination in UM-UC-3 cells, the increase in pH3 cells suggests mitotic accumulation and a later timepoint may have shown apoptosis. The cPARP signal seen in RT112 cells was much greater with the combination that the single agents.

3.4.4 Scheduling of MLN8237 and paclitaxel combination in T24 cells

With CYC3 and paclitaxel, maximum synergy was seen with concurrent dosing (3.2.4). To explore this with MLN8237 and paclitaxel in T24 cells, rather than selecting just the combination of most interest as before, I chose to look at the whole concentration-combination grid as this would also allow me to see shifts in dose response. Flow cytometry data had shown that changes to the cell cycle profile could be seen after only six hours exposure to paclitaxel (Figure 3-22). As before, cells were first treated with

either agent for six or 24 hours, followed by washout and a media change before the second drug was added for the remaining time period to 72 hours (ie either 66 hours (for initial six hour treatment) or 48 hours (for initial 24 hour treatment). The end result was measured using SRB assay and compared to continuous dosing of both drugs (Figure 3-17).

For the combinations where paclitaxel was dosed first for six hours, a shift in the single agent dose response curve for paclitaxel was seen, with 64±15% growth with paclitaxel 30 nM compared to 11±2% after 72 hours continuous exposure (Figure 3-29). However, a significant area of synergy was still observed when MLN8237 was combined with higher concentrations of paclitaxel.

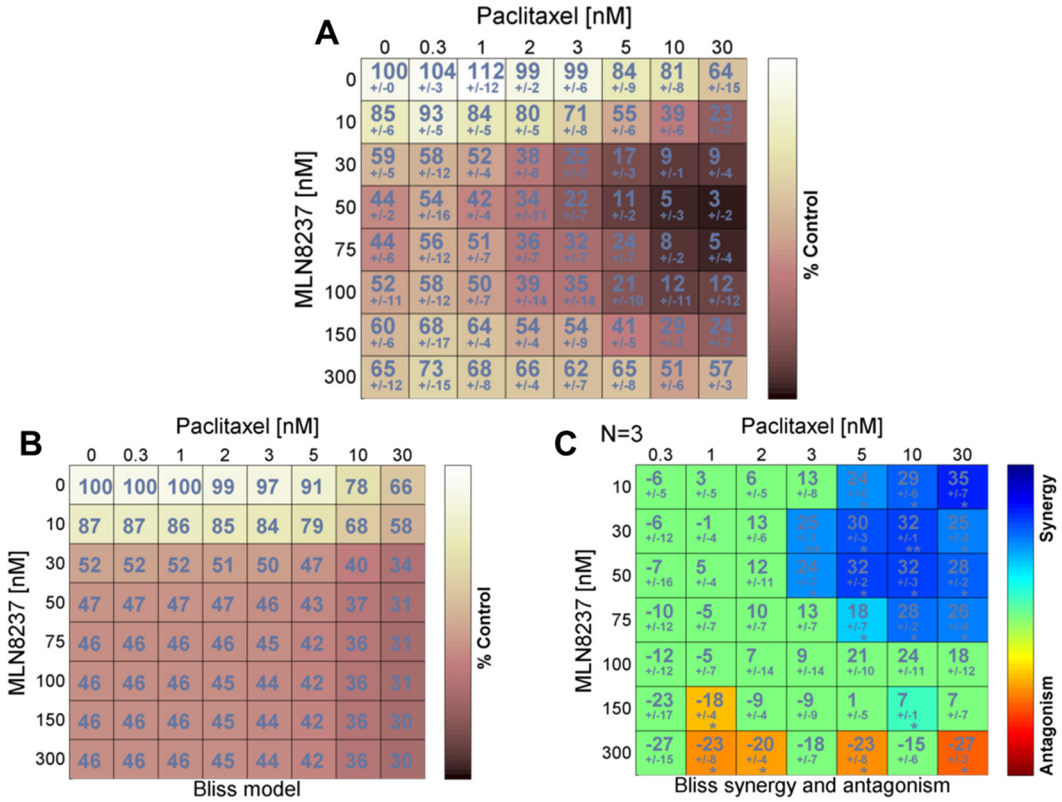

Figure 3-29: Combination of MLN8237 and paclitaxel in T24 cells with cells initially exposed to paclitaxel for six hours, followed by MLN8237 for remaining 66 hours.
T24 cells were seeded in 96-well plates and treated with combinations of paclitaxel for six hours followed by MLN8237 for the remaining time period to 72 hours.

When paclitaxel was dosed first for 24 hours (Figure 3-30), only 2±3% growth was seen for paclitaxel 30 nM, indicating nearly 100% growth inhibition. A similar region of synergy was seen with only 24 hours exposure to paclitaxel, followed by 48 hours MLN8237 compared to 72 hours continuous exposure to the combination (Figure 3-30). The schedule of 2 nM paclitaxel for 24 hours followed by MLN8237 50 nM for 48 hours reached a synergy score of 37±10 (very similar to the score of 33±1 seen with combined continuous 72 hour exposure to the combination in Figure 3-17), but 40±10%

cell growth was seen at this point compared to 19±1% seen with the continuous 72 hour exposure to both drugs (i.e 60±10% growth inhibition compared to 81±1%).

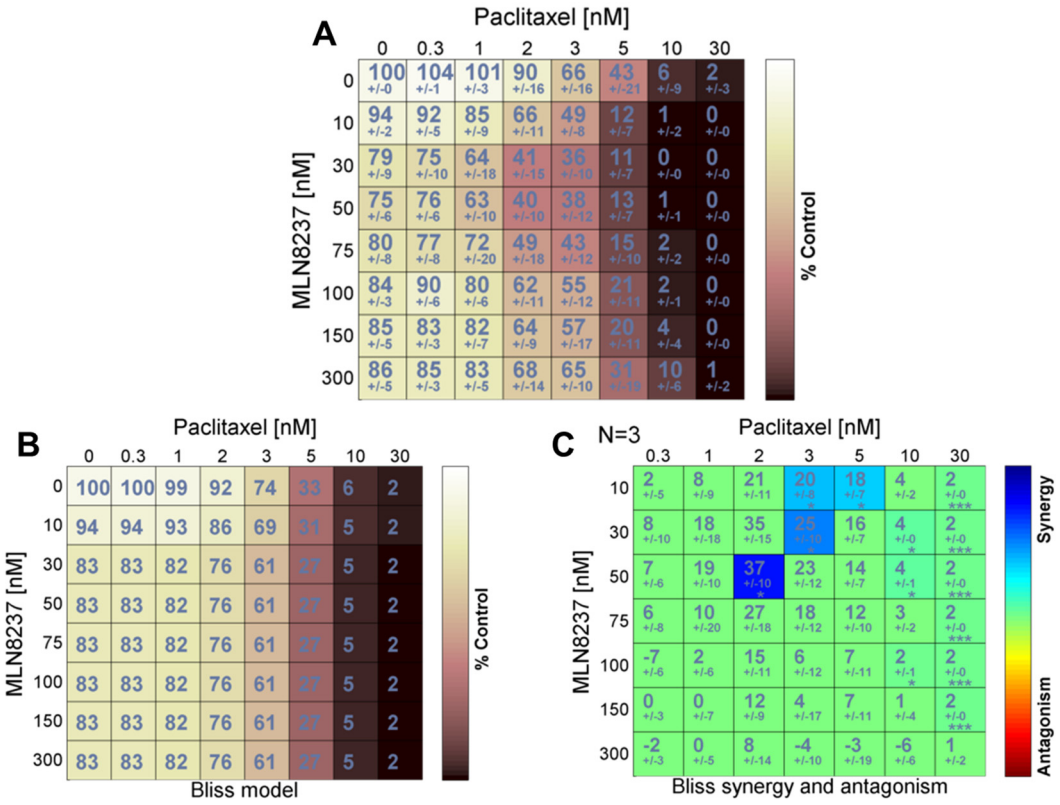

Figure 3-30: Combination of MLN8237 and paclitaxel in T24 cells with cells initially exposed to paclitaxel for 24 hours, followed by MLN8237 for remaining 48 hours.
T24 cells were seeded in 96-well plates and treated with combinations of paclitaxel for 24 hours followed by MLN8237 for the remaining time period to 72 hours.

For the experiments where MLN8237 was dosed first for six hours, followed by 66 hours of paclitaxel, there was no significant inhibition with single agent MLN8237. However, it may have had some effect as a region of synergy was seen, maximal with MLN8237 75 nM and paclitaxel 3 nM, with growth of 33±2% (Figure 3-31).

When cells were exposed to MLN8237 alone for 24 hours, followed by 48 hours of paclitaxel, the dose response curve for MLN8237 after 24 hours exposure was similar to that seen with 72 hours (Figure 3-32). However, a largely additive picture was seen with no significant synergy.

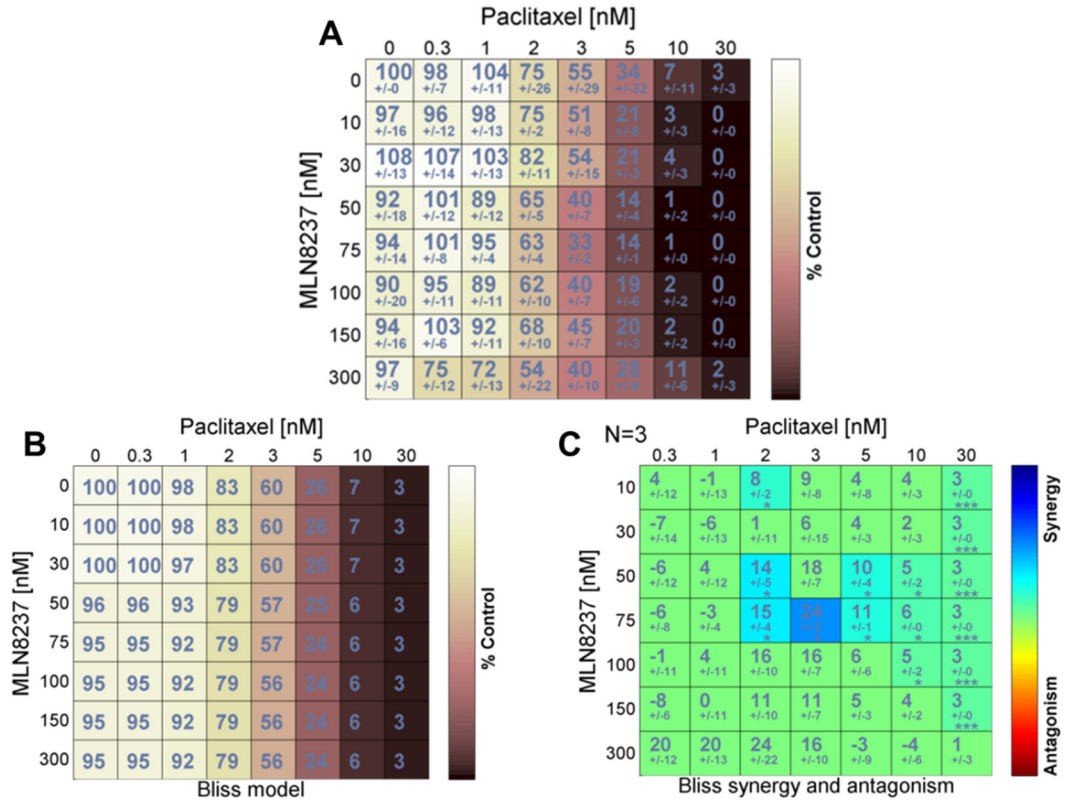

Figure 3-31: Combination of MLN8237 and paclitaxel in T24 cells with cells initially exposed to MLN8237 for six hours, followed by paclitaxel for remaining 66 hours.
T24 cells were seeded in 96-well plates and treated with combinations of MLN8237 for six hours followed by paclitaxel for the remaining time period to 72 hours.

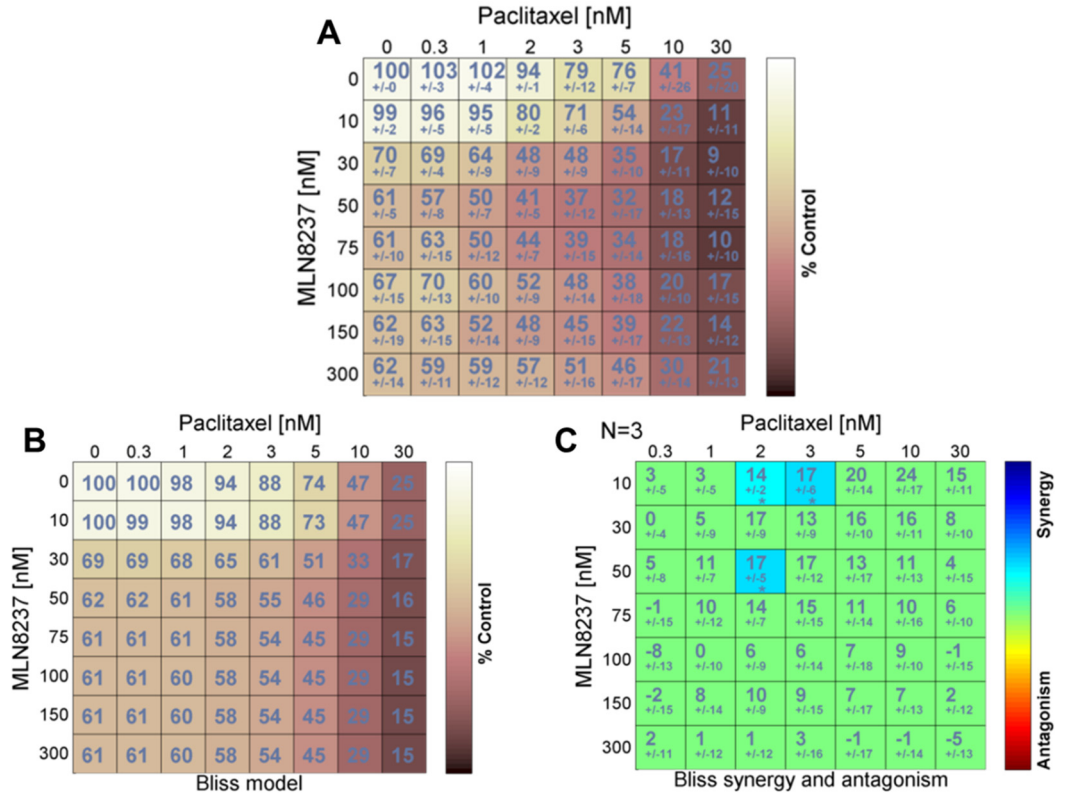

Figure 3-32: Combination of MLN8237 and paclitaxel in T24 cells with cells initially exposed to MLN8237 for 24 hours, followed by paclitaxel for remaining 48 hours.
T24 cells were seeded in 96-well plates and treated with combinations of MLN8237 for six hours followed by paclitaxel for the remaining time period to 72 hours.

On comparison of these results with the continuous 72 hour dosing (Figure 3-17), it is notable that the antagonism seen with concentrations of paclitaxel ≥5 nM and MLN8237 ≥ 100 nM was reduced when either paclitaxel or MLN8237 were dosed first (Figure 3-29 to Figure 3-32). However, to achieve maximal growth inhibition at synergistic concentrations, I concluded that simultaneous dosing with MLN8237 and paclitaxel was the optimal schedule, as used in the majority of reports. In contrast, Zhou *et al.* report that maximal synergy (calculated using the combination index) was achieved when cells were exposed to MLN8237 first followed by paclitaxel, and reported antagonism with concurrent treatment (121). However, their experimental design compared single agent or concurrent combination exposure for 48 hours (measured at 48 hours) with sequential exposure where one drug was added for 48 hours, followed by the second drug for a further 48 hours (measured at 96 hours). I believe this difference in the duration of the assay will affect the results and thus was a flawed approach. In my experiments, I ensured the total cell incubation period was kept the same. Certainly subsequent translational exposure-efficacy modeling of the combination of MLN8237 and taxanes using *in vivo* data by others showed additive and synergistic effects in a range of mouse models with concurrent dosing (261).

3.4.5 Colony forming assay with the combination of MLN8237 and paclitaxel

To gain insight into the longer term effects of exposure to paclitaxel and MLN8237 both as single agents and as a combination in the three cell lines where synergy had been seen, the colony forming assay was used.

3.4.5.1 T24 colony forming assay

After 24 hours (Figure 3-33A), 57±7% colonies survived exposure to paclitaxel 2 nM with only 19±5% remaining with MLN8237 50 nM. Both these results contrast to the SRB assay after 24 hours of exposure to paclitaxel 2 nM (90±16% cell growth, Figure 3-30) and after MLN8237 50 nM for 24 hours (61±5% cell growth, Figure 3-32). Colony formation was inhibited with the combination of MLN8237 50 nM and paclitaxel 2 nM to a similar extent to paclitaxel 30 nM with 2±1% colonies surviving (no significant difference p=0.39).

After exposure to drugs for 72 hours (Figure 3-33 B) whilst 45±9% colonies survived exposure to paclitaxel 2 nM, only 3±1% remained in those exposed to single agent MLN8237 50 nM, again far less than predicted from the SRB assay (57±7%, Figure

3-17). No colonies remained with either the combination treatment or paclitaxel 30 nM. The only other report of long term viability of T24 cells post-exposure to treatment comes from single agent data after 48 hours exposure to MLN8237 100 nM and MLN8237 1 μM, where less than 10% and 1% cells survived respectively (121). My data shows greater effect than that publication, with effective colony inhibition with MLN8237 50 nM at 24 hours. The combination of paclitaxel 2 nM and MLN8237 50 nM is at least as effective as that seen by them at higher concentrations.

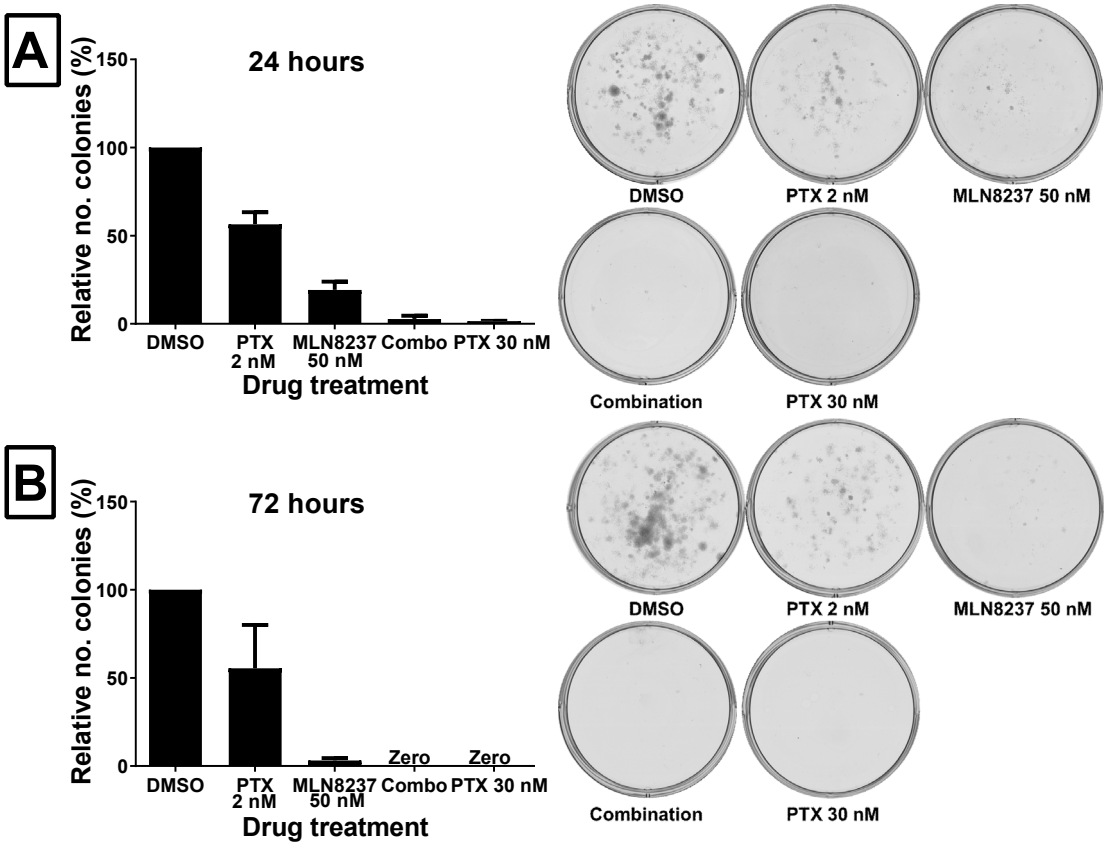

Figure 3-33: Colony forming assay in T24 cells exposed to paclitaxel and/or MLN8237.
Relative number of colonies observed after A. 24 hours and B. 72 hours exposure to either paclitaxel 2 nM, MLN8237 50 nM, the combination of MLN8237 50 nM and paclitaxel 2 nM or paclitaxel 30 nM. After drug exposure, equal numbers of viable cells were re-plated in fresh medium and allowed to grow for seven days. The quantification of the plates using GelCount is presented. These data are the mean of three replicates with SD shown. Representative photographs of the colony plates are shown during quantification using GelCount. Abbreviations: PTX=paclitaxel, combo/combination=combination MLN8237 50 nM and paclitaxel 2 nM.

3.4.5.2 RT112 colony forming assay

After exposure to drugs for 24 hours (Figure 3-34 A), 77±4 % colonies survived with paclitaxel 2 nM and with MLN8237 50 nM, more colonies were present than in DMSO control (130±4%). However, when the two drugs were combined, 23±6% colonies survived, compared to paclitaxel 30 nM at 3.1%±1. Even after 72 hours (Figure 3-34 B), 69±19 % colonies survived exposure to paclitaxel 2 nM and 54±14% colonies survived

MLN8237 50 nM, results less than the cell growth seen at 72 hours for the single agents in the SRB assay (84±5% with paclitaxel 2 nM and 87±10% with MLN8237 50 nM, Figure 3-19). No colonies survived in either the combination or paclitaxel 30 nM groups, whereas 42±7% cell growth had been seen in the SRB assay with the combination. The difference between the relatively high percentages of cells which survived the single agent treatments and the combination was marked.

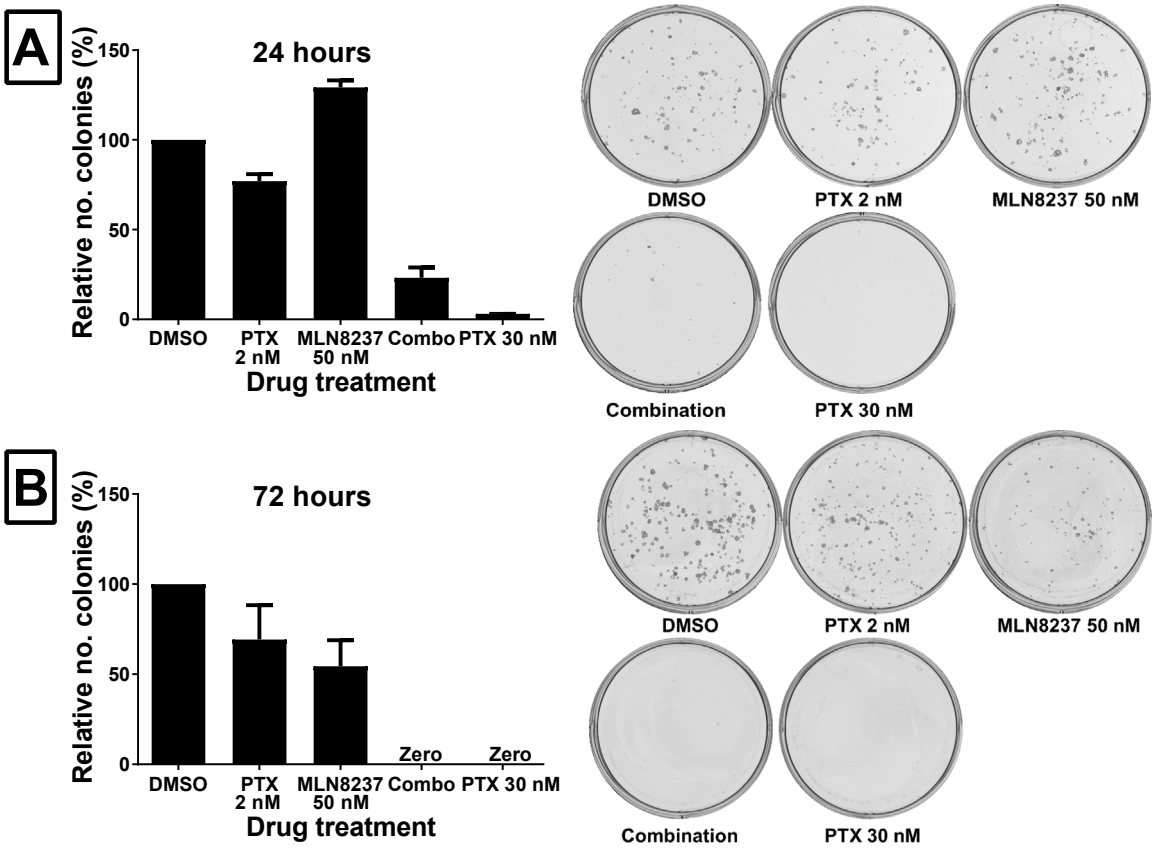

Figure 3-34: Colony forming assay in RT112 cells exposed to paclitaxel and/or MLN8237.
Relative number of colonies observed after A. 24 hours and B. 72 hours exposure to either paclitaxel 2 nM, MLN8237 50 nM, the combination of MLN8237 50 nM and paclitaxel 2 nM or paclitaxel 30 nM. After drug exposure, equal numbers of viable cells were re-plated in fresh medium and allowed to grow for seven days. The quantification of the plates using GelCount is presented. These data are the mean of three replicates with SD shown. Representative photographs of the colony plates are shown during quantification using GelCount. Abbreviations: PTX=paclitaxel, combo/combination=combination MLN8237 50 nM and paclitaxel 2 nM.

3.4.5.3 UM-UC-3 colony forming assay

After exposure to drugs for 24 hours (Figure 3-35 A), the colonies appeared particularly sensitive to paclitaxel 2 nM with only 29±3% colonies surviving compared to MLN8237 50 nM with 74±5%. With the combination 6.0±3% colonies survived, compared to paclitaxel 30 nM at 0.62%±0.32. After exposure to drugs for 72 hours (Figure 3-35 B) 34±8% colonies survived with paclitaxel 2 nM compared to MLN8237 50 nM with 40±5% (cell growth of 81±5% for paclitaxel 2 nM and 85±14% for MLN8237 50 nM in SRB assay, Figure 3-20). In both the combination and paclitaxel 30

nM groups, no colonies survived, whereas 35±8% cell growth had been seen with the combination in the SRB assay.

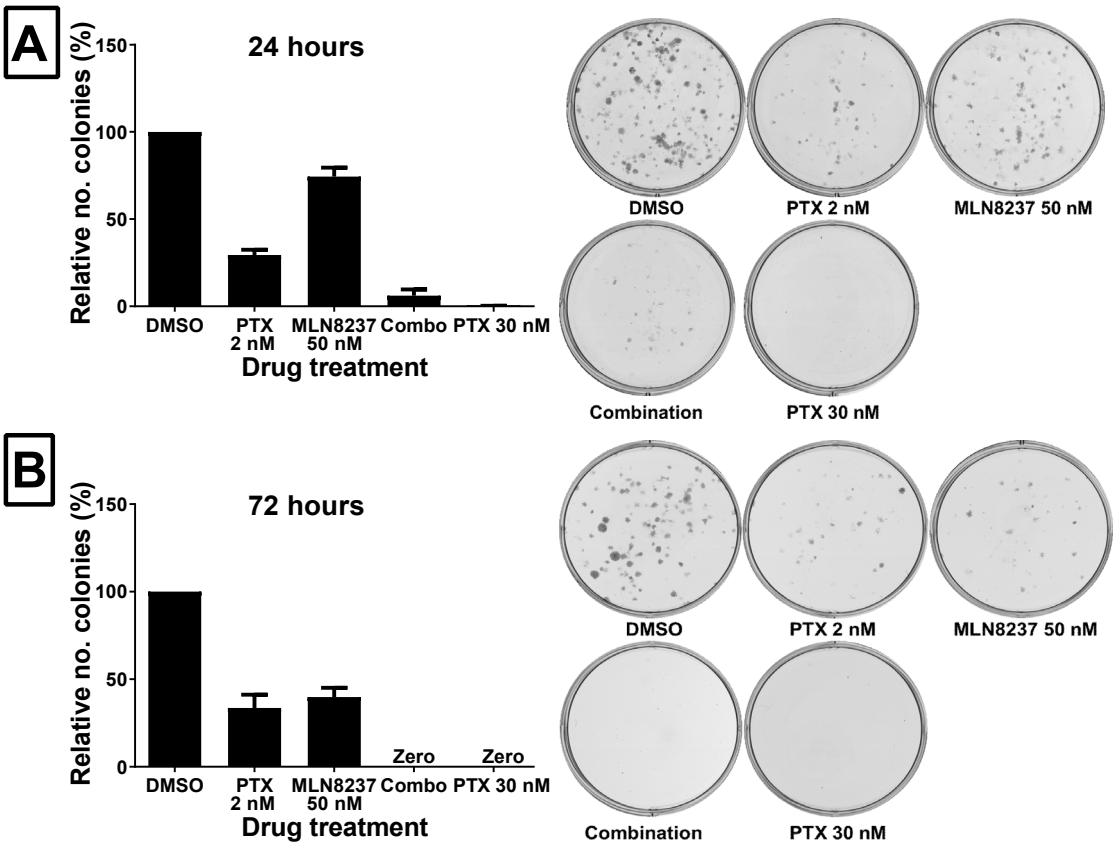

Figure 3-35: Colony forming assay in UM-UC-3 cells exposed to paclitaxel and/or MLN8237. Relative number of colonies observed after A. 24 hours and B. 72 hours exposure to either paclitaxel 2 nM, MLN8237 50 nM, the combination of MLN8237 50 nM and paclitaxel 2 nM or paclitaxel 30 nM. After drug exposure, equal numbers of viable cells were re-plated in fresh medium and allowed to grow for seven days. The quantification of the plates using GelCount is presented. These data are the mean of three replicates with SD shown. Representative photographs of the colony plates are shown during quantification using GelCount. Abbreviations: PTX=paclitaxel, combo/combination=combination MLN8237 50 nM and paclitaxel 2 nM.

3.4.5.4 Summary of colony forming assay

Therefore across all three cell lines where synergy had been seen in the SRB assay, the strongest reduction in clonogenic ability of cells was with the combination of MLN8237 50 nM and paclitaxel 2 nM. Greater sensitivity was seen using this clonogenic assay than in the SRB data, perhaps reflecting that cells were viable but had lost proliferative potential at the end of the 72 hour incubation period of the SRB assay. Thus the SRB assay may have underestimated the efficacy of the combination. The colony assay also demonstrated that 24 hours of treatment with the combination was sufficient to have extensive growth inhibitory effect, strengthening the interest in taking this combination into pre-clinical and clinical studies.

3.4.6 Assessment of the combination of MLN8237 and docetaxel in bladder cancer cell line panel

Docetaxel is an alternative taxane, with a similar structure and mechanism of action, which can be used as a second line option in metastatic bladder cancer following cisplatin and gemcitabine, similarly to paclitaxel (262). I was therefore interested in comparing the results I had seen with paclitaxel. The combination of MLN8237 and docetaxel has been reported to enhance apoptosis and anti-tumour activity in oesophageal cancer, breast cancer and mantle cell lymphoma (231, 232, 261). Similar results have been seen with the combination of alternative AK-A inhibitors and docetaxel (217, 263) but not in bladder cancer.

3.4.6.1 Assessment of MLN8237 and docetaxel combination in SRB assay

The results are summarised in Table 3-12 (the individual plots are not shown for brevity) and show synergy was seen with RT112, T24 and UM-UC-3 cells, albeit with a lower synergy score than with paclitaxel. The synergy seen in these three cell lines was in the range of MLN8237 30-75 nM and docetaxel 0.3-3 nM. Therefore this combination may show promise in the same cell lines as seen with paclitaxel – T24, UM-UC-3 and RT112.

Cell line	SS	GI at max SS point (%)	[MLN8237] at this point (nM)	[Docetaxel] at this point (nM)
HT1197	7.2±9	17±9	50	0.3
J82	14±7	44±7	50	1
RT4	17±1	41±1	30	1
RT112	33±4	77±4	75	0.3
SW780	4.1±8	33±8	100	0.3
T24	22±9	69±9	75	1
UM-UC-3	24±12	55±12	10	1

Table 3-12: Summary of SRB assay data for bladder cell lines with MLN8237 together with docetaxel.
The highest synergy score is shown, together with the extent of growth inhibition at this point and the relevant MLN8237 and docetaxel concentrations. Growth inhibition calculated from percentage growth compared to control with mean and standard deviation shown (n=3). Abbreviations: SS=synergy score, GI=growth inhibition.

3.4.6.2 Comparison of MLN8237 and taxane combinations in T24 cell line

In T24, UM-U-3 and RT112 cells, cPARP signal consistent with apoptosis had been seen after 24 hours exposure to the combination of MLN8237 50 nM and paclitaxel 2 nM. Death in mitosis involves the intrinsic (mitochondrial mediated) apoptotic pathway, initiated by CC9 ultimately causing activation of caspases such as CC3 and then cPARP cleavage. To investigate the effect of the combination of MLN8237 and docetaxel on

T24 cells and compare this with that already seen with MLN8237 and paclitaxel, I performed Western blotting of T24 cells following exposure to the drugs of interest assessing CC9 and CC3 as well as cPARP at 24, 30 and 48 hours. The combination of MLN8237 50 nM and docetaxel 1 nM was selected as this allowed the same concentration of MLN8237 to be assessed and it had shown growth inhibition of 67±9% and a SS of 20±9, very similar to the results at the highest SS with MLN8237 75 nM and docetaxel 1 nM (Table 3-12).

Whilst little effect was seen with either paclitaxel 2 nM, docetaxel 1 nM or MLN8237 50 nM at 24 or 30 hours, by 48 hours there had been a slight increase in CC9 and CC3 signal and cPARP was visible with docetaxel 1 nM (lane 3) and MLN8237 50 nM (lane 4). With the combinations, CC3 and CC9 signal was present by 24 hours, corresponding to the cPARP signal seen but was stronger with the higher concentration of single agent taxanes. By 48 hours, the cPARP signal was very similar between either combination or higher concentration of single agent taxanes, suggesting that both the low concentration of paclitaxel and docetaxel combinations with MLN8237 50 nM were as effective in terms of inducing apoptosis.

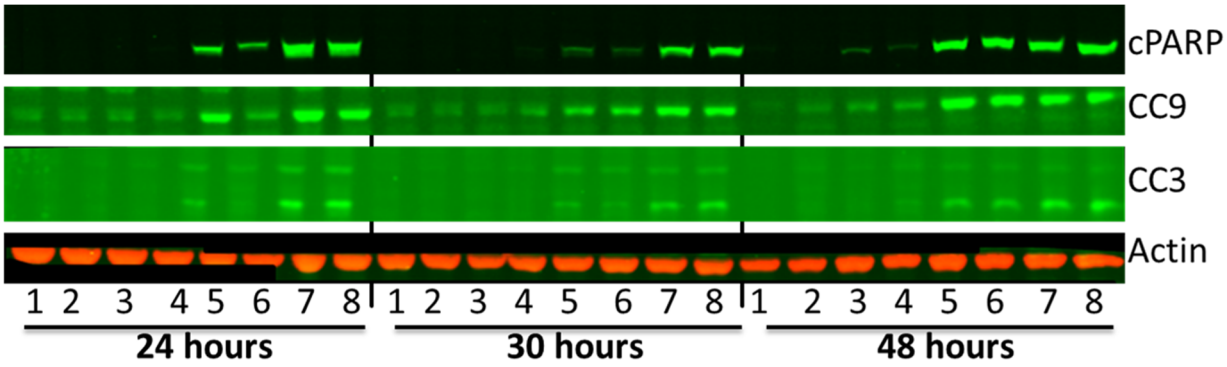

Figure 3-36: Western blots for proteins of interest in T24 cells exposed to docetaxel, paclitaxel and MLN8237 as labelled for 24, 30 and 48 hours.
T24 cells exposed to the following drug treatments 1. DMSO 2. Paclitaxel 2 nM 3. Docetaxel 1 nM 4. MLN8237 50 nM 5. Combination of paclitaxel 2 nM and MLN8237 50 nM 6. Combination of docetaxel 1 nM and MLN8237 50 nM 7. Paclitaxel 30 nM 8. Docetaxel 30 nM for 24, 30 and 48 hours. Proteins of interest shown in green channel with actin as control (red channel).

The CC9 signal confirms the activation of the intrinsic apoptosis pathway. CC3 is a marker that can be detected in tumours by immunohistochemistry and this would be an appropriate indicator of apoptosis that can be used for future *in vivo* studies. This experiment confirms that either paclitaxel 2 nM or docetaxel 1 nM in combination with MLN8237 50 nM can induce a similar degree of apoptosis to that seen with a higher concentration of single agent taxanes.

3.5 Summary of chapter

In this chapter, I initially tested a range of novel aurora kinase inhibitors in the T24 bladder cancer cell line as at the time of this work it was unclear whether an AK-A, AK-B or pan-AKI would be most effective. I identified that AK-A-specific inhibitors, exemplified by CYC3, were the most potent in synergy with paclitaxel. The use of a matrix to test a range of eight by eight concentration combinations proved particularly helpful as synergy was seen at low concentrations of paclitaxel (GI_{20} to GI_{40}) with antagonism at higher concentrations. Subsequent investigations including live cell imaging confirmed the cytotoxic effect of the combination. A range of schedules were examined but concurrent dosing seemed the most effective. Although some synergy was seen in the other bladder cancer cell lines, it appeared most apparent in the T24 cell line. At the time, CYC3 was the best AK-A inhibitor available to me and therefore it was used in further experiments comparing the combination in non-cancer cell lines (Chapter 4) and it was taken forward into initial *in vivo* studies (Chapter 6).

However, later in my research, I was able to obtain access to an alternative AK-A inhibitor, MLN8237. Synergy was seen in T24, UM-UC-3 and RT112 cell lines with the combination of MLN8237 and paclitaxel, again with concentrations of paclitaxel $\leq GI_{50}$. Enhanced cell death was confirmed using live cell Incucyte™ imaging, flow cytometry, Western blotting and long term clonogenic assays. Docetaxel also showed potential in combination with MLN8237 in the same cell lines. These results are consistent with reports of synergy between AK-A specific inhibitors and taxanes, reported during my studies. Given its improved AK-A selectivity and the more promising synergy seen in multiple cell lines, together with the fact that MLN8237 was further developed and entering clinical trial testing, all further experiments and the majority of my *in vivo* work was performed using MLN8237 instead of CYC3.

Whilst T24 and UM-UC-3 are derived from high grade tumours (Grade 3), RT112 cells are from a Grade 2 tumour (Table 3-5). Synergy was not seen in the other four bladder cell lines, including other high grade tumours (such as J82). The variability between cell line responses to each anti-cancer drug as a single agent and in combination reflects the heterogeneity seen within each cancer type, now comprehensively studied in bladder cancer (107). Both the TP53 and TP73 status of cell lines may be important in determining the cell fate of cells in response to AKI, with some studies showing cell lines with a compromised p53/p21 post-mitotic checkpoint or with p53 mutations are more sensitive to pan-AKI and AK-A specific AKI and more likely undergo apoptosis

than cells with intact checkpoint function (264-266). In the bladder cancer cell panel I studied, T24, RT112 and UM-UC-3 had p53 mutations considered deleterious (whilst J82 does have mutations in p53, these have been reported as neutral in terms of effect on cells (IARC database, http://p53.iarc.fr/ version R18 (267)). TP73 has been shown to play a significant role in determining cell fate in p53 deficient cells exposed to AK-A inhibitors (129-132), with p73 potentially able to compensate for lack of p53 function in tumour cells. To investigate the role of TP53 and TP73 in the response seen, I did perform experiments attempting siRNA knockdown of p73 in T24 cells and with isogenic p53 mutant/null HCT116 cell lines, but the results were not sufficiently robust to draw definitive conclusions. A subsequent study combining MLN8237 and docetaxel in upper gastro-intestinal cancer models concluded that the combination was effective independent of p53 status (232).

In parallel studies that we have published (Appendix 1), we demonstrated that CYC3 synergised with low concentration paclitaxel to suppress the growth and viability of pancreatic cancer cells, with the combination approaching the efficacy of higher concentrations of single agent paclitaxel (258). The concept of dose reduction potential where a combination can achieve similar responses but with reduced toxicity is also important when assessing combination effects. These results suggested the combination of concentrations of paclitaxel below GI_{50} and AK-A inhibitors may provide a better therapeutic window compared to high concentration paclitaxel. Therefore, I next examined the combination in “normal” cell line models and with the CFU-GM assay to confirm whether a therapeutic window could be achieved.

4 *ASSESSMENT OF THE EFFECT OF AK-A SPECIFIC INHIBITORS IN NON-CANCER CELL LINES COMPARED TO T24 CELLS*

4.1 Introduction

With promising results from the cytotoxicity assays showing synergy between low concentrations of paclitaxel and two different AK-A specific AKI, CYC3 and MLN8237 in some bladder cancer cell lines, it was important to assess the effect of these combinations in non-cancer cell lines. Differences between cancer cell lines and non-transformed cell lines in their response to various anti-mitotic drug treatments have been previously reported using live cell imaging techniques (268-270). Encouragingly these have all shown a differential response, with an increase in cell death seen in the cancer cell lines compared to the non-transformed cell lines. This could translate into an effective treatment with reduced toxicity to normal cells. However, neutropenia was frequently dose limiting in the Phase 1 single agent studies (Table 1-2 to Table 1-4) and the combination with a taxane could increase this further. Hence the effect of these combinations was assessed in non-cancer cell lines. I then tested the combination in the CFU-GM assay using primary bone marrow cells, which has been validated as a useful predictor of the risk of neutropenia from drug regimens (271, 272).

Contribution of others to this experimental work: Live cell imaging and immunostaining (4.3) was performed in collaboration with Dr Yao Lin. He also assisted with manual colony counting (4.4).

4.2 Comparison of the efficacy *in vitro* of AK-A inhibitors and paclitaxel in IMR-90 and ARPE-19 cell lines

Two different cell lines were used for comparisons with the T24 cell line using the SRB assay – IMR-90 and ARPE-19. IMR-90 is a primary diploid lung fibroblast line (273) and ARPE-19 is a human retinal pigment epithelial cell line with differentiated properties (274). Initial experiments were performed with both CYC3 and MLN8237 in IMR-90 cells. However, IMR-90 cells have a tendency to senesce with repeated passaging and need to be grown in low oxygen conditions, meaning that assays such as live cell imaging were not technically possible. Given this and the synergy seen in

MLN8237 in several bladder cancer cell lines, I subsequently concentrated on the combination of MLN8237 and paclitaxel in ARPE-19 cells.

4.2.1 Single agent response to paclitaxel and AKI

IMR-90 cells were sensitive to single agent paclitaxel, with a GI_{50} of 3.2 nM (Figure 4-1 B), comparable to that seen in the T24 bladder cancer cell line (GI_{50} 3.8 nM). IMR-90 cells were resistant to both MLN8237 (Figure 4-1 B) and CYC3 (Figure 4-1 C) with only 20% maximum inhibition seen with either drug, even when higher concentrations of drug were tested (data not shown).

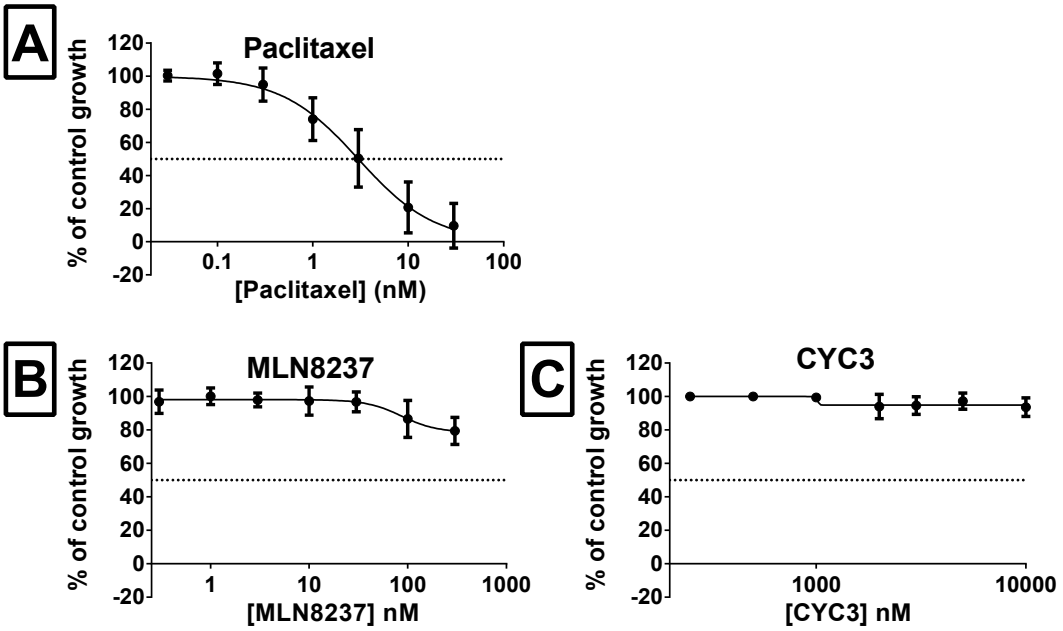

Figure 4-1: Dose response curves for IMR-90 cells exposed to paclitaxel, MLN8237 and CYC3. IMR-90 cells were exposed to a range of concentrations of A. Paclitaxel B. MLN8237 and C. CYC3 for 72 hours, then analysed using SRB assay. Each graph shows the data for % control cell growth at each concentration of three replicates with SD and then a curve fitted to the data using GraphPad Prism. The dotted line shows 50% cell growth and this was used to identify the GI_{50} from the graph.

ARPE-19 cells were sensitive to paclitaxel, with a GI_{50} of 1.4 nM (Figure 4-2 A). MLN8237 did show an effect in ARPE-19 cells (GI_{50} 50 nM) but this plateaued at 50% growth inhibition (Figure 4-2 B).

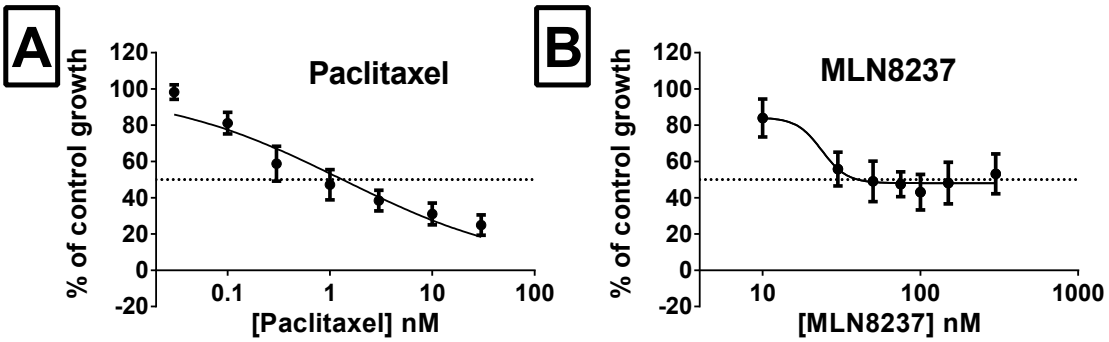

Figure 4-2: Dose response curves for ARPE-19 cells exposed to paclitaxel and MLN8237.
ARPE-19 cells were exposed to a range of concentrations of A. Paclitaxel B. MLN8237 for 72 hours, then analysed using SRB assay. Each graph shows the data for % control cell growth at each concentration of three replicates with SD and then a curve fitted to the data using GraphPad Prism. The dotted line shows 50% cell growth and this was used to identify the GI_{50} from the graph.

4.2.2 Combination of AK-A inhibitors with paclitaxel

When the combination of CYC3 and paclitaxel was studied in IMR-90 cells (Figure 4-3), there were a few concentration-combinations associated with synergy (for example CYC3 2000 nM and paclitaxel 1 nM) but no consistent region. Synergy was detected with very high concentrations of CYC3 (10000 nM), but these are concentrations at which it is likely to be also targeting other kinases such as AK-B.

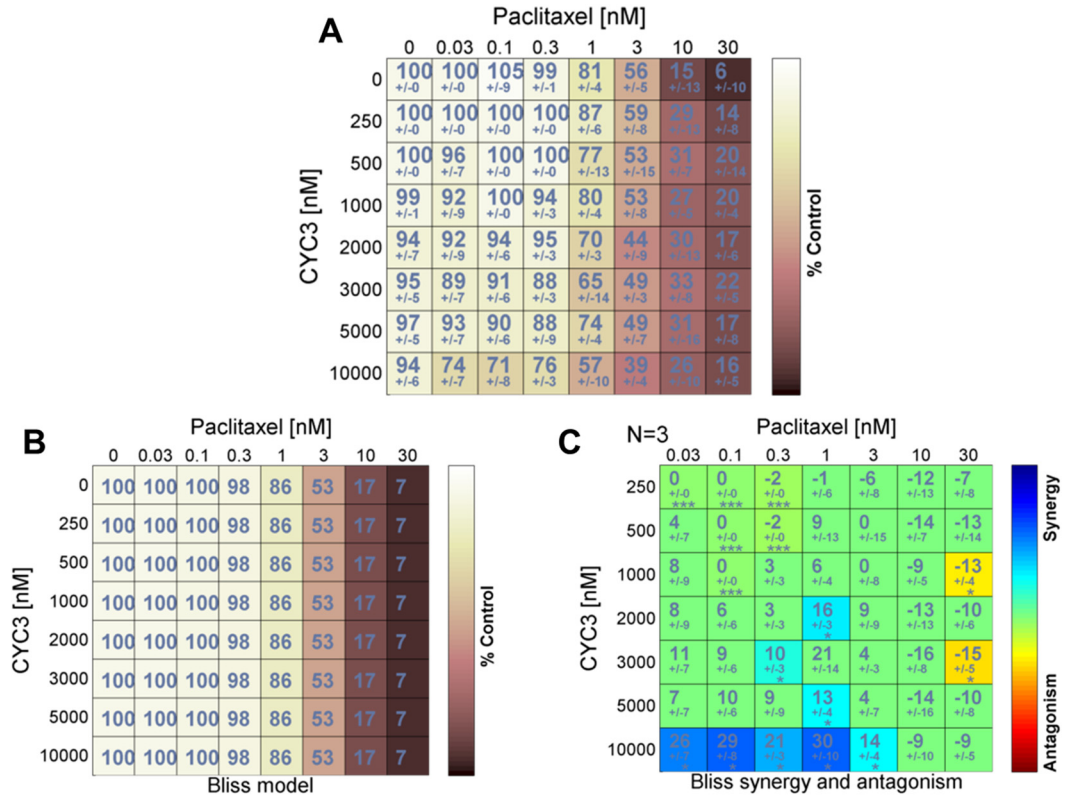

Figure 4-3: Combination of CYC3 and paclitaxel in IMR-90 cells.
IMR-90 cells were seeded in 96-well plates and treated with combinations of paclitaxel and CYC3 for 72 hours.

There was no significant synergy seen with MLN8237 and paclitaxel (Figure 4-4), with the effects seen close to single agent paclitaxel at the same concentrations, consistent with the limited dose response seen in Figure 4-1.

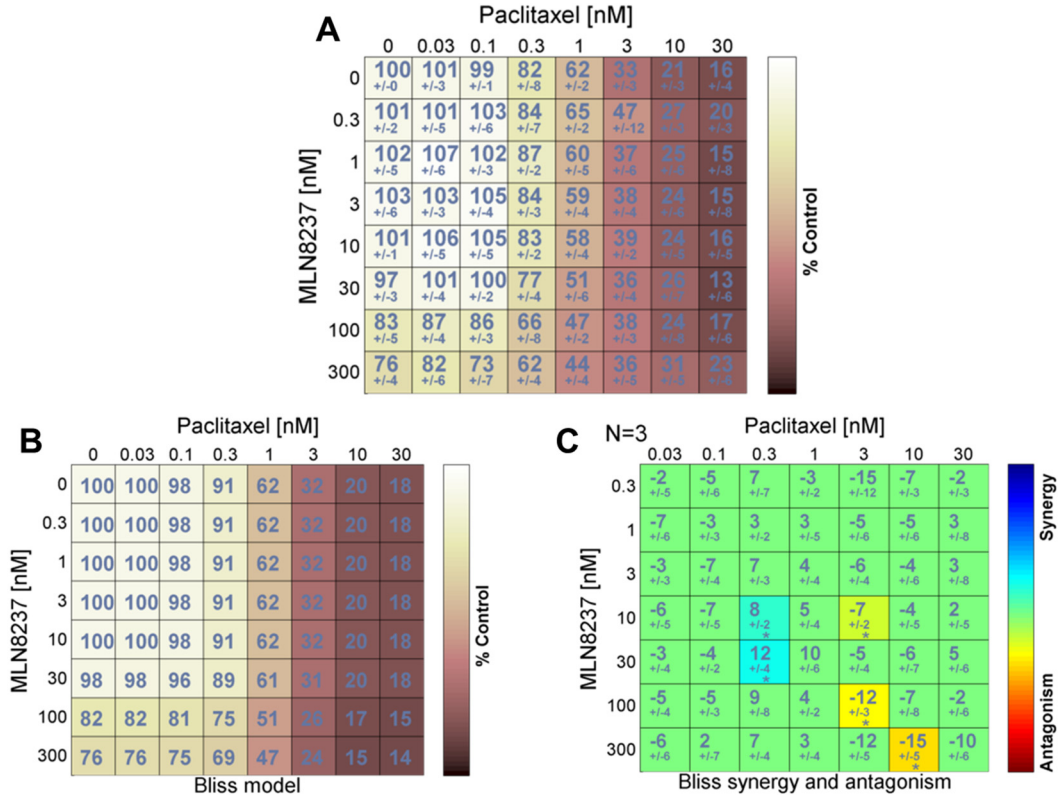

Figure 4-4: Combination of MLN8237 and paclitaxel in IMR-90 cells.
IMR-90 cells were seeded in 96-well plates and treated with combinations of paclitaxel and MLN8237 for 72 hours.

With the combination of MLN8237 and paclitaxel in ARPE-19 cells (Figure 4-5), no significant synergy was seen, despite the fact that the GI_{50} was reached for both drugs. Indeed the areas of yellow and orange seen in the Bliss model (Figure 4-5 C) suggest antagonism, particularly at paclitaxel concentrations ≥5 nM. At the concentration-combination of MLN8237 50 nM and paclitaxel 2 nM where maximum synergy was seen in T24 cells, growth inhibition was 60±8% compared to 81±1% in T24 cells.

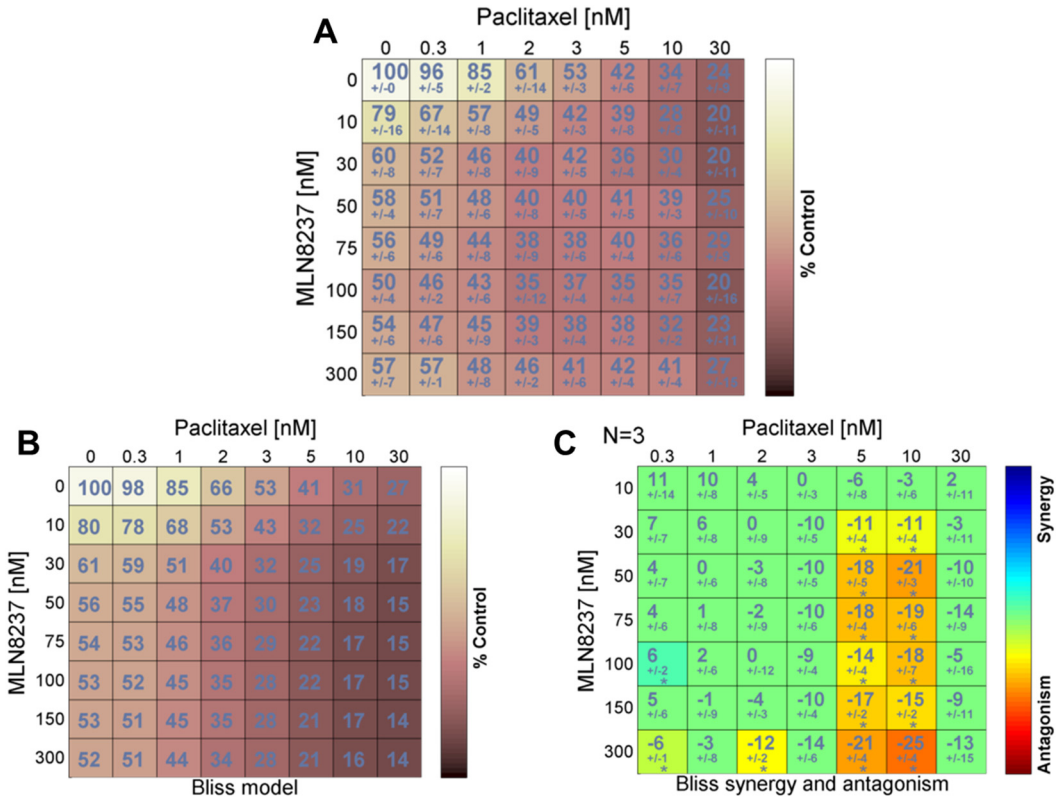

Figure 4-5: Combination of MLN8237 and paclitaxel in ARPE-19 cells.
ARPE-19 cells were seeded in 96-well plates and treated with combinations of paclitaxel and MLN8237 for 72 hours.

4.2.3 Investigation of SRB findings in ARPE-19 cells exposed to paclitaxel and MLN8237

To further explore the combination of MLN8237 and paclitaxel, the ARPE-19 cell line was used.

4.2.3.1 IncuCyte™ live cell imaging

The paclitaxel dose response curve was relatively steep, particularly between 1 nM (final confluency 80±18%) and 2 nM (final confluency 29±3%) (Figure 4-6 A). There was a more gradual dose-response effect with MLN8237: the final cell confluency was 59±10% with MLN8237 30 nM, 50±11% MLN8237 50 nM and 42±5% with MLN8237 100 nM. With the combination of MLN8237 50 nM and paclitaxel 2 nM (Figure 4-6 B), the final cell confluency with the combination at endpoint was suppressed at 24±2%, a greater effect than seen in the SRB assay (40±8% (Figure 4-5)).

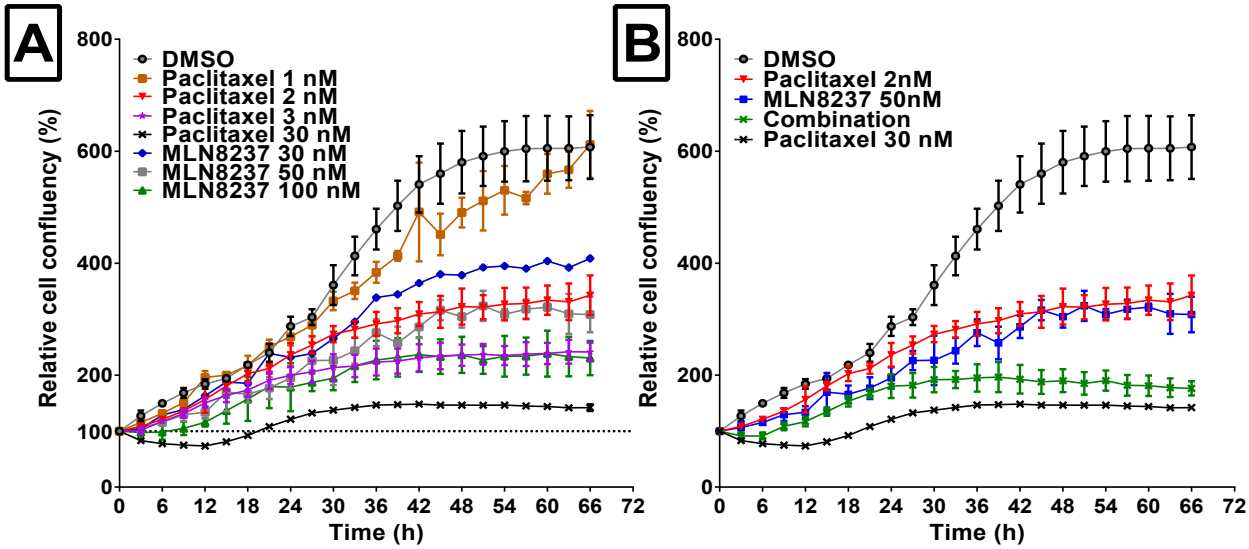

Figure 4-6: Relative cell confluency over time in ARPE-19 cells exposed to drugs as indicated. ARPE-19 cells were seeded in 96-well plates and allowed to grow for 24 hours. They were then dosed with A. a range of concentrations of MLN8237 and paclitaxel as single agents B. single agent paclitaxel 2 nM, MLN8237 50 nM, the combination of MLN8237 50 nM and paclitaxel 2 nM or paclitaxel 30 nM. They were imaged using IncuCyte™ for 66 hours and percentage confluency relative to the start of imaging was calculated and plotted. These data are the mean of three replicates with SD. Combination= MLN8237 50 nM and paclitaxel 2 nM.

The ARPE-19 IncuCyte™ results are comparable to the findings in T24 cells where the final cell confluency with the same combination was 15±1% of control at endpoint (Figure 3-25 A). This suggests that there may not be a large therapeutic window for the combination, with similar effects on bladder cancer cells and on highly proliferative normal epithelia. Therefore, to gain some insight into the longer term effects of exposure to both drugs both as single agents and as a combination, the colony forming assay was used.

4.2.3.2 Colony forming assay

After exposure to drugs for 24 hours, 50±5% colonies survived with paclitaxel 2 nM and 15±8% with MLN8237 50 nM, compared to the combination with 0.71±0.5% (Figure 4-7). Whereas the SRB and IncuCyte™ data had suggested approximately 50% cell growth in the presence of MLN8237 50 nM for up to 72 hours, after 24 hours exposure the surviving fraction was only 15%. One explanation for this could be that although cells were able to maintain their protein content (as measured by SRB) in the presence of MLN8237 and maintain cell confluency (as seen in the IncuCyte™ assay), their ultimate cell fate was already determined and in longer term assays this became clear. After exposure to drugs for 72 hours, 39±5% colonies survived with paclitaxel 2

nM and 27±11% with MLN8237 50 nM, compared to combination with 0.64±0.5% (Figure 4-7 B).

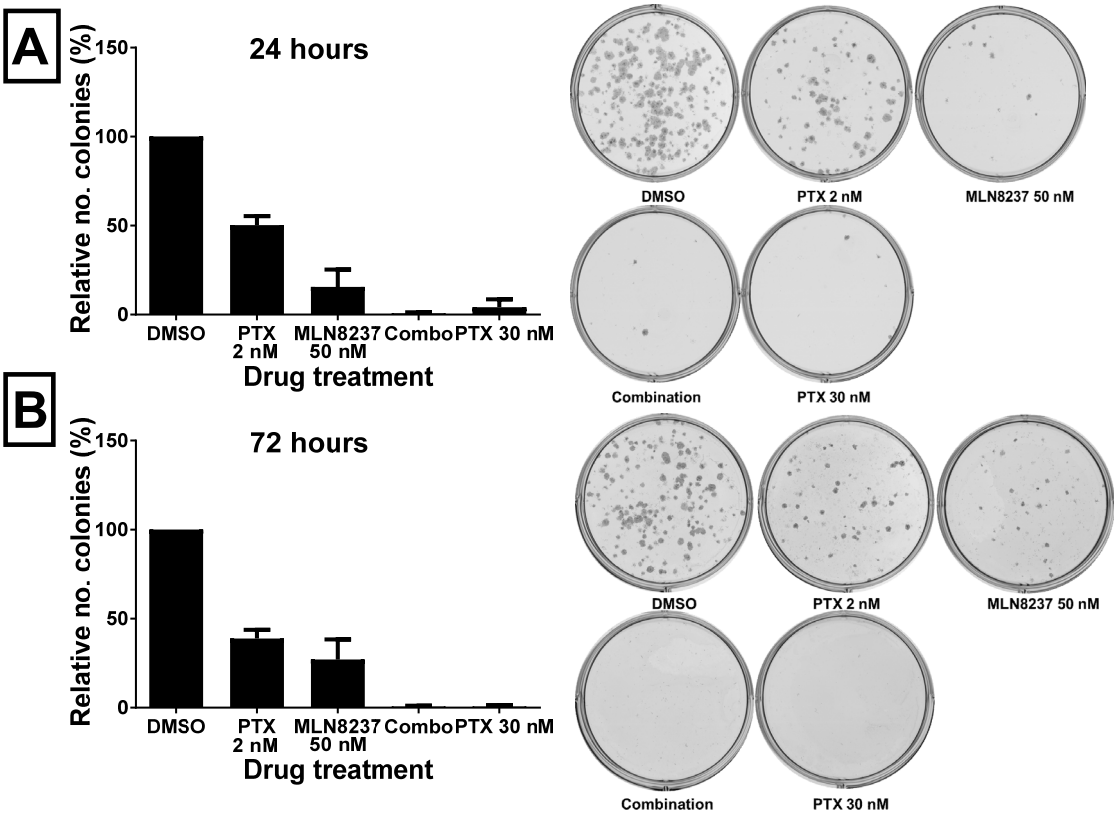

Figure 4-7: Relative number of colonies observed after 24 hours and 72 hours exposure to paclitaxel and/or MLN8237 in ARPE-19 cells together with representative photographs of the colony plates.
Relative number of colonies observed after A. 24 hours and B. 72 hours exposure to either paclitaxel 2 nM, MLN8237 50 nM, the combination of MLN8237 50 nM and paclitaxel 2 nM or paclitaxel 30 nM. After drug exposure, equal numbers of viable cells were re-plated in fresh medium and allowed to grow for seven days. The quantification of the plates using GelCount is presented. These data are the mean of three replicates with SD shown. Representative photographs of the colony plates are shown during quantification using GelCount. Abbreviations: PTX=paclitaxel, combo/combination=combination MLN8237 50 nM and paclitaxel 2 nM.

Therefore after both 24 and 72 hours exposure to the combination of MLN8237 and paclitaxel 2 nM, the combination appeared as toxic as paclitaxel 30 nM. These results are similar to those seen in T24, UM-UC-3 and RT112 cells in the colony forming assay, suggesting that there is potential for synergistic toxicity in non-cancer epithelial cells. Certainly on review of the SRB assay data (Figure 4-5), although no synergy was seen with this combination, 60±8% growth inhibition was seen, which is not dissimilar to that seen in RT112 (68±7%) and UM-UC-3 (65±8%) cells (where significant synergy was identified).

4.3 Comparison of effects of MLN8237 and paclitaxel in ARPE-19 and T24 cells using live cell imaging and immunostaining

The SRB assay showed additivity with the combination of MLN8237 and paclitaxel in ARPE-19 cells, but the IncuCyte™ and colony forming assays both showed that the combination of MLN8237 50 nM and paclitaxel 2 nM suppressed cell growth. The differential responses between non-transformed cell lines and cancer cell lines previously reported have used time-lapse live cell imaging to allow the individual fate of cells to be studied (268-270), so we utilised this technique together with immunostaining to further explore the effects on mitosis of this combination in both T24 and ARPE-19 cells. These experiments were devised and carried out in collaboration with Dr Yao Lin.

4.3.1 Live cell imaging in T24 and ARPE-19 cells exposed to MLN8237 and paclitaxel

Live cell imaging with bright field morphology analysis was performed in both T24 and ARPE-19 cells, exposed to paclitaxel 2 nM and 30 nM, MLN8237 50 nM and the combination of MLN8237 50 nM and paclitaxel 2 nM. The mitotic fates of cells entering their first mitosis were divided into four categories, either normal mitotic division with two daughter cells, division with more than two daughter cells, one cell remaining, or mitotic death (Figure 4-8 with representative images in Figure 4-9). Of note, for the cells labelled as one daughter cell, the cell rounded up and entered mitosis but after a period of time, it exited but remained one cell (example shown in Figure 4-9). Whilst these are categorised in our analysis as cells having passed into mitosis into the next G1 with only one daughter cell, without definite evidence to prove this, it is also possible that the original cell failed mitosis and flattened out again but still in G2. The fates of daughter cells at their next division were either death, being able to divide again or viable but without further division. In this analysis, for each of the cells that divided, one daughter cell was selected at random and its fate was determined.

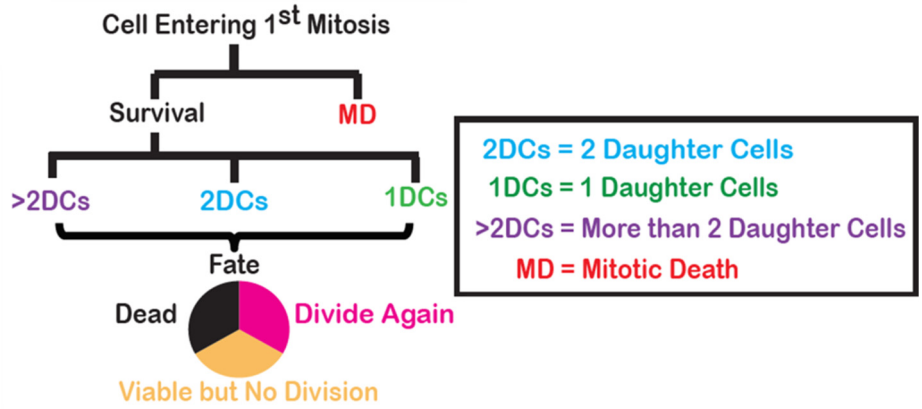

Figure 4-8: Diagram depicting the various fates of a cell and its daughter cells after first mitosis.

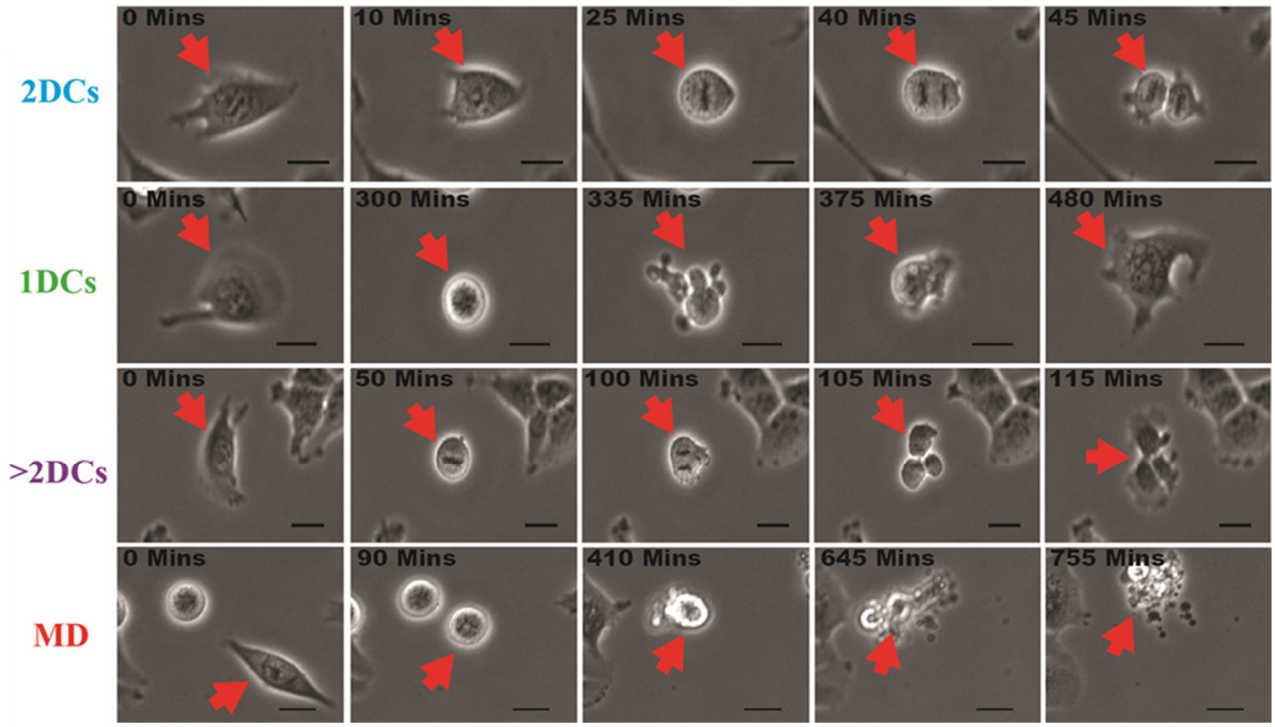

Figure 4-9: Representative images of T24 cells undergoing each different mitotic fate.
Cell fates - normal division with two daughter cells (2DCs), only one daughter cell (1 DCs), division with more than two daughter cells (>2DCs) or mitotic death (MD). T24 cells were seeded in Ibidi eight-chamber slides at 5000 cells/chamber. After 24 hours, cells were exposed to drugs and sent for 72 hour live cell imaging detection with five minute gaps between frames.

4.3.1.1 Live cell imaging in T24 cells

I have shown that paclitaxel 2 nM alone did not induce strong growth inhibition in T24 cells in SRB experiments (12±7% in the combination data in Figure 3-17 and IncuCyte™ data in Figure 3-25 A). Here Figure 4-10 and Table 4-1 demonstrate that although it did not induce any mitotic death, it did significantly extend the average mitotic duration (149±52 mins vs 54±10 mins in DMSO) and was capable of inducing aberrant divisions leading to >2 daughter cells (30% vs 0% in DMSO). This indicates that cells can undergo multi-polar mitosis when exposed to paclitaxel 2 nM. The

average mitotic duration with MLN8237 alone (265±136 mins) was five times longer than in control (as expected for an AK-A inhibitor) but no mitotic death occurred. With the combination, the average time in mitosis extended further to 405±217 minutes. This compared to 641±319 minutes with paclitaxel 30 nM. When cells were co-treated with MLN8237, induction of mitotic death was observed compared to either single agent alone (23% vs 0%), and with paclitaxel 30 nM it was 43% (Table 4-1). It is clear there is a threshold of time spent in mitosis of around 500 minutes, above which the cells are more likely to undergo mitotic death (Figure 4-10), consistent with previous observations (144).

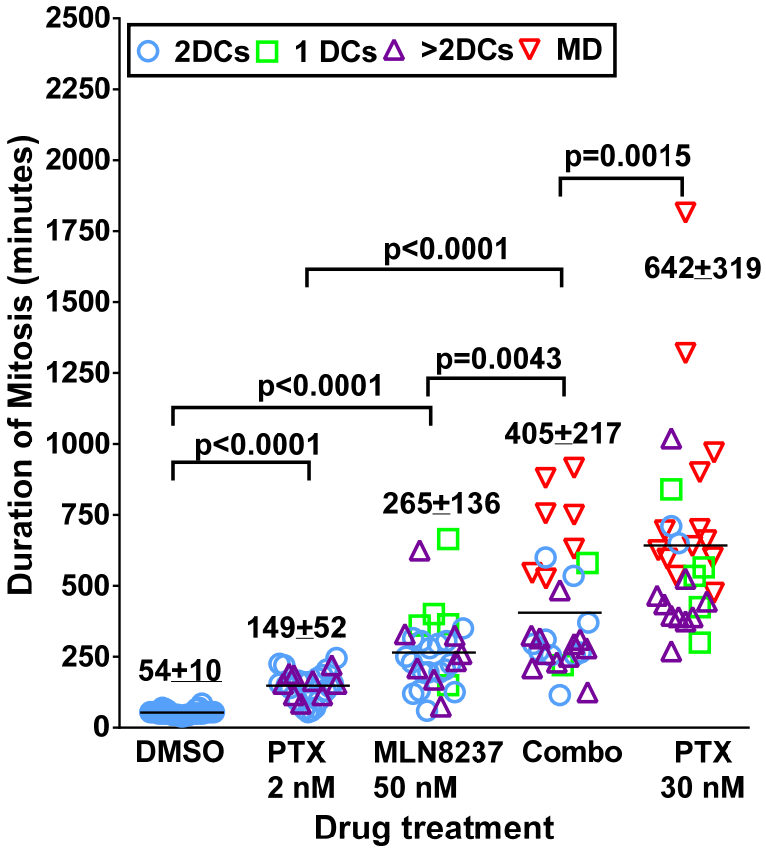

Figure 4-10: T24 live cell imaging.
T24 cells were seeded in Ibidi 8-chamber slides at 5000 cells/chamber. After 24h, cells were exposed to drugs as labelled (Combo=combination of MLN8237 50 nM and paclitaxel 2 nM) and sent for 72h live cell imaging detection with five minutes gap between frames. For each treatment, 30 cells were counted and the fate of cells using the four categories illustrated in Figure 4-8 is shown. The duration of mitosis is defined as the time between nuclear envelope breakdown and chromatin decondensation and is shown for each treatment together with SD. The p value was calculated using the two-column t-test in GraphPad Prism.

Cell fate	DMSO	Paclitaxel 2 nM	MLN8237 50 nM	Combination	Paclitaxel 30 nM
2 DCs (%)	100	67	57	33	7
1 DCs (%)	0	3	17	7	17
>2DCs (%)	0	30	27	37	33
MD (%)	0	0	0	23	43

Table 4-1: Proportion of cell fates for each T24 cell entering mitosis for each drug treatment.
Fate of cells determined according to the categories in Figure 4-8 (two daughter cells (2DCs), only one daughter cell (1 DCs), division with more than two daughter cells (>2DCs) or mitotic death (MD)), with 30 cells counted for each treatment. Drug treatments as labelled, combination=MLN8237 50 nM and paclitaxel 2 nM.

The proportion of cells dying in mitosis in each of the different treatment groups, as assessed here by live cell imaging correlates well with the c-PARP levels observed in western blots shown in Figure 3-26.

Even in the cells exposed to the combination which successfully exited mitosis, none of the daughter cells were able to divide again, with the majority dying (63% with combination, 82% with paclitaxel 30 nM) and the rest not able to undergo mitosis, whilst looking viable (Table 4-2).

Drug treatment	Divide again (%)	Viable, no division (%)	Dead (%)
DMSO	100	0	0
Paclitaxel 2 nM	80	0	20
MLN8237 50 nM	30	49	21
MLN8237 50 nM and paclitaxel 2 nM	0	37	63
Paclitaxel 30 nM	0	18	82

Table 4-2: Fate of T24 daughter cells following first mitosis in cells exposed to drug treatments as labelled.
For each of the cells that divided, one daughter cell was selected at random and its fate determined, n=30.

4.3.1.2 Live cell imaging in ARPE-19 cells

Previous experiments had shown growth inhibition with paclitaxel 2 nM alone in the SRB assay in ARPE-19 cells (39±14%) (Figure 4-5). Here although the average mitotic duration significantly increased (to a similar extent to that seen in T24) from 39±6 minutes in DMSO to 166±137 minutes, only one abnormal division was observed and no cell death (Figure 4-11 and Table 4-3). Although these cells successfully divided, 8% of the daughter cells died in the subsequent mitosis and 51% did not divide whilst appearing viable (Table 4-4). MLN8237 50 nM did not extend time in mitosis to the same degree (74±47 minutes) and little abnormal division was observed (Figure 4-11 and Table 4-3), although again the daughter cells were affected with 5% dying and 42% appearing viable but not dividing again (Table 4-4).

With the combination, time in mitosis was extended to 279±255 minutes (a shorter duration to that seen in T24 cells), with 50% of divisions aberrant (Figure 4-11 and Table 4-3). Whilst only 2% of the daughter cells divided again, the majority appeared viable but not dividing and only 17% died (Table 4-4), in contrast to T24 cells where 63% of cells died. It was particularly striking that with both the combination and paclitaxel 30 nM treated cells, no mitotic death was seen in the initial mitosis whereas the treatments had induced 23% and 43% cell death respectively in T24 cells. In the paclitaxel 30 nM treated cells, this was despite mitosis being extended much further (1050±497 minutes) (Figure 4-11 and Table 4-3). However, aberrant division occurred in 67% of cells exposed to paclitaxel 30 nM and none of the daughter cells divided again, although 38% appeared viable. There was a difference in the fate of daughter cells when the combination treatment was compared to paclitaxel 30 nM between the two cell lines. A greater proportion of ARPE-19 cells appeared viable (81% vs 37% of T24 cells) with the combination and compared to paclitaxel 30 nM (38% still appeared viable compared to 18% of T24 cells).

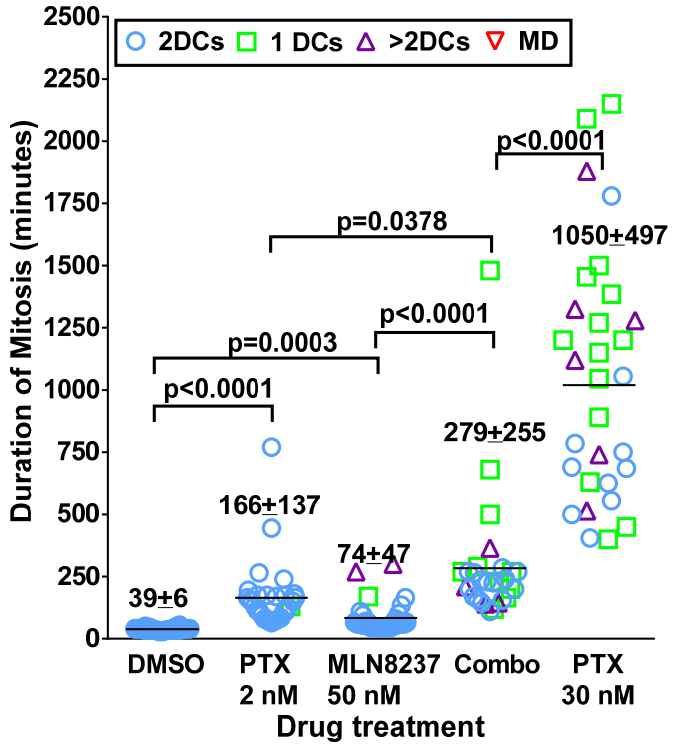

Figure 4-11: ARPE-19 live cell imaging.
ARPE-19 cells were seeded in Ibidi 8-chamber slides at 5000 cells/chamber. After 24h, cells were exposed to drugs as labelled (Combo=combination of MLN8237 50 nM and paclitaxel 2 nM) and sent for 72h live cell imaging detection with five minutes gap between frames. For each treatment, 30 cells were counted and the fate of cells using the four categories illustrated in Figure 4-8 is shown. The duration of mitosis is defined as the time between nuclear envelope breakdown and chromatin decondensation and is shown for each treatment together with SD. The p value was calculated using the two-column t-test in Graphpad Prism.

Cell fate	DMSO	Paclitaxel 2 nM	MLN8237 50 nM	Combination	Paclitaxel 30 nM
2 DCs (%)	100	97	93	50	33
1 DCs (%)	0	3	3	37	47
>2DCs (%)	0	0	4	13	20
MD (%)	0	0	0	0	0

Table 4-3: Proportion of cell fates for each ARPE-19 cell entering mitosis for each drug treatment. Fate of cells determined according to the categories in Figure 4-8 (two daughter cells (2DCs), only one daughter cell (1 DCs), division with more than two daughter cells (>2DCs) or mitotic death (MD)), with 30 cells were counted for each treatment. Drug treatments as labelled, combination=MLN8237 50 nM and paclitaxel 2 nM.

Drug treatment	Divide again (%)	Viable, no division (%)	Dead (%)
DMSO	100	0	0
Paclitaxel 2 nM	41	51	8
MLN8237 50 nM	53	42	5
MLN8237 50 nM and paclitaxel 2 nM	2	81	17
Paclitaxel 30 nM	0	38	62

Table 4-4: Fate of ARPE-19 daughter cells following first mitosis in cells exposed to drug treatments as labelled.
For each of the cells that divided, one daughter cell was selected at random and its fate determined (n=30).

The combination was less toxic to the ARPE-19 cells than the T24 cells, raising the possibility that in ARPE-19 cells although mitosis is still significantly prolonged, the cells remain viable after drug exposure with the opportunity to recover whereas T24 cells are more likely to die in subsequent cell divisions. This is consistent with observations by others. When non-transformed human RPE-1 cells are exposed to low concentrations of paclitaxel 5 nM, mitosis is prolonged but 99% of cells survived, by constructing abnormal but functional spindles which were able to satisfy the SAC, and allow subsequent aneuploid division in 90% daughter cells (275). Further experiments confirmed a differential response between cancer cell lines such as HeLa and U2OS and non-transformed RPE-1 cells. The cancer cell lines were less likely to survive their first mitosis when exposed to microtubule poisons and even those that were able to satisfy the SAC are more likely to die shortly after entering the next G1 (268, 269).

4.3.2 Immunostaining in T24 and ARPE-19 cells exposed to MLN8237 and paclitaxel

To further explore the observations that non-transformed cell lines were better able to construct functional bipolar spindles than cancer cell lines, immunostaining was used to investigate the spindles and centrosomes of the T24 and ARPE-19 cells exposed to the same drug treatments.

4.3.2.1 Immunostaining in T24 cells

When the mitotic cells were assessed, 80% of cells exposed to DMSO underwent a normal bipolar mitosis (Figure 4-12). In contrast paclitaxel 2 nM alone was sufficient to induce acentrosomal multipolar mitosis (62% of mitotic cells vs 17% in DMSO control), with an example of a multipolar division, with three poles but only two centrosomes (CDK5RAP2 spots) shown in Figure 4-12 A. MLN8237 50 nM also led to abnormal mitosis but here 52% of cells were monopolar and 24% multipolar. With both the combination and paclitaxel 30 nM, no bipolar division was seen, with the majority of divisions multi-polar (80% and 92% respectively) (Figure 4-12).

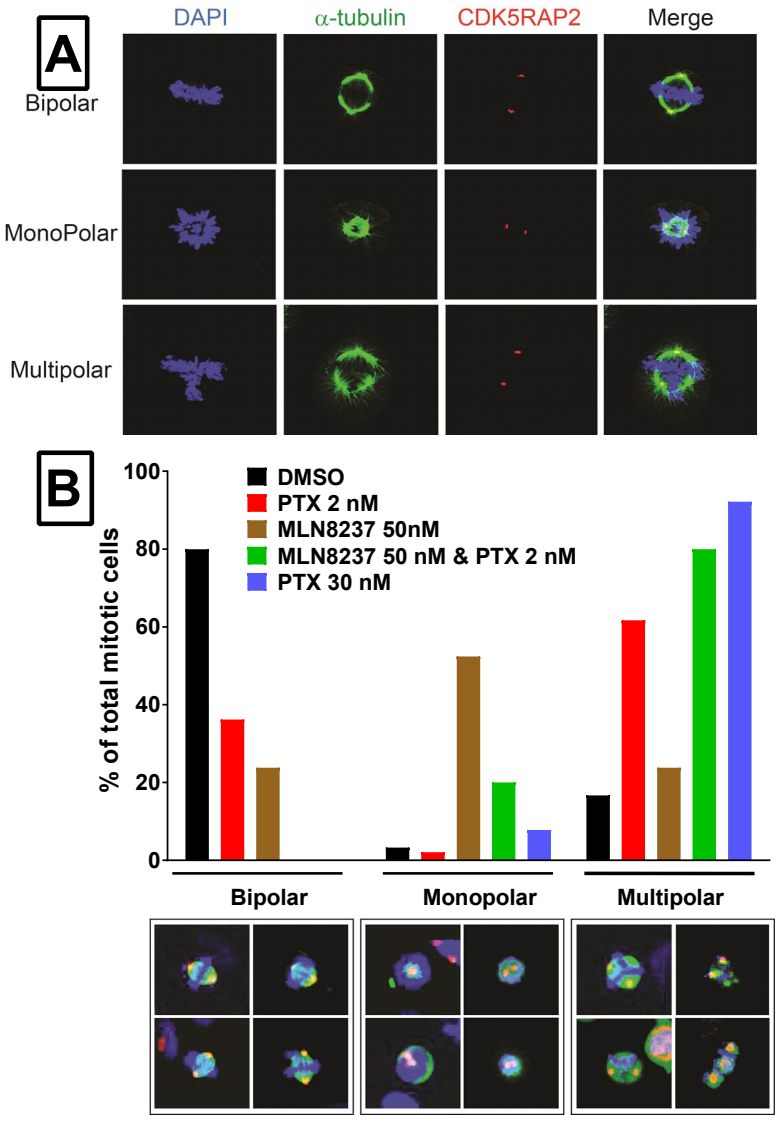

Figure 4-12: Percentage of total mitotic T24 cells exposed to drug treatments as labelled.
A total of 5000 cells were seeded in eight-well Ibidi slides and treated with the indicated drugs for 24 hours before immunofluorescent detection of CDK5RAP2 (red), α-tubulin (green) and DAPI (blue). Representative images of bipolar, monopolar and multipolar mitoses are shown in A. The proportions of cells in different stages were calculated using CompuCyte Icys® imaging cytometer and are shown in B together with further merged images of each cell fate captured by Icys®. At least 30 cells were counted for each treatment. Immunostaining performed by Dr Yao Lin. Abbreviation: PTX=paclitaxel.

When the nuclei of interphase cells were examined, aberrant nuclei were seen even in DMSO cells (19%) but the proportion increased with the drug treatments- 44% with paclitaxel 2nM, 58% with MLN8237 50 nM, 72% with the combination and 93% with paclitaxel 30 nM (Figure 4-13).

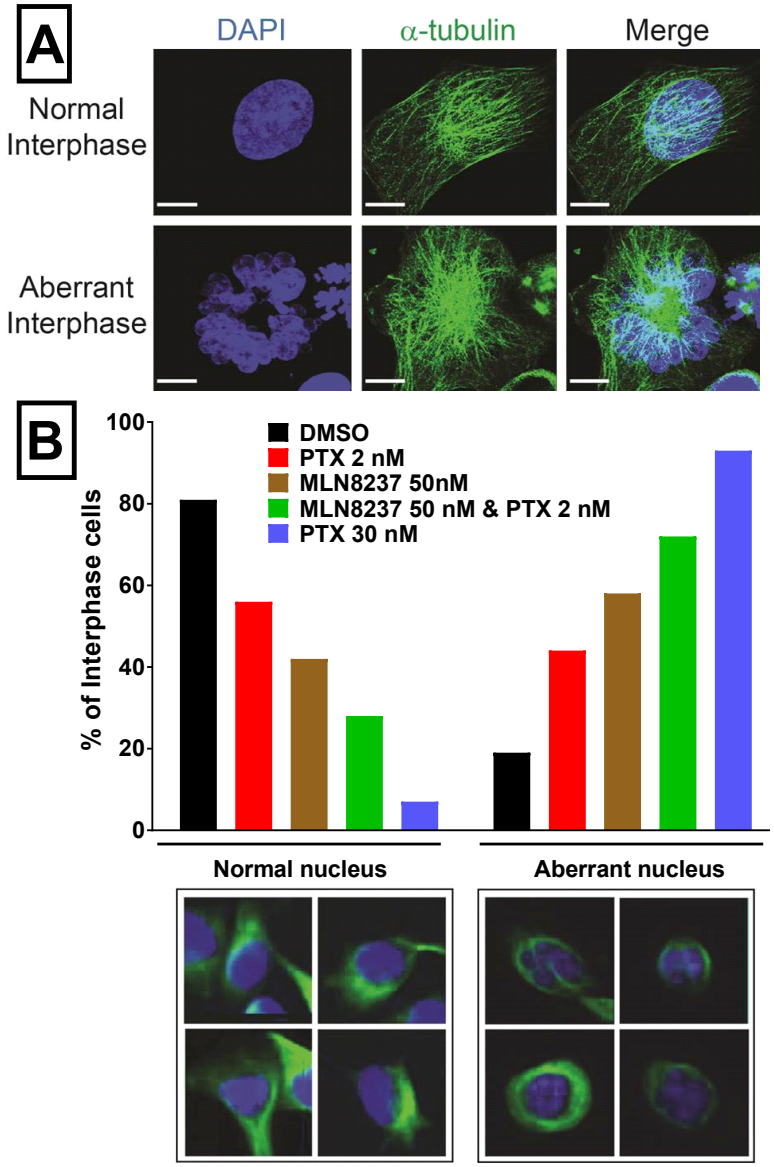

Figure 4-13: Percentage of T24 in interphase with normal or aberrant nuclei following exposure to drug treatments as labelled.
A total of 5000 cells were seeded in eight-well Ibidi slides and treated with the indicated drugs for 24 hours before immunofluorescent detection of α-tubulin (green) and DAPI (blue). Representative images of normal and aberrant nuclei are shown in A. The proportions of cells that were the products of aberrant division were calculated using CompuCyte Icys® imaging cytometer and are shown in B together with further merged images of each cell fate captured by Icys®. At least 30 cells were counted for each treatment. Immunostaining performed by Dr Yao Lin. Abbreviation: PTX=paclitaxel.

In summary, the combination of paclitaxel 2nM and MLN8237 50nM was shown to greatly induce multipolar mitosis and abnormal interphase nuclei formation in T24 cells, achieving similar effects as paclitaxel 30nM.

4.3.2.2 Immunostaining in ARPE-19 cells

Paclitaxel 2 nM and MLN8237 50 nM as single agents led to largely bipolar divisions (77% and 71% respectively compared to 90% in DMSO control) (Figure 4-14). With the combination this fell to 39%, with the aberrant divisions being either mono- or multi-polar, and paclitaxel 30 nM showed the greatest change with only 17% bipolar divisions (Figure 4-14).

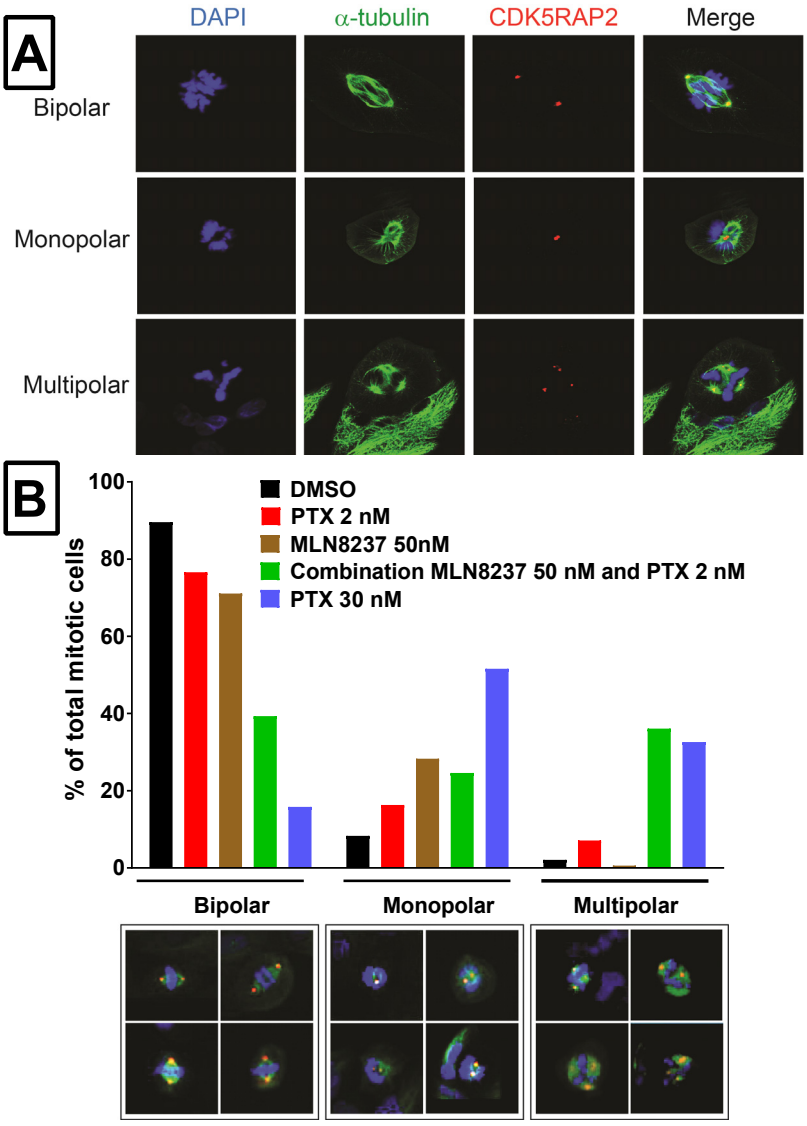

Figure 4-14: Percentage of total mitotic ARPE-19 cells exposed to drug treatments as labelled.
A total of 5000 cells were seeded in eight-well Ibidi slides and treated with the indicated drugs for 24 hours before immunofluorescent detection of CDK5RAP2 (red), α-tubulin (green) and DAPI (blue). Representative images of bipolar, monopolar and multipolar mitoses are shown in A. The proportions of cells in different stages were calculated using CompuCyte Icys® imaging cytometer and are shown in B together with further merged images of each cell fate captured by Icys®. At least 30 cells were counted for each treatment. Immunostaining performed by Dr Yao Lin. Abbreviation: PTX=paclitaxel.

However, the proportion of cells undergoing bipolar division despite exposure to the combination or paclitaxel 30 nM differs to the result in T24 cells where no bipolar

divisions were seen (Figure 4-12). Although less aberrant nuclei were seen with the single agents paclitaxel 2 nM (36%) and MLN8237 (26%) compared to T24 cells, 74% were observed with the combination, compared to 91% with paclitaxel 30 nM (Figure 4-15), similar to T24 cells (Figure 4-13). Hence whilst the combination and paclitaxel 30 nM treatments did not induce the same degree of multi-polar division in ARPE-19 as in T24 cells, the results of the interphase cells are very similar, with aberrant nuclei.

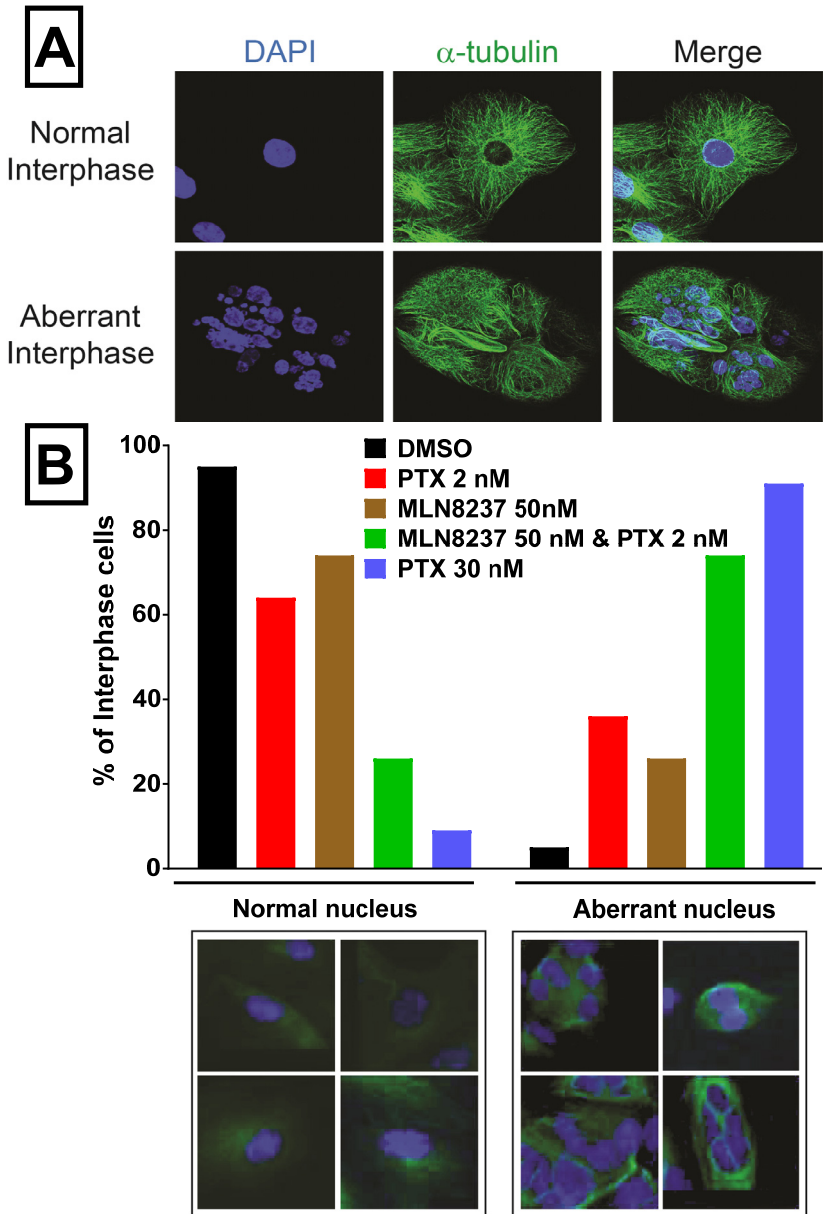

Figure 4-15: Percentage of ARPE-19 cells in interphase with normal or aberrant nuclei following exposure to drug treatments as labelled.
A total of 5000 cells were seeded in eight-well Ibidi slides and treated with the indicated drugs for 24 hours before immunofluorescent detection of α-tubulin (green) and DAPI (blue). Representative images of normal and aberrant nuclei are shown in A. The proportions of cells that were the products of aberrant division were calculated using CompuCyte Icys® imaging cytometer and are shown in B together with further merged images of each cell fate captured by Icys®. At least thirty cells were counted for each treatment. Immunostaining performed by Dr Yao Lin. Abbreviation: PTX=paclitaxel.

4.3.3 Summary of data in ARPE-19 and IMR-90 cell lines

With the combination of an AK-A inhibitor and paclitaxel, no synergy was seen in ARPE-19 or IMR-90 cells in the SRB assay but the combination did still reduce cell growth and long term viability as assessed by IncuCyte™ and colony forming assays. Others have commented that under experimental conditions where a significant proportion of cells die in the first mitosis (as seen here), many of the cell based assays traditionally used, where cancer cell lines are exposed to drugs for up to 72 hours, may be contaminated with dead or dying cells (269). Hence live cell imaging offers the best opportunity to assess early drug response. This showed a differential response, with more ARPE-19 cells remaining viable after exposure to the combination than T24 cells. Immunostaining confirmed ARPE-19 cells exposed to the combination were able to undergo bipolar mitotic division, whereas no T24 cells could. However, a similar proportion of cells in interphase with aberrant nuclei were seen. The reason for this may centre around the mechanism by which centrosomes become clustered (hence leading to bipolar mitosis) in the two cell lines. The T24 cell line has been recently reported to have 23% aberrant centrosomes (276) but further experiments to explore this were not performed in this work.

Since these experiments were performed, clinical trials of single agent MLN8337 have largely shown dose-limiting haematological rather than epithelial cell toxicity. For example, in a large Phase 2 study the most common Grade 3-4 toxicities were neutropenia (43%) and leucopenia (21%) compared to stomatitis (8%) or diarrhoea (1%) (211). This suggests that although ARPE-19 cells may be able to give some information about normal cell toxicity, the effect of the combination on the bone marrow may be the most relevant.

4.4 Myelotoxicity of combination of AK-A inhibitors and paclitaxel

Given the incidence of neutropenia seen with AK-A specific AKI in clinical trials, I investigated the impact of the combination of an AK-A inhibitor with paclitaxel compared to the high-concentration single-agent paclitaxel on the bone marrow using the CFU-GM assay with human bone marrow cells. Firstly the single agent dose responses of paclitaxel, CYC3 and MLN8237 were assessed (Figure 4-16). These experiments were performed with Dr Yao Lin, who assisted with the manual colony counting (CYC3 data published in (258)).

With single agent paclitaxel, there is a steep dose response in colony inhibition from 3 nM to 10 nM (GI_{50} 10 nM, Figure 4-16), consistent with previous reports (258, 277, 278). Shallower dose response curves are seen with CYC3 and MLN8237 and the GI_{50} are slightly lower to those in T24 cells (CYC3 1100 nM compared to 1900 nM and MLN8237 20 nM compared to 30 nM, Figure 4-16).

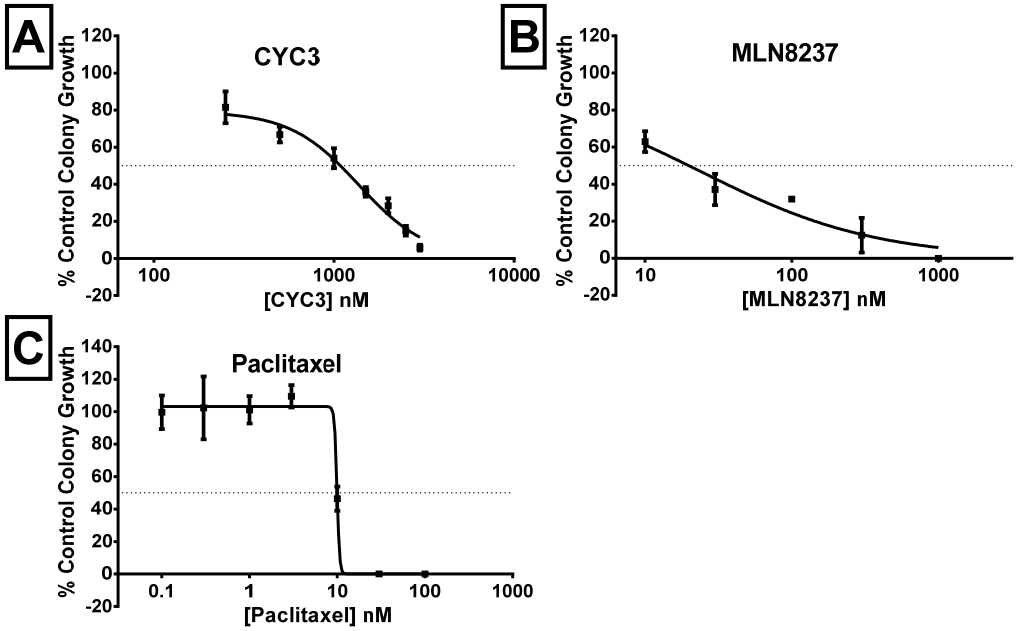

Figure 4-16: CFU-GM assay for CYC3, MLN8237 and paclitaxel.
Human bone marrow cells were exposed to a range of concentrations of A. CYC3 B. MLN8237 and C. paclitaxel for 14 days in CFU-GM assays. Each graph shows the data for percentage control colony growth at each concentration of three replicates with SD and then a curve fitted to the data using GraphPad Prism. The dotted line shows 50% colony growth and this was used to identify the GI_{50} from the graph.

Having confirmed the sensitivity of bone marrow cells to paclitaxel, I next investigated combinations of CYC3 and MLN8237 with paclitaxel. Concentrations of paclitaxel ranging from 1-3 nM were used, which showed little impact on colony growth as a single agent (Figure 4-17). Whereas no colonies survived with paclitaxel 30 nM treatment, the combinations with CYC3 and paclitaxel were less toxic, with similar colony numbers to those seen with the single agent CYC3 (Figure 4-17 A and B). For the MLN8237 and paclitaxel combinations, more colonies actually survived than with the single agent MLN8237 (Figure 4-17 C-F), reaching significance for MLN8237 100 nM with paclitaxel 1 nM ($p=0.0019$) and MLN8237 100 nM and paclitaxel 3 nM

(p=0.026).

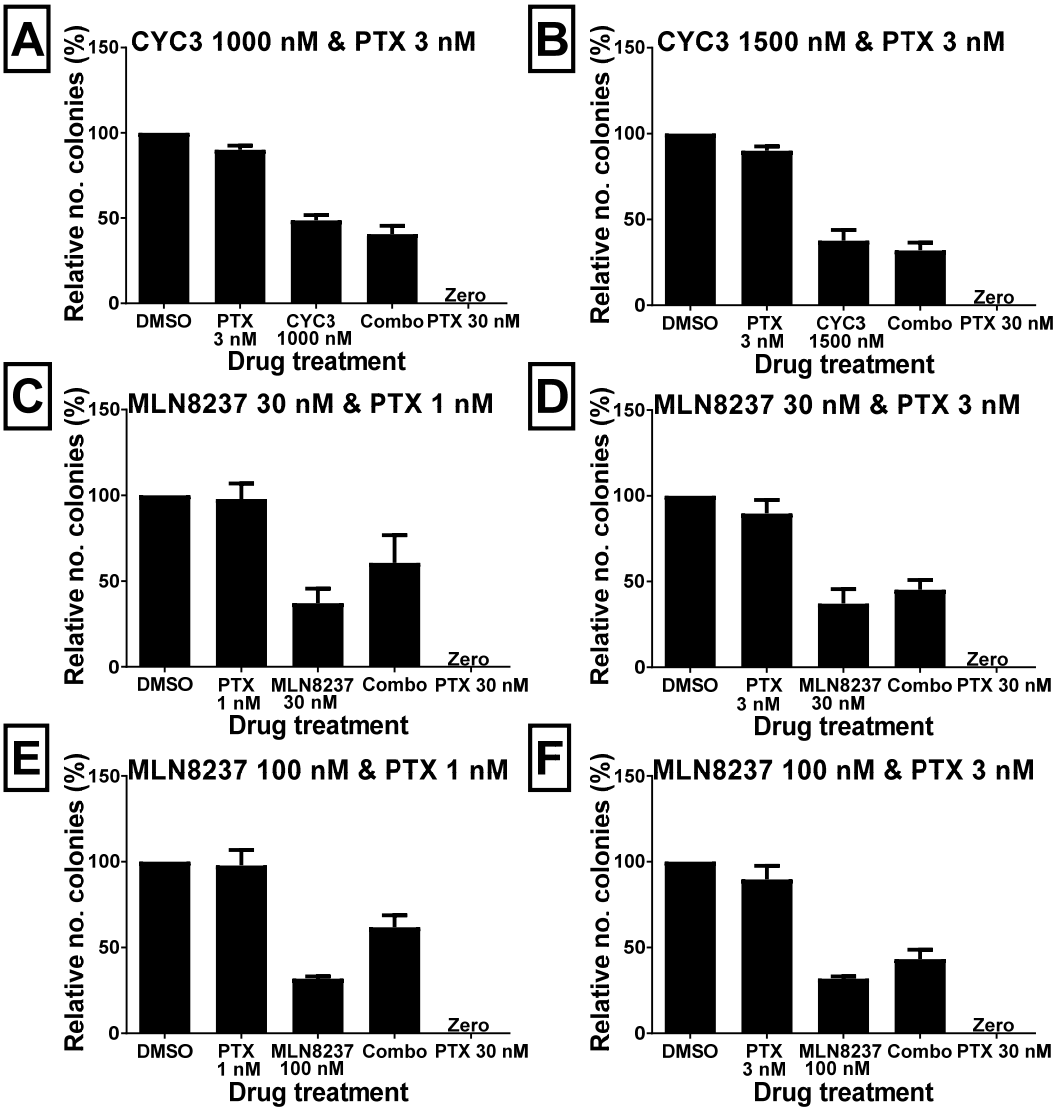

Figure 4-17: CFU-GM assay results for combinations of CYC3 or MLN8237 together with paclitaxel.
Human bone marrow cells were treated with the combination of A. CYC3 1000 nM and paclitaxel 3 nM B. combination of CYC3 1500 nM and paclitaxel 3 nM C. MLN8237 30 nM and paclitaxel 1 nM D. MLN8237 30 nM and paclitaxel 3 nM E. MLN8237 100 nM and paclitaxel 1 nM F. MLN8237 100 nM and paclitaxel 3 nM. No colonies grew in the presence of paclitaxel 30 nM. These data are the mean of three replicates with SD. The p value was calculated using the two-column t-test in Graphpad Prism. Abbreviations: PTX=paclitaxel, combo=combination of AKI and paclitaxel as labelled in graph title.

Hence whereas the combinations of AK-A specific inhibitors with low concentrations of paclitaxel showed synergistic cytotoxicity in cancer cell lines, antagonism was seen in the CFU-GM assay when MLN8237 was combined with low concentrations of paclitaxel. Whilst in cancer cells the combination could be as effective as high concentration paclitaxel, high dose paclitaxel is much more toxic than the combination in the CFU-GM assay. This suggests there may be reduced clinically relevant toxicity with the combination, compared to high dose single agent taxanes.

4.5 Summary of chapter

Comparing the effect of CYC3 and MLN8237 in two non-transformed cell lines in the SRB assay suggested that rather than the synergy seen in some bladder cancer cell lines, an additive or even antagonistic effect may be seen with the combination of an AK-A inhibitor and paclitaxel. However, subsequent IncuCyte™ imaging showed the final cell confluency with the combination at endpoint was suppressed to a greater extent than expected, comparable to that seen in T24 cells, and with the colony forming assay, very few colonies survived. This suggests that there may not be a large therapeutic window.

Live cell imaging in T24 and ARPE-19 cells demonstrated a differential response, with more cells remaining viable after exposure to the combination in ARPE-19 cells compared to T24 cells, as discussed in 4.3.3. Further analysis to track the cell cycle phase in more detail (particularly to clarify the mitotic status of those labelled in our analysis as "one daughter cell") could include use of techniques such as FUCCI-labelling of cells. Immunostaining confirmed less non-bipolar cell division in ARPE-19 cells than T24, despite a similar degree of aberrant nuclei in interphase, suggesting the potential for more normal cells to recover after exposure to these drugs. These results suggest that the combination may be more able to effectively target transformed cells with a lesser effect on normal cells, compared to a higher concentration of single agent paclitaxel.

Although ARPE-19 cells are non-transformed and have been used in many studies as a model, the process of isolating and culturing cells causes adaptation to culture conditions (279), and it remains to be determined how valid this cell line is as a model for toxicity testing and predicting clinical effects. Efforts have previously been made to develop *in vitro* toxicity assays for predicting therapeutic index, made harder by the difficulty of culturing primary cells. When a panel of four types of normal cells (renal (HRPTEpiC), epithelial (hTERT-RPE1), lymphocyte and FMCA-GM14 (CD34(+) progenitor cells)) was tested against anti-cancer drugs, they were shown to largely reflect known clinical renal and bone marrow toxicity profiles (280). These may form an increasing part of the assessment of new drugs prior to their translation to the clinic, as may the use of new organoid models for toxicity testing (281).

Given the haematological toxicity seen with MLN8237 as a single agent, the results of the CFU-GM assay were promising, indicating that the MLN8237 combination with low concentration paclitaxel may be less myelotoxic than higher paclitaxel as a single agent. However, whilst the assay has been validated and shown to have a high

predictive potential, there are technical issues with the method. A prolonged incubation period is required to allow colonies to grow to a sufficient size to be counted, and this has to be in the continued presence of drug because the cells cannot be washed and re-plated. Thus the assay does not reflect clinical pharmacokinetics of the drugs being tested. Scoring is done manually using an inverted microscope, which can be difficult, with considerable inter-individual variability, and heterogeneity in colony morphology. Although media and growth factors were selected to optimise the growth of CFU-GM colonies and specifically looked for their distinctive appearance, it is possible that other progenitors were also represented in these colony counts. The viscosity of the MethoCult™ medium also made analysis of images using GelCount difficult, but this was the best equipment available to us at the time. Stem Cell Technologies have now developed the STEMvision™ automated instrument and computer system, which has shown promise in standardising counts. Other techniques to model chemotherapy-induced myelosuppression have been published (282) but most models require *in vivo* data. A specific model for MLN8237 in combination with docetaxel has now been developed, discussed in 7.5.2 (283).

I have now not only demonstrated synergy in bladder cancer cell lines with the combination of two different AK-A inhibitors with low concentrations of paclitaxel (in Chapter 3) but also identified a potential differential response between cancer and non-cancer cells. A potential factor that may influence both the specificity and selectivity of the combination may be the extent of AK-A expression in the cell lines, which could be a potential biomarker to test in future *in vivo* studies and this will therefore be explored next.

5 *EXPLORING THE INFLUENCE OF AK-A EXPRESSION ON RESPONSE TO AKI AND PACLITAXEL*

5.1 Introduction

The work in previous chapters has demonstrated synergy with MLN8237 and paclitaxel in some bladder cancer cell lines, which appears to be selective compared to a non-cancer cell line. This is similar to the effect we observed with CYC3 in both bladder and pancreatic cancer cells (258), suggesting the synergy between AK-A inhibition and low concentration paclitaxel may apply to multiple tumour types. I investigated whether the extent of AK-A expression in the cell lines contributed to sensitivity to the drug combination. An *in vitro* cell model was created to assess in more detail the effect AK-A over-expression had on the response to taxanes.

Contribution of others to this experimental work: Dr David Perera assisted with the creation of the HeLa AK-A inducible cell line (5.3.1). Dr Siang Boon Koh performed the immunofluorescence experiment shown in Figure 5-4 *and the live cell imaging experiments in 5.3.3 were performed and analysed with him.*

5.2 Relative levels of AK-A in the cell lines tested

The AK-A expression in the bladder cancer cell line panel I used has not been published. Therefore, to explore the relationship between the relative baseline level of AK-A in the cell lines tested and whether there was any correlation with the dose response curves seen in Chapter 3, I compared the relative AK-A expression in the cell lines used in this work using Western blotting.

The total AK-A signal was relatively low in all the bladder cancer cell lines and in ARPE-19 cells compared to HeLa cells (Figure 5-1). The signal in J82 cells was higher than in the other bladder cancer cell lines – this may have contributed to its insensitivity to AK-A inhibitors (GI_{50} not reached with either CYC3 or MLN8237). However, the AK-A signal was similar between the T24 and HT1197 cell lines, yet for MLN8237, the GI_{50} in the T24 cell line was 30 nM and it was not reached in HT1197 cells. There did not appear to any relationship to cell line doubling time.

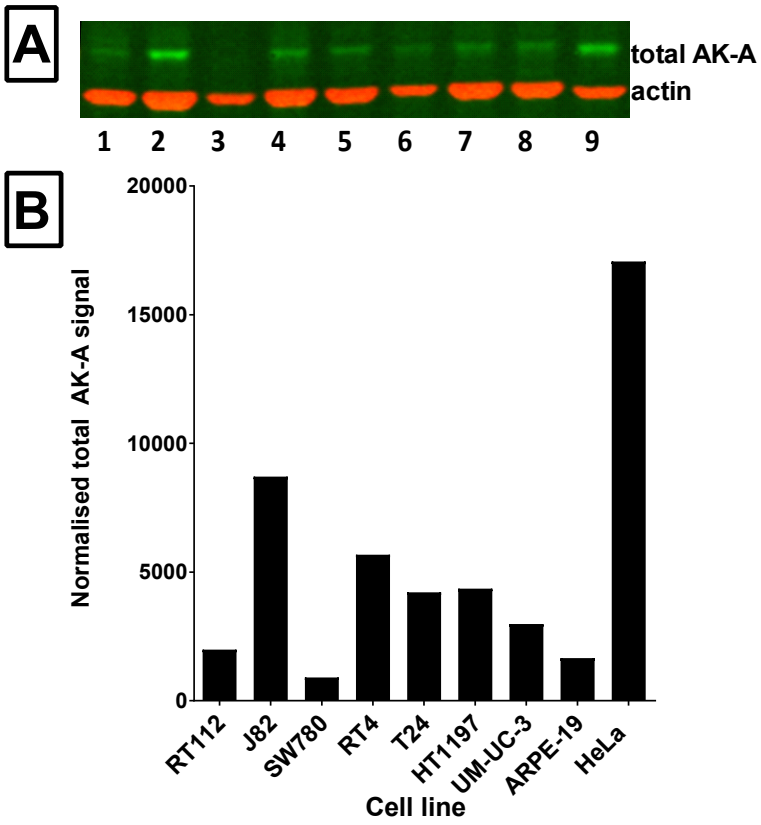

Figure 5-1: Total AK-A quantification in cell lines tested as labelled.
Cells were grown for 24 hours before harvesting and preparation. A. shows Western blot for total AK-A. Cell lines are 1. RT112, 2. J82, 3. SW780, 4. RT4, 5. T24, 6. HT1197, 7. UM-UC-3 8. ARPE-19 9. HeLa. Actin used as loading control. B. shows total AK-A signal for each signal normalised to its actin signal using Image Studio.

Others have reported only a weak association between the level of AK-A in cell lines and response to pan-AKI (265). Given this apparent lack of correlation and to investigate this further, I created a cell line where it was possible to induce expression of AK-A.

5.3 Use of *in vitro* HeLa cell model to assess AK-A over-expression

5.3.1 Creation of HeLa AK-A inducible cell line

Whilst I would have liked to use a bladder cancer cell line for this model, it proved difficult to source an appropriate parent line. Therefore, a tetracycline inducible HeLa cell line was created with the assistance of Dr David Perera and with the gift of constructs from Professor Stephen Taylor. A Myc tag allowed the inducible AK-A to be identified on Western blots. A pooled sample and individual clones were tested to select the cell line with the greatest inducible AK-A expression and conditions were optimised for experiments.

Early time point experiments showed that following addition of doxycycline, induced AK-A signal started to rise at two hours and was strongly present from four hours (Figure 5-2). Concentrations of both 1 µg/ml and 2 µg/ml doxycycline produced a similar degree of AK-A expression.

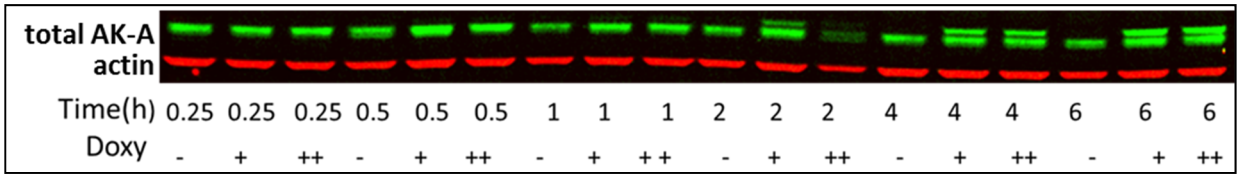

Figure 5-2: Western blot showing total AK-A (green channel) with actin as control (red channel). Endogenous AK-A is a green band in all samples, the doxycycline-inducible AK-A appears as a larger band due to the Myc-tag. Experiment shows AK-A levels at 0.25, 0.5, 1, 2, 4 and 6 hours either without doxycycline or with doxycycline 1 µg/ml (indicated as +) or 2 µg/ml (indicated as ++). Note: technical issue with the 2 hour 2 µg/ml doxycycline sample, which was not seen in repeat experiments.

When the degree of AK-A induction was assessed at 24, 48 and 72 hours, maximal expression of exogenous AK-A was achieved by 24 hours, such that the sum of the exogenous and endogenous levels of AK-A was five times that of the non-induced cells (Figure 5-3). By 72 hours, the signal fell to around two-fold above baseline and similar expression was seen at 96 hours. Re-induction with the addition of fresh doxycycline every 24 hours did not make a significant difference to the degree of AK-A expression seen. Overall the expression of AK-A in the induced cells was at least two fold for 96 hours.

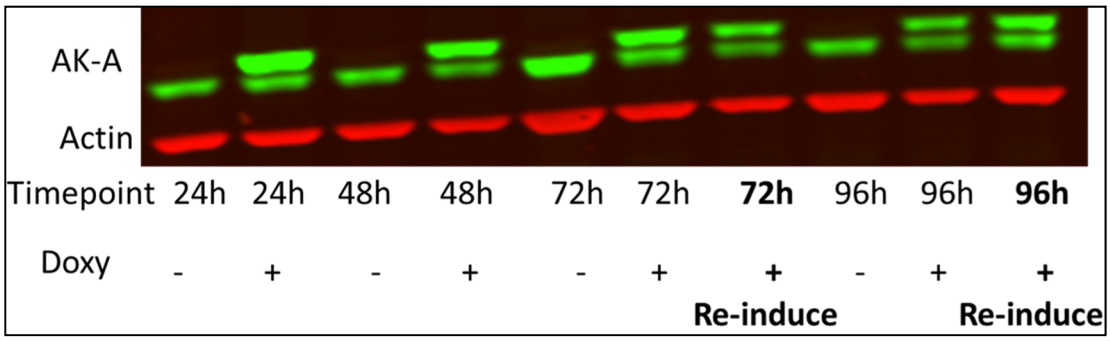

Figure 5-3: Western blot showing total AK-A (green channel) with actin as control (red channel). The doxycycline-inducible AK-A appears as a larger band than the endogenous due to the Myc-tag. Experiment shows AK-A levels at 24, 48, 72 and 96 hours with and without doxycycline and the effect of re-induction with repeated dosing of doxycycline every 24 hours on levels at 72 and 96 hours.

Immunofluorescence showed that AK-A over-expression and presence of the Myc-tag did not affect protein localisation, with the Myc tag co-localised with AK-A in the over-expressing (induced) cells, and its location at the mitotic spindle poles matching that of AK-A in the non-induced cells (Figure 5-4, experiment performed by Dr Siang Boon Koh).

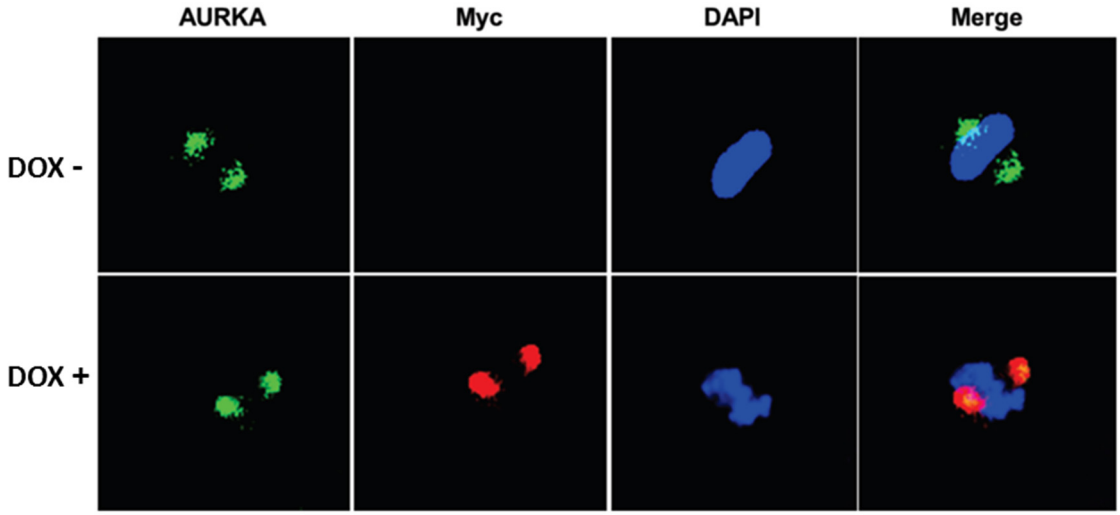

Figure 5-4: Immunofluorescence staining of mitotic HeLa AK-A inducible cells with and without doxycycline.
Cells stained for AK-A, Myc, DAPI and then merged images. Experiment performed and images processed by Dr Siang Boon Koh. Abbreviation: DOX=doxycycline

Therefore, given reports of two to five fold increase of AK-A expression in most cancer cell lines (123), the HeLa AK-A inducible cells should be a physiologically relevant *in vitro* model to use further.

5.3.2 Effects of AK-A over-expression on sensitivity to MLN8237 and paclitaxel

5.3.2.1 Single agent response curves in HeLa AK-A inducible cells

To ensure that the effects on HeLa AK-A inducible cells of drug treatments in the SRB assay were assessed during the time period when AK-A expression was elevated, cells were plated as normal and left overnight. Doxycycline was added the following day, followed by the drugs of interest four to six hours later as induced AK-A expression was rising.

When MLN8237 and paclitaxel were assessed as single agents, the IC_{50} and GI_{50} were not significantly different between the cells with or without AK-A over-expression for either drug after 72 hours (Figure 5-5 and Table 5-1).

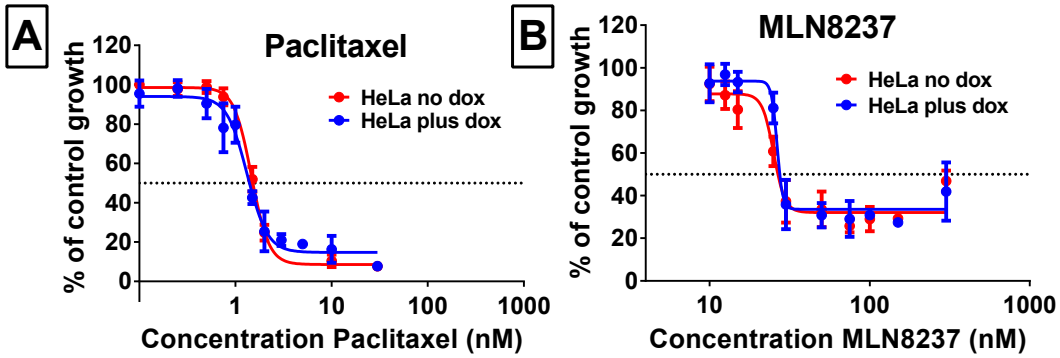

Figure 5-5: Dose response curves for HeLa AK-A inducible cells, with and without induction of AK-A expression with doxycycline.
Cells were exposed to a range of concentrations of A. Paclitaxel B. MLN8237 for 72 hours, then analysed using SRB assay. Each graph shows the data for percentage control cell growth at each concentration of at least three replicates with SD and then a curve fitted to the data using GraphPad Prism to calculate IC_{50}. The dotted line shows 50% cell growth and this was used to identify the GI_{50} from the graph. Abbreviation: Dox=doxycycline.

Drug	IC_{50} (nM)	GI_{50} (nM)
Paclitaxel (no dox)	1.3	1.4
Paclitaxel (plus dox)	1.5	1.5
MLN8237 (no dox)	25	26
MLN8237 (plus dox)	26	28

Table 5-1: IC_{50} and GI_{50} of paclitaxel and MLN8237 in HeLa AK-A inducible cell line.
Measured from dose response curves shown in Figure 5-5. Abbreviation: Dox=doxycycline.

I had expected AK-A over-expression would induce paclitaxel resistance based on previous reports (1.8.2). In the most cited publication, when mock transfected and AK-A over-expressing cells (reported to have level of expression of AK-A about five-fold greater than endogenous cells) were exposed to paclitaxel for 72 hours, less apoptosis was seen in the AK-A over-expressing cells; 45% with paclitaxel 150 nM in the AK-A overexpressing cells compared to 65% apoptotic cells in the mock transfected cells (2). However, the method of assessment was different from mine: the percentage of apoptotic cells (defined as sub G1 population) was calculated using propidium iodide staining and flow cytometry. Quantification of the sub G1 population is no longer accepted as a valid method for quantification of apoptotic cells, and the sensitivity to paclitaxel appears surprisingly low in that study. Despite these differences in study endpoint, I had expected that a cell line over-expressing AK-A would have been more resistant to an AK-A inhibitor such as MLN8237.

5.3.2.2 Combination of MLN8237 and paclitaxel in HeLa AK-A inducible cells using SRB assay

Next I explored whether there was a difference when both drugs were combined, in cells with and without the addition of doxycycline. Initially a concentration range

covering up to 30 nM paclitaxel was selected (images not shown) but as the cell growth inhibition at 2 nM was around 80%, this range did not allow scope to see any dose response to the combination and the narrow range of 0.1 to 2 nM was used.

In the HeLa AK-A inducible cells without doxycycline (Figure 5-6), a significant region of synergy was seen with the combination, with a maximum synergy score of 36±4 with paclitaxel 1 nM and MLN8237 15 nM, and 74±4% growth inhibition.

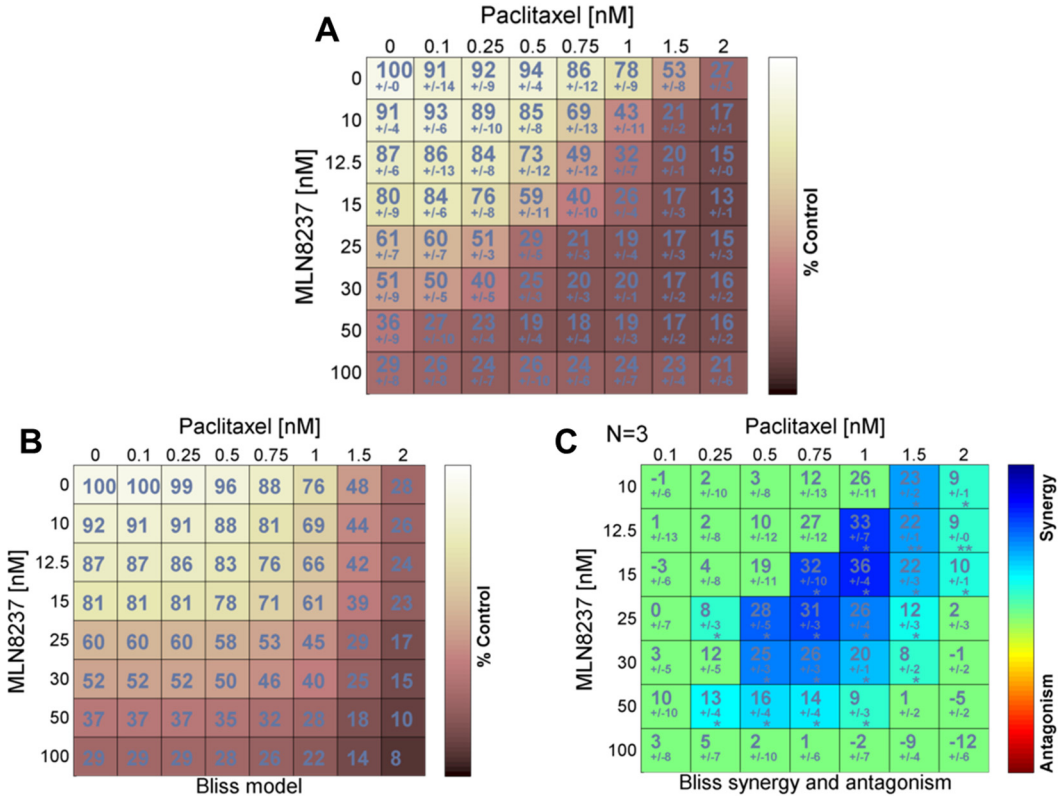

Figure 5-6: Combination of MLN8237 and paclitaxel in HeLa AK-A inducible cells without doxycycline.
HeLa AK-A inducible cells were seeded in 96-well plates and treated with eight x eight combinations of paclitaxel and MLN8237 for 72 hours.

With the addition of doxycycline to induce AK-A expression, synergy was still seen in the same region but to a slightly lesser extent (Figure 5-7), with a synergy score of 25±9 with paclitaxel 1 nM and MLN8237 15 nM and 66±9% growth inhibition. Thus AK-A over-expression may have resulted in cells being marginally more resistant to the synergistic combination, but there was no appreciable difference in the dose response curves to single agents, as measured by the SRB assay.

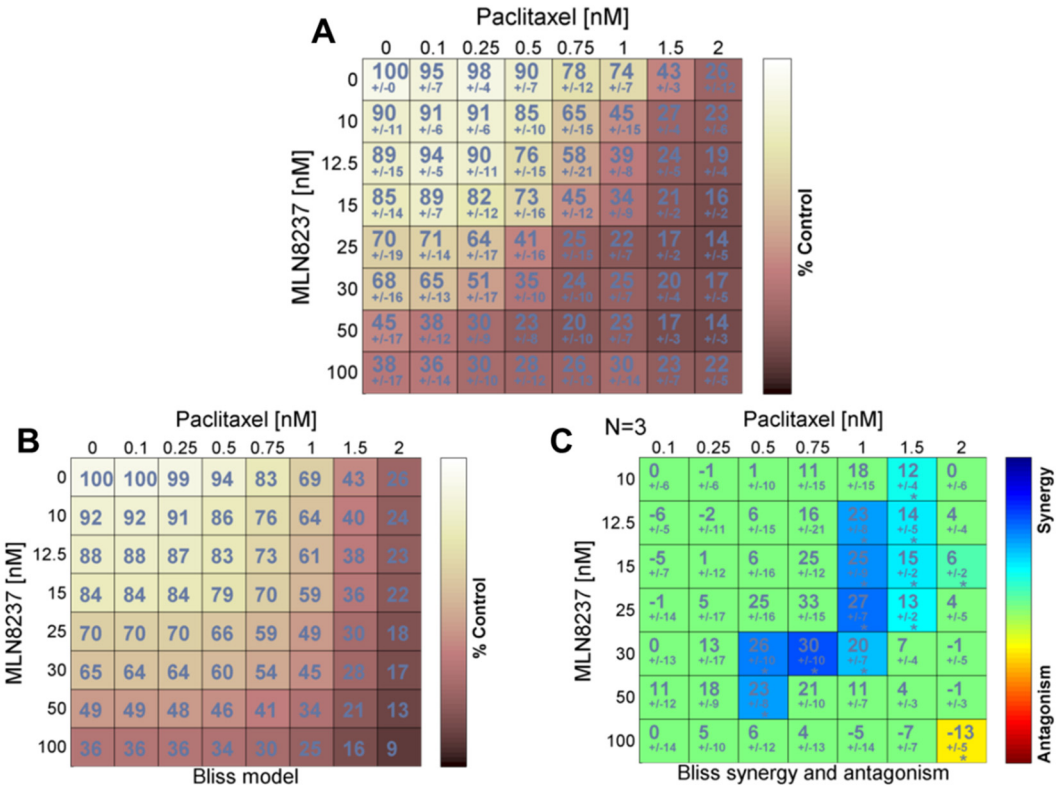

Figure 5-7: Combination of MLN8237 and paclitaxel in HeLa AK-A inducible cells with doxycycline.
HeLa AK-A inducible cells were seeded in 96-well plates and treated with eight x eight combinations of paclitaxel and MLN8237 for 72 hours.

5.3.2.3 IncuCyte™ imaging to assess effects of MLN8237 and paclitaxel in HeLa AK-A inducible cell line

Using IncuCyte™ imaging to directly determine the growth profile of the cells, concentrations of paclitaxel and MLN8237 around the region of synergy (paclitaxel 0.5, 0.75 and 1 nM and MLN8237 15, 25 and 30 nM) were tested as single agents and in combination, with the combination of paclitaxel 1 nM and MLN8237 15 nM shown (Figure 5-8).

The growth curves for the DMSO treated cells with or without doxycycline are very similar. For the paclitaxel single agent, the curves for 0.5 nM and 0.75 nM were also similar with a small growth advantage in the over-expressing cells (not shown) but after 24 hours there was a significant difference in the curves with paclitaxel 1 nM where the cells with doxycycline reached higher relative confluency at each timepoint (suggesting resistance to paclitaxel) ($p<0.0001$). Repeat experiments done by myself and Dr Siang Boon Koh confirmed that at concentrations of paclitaxel up to 3 nM, paclitaxel appeared to inhibit proliferation slightly less in the AK-A over-expressing cells than in the non-induced cells. At concentrations above this, almost total growth inhibition was seen even in the AK-A over-expressing cells.

Over-expression of AK-A did appear to lead to some resistance to the effect of MLN8237 with slightly higher confluency in the induced cells, illustrated here with MLN8237 15 nM ($p<0.0001$). However, the small growth advantage in the over-expressing cells exposed to the single agents was abolished with both the combination of MLN8237 15 nM and paclitaxel 1 nM and with paclitaxel 10 nM, with no significant difference seen in the cells over-expressing AK-A. Growth was suppressed in the combination after 24 hours with final cell confluency relative to DMSO of 19±6% in the induced cells vs 17±4%. The combination was almost as effective as paclitaxel 10 nM.

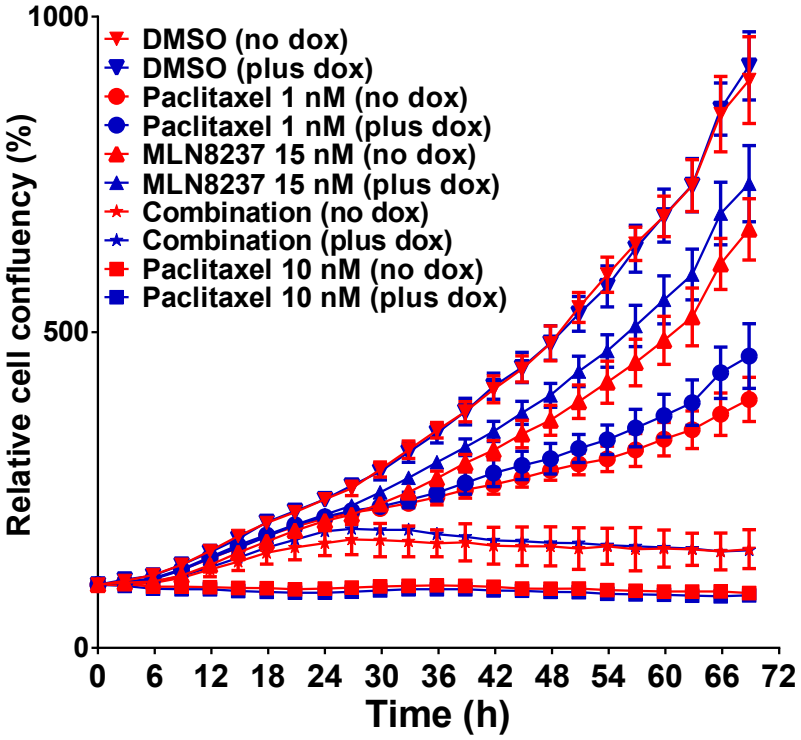

Figure 5-8: Relative cell confluency for HeLa AK-A inducible cells exposed to paclitaxel and MLN8237 as labelled.
HeLa AK-A inducible cells were seeded in 96-well plates and allowed to grow for 24 hours. They were then dosed with drugs as indicated and imaged using IncuCyte™ for 72 hours. Percentage confluency relative to the start of imaging was calculated and plotted for DMSO, paclitaxel 1 nM, MLN8237 25 nM, the combination and paclitaxel 10 nM (with and without doxycycline). These data are the mean of eight replicates with SD. Statistical analysis performed in GraphPad Prism using matched 2 way ANOVA over time. Abbreviation: Dox=doxycycline.

Thus, induced AK-A over-expression only caused a modest reduction in drug sensitivity with low concentrations of either paclitaxel or MLN8237 as single agents and did not significantly change sensitivity to the combination.

5.3.3 Live cell imaging in HeLa AK-A cells with paclitaxel

To investigate if there was a difference in longer term mitotic fate in the HeLa AK-A over-expressing cells, time-lapse microscopy was used to directly quantify the mitotic

duration of the HeLa AK-A cells with and without doxycycline induction. These experiments were devised and analysed together with Dr Siang Boon Koh.

Based on the differences seen with the IncuCyte™ data (Figure 5-8), paclitaxel 1 nM, 2 nM and 10 nM were selected. In cells treated with DMSO alone, the mitotic duration in the HeLa AK-A induced cells (54±20 minutes) was significantly shorter than that of the non-overexpressing cells (74±32 minutes) (p=0.0002), consistent with the hypothesis that over-expression of AK-A would allow cells to override the spindle assembly checkpoint (Figure 5-9). Paclitaxel 1 nM was sufficient to increase the average time in mitosis to a greater extent in non-induced (191±219 minutes) than induced cells (120±141), although considerable variability was seen. Mitotic duration was extended further with paclitaxel 2 nM to 205±194 minutes in non-induced versus 125±109 minutes in the induced cells. Paclitaxel 10 nM increased the time in mitosis compared to DMSO in cells both with (448±160 minutes) and without AK-A over-expression (502±167 minutes) but there was no significant difference between the groups.

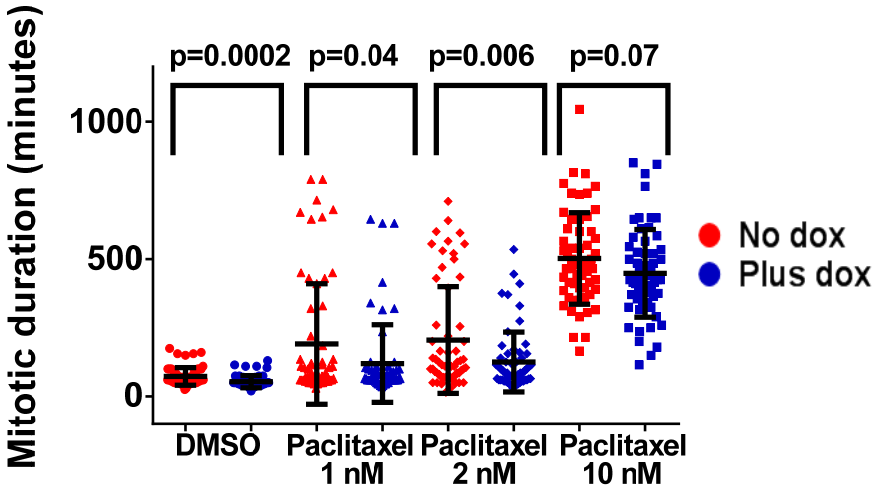

Figure 5-9: Mitotic duration of HeLa AK-A inducible cells with or without doxycycline in cells exposed to DMSO or paclitaxel.
Cells were seeded in eight-well Ibidi chamber slides (5000 cells/chamber) and DMSO or paclitaxel added 24 hours later. Imaging was performed using phase-contrast time-lapse microscopy every five minutes. Each dot represents a single cell with mean and standard deviation derived from three independent experiments, 60 cells in total for each condition. Mitotic duration was defined as the time between nuclear envelope breakdown and chromatin decondensation. Statistical analysis performed in GraphPad Prism and p value for unpaired t test comparing each treatment with cells with and without doxycycline in shown. Abbreviation: Dox=doxycycline.

A range of cell fates were seen (Figure 5-10), with a time in mitosis greater than 200 minutes associated with either aberrant/failed division or mitotic death (Figure 5-11).

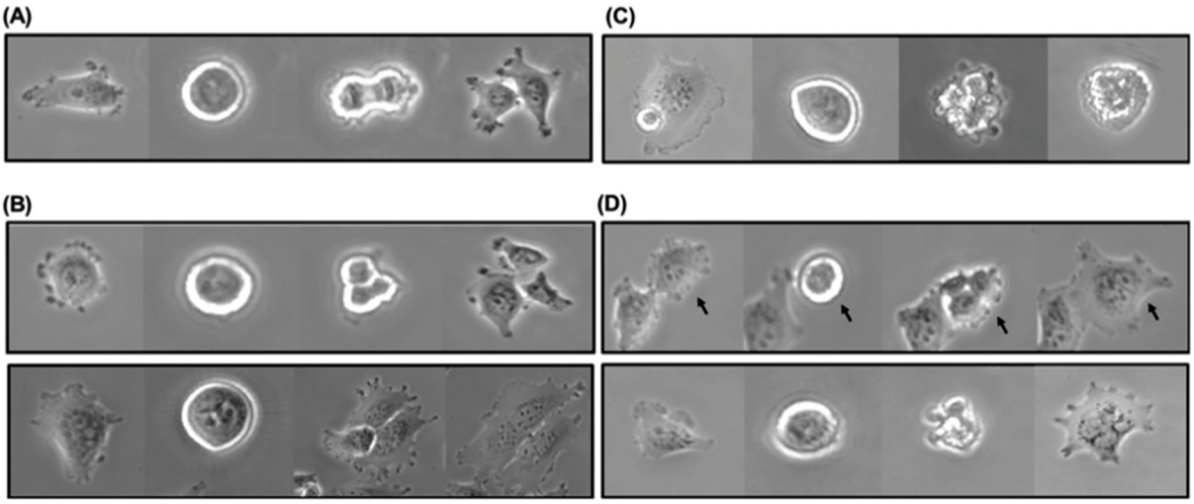

Figure 5-10: Representative photographic images of HeLa AK-A inducible cells undergoing different mitotic phenomena when exposed to paclitaxel 1 nM and paclitaxel 2 nM.
Images show A. normal division with two daughter cells, B. Aberrant division either with more than two daughter cells (upper panel) or or pseudo-tripolar division (lower panel) where three daughter cells arose transiently before fusing into two C. Mitotic death. D. examples of failed division which occurred as pseudo-division (upper panel) where separation was momentarily observed but failed eventually, or when cell returned to interphase-like state following a mitotic attempt.

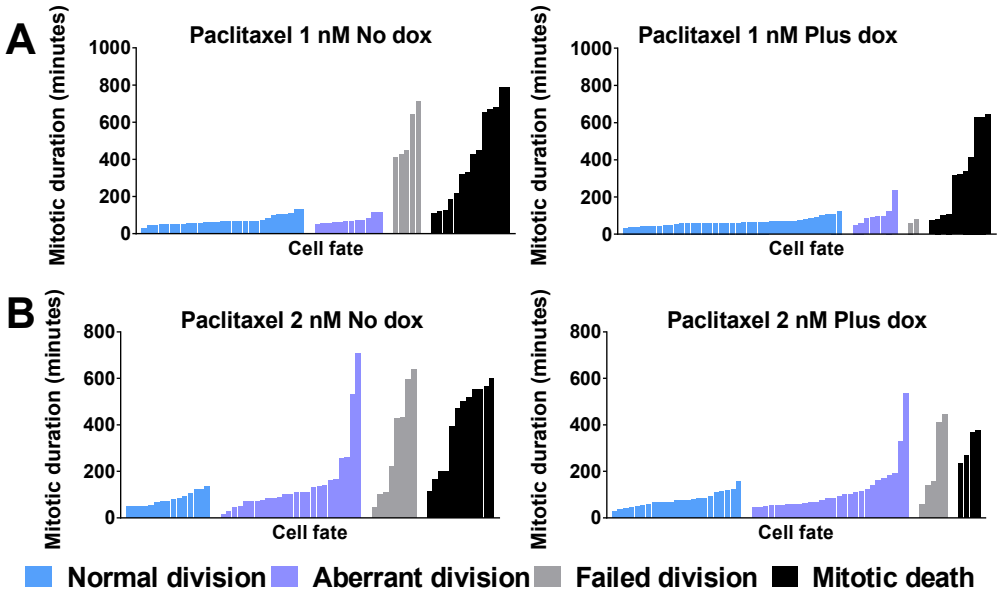

Figure 5-11: Mitotic duration and cell fate for HeLa AK-A cells exposed to paclitaxel 1 nM and 2 nM with and without doxycycline induction.
Mitotic duration and cell fate for cells exposed to A. Paclitaxel 1 nM with and without doxycycline induction B. Paclitaxel 2 nM with and without doxycycline induction. Cells were seeded in eight-well Ibidi chamber slides (5000 cells/chamber) and drugs added 24 hours later. Imaging was performed using phase-contrast time-lapse microscopy every five minutes. Each bar represents a single cell with the length of the bar indicating mitotic duration and the colour of the bar indicating cell fate, with 60 cells in total for each condition derived from three independent experiments. Abbreviation: Dox=doxycycline.

Cells over-expressing AK-A had a survival advantage, with more normal divisions and less mitotic death when exposed to paclitaxel 1 nM and paclitaxel 2 nM (Table 5-2).

Drug treatment	Normal division (%)	Aberrant division (%)	Failed division (%)	Mitotic death (%)
Paclitaxel 1 nM (no dox)	45	20	8	23
Paclitaxel 1 nM (plus dox)	65	13	3	18
Paclitaxel 2 nM (no dox)	25	42	13	20
Paclitaxel 2 nM (plus dox)	38	47	8	7

Table 5-2: Cell fate for HeLa AK-A cells exposed to paclitaxel 1 nM and 2 nM with and without doxycycline (dox) induction.

When the fate of daughter cells whose parents successfully underwent mitosis in the presence of paclitaxel was analysed, the percentage of daughter cells that entered mitosis was also greater in the AK-A over-expressing cells (87% vs 73% with paclitaxel 1 nM, 53% vs 45% with paclitaxel 2 nM), and less cell death was seen (4% versus 20% with paclitaxel 1 nM, and 35% versus 50% with paclitaxel 2 nM) (Figure 5-12)

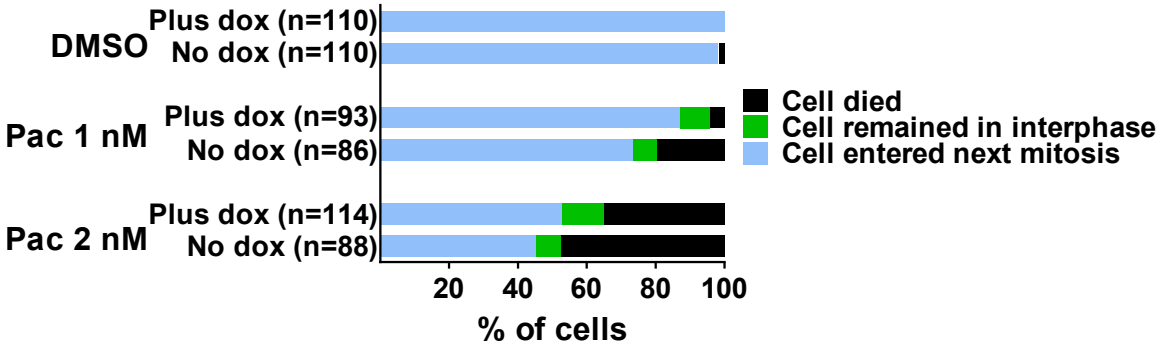

Figure 5-12: HeLa AK-A inducible cell line daughter cell fate following paclitaxel treatment. Cells were seeded in eight-well Ibidi chamber slides (5000 cells/chamber) and drugs added 24 hours later. Imaging was performed using phase-contrast time-lapse microscopy every five minutes. One daughter cell was chosen at random from a successful mitotic division and tracked for its fate over the following 72 hours. Results were pooled from two independent experiments. Bracketed n represents number of daughter cells tracked in each population. Abbreviation: Dox=doxycycline.

In summary, these experiments demonstrated that the cells with induced AK-A over-expression had a significantly shorter mitotic duration when exposed to paclitaxel 1 nM and 2 nM, with more normal division and less mitotic death. The daughter cells with AK-A over-expression also had a survival advantage at low concentrations of paclitaxel.

5.3.4 Colony forming assay in HeLa AK-A cells with paclitaxel

Given the survival advantage seen in the live cell imaging, the colony forming assay was used to assess whether this affected proliferative potential, using the same concentrations of paclitaxel. With both paclitaxel 1 nM and paclitaxel 2 nM, more colonies survived in the HeLa AK-A induced cells compared to the non-induced cells, reaching significance with paclitaxel 1 nM ($p=0.015$), confirming the modest survival

advantage seen in the other assays in the presence of AK-A over-expression. (Figure 5-13).

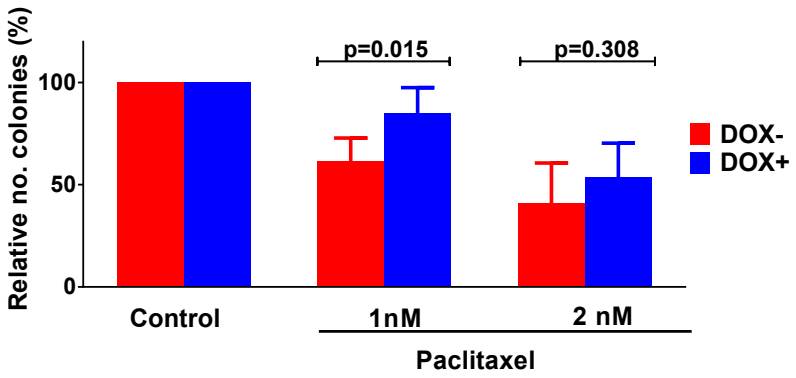

Figure 5-13: Relative number of colonies observed after 24 hours exposure to paclitaxel in HeLa AK-A inducible cells.
HeLa AK-A inducible cells were incubated with or without doxycycline with paclitaxel for 24 hours and were then re-seeded in duplicate without drug. The quantification of the plates after seven days using GelCount is presented. The results are expressed as a percentage of control. Mean and standard deviation as shown, n=5. Statistical analysis performed in GraphPad Prism with unpaired t test. Abbreviation: Dox=doxycycline.

5.3.5 Western blotting with the combination of MLN8237 and paclitaxel

To assess if the small survival advantage seen with paclitaxel 1 nM was reflected in differences seen in pH3, CC3 and cPARP, I assessed the synergistic combination of MLN8237 15 nM and paclitaxel 1 nM. Paclitaxel 10 nM was used as a comparator as 100% growth inhibition had been seen in initial SRB assays.

Consistent with previous experiments, total AK-A (exogenous and endogenous) expression was three times greater in the induced vs non-induced control samples at 24 and 48 hours. Induction of cell death as measured by CC3 and cPARP was most prominent in the combination and paclitaxel 10 nM samples at 48 hours, and when the intensity of signal for these proteins was quantified in ImageQuant, it was three times greater in the non-induced cells (Figure 5-14). This suggests that there was again a small survival advantage in the cells over-expressing AK-A.

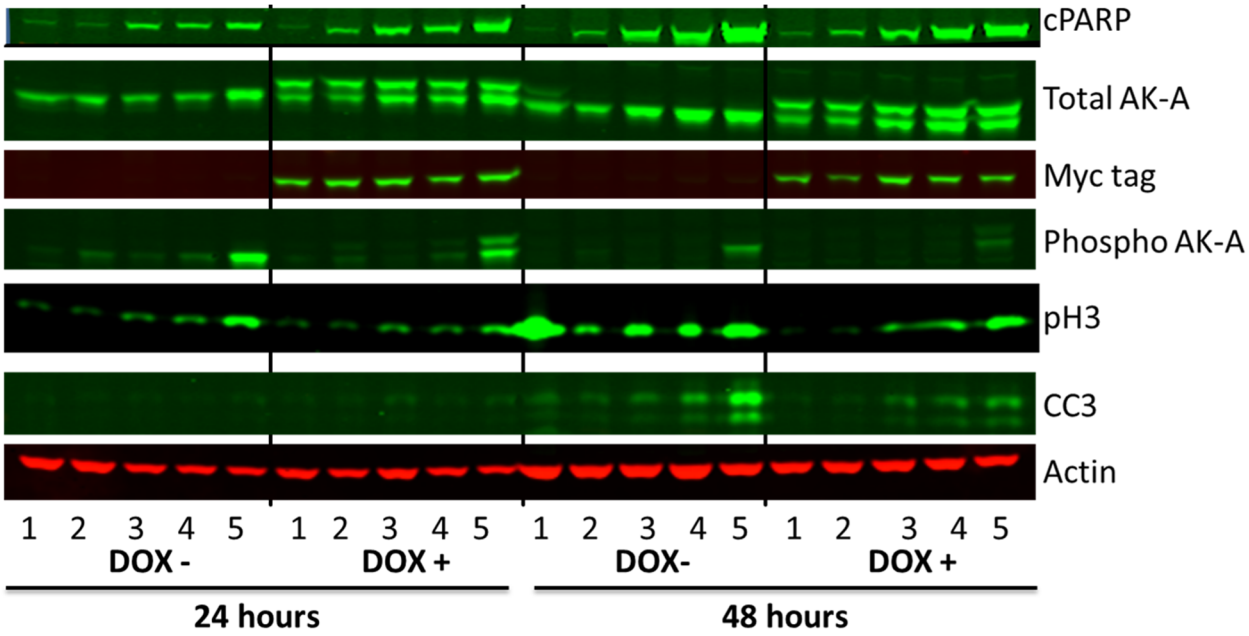

Figure 5-14: Western blots of HeLa AK-A cells with and without doxycycline after 24 or 48 hours of exposure to MLN8237 or paclitaxel.
HeLa AK-A inducible cells were exposed to either 1. DMSO 2. Paclitaxel 1 nM 3. MLN8237 15 nM 4. Combination of MLN8237 15 nM and paclitaxel 1 nM 5. Paclitaxel 10 nM for 24 or 48 hours as labelled. Proteins of interest (green channel) with actin as control (red channel). Note: in the pH3 samples at 48 hours, there was an experimental error with the DMSO sample, with the lane merging with the previous paclitaxel 10 nM lane where high pH3 expression had been seen. Abbreviation: Dox=doxycycline.

5.4 Summary of chapter

In this chapter, I firstly explored whether there was an association between the extent of AK-A expression in the cell lines and the response I had seen with the combination of MLN8237 and paclitaxel, concluding that the total AK-A expression did not correlate with the response seen. To further investigate this, I created a HeLa AK-A inducible cell line, with AK-A over-expression at a similar level to that seen clinically. Although no clear difference was seen between the HeLa AK-A inducible cells with or without AK-A over-expression in the SRB assay, when the cells were examined in real time using live cell imaging, there was a modest survival advantage in cells which over-express AK-A in the presence of low concentrations of paclitaxel. However, the small magnitude of effect is unlikely to be clinically significant in determining the response to an AK-A inhibitor/taxane combination in tumours with AK-A over-expression. Certainly this degree of taxane resistance was not overcome by the addition of MLN8237 when assessed using IncuCyte™ imaging, although it would have been interesting to have used live cell imaging to study cell fates with the combination.

These findings are contrary to the accepted dogma that AK-A over-expression is likely to induce resistance to taxanes, which is largely based on publications using flow cytometry methods which would not now be considered sufficient (2, 232).

My work suggests that the combination of MLN8237 and paclitaxel is likely to be equally effective in tumours whether or not AK-A is over-expressed, and therefore AK-A expression is unlikely to be useful as a biomarker for patient selection in clinical trials. Indeed when subsequent clinical trials with MLN8237 attempted to correlate response with tumour AK-A expression levels and AK-A gene copy number in archived tumour samples, no association was found between these and response (210). In the MLN8237 trial in patients with bladder cancer, pre-treatment tumour samples were assessed for AK-A expression, with high nuclear immunoreactivity for AK-A seen in the majority of tumours meaning no correlation could be seen between expression and response (178).

Therefore, with the data on scheduling of the drug combination from Chapter 3, and the information on the drug-induced phenotype from live cell imaging in Chapter 4, I next chose to explore the tolerability and efficacy of an AK-A inhibitor with taxanes *in vivo*. However, based on the work in this Chapter, I decided not to assess AK-A expression.

6 *IN VIVO STUDIES*

6.1 Introduction

To explore the combination of an AK-A inhibitor in combination with paclitaxel further, I established a T24 bladder cancer subcutaneous xenograft model in Balb/c nude mice, together with the CRUK-CI BRU. CYC3 and taxanes were then tested as single agents for pharmacokinetics (PK), potential pharmacodynamic (PD) markers of response and tolerability. Subsequently MLN8237 was substituted as the AK-A inhibitor of choice and studies carried out with it, both as a single agent and in combination with taxanes, assessing evidence of tolerability, particularly on the bone marrow, and anti-tumour efficacy.

Contribution of others to this experimental work: As described in 2.3, staff of the CRUK-CI Biological Resources Unit were responsible for the routine care of the animals, including health assessments, weights and assessment of tumour volumes. They also administered the drugs tested in these experiments and assisted with the mid-term bleeds. Dr Frances Richards assisted with drug formulation and performed the mouse necropsies. The CRUK-CI histopathology department sectioned and stained tissues and also developed and optimised the image analysis algorithms. LC-MS/MS analysis was performed by Dr Tashinga Bapiro (2.2.11). Jo Bramhall performed the M30/M65 ELISA experiment. All other sample preparation and all the data analysis was performed by me.

6.2 Establishment of T24 bladder cancer xenograft model

Whilst there have been previous publications using T24 xenografts, the original paper reported that T24 cells are non-tumorigenic (284). Subsequent cytogenetic studies have shown different T24 sublines and that the tumorigenic subline contains fewer chromosomes (285). I therefore carried out a pilot study in thirty mice injected subcutaneously with $2x10^6$ T24 cells (obtained directly from CLS and STR genotyped). There was variability in the growth rate between mice, with an 80% take rate (Figure 6-1). Of the tumours that grew, the mean doubling time was 8.4±6.4 days (Figure 6-1 B). The mice in which tumours grew were used between Days 30-45 for PK studies.

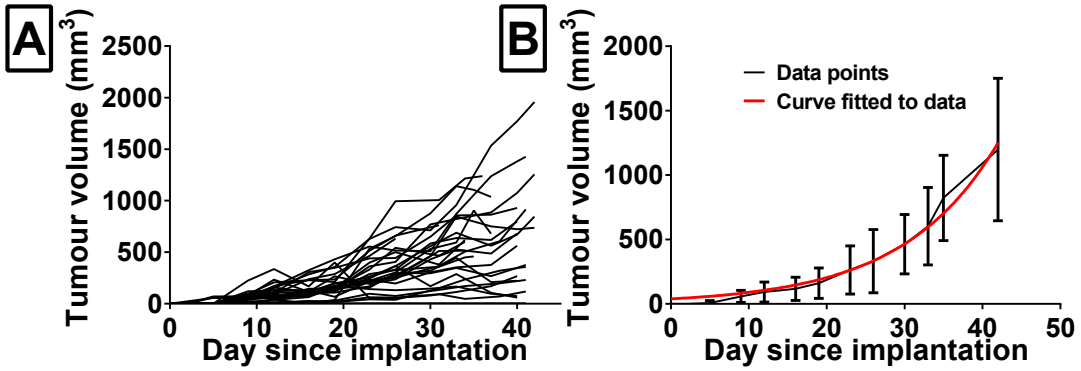

Figure 6-1: Tumour growth over time in T24 xenografts.
A. shows the individual tumour growth curves for the 30 tumours. B. shows the mean tumour growth over time and standard deviation with the fitted curve giving the tumour doubling time.

6.3 Initial pilot studies with AKI and paclitaxel

Based on cell culture medium concentrations of CYC3 and paclitaxel that showed synergy *in vitro* in T24 cells, target PK profiles were identified as CYC3 1 µM sustained for 72 hours and paclitaxel 3 nM sustained for at least 24 hours. As we had also shown synergy *in vitro* in MIA PaCa-2 cells and this was an established tumour xenograft in our institution, PK studies were also performed using this model. Time course experiments were undertaken in both T24 and MIA PaCa-2 xenografts with CYC3 and paclitaxel, with mice killed at set time points after a single dose of drug, collecting plasma and tumour tissue for LC-MS/MS analysis of drug concentrations as detailed in 2.2.11. Having decided to proceed further with AK-A inhibitor MLN8237 instead of CYC3, PK studies were also performed with MLN8237, aiming to identify a dose schedule to achieve the target PK profile of 50 nM for 72 hours.

In these initial pilot studies, tumour sections were stained by the CRUK-CI Histopathology Core Facility for Ki67 (to assess tumour cell proliferation), cleaved caspase 3 (CC3) (as a marker of apoptosis) and phospho-histone H3 (pH3) (as both a marker of mitosis and AK-A inhibition). Given that there were only two or three mice per treatment group, with intra-group variation, statistical testing was not performed but these experiments allowed me to test which would be most useful for analysis in subsequent studies and gave helpful information about the magnitude of change that could be seen with each stain.

At necropsy, all of the T24 tumours were pink and soft, and many of the tumours were cystic, with large regions of necrosis. This has implications for future studies as it may lead to an over-estimate of tumour growth due to the serous component of the tumour. It also meant that the analysis algorithms in Aperio were scoring aberrant positive cells

within the areas of necrosis. Therefore, after discussion with the CRUK-CI Histopathology core facility, the T24 studies were re-analysed using HALO as described in 2.3.5.1 to allow necrotic areas to be identified and excluded from analysis.

6.3.1 CYC3 pilot studies in MIA PaCa-2 and T24 xenograft models

6.3.1.1 CYC3 tolerability

To assess oral bioavailability, a single dose of CYC3 20 mg/kg was administered either by intraperitoneal injection (IP) or oral gavage (OG) in the MIA PaCa-2 xenograft mice. In the mice dosed IP, both with vehicle only and with CYC3, the mice exhibited signs of discomfort after half the volume of solution had been injected. With the CYC3 IP-dosed mice, four of the mice became somnolent 15 minutes after dosing and one mouse became hunched and hypomotile within 10 minutes of dosing and was killed early. As the IP route was not tolerated, only the OG route (which was tolerated) was used with the T24 xenograft mice and future studies.

6.3.1.2 CYC3 pharmacokinetics

With CYC3 20 mg/kg OG, sampling in the T24 xenografts showed that the plasma C_{max} at 1 hour was 6.5 μM, with levels in the tumours over 3 μM (for example 1.5 ng/mg estimated at 3.4 μM) (Figure 6-2 A). However, CYC3 was present at levels above the target concentration of 1 μM for less than eight hours.

Although the T24 xenografts were more cystic, similar findings were seen in the MIA PaCa-2 xenografts. With the CYC3 20 mg/kg dosing, the highest tumour concentration achieved for CYC3 OG was less than 2 μM and the tumour concentration remained above 1 μM for less than four hours (Figure 6-2 B). C_{max} for IP dosing was higher at around 5 μM but again the concentration was sustained above 1μM for less than four hours (Figure 6-2 C). As the IP dose was not well tolerated, a further cohort of mice with MIA PaCa-2 xenografts were given a single dose of 50 mg/kg of CYC3 OG (Figure 6-2 D). Tumour concentration varied at one hour and again the tumour concentration remained above 1μM for less than four hours.

Even with 50 mg/kg CYC3, the target tumour concentration of >1 μM was not sustained for more than two hours. With this formulation, it is unlikely a higher dose could be given. With this PK profile, CYC3 would probably need to be dosed three or four times per day in an efficacy study to maintain the target concentration. This schedule was not considered feasible.

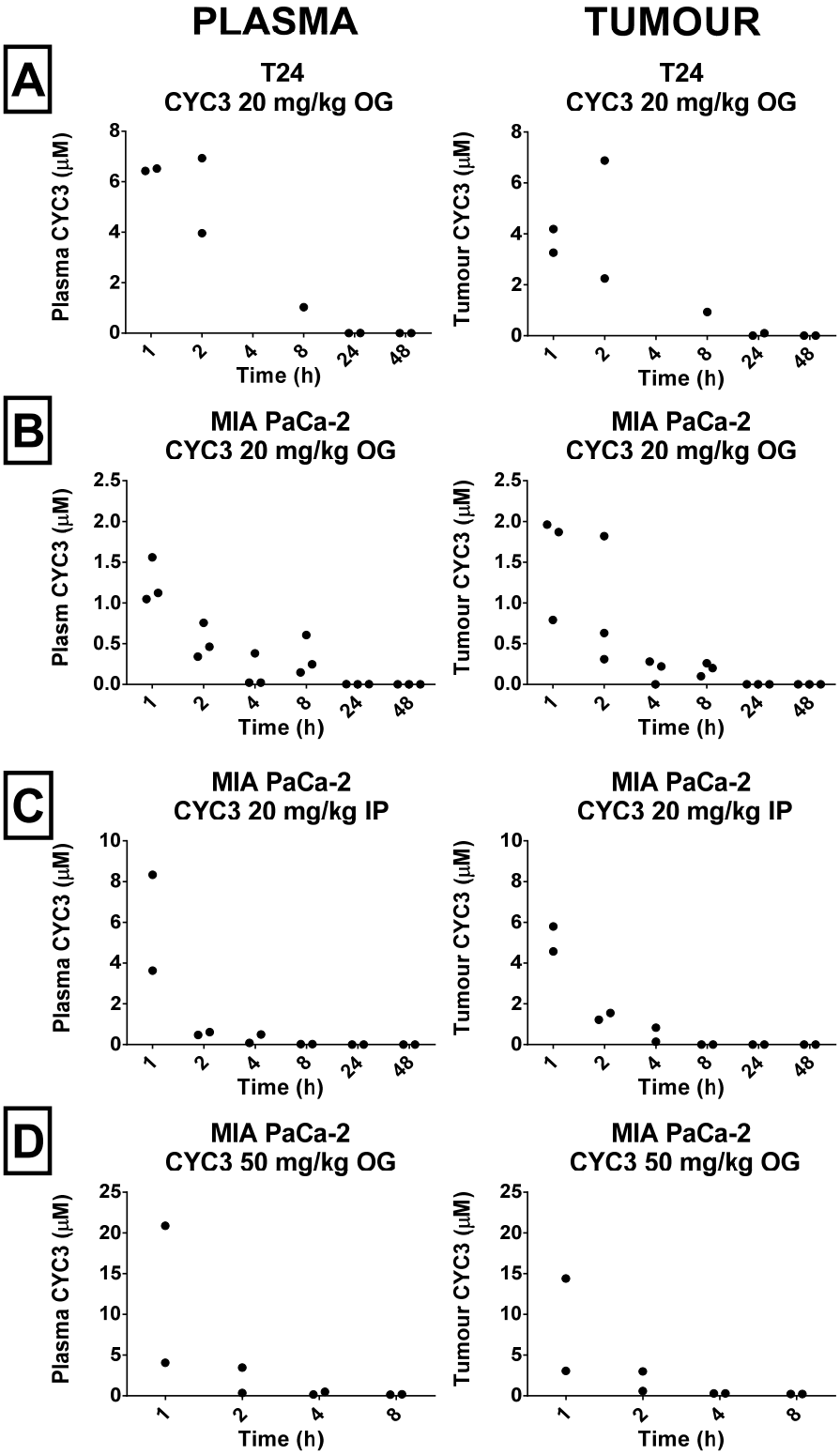

Figure 6-2: Pharmacokinetic analysis of CYC3 concentrations in plasma and tumour in T24 and MIA PaCa-2 xenografts.

A. plasma and tumour PK following single dose of CYC3 20 mg/kg OG in T24 xenografts, n=9, B. plasma and tumour PK following single dose of CYC3 20mg/kg OG in MIA PaCa-2 xenografts, n=18, C. plasma and tumour PK following single dose of CYC3 20 mg/kg IP in MIA PaCa-2 xenografts, n=12, D. plasma and tumour PK following single dose of CYC3 50 mg/kg OG in MIA PaCa-2 xenografts, n=8. Note: tumour values measured in ng/mg tissue and converted to a molar concentration. Abbreviation: OG=oral gavage.

6.3.1.3 Effect of CYC3 on PD markers

In the T24 xenografts given a single dose of CYC3 20 mg/kg (Figure 6-3), the percentage of Ki67 positive cells was reduced at each timepoint compared to vehicle but was similar across the timepoints, indicating a potential drug effect in reducing proliferation. The percentage of CC3 positive tissue reduced over the timepoints compared to vehicle, suggesting there was no significant induction of apoptosis from a single dose of CYC3. With pH3, there was an increase in the percentage of positive cells from eight hours, maintained at 48 hours. Whilst the difference is small, this may indicate AK-A inhibition as an increase in pH3 positive cells has been shown in tumour samples previously with other AK-A inhibitors (205). As seen in Figure 6-3 D, the percentage of tissue identified as necrotic using the HALO™ classifier was higher in all the CYC3 treated tumours, peaking at two hours post-dose.

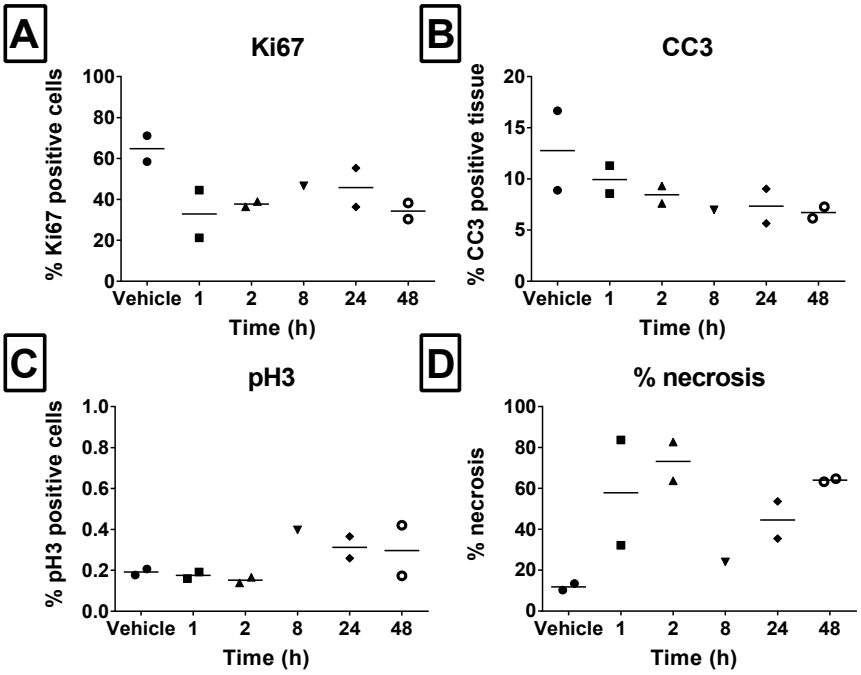

Figure 6-3: Time course experiment to establish PD parameters following single dose of CYC3 in T24 xenografts.
Analysis of A. percentage positive cells for Ki67, B. percentage positive tissue for CC3 and C. percentage positive cells for pH3 after a single dose of CYC3 20 mg/kg OG, analysed in HALO™ (as described in 2.3.5.1). D. shows percentage of necrosis for slides analysed in HALO™, n=11.

For the MIA PaCa-2 xenografts, the data is shown for the CYC3 50 mg/kg OG dosing cohort (Figure 6-4). There were no clear trends in the percentage of Ki67 or CC3 positive cells, although the percentage of CC3 positive cells was higher at 48 hours compared to vehicle, suggesting induction of apoptosis. An increase in the percentage of pH3 positive cells was seen between four and twenty-four hours, consistent with AK-A inhibition but by 48 hours this difference was not seen.

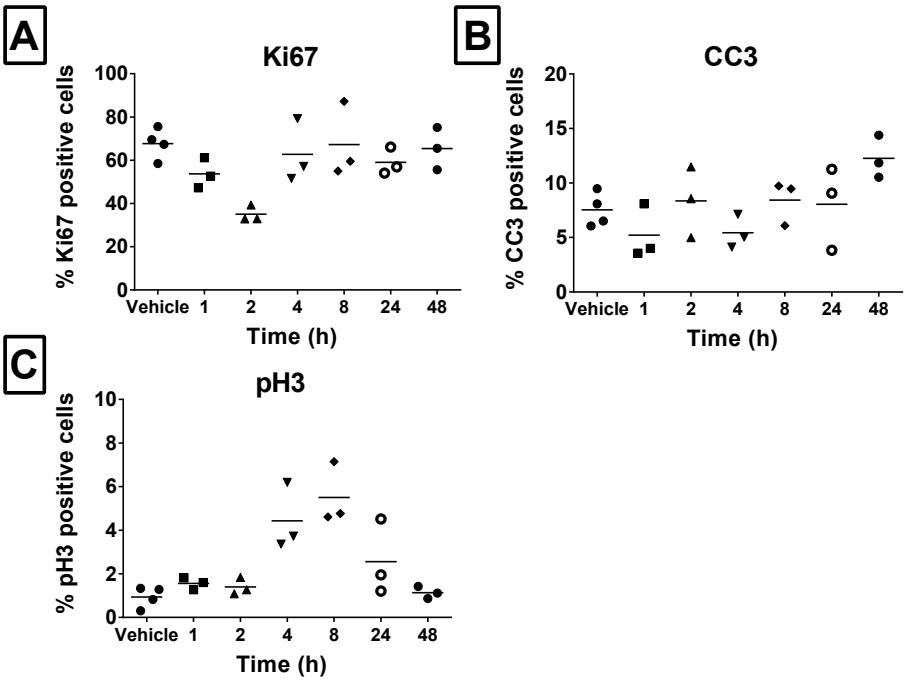

Figure 6-4: Time course experiment to establish PD parameters following single dose of CYC3 in MIA PaCa-2 xenografts.
Analysis of percentage positive cells for A. Ki67, B. CC3 and C. pH3 after a single dose of CYC3 20 mg/kg OG, using Aperio (as described in 2.3.5.1), n=22.

6.3.2 MLN8237 pilot study in T24 xenograft model

6.3.2.1 MLN8237 Tolerability

The maximum tolerated dose of MLN8237 in other mouse xenograft models was reported as 20 mg/kg twice a day or 30 mg/kg once daily when dosed continuously for 21 days. Intermittent dosing had also demonstrated anti-tumour activity (205, 286). Analysis of tumour tissue from HCT-116 xenografts treated with increasing doses of MLN8237 suggested a plasma concentration between 1–2 μM was required to inhibit AK-A *in vivo* (205). Here the T24 xenograft mice tolerated a single dose of 30 mg/kg MLN8237 well with no adverse effects seen.

6.3.2.2 MLN8237 pharmacokinetics

The PK profile showed that the concentration of MLN8237 in both tumour and plasma was at its maximum 0.5 hours after a single dose of MLN8237 30 mg/kg OG but remained above 1 μM after 24 hours (Figure 6-5). Hence the levels achieved appear to be in the range previously reported to cause AK-A inhibition in HCT-116 xenografts.

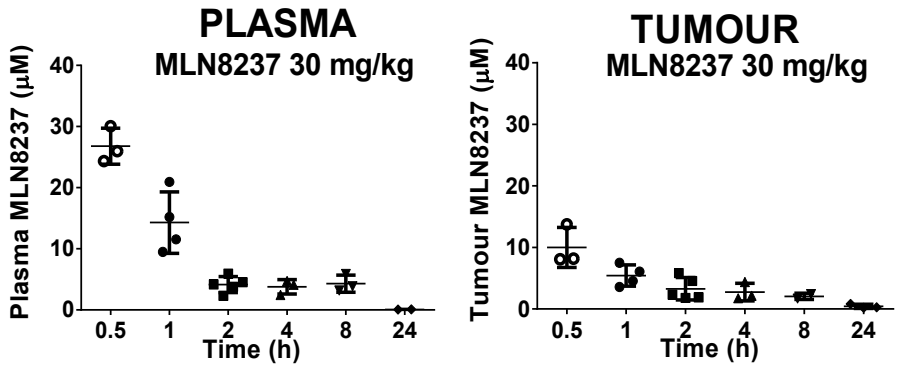

Figure 6-5: Pharmacokinetic analysis of MLN8237 concentrations in plasma and tumour of T24 xenografts.
Plasma and tumour PK after single dose of MLN8237 30 mg/kg OG, n=21. Note: tumour values measured in ng/mg tissue and converted to a molar concentration.

6.3.2.3 Effect of MLN8237 on PD markers

There were no clear changes in the percentage of Ki67, CC3 or pH3 positive cells (Figure 6-6). There was considerable variability in the percentage necrosis seen for example ranging from 12-73% in the vehicle group consistent with my earlier observations surrounding the degree of necrosis seen in these tumours, even when untreated (Figure 6-6 D).

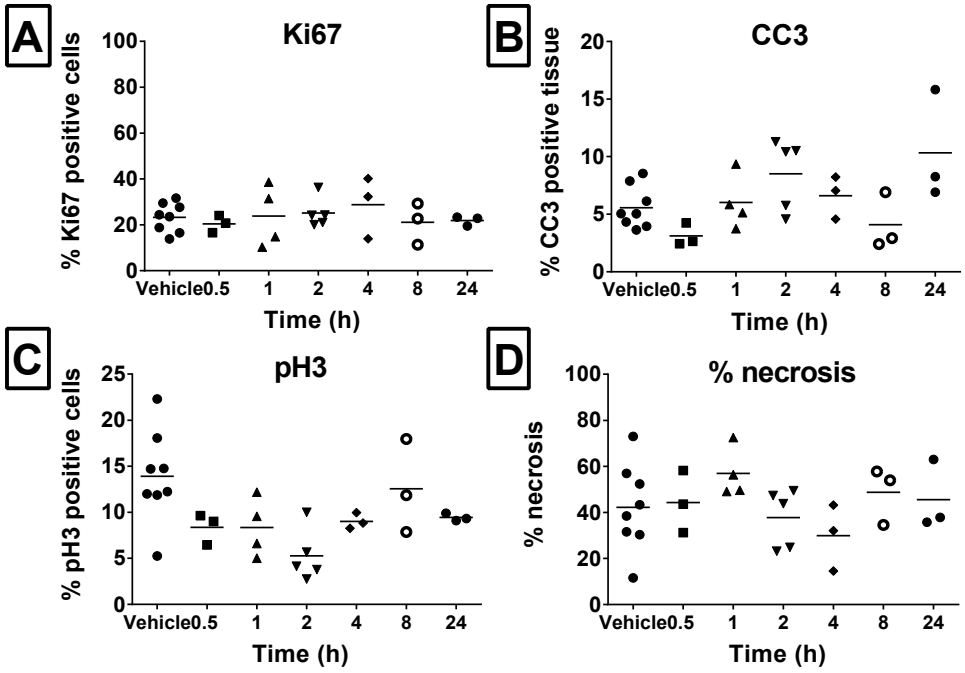

Figure 6-6: Time course experiment to establish PD parameters in T24 xenografts after a single dose of MLN8237 30 mg/kg OG.
Analysis of A. percentage positive cells for Ki67, B. percentage positive tissue for CC3 and C. percentage positive cells for pH3 after a single dose of MLN8237 30 mg/kg OG, analysed in HALO™ (as described in 2.3.5.1). D. shows percentage of necrosis for slides analysed in HALO™, n=29.

6.3.3 Paclitaxel pilot study in T24 xenograft model

6.3.3.1 Paclitaxel tolerability

Prior to *in vivo* combination experiments, paclitaxel PK were assessed in T24 xenografts. Doses of 20 mg/kg intravenously have been previously reported to be well tolerated (287), and no acute toxicities were seen here after a single intravenous dose.

6.3.3.2 Paclitaxel pharmacokinetics

Plasma concentrations were above 2000 nM at one hour and remained above 1000 nM at two hours. However, by 24 hours, paclitaxel was barely detectable (2-3 nM) and it could not be detected at 48 hours. In contrast, peak concentrations in tumour (around 3000 nM) were seen at two hours, remained around 1000 nM 24 hours later, and were still ≥50 nM at 48 hours (Figure 6-7).

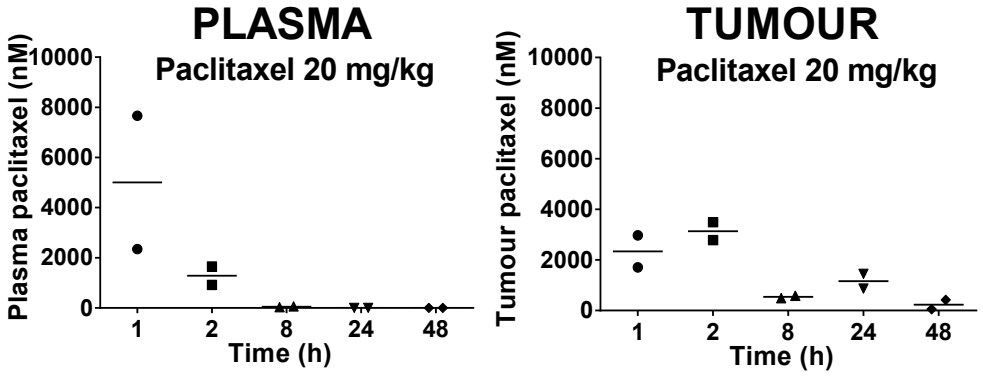

Figure 6-7: Pharmacokinetic analysis of paclitaxel concentrations in plasma and tumour of xenografts.
Plasma and tumour PK after single dose of paclitaxel 20 mg/kg in T24 xenografts, dosed intravenously, n=10. Note: tumour values measured in ng/mg tissue and converted to a molar concentration.

Hence paclitaxel was sustained in the tumour at much greater concentrations than those targeted when given at 20 mg/kg. Previous reports had shown paclitaxel concentrated intracellularly, reaching micromolar levels (288, 289). Since these experiments were performed, analysis of plasma and tumour samples from patients with breast cancer confirmed intra-tumoural concentration of paclitaxel, up to 70 fold that of plasma and indicated that clinically relevant plasma levels of paclitaxel are in the low nM range (290).

6.3.3.3 Effect of paclitaxel on PD markers

After a single dose of paclitaxel 20 mg/kg the percentage of Ki67 positive cells was reduced in all the treated samples, particularly at 48 hours (Figure 6-8 A). The percentage of CC3 positive cells was slightly reduced compared to vehicle in the treated

tumours (Figure 6-8 B). The percentage of pH3 positive cells was less than 1% as seen with CYC3 but did increase between two and 24 hours compared to vehicle control, suggestive of cells arrested in mitosis (Figure 6-8 C). Necrosis (as measured with the tissue classifier in HALO™) was increased in the treated tumours, peaking at eight hours (apart from the single tumour at 24 hours). These data suggest an active intra-tumoural concentration of paclitaxel was achieved, but with only two samples per timepoint no statistical signficance could be calculated.

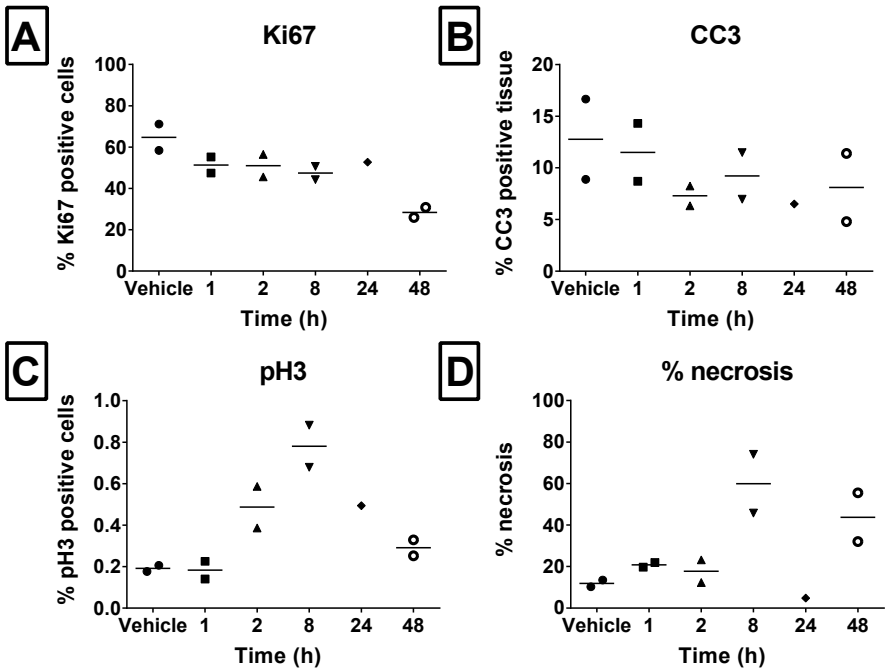

Figure 6-8: Time course experiment to establish PD parameters following single dose of paclitaxel in T24 xenografts.
Analysis of A. percentage positive cells for Ki67, B. percentage positive tissue for CC3 and C. percentage positive cells for pH3 after a single dose of paclitaxel 20 mg/kg iv, analysed in HALO™ (as described in 2.3.5.1), n=11 as it was not possible to fix all of the tumours from the 24 hour timepoint. D. shows percentage of necrosis for slides analysed in HALO™.

6.3.4 Summary of pilot studies

In the CYC3 studies, the target CYC3 concentrations were not achieved in tumour for a sufficient time period with once daily dosing and the dosing schedule likely to be required of three to four times a day was not feasible. In contrast, with MLN8237 30 mg/kg once daily dosing by oral gavage, target PK concentrations were achieved and hence this AK-A inhibitor was selected for further investigation. With paclitaxel 20 mg/kg, concentrations in both plasma and tumour were sustained at levels above the target range for 24 hours. My earlier work supported a combination of an AK-A inhibitor with low concentrations of paclitaxel. Hence rather than pursue further dosing with paclitaxel 20 mg/kg alone, I chose to investigate lower concentrations of paclitaxel in my further experiments. The preliminary PD analysis did not show any clear trends in

the MLN8237 timecourse experiments, but there was potentially evidence of a PD effect in the percentage necrosis and pH3 results in the paclitaxel study.

6.4 Single agent efficacy studies in T24 xenograft model

6.4.1 Efficacy of single agent paclitaxel and docetaxel

Because of its poor aqueous solubility, paclitaxel is formulated in Cremophor EL. Severe hypersensitivity reactions were seen in Phase 1 clinical trials with paclitaxel (due to Cremophor EL) and therefore pre-medication is administered with steroids and anti-histamines (291). Efficacy studies with multiple doses of paclitaxel *in vivo* can therefore be complicated by an anaphylaxis reaction. Although the mice tolerated a single dose of paclitaxel intravenously in the pilot experiments, I also tested the efficacy of docetaxel which is more soluble, can be formulated without Cremophor EL and can be dosed intraperitoneally.

Mice were randomised into groups on Day 21 after T24 cell implantation and dosed with either intravenous paclitaxel or intraperitoneal docetaxel at a range of dose levels (as detailed in Table 6-1 together with the vehicle formulations) once weekly for a total of four doses (Days 1, 7, 14 and 21) and compared to vehicle. As can be seen in Table 6-1, the concentration of Cremophor EL required for the paclitaxel 20 mg/kg group was 25% compared to 5% at lower dosing levels.

Treatment group	Vehicle
Vehicle	5:5:90 ethanol:polysorbate80: saline (sterile)
Paclitaxel 20 mg/kg	25% Cremophor EL, 25% ethanol, 50% saline (sterile)
Paclitaxel 6 mg/kg	5% Cremophor EL, 5% ethanol, 90% saline (sterile)
Paclitaxel 2 mg/kg	5% Cremophor EL, 5% ethanol, 90% saline (sterile)
Docetaxel 20 mg/kg	5:5:90 ethanol:polysorbate80: saline (sterile)
Docetaxel 6 mg/kg	5:5:90 ethanol:polysorbate80: saline (sterile)

Table 6-1: Vehicle formulation used for each dosing level of paclitaxel and docetaxel.

6.4.1.1 Tolerability of paclitaxel and docetaxel

There were no significant changes in weight during dosing across groups with none of the weights falling by more than 10% relative to weight on the first day of dosing, over the course of 4 weeks of dosing (Figure 6-9). Adverse events were seen in the paclitaxel 20 mg/kg group after only one dose. Three of the five mice in this cohort were hypomotile for 10 minutes after their first dose but recovered. A similar period of hypomotility was seen in one mouse after the second dose was administered, and another mouse died immediately following the second dose. Because of these reactions (presumed to be due to hypersensitivity), further doses of paclitaxel 20 mg/kg were not

given. In the paclitaxel 2 mg/kg group, one mouse had to be killed after two doses due to a necrotic tail at the intravenous injection point, and another because the large cystic tumour was impeding movement (but after all four doses of drug had been successfully administered).

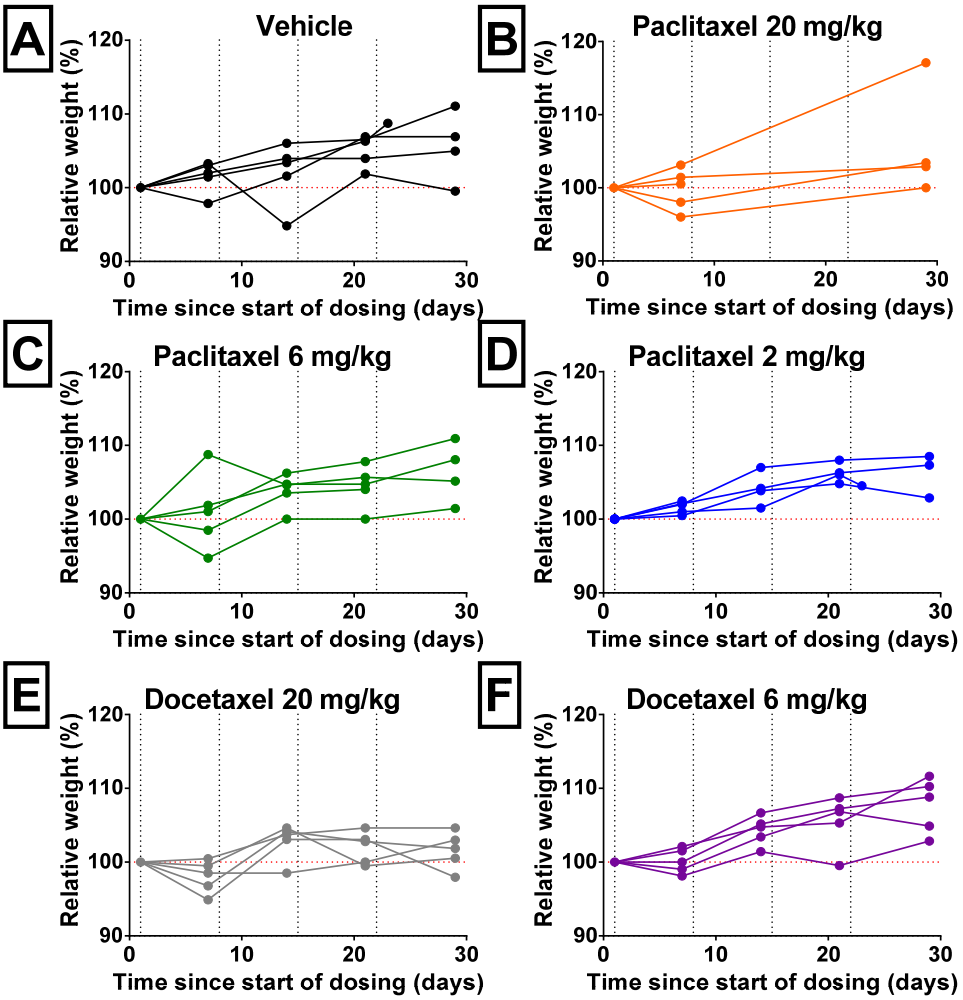

Figure 6-9: Percentage body weight relative to Day 1 of dosing over days since first dose for each individual mouse dosed with paclitaxel and docetaxel on days 1, 7, 14 and 21.
Individual mouse body weight plotted for each group for A. Vehicle B. Paclitaxel 20 mg/kg C. Paclitaxel 6 mg/kg D. Paclitaxel 2 mg/kg E. Docetaxel 20 mg/kg F. Docetaxel 6 mg/kg. Mice were weighed prior to each weekly dose, with vertical black dotted lines indicating each weekly dose, n=5 for each group. Paclitaxel dosed intravenously, Docetaxel dosed using intraperitoneal route. Only two doses of paclitaxel 20 mg/kg administered – final weight taken at day 29, the endpoint of study.

Endpoint blood tests were taken on Day 29 (eight days after the last dose of drug for the groups apart from the paclitaxel 20 mg/kg group where last dose was on Day 7 and in cases where mice were killed early due to tumour size). Of particular interest given the clinical concern about neutropenia with the combination of AK-A inhibitors and paclitaxel were the overall white cell count (WBC) and the granulocyte count (as neutrophils are the most abundant type of granulocytes). However, the timing of testing

may mean the bone marrow had sufficient time to recover from weekly drug dosing (292).

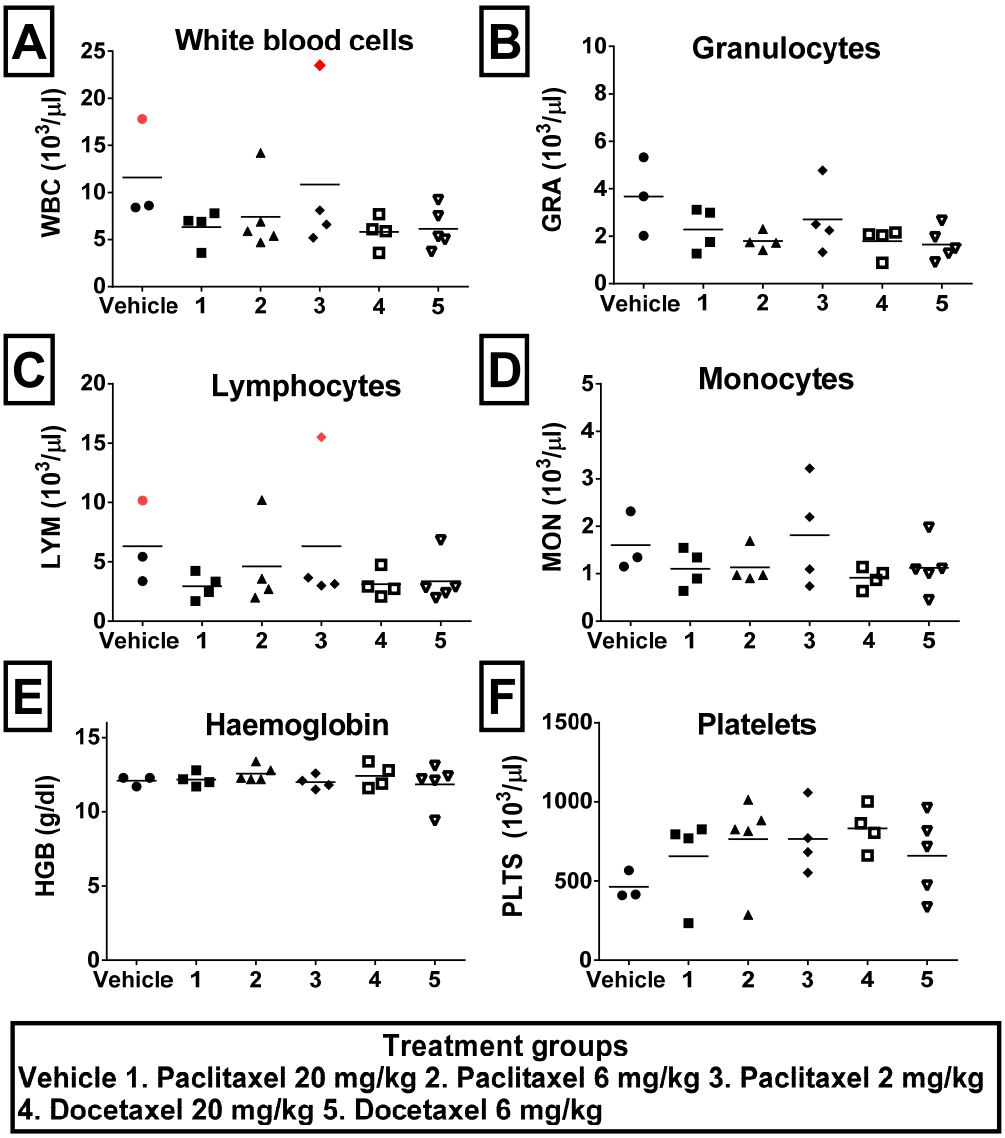

Figure 6-10: Blood counts for study comparing the effect of multiple dosing of paclitaxel or docetaxel on days 1, 7, 14 and 21, compared with vehicle.
Mice were dosed with either Vehicle, 1. Paclitaxel 20 mg/kg 2. Paclitaxel 6 mg/kg 3. Paclitaxel 2 mg/kg 4. Docetaxel 20 mg/kg 5. Docetaxel 6 mg/kg, with paclitaxel dosed intravenously and docetaxel dosed using intraperitoneal route. Only two doses of paclitaxel 20 mg/kg administered. Samples were taken at Day 29 (eight days after last dose for vehicle and groups 2-5 but 22 days after last dose for group 1). Parameters measured are A. total white blood cell count (WBC), B. granulocytes (gra), C. lymphocytes (lym), D. monocytes (mon), E. haemoglobin (HGB) and F. platelets (plts). Mice killed early with higher overall WBC and lymphocyte count are indicated with red dots. Statistical analysis performed with ordinary one way ANOVA and Dunnett's multiple comparison test compared to vehicle in GraphPad Prism.

As seen in Figure 6-10, the overall WBC count was slightly suppressed in the treatment groups compared to vehicle (although not statistically significant, p=0.31) with a corresponding trend towards a reduction in granulocytes (p=0.11) and lymphocytes. Despite the time since last dose of paclitaxel, in the paclitaxel 20 mg/kg group (group 1), WBC remained suppressed to a similar extent to the other groups, although this was

not statistically significant (p=0.31). Both of the mice killed on Day 23 (one in the paclitaxel 2 mg/kg group and one in the vehicle group) due to tumour size had a raised white cell count with lymphocytosis (indicated in Figure 6-10 with red spots), potentially due to infection. Haemoglobin was stable across the treatment groups. There was variability in the platelet count, but with an apparent non-significant increase in treatment groups compared to vehicle (p=0.35).

Therefore, both paclitaxel 6 mg/kg or 2mg/kg and docetaxel 20 mg/kg or 6 mg/kg were tolerated as measured by the blood cell counts, with a non-significant reduction in WBC and granulocyte counts.

6.4.1.2 Effect of paclitaxel and docetaxel on tumour growth

As can be observed in Figure 6-11 A, there was variance in tumour volumes, even within the vehicle group. This is partly because many of the tumours contained fluid-filled cysts and necrotic areas and so the total volume of the subcutaneous nodules did not always correlate precisely with the amount of tumour cellular tissue. Despite this, there was a significant difference in tumour growth ($p<0.0001$) between the treatment groups compared to vehicle. Although we could only give two of the planned four doses of paclitaxel 20 mg/kg, tumour growth was suppressed compared to vehicle (p=0.0064, Figure 6-11 B). Paclitaxel 6 mg/kg given weekly for four weeks also reduced tumour growth significantly (p=0.031, Figure 6-11 C) but paclitaxel 2 mg/kg did not suppress tumour growth (p=0.19, Figure 6-11 D). With docetaxel, there was significant tumour growth inhibition with docetaxel 20 mg/kg (p=0.0001, Figure 6-11 E) but little difference between the vehicle and docetaxel 6 mg/kg group (p=0.85, Figure 6-11 F). These results confirm the known utility of both paclitaxel and docetaxel in bladder cancer at the higher dose levels (20 mg/kg) but also reveal potential efficacy at a lower dose (6 mg/kg) of paclitaxel.

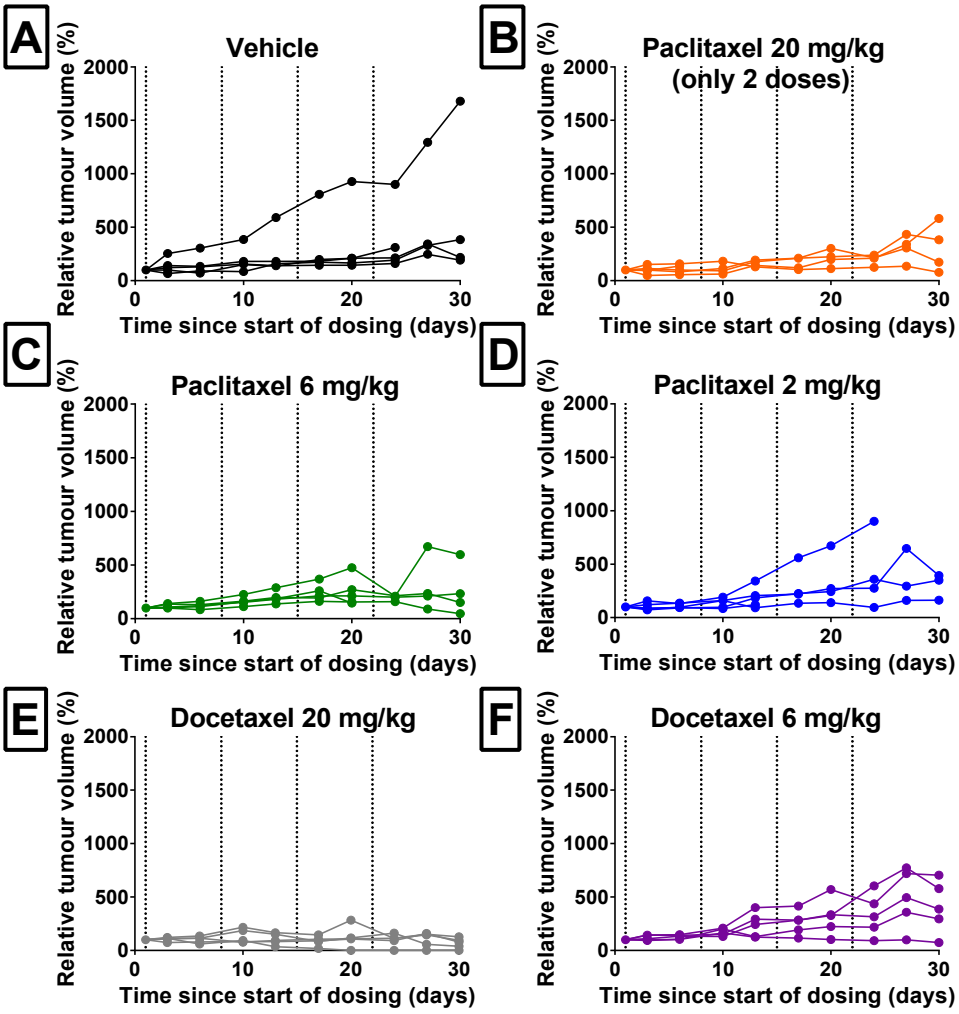

Figure 6-11: Relative tumour growth expressed as volume measured over time since start of dosing in mice dosed weekly with either vehicle, paclitaxel or docetaxel, on days 1, 7, 14 and 21.
Mice were dosed with either A. vehicle B. paclitaxel 20 mg/kg C. paclitaxel 6 mg/kg D. paclitaxel 2 mg/kg E. docetaxel 20 mg/kg or F. docetaxel 6 mg/kg on days 1, 7, 14 and 21. Only two doses of paclitaxel 20 mg/kg administered. Mice were dosed with paclitaxel intravenoulsy, docetaxel dosed using intraperitoneal route. Tumour volumes were measured approximately every 72 hours after dosing using calipers. Endpoint was at Day 29. Statistical testing was performed using ordinary two way ANOVA with Dunnett's multiple comparison test comparing each treatment group to vehicle in GraphPad Prism.

6.4.1.3 Effect of paclitaxel and docetaxel on PD markers

Despite the effects on tumour growth demonstrated in Figure 6-11, there were no significant differences in Ki67, CC3 and pH3 for the treatment groups compared to vehicle, although there was a non-significant slight increase in both CC3 positive tissue and pH3 positive cells in the paclitaxel 6 mg/kg group (Figure 6-12). The amount of time that had elapsed after the last dose (eight days) may have masked changes in these dynamic measures. The percentage of necrosis was variable both within and between treatment groups, with a non-significant increase in necrosis in the paclitaxel treatment groups (most pronounced with paclitaxel 6 mg/kg) and decrease in the docetaxel treatment groups.

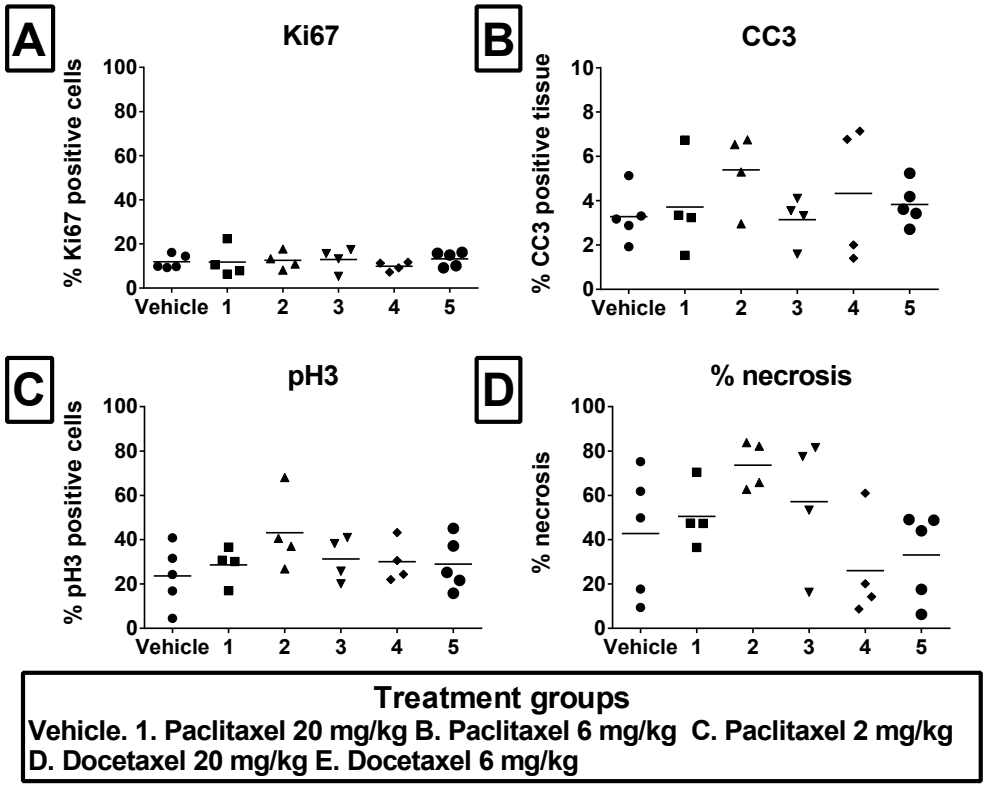

Figure 6-12: Pharmacodynamic analysis of T24 xenograft tumours of mice treated with either vehicle, paclitaxel or docetaxel on days 1, 7, 14 and 21.
A. percentage positive cells for Ki67 B. percentage positive tissue for CC3 and C. percentage positive cells pH3 after dosing with either vehicle, paclitaxel or docetaxel on days 1, 7, 14 and 21 as described in Figure 6-11. Tumour samples were taken at the endpoint of the study, Day 29 from start of dosing. Three mice were killed early and samples were not collected. Slides analysed in HALO™ (as described in 2.3.5.1). D. shows percentage of necrosis for slides analysed in HALO™. Statistical testing was performed using ordinary one way ANOVA with Dunnett's multiple comparison test comparing each treatment group to vehicle in GraphPad Prism.

6.4.1.4 Summary of paclitaxel and docetaxel efficacy study

Based on these results, the greatest effect on tumour growth was achieved by docetaxel 20 mg/kg. Although repeated dosing of paclitaxel 20 mg/kg was not possible due to issues with tolerability, growth was still significantly suppressed. Paclitaxel 6 mg/kg still showed an effect on tumour growth and was better tolerated. Both paclitaxel 2 mg/kg and docetaxel 6 mg/kg showed no significant anti-tumour effect.

6.4.2 Efficacy of single agent MLN8237

MLN8237 was my AK-A inhibitor of choice for combination studies and was assessed as a single agent at both the reported maximum tolerated dose of 30 mg/kg and at a lower dose level of 15 mg/kg in case of toxicities when the drugs were combined. Mice with T24 xenografts received five cycles of either MLN8237 30 mg/kg, MLN8237 15 mg/kg or vehicle with a cycle consisting of dosing by oral gavage once daily for five consecutive days per week for five weeks, with eleven mice in each treatment group. A

final dose of MLN8237 was given between two to six hours prior to the study endpoint to evaluate PD biomarkers.

6.4.2.1 MLN8237 tolerability

The treatment appeared reasonably well tolerated but statistical testing of body weight relative to Day 1 dosing showed a significant difference in weight for both treatment groups compared to vehicle (p=0.0001 for both). One mouse in the MLN8237 30 mg/kg group was found dead at the end of the second cycle. There had been no abnormal clinical signs, although it had lost 10% of body weight based on the weight the day before it died (blue dot marked in Figure 6-13 B at Day 11). One other mouse in the MLN8237 30 mg/kg group had lost 10% of body weight at the end of study with body weight close to this from Day 25 (blue dots marked in Figure 6-13 B).

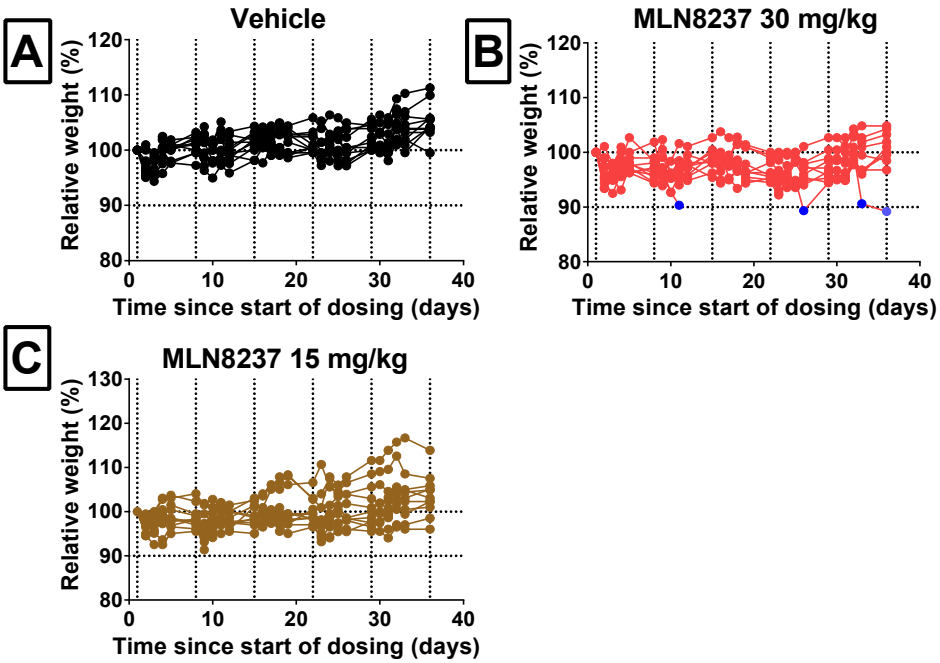

Figure 6-13: Percentage body weight relative to Day 1 of dosing over days since first dose for each individual mouse dosed with MLN8237 once daily for five consecutive days of a weekly cycle for five weeks.
Individual mouse body weight plotted for each group for A. Vehicle B. MLN8237 30 mg/kg C. MLN8237 15 mg/kg. Mice were weighed prior to each cycle, with vertical black dotted lines indicating the start of each cycle. Blue dots used to indicate body weights meeting loss of 10% body weight. MLN8237 dosed daily by oral gavage for five consecutive days of a weekly cycle for total of five cycles with final dose administered on day 36 two to six hours prior to endpoint. Statistical testing was performed using ordinary one way ANOVA with Dunnett's multiple comparison test comparing each treatment group to vehicle in GraphPad Prism.

On the endpoint blood tests (Figure 6-14), the overall white blood count (WBC) was significantly lower than vehicle following administration of either MLN8237 treatment (p=0.038). As two of the mice in the vehicle group had a raised total white cell count with lymphocytosis (shown in red dots in Figure 6-14 A), these outliers were excluded. When the data was re-analysed, the difference between the MLN8237 treatment groups

compared to vehicle remained significant (p=0.041), although there was not a significant difference between each individual group compared to vehicle (p=0.062 for MLN8237 30 mg/kg, p=0.099 for MLN8237 15 mg/kg). When the components of the WBC count were analysed, there was a decrease in granulocytes, lymphocytes and monocytes in the MLN8237 treatment groups, compared to vehicle. This reached significance for granulocytes (p=0.0012) and monocytes (p=0.0007).

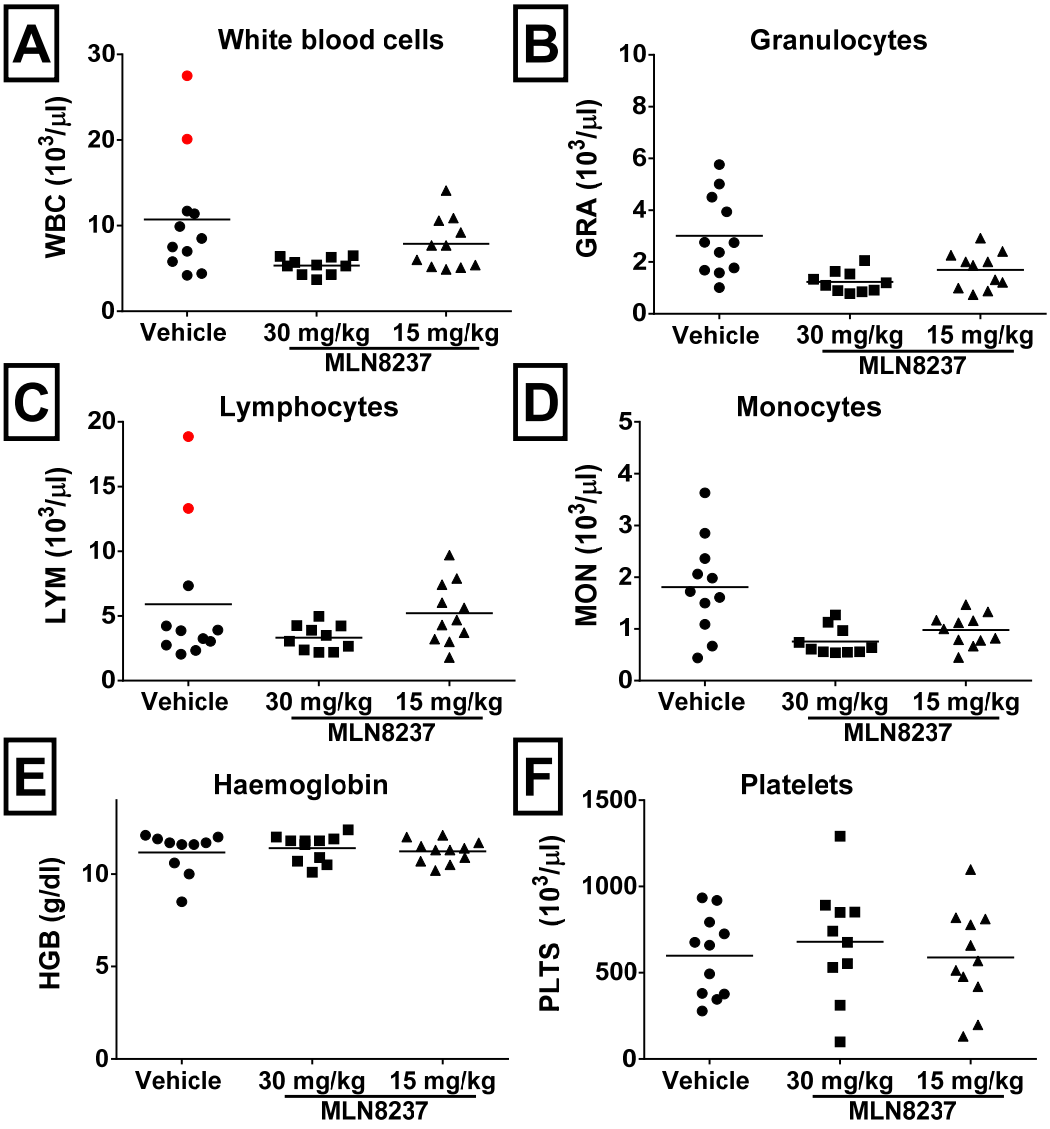

Figure 6-14: Blood counts for study comparing the effect of multiple dosing (once daily for five consecutive days of a weekly cycle for five weeks) of MLN8237 30 mg/kg or MLN8237 15 mg/kg compared to vehicle.
MLN8237 dosed as described in Figure 6-13. Samples were taken at Day 36 (between two and six hours after last dose of MLN8237). Parameters measured are A. total white blood cell count (WBC), B. granulocytes (gra), C. lymphocytes (lym), D. monocytes (mon), E. haemoglobin (HGB) and F. platelets (plts). Two mice with higher overall WBC and lymphocyte count in the vehicle group are indicated with red dots. Statistical testing was performed using ordinary one way ANOVA with Dunnett's multiple comparison test comparing each treatment group to vehicle in GraphPad Prism.

These results are consistent with reports of lower white cell counts and neutropenia (granulocytes reduced) with single agent MLN8237 in clinical trials (204). There was no significant difference in haemoglobin. There was a very wide range of platelet counts within each treatment group, with no obvious increase or decrease induced by MLN8237.

The results from the endpoint blood tests with the lower WBC in the MLN8237 treated mice indicated an effect of the drugs on the bone marrow, which was therefore assessed in the mouse femurs. I reviewed these and an opinion on a blinded series was sought from a histopathologist, Dr Penny Wright. She commented that in mice treated with MLN8237 30 mg/kg, haemosiderin staining was seen, indicative of haemosiderin-laden macrophages involved in phagocytosis of dead/dying cells. More megakaryocytes were identified (bone marrow cells responsible for production of platelets). There was also a shift in the normal myeloid/erythroid cell ratio – a so called “left shift” where more immature WBC are seen, particularly myeloid precursors. These changes are consistent with the effect of drugs on the bone marrow, which is then recovering. Whilst occasional haemosiderin staining was seen in the MLN8237 15mg/kg group, a “left shift” was not seen. Representative images are shown in Figure 6-15.

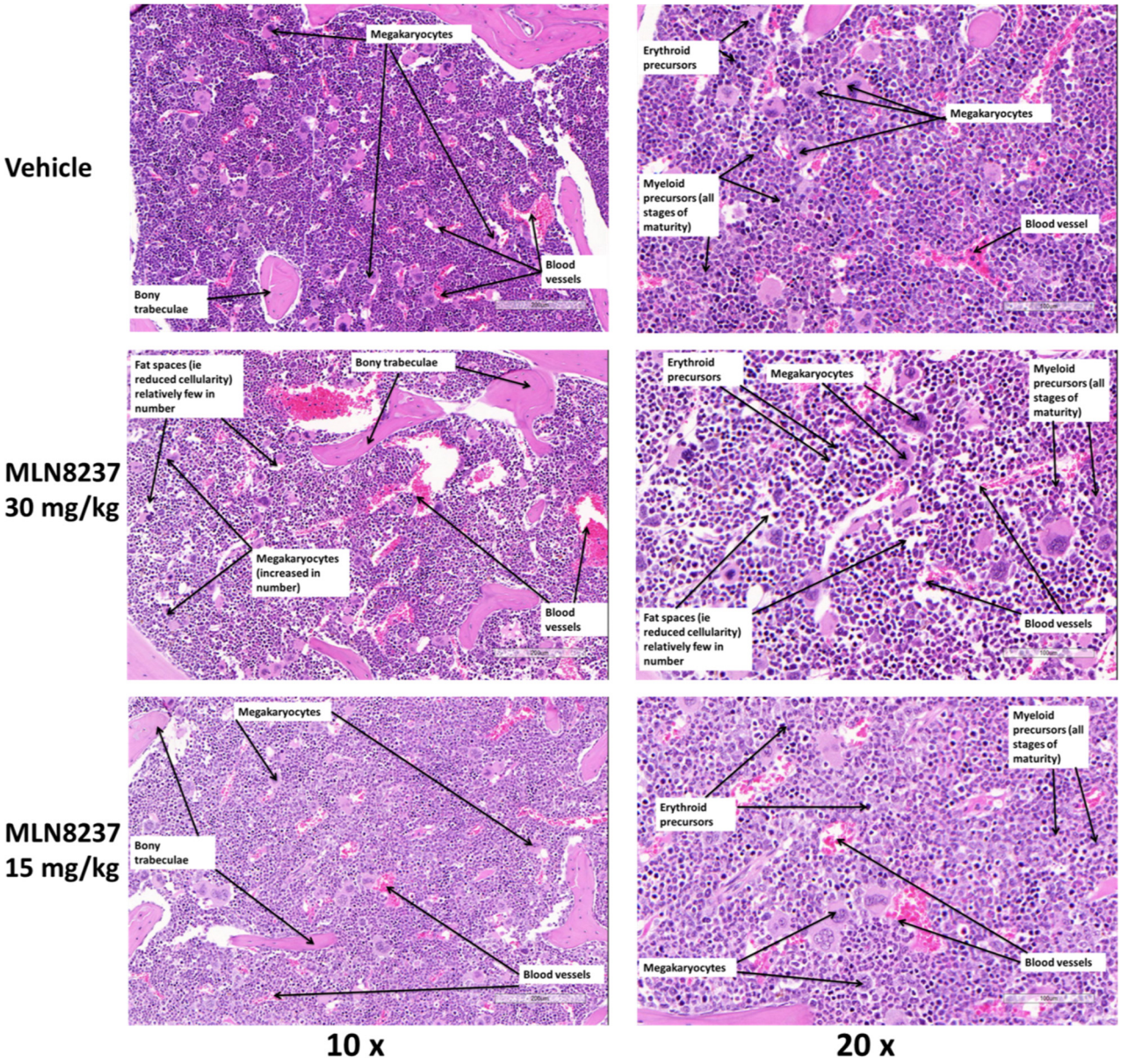

Figure 6-15: Representative bone marrow images of femurs of mice comparing the effect of multiple dosing (once daily for five consecutive days of a weekly cycle for five weeks) of MLN8237 30 mg/kg or MLN8237 15 mg/kg compared to vehicle.
MLN8237 dosed as described in Figure 6-13. In both MLN8237 15 mg/kg and MLN8237 30 mg/kg, reduced cellularity and increase in megakaryocytes and myeloid precursors seen as labelled. Images stained with H&E. Left hand side scale bars 200 µm, right hand scale bar 100 µm. Femurs from mice prepared and stained as described in 2.3.5.3.

Dr Wright also suggested staining the bone marrow slides for anti-Myeloperoxidase (MPO), which detects granulocytes and monocytes in blood and precursors of granulocytes in the bone marrow. It strongly labels myeloid cells at all stages of maturation, whereas cells of monocytic origin are typically weakly positive or negative and erythroid precursors, megakaryocytes, lymphoid cells, plasma cells and blood vessels are negative (293) and hence could have given a useful indicator of relevant changes in the bone marrow. However, there was no significant different in the percentage of MPO positive cells between treatment groups (Figure 6-16). Thus, this

marker did not identify the MLN8237-induced change in myeloid precursors identified on the H&E stains and hence could not replace individual image analysis by an expert pathologist in these studies.

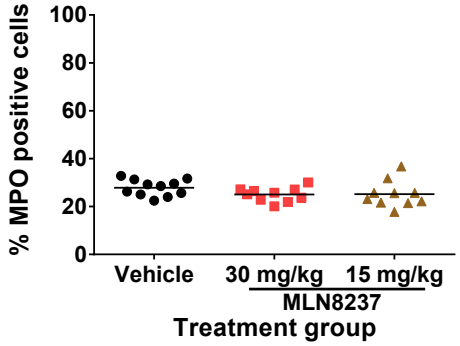

Figure 6-16: Myeloperoxidase (MPO) positive cells in bone marrow of femurs of mice with T24 xenografts comparing the effect of multiple dosing (once daily for five consecutive days of a weekly cycle for five weeks) of MLN8237 30 mg/kg or MLN8237 15 mg/kg compared to vehicle.
MLN8237 dosed as described in Figure 6-13. Samples were taken at Day 36 (between two and six hours after last dose of MLN8237.) Statistical testing was performed using ordinary one way ANOVA with Dunnett's multiple comparison test comparing each treatment group to vehicle in GraphPad Prism.

6.4.2.2 Effect of MLN8237 on tumour growth

There was a significant difference in tumour growth between vehicle and MLN8237 treated mice ($p<0.0001$ for both MLN8237 30 mg/kg and 15 mg/kg), despite the variable growth in the vehicle group (Figure 6-17). There was no significant difference in tumour growth between the two different doses of MLN8237 ($p=0.98$).

In clinical practice, tumour response to treatment is assessed using RECIST criteria (294). These are:

- Complete response (CR): Disappearance of all target lesions
- Partial Response (PR): At least a 30% decrease in the sum of the longest diameter (LD) of target lesions, taking as reference the baseline sum LD
- Stable Disease (SD): Neither sufficient shrinkage to qualify for PR nor sufficient increase to qualify for PD, taking as reference the smallest sum LD since the treatment started
- Progressive Disease (PD): At least a 20% increase in the sum of the LD of target lesions, taking as reference the smallest sum LD recorded since the treatment started or the appearance of one or more new lesions

When the change in tumour volume was compared to Day 1 of dosing using a waterfall plot (Figure 6-18), 9/11 vehicle tumours showed PD, the MLN8237 30 mg/kg group had 6/10 PD, 3/10 PR and 1/10 SD; and the MLN8237 15 mg/kg group had 5/10 PD,

2/10 CR, 1/10 PR and 3/10 SD. This confirms the differences seen in mean tumour growth over time illustrated in Figure 6-17.

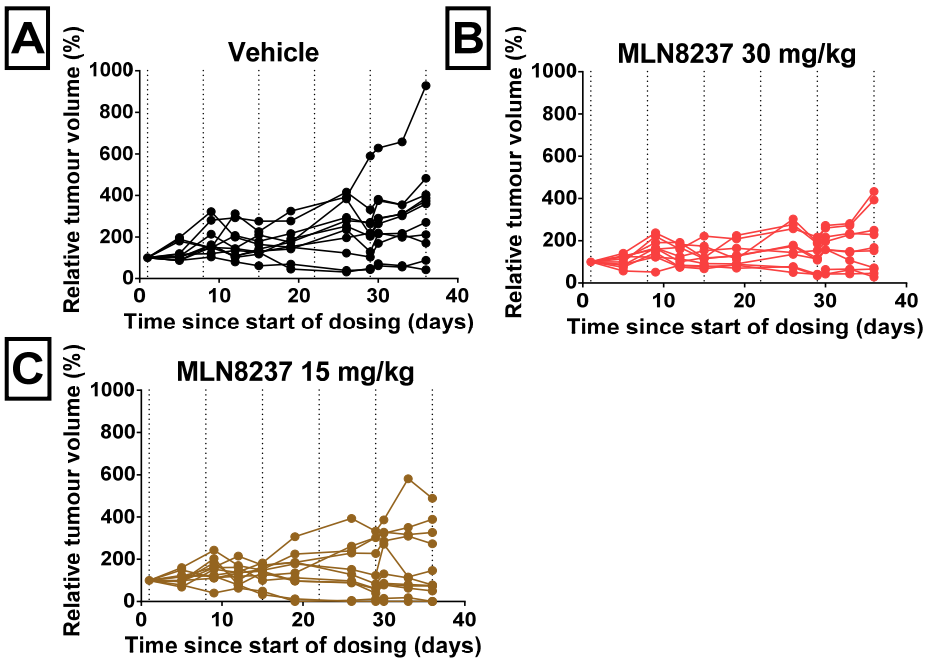

Figure 6-17: Relative tumour growth expressed as volume measured over time since start of dosing comparing the effect of multiple dosing (once daily for five consecutive days of a weekly cycle for five weeks) of MLN8237 30 mg/kg or MLN8237 15 mg/kg compared to vehicle.
Mice were dosed with either A. vehicle B. MLN8237 30 mg/kg, C. MLN8237 15 mg/kg. MLN8237 dosed as described in Figure 6-13, with vertical black lines indicating start of each cycle. Tumour volumes were measured approximately every 72 hours after dosing using calipers. Endpoint was at day 36. Statistical testing was performed using ordinary two way ANOVA with Tukey's multiple comparison test comparing each treatment group in GraphPad Prism.

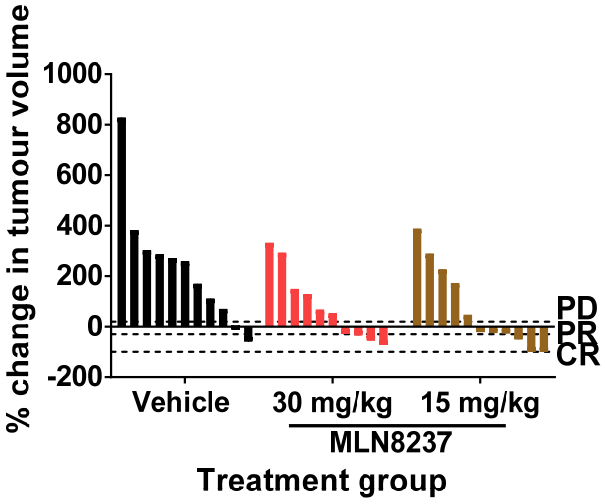

Figure 6-18: Waterfall plot of percentage change in tumour volume at endpoint comparing the effect of multiple dosing (once daily for five consecutive days of a weekly cycle for five weeks) of MLN8237 30 mg/kg or MLN8237 15 mg/kg compared to vehicle.
Percentage tumour volume at endpoint compared to Day 1 dosing in mice dosed with vehicle, MLN8237 30 mg/kg or MLN8237 15 mg/kg. MLN8237 dosed dosed as described in Figure 6-13. Tumour volumes were measured approximately every 72 hours using calipers. The black dotted lines indicate progressive disease (PD) with 20% increase in tumour volume, partial response (PR) with 30% decrease in tumour volume and complete response (CR) with complete regression of tumour.

Given the issue with fluid-filled cysts in the tumours, the tumours were also weighed after dissection, once the cyst fluid had drained out to investigate if there was a relationship between endpoint tumour volume and tumour weight. There was a significant correlation between tumour volume and tumour weight, with a of r=0.925 (CI 0.8506 to 0.963, p<0.0001) (Figure 6-19 A). Although there was a difference in mean tumour weight between the groups, this was non-significant, with variation reflected in the standard deviations (mean and SD vehicle 0.42±0.22 g, MLN8237 30 mg/kg 0.21±0.15 g and MLN8237 15 mg/kg 0.30±0.33 g). However, tumour inhibition rate (calculated using the formula = (1-mean tumour weight treated/mean tumour weight control as in (261)) confirmed a treatment effect. This was 54% in the MLN8237 30 mg/kg group versus 27% in the MLN8237 15 mg/kg group showing MLN8237 30 mg/kg was more effective overall, even though there were two CR in the MLN8237 15 mg/kg group.

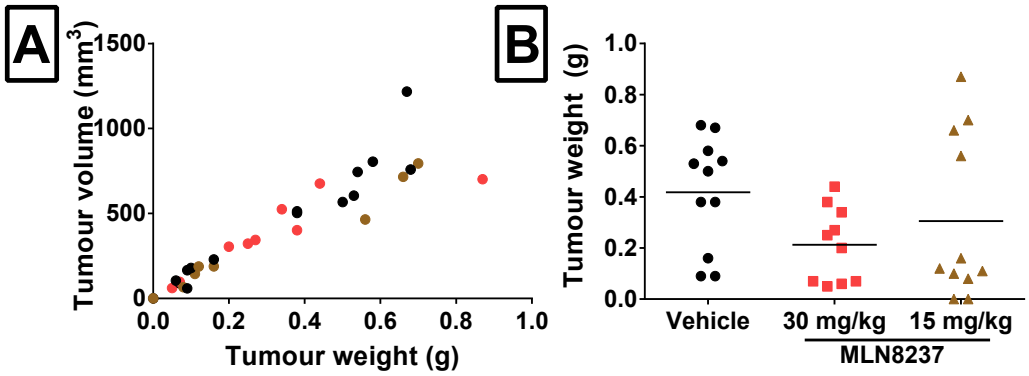

Figure 6-19: Relationship between tumour volume and tumour weight comparing the effect of multiple dosing (once daily for five consecutive days of a weekly cycle for five weeks) of MLN8237 30 mg/kg or MLN8237 15 mg/kg compared to vehicle.
Tumour volume compared with tumour weight in each treatment group at end of study in mice dosed with vehicle (shown in black), MLN8237 30 mg/kg (shown in red) or MLN8237 15 mg/kg (shown in brown). A. shows the relationship between tumour weight and tumour volume at endpoint, B. shows the tumour weights for each group. MLN8237 dosed dosed as described in Figure 6-13. Tumour volumes were measured using calipers every 72 hours, tumour weights measured following drainage of any cysts after dissection at endpoint of study. Pearson correlation coefficient calculated by GraphPad Prism.

6.4.2.3 Effect of MLN8237 on PD markers

There was a statistically significant increase in the percentage of CC3 positive tissue between the vehicle and MLN8237 treatment groups (Figure 6-20 B, p=0.040) with the difference remaining significant when MLN8237 30 mg/kg alone was compared with vehicle (p=0.039) but not for MLN8237 15 mg/kg (p=0.089), suggesting that with MLN8237 30 mg/kg an active anti-tumoural concentration may have been achieved. There was no significant difference in Ki67 or pH3 between the vehicle and MLN8237 treated groups (Figure 6-20 A and C). Whilst others have reported a reduction in Ki67

positive cells, the exact timing of their endpoint compared to last dose of drug is not clear as they state *"on completion of treatment"* (121), which could potentially influence results seen. The percentage of necrosis was very variable within each group and there was no significant difference between groups (Figure 6-20 D).

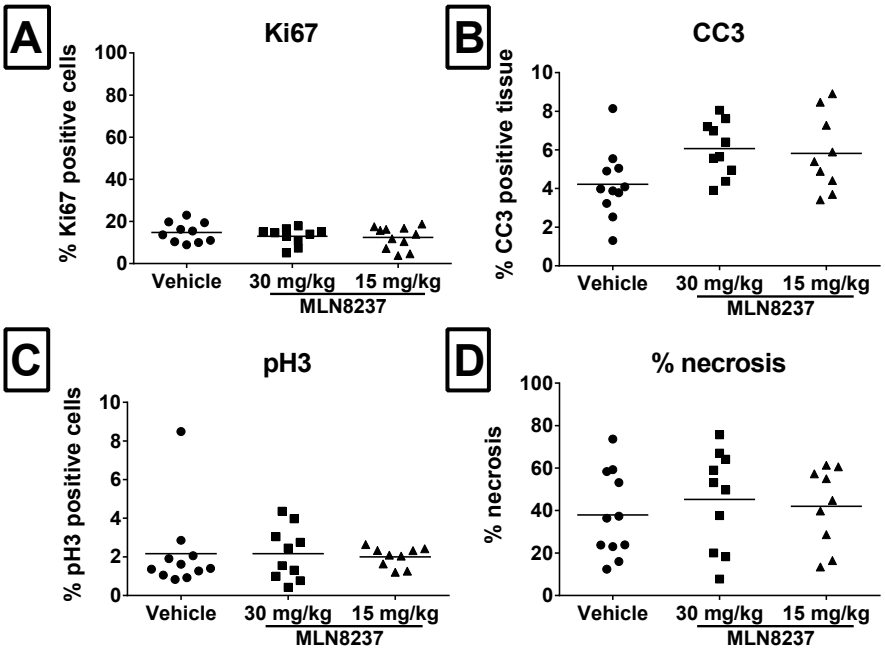

Figure 6-20: Pharmacodynamic markers measured at endpoint comparing the effect of multiple dosing (once daily for five consecutive days of a weekly cycle for five weeks) of MLN8237 30 mg/kg or MLN8237 15 mg/kg compared to vehicle.
A. percentage positive cells for Ki67, B. percentage positive tissue for CC3, C. percentage positive cells pH3, after dosing with either vehicle, MLN8237 30 mg/kg or MLN8237 15 mg/kg as described in Figure 6-13. Tumour samples were taken at the endpoint of the study, Day 36 from start of dosing with a final dose of MLN8237 administered two to six hours prior to endpoint. Slides analysed in HALO™ (as described in 2.3.5.1). D. shows percentage of necrosis for slides analysed in HALO™. One mouse in the MLN8237 30 mg/kg was found dead after the second cycle and samples were not collected. Two of the mice in MLN837 15 mg/kg group had a complete response and no tumour remained for analysis. Statistical testing was performed using ordinary one way ANOVA with Dunnett's multiple comparison test comparing each treatment group to vehicle.

6.4.2.4 Summary of MLN8237 efficacy study

The MLN8237 treatments were tolerated, although two mice in the MLN8237 30 mg/kg did show a reduction in weight. With both the MLN8237 30 mg/kg and 15 mg/kg treatment groups, a significant reduction in overall WBC and granulocytes was seen compared to vehicle, consistent with previous reports. There was a significant difference in tumour growth for both treatment groups compared to vehicle, but a greater tumour inhibition rate was seen in the 30 mg/kg group compared to the 15 mg/kg group. The increase in CC3 positive tissue seen with MLN8237 30 mg/kg suggests sufficient tumour concentrations may have been achieved to show an anti-tumour effect.

6.4.3 Summary of single agent efficacy studies

Whilst repeated dosing of paclitaxel 20 mg/kg was not tolerable, paclitaxel 6 mg/kg showed some evidence of anti-tumour effect. Docetaxel 20 mg/kg was tolerated and showed the greater anti-tumour effect. Although no anti-tumour efficacy was seen with either paclitaxel 2 mg/kg or docetaxel 6 mg/kg, it is possible that they could provide a synergistic combination with an AK-A inhibitor, as seen in the *in vitro* studies with low concentrations of paclitaxel and docetaxel.

MLN8237 30 mg/kg and 15 mg/kg led to tumour responses but the greatest effect was seen with MLN8237 30 mg/kg where target PK was achieved. The endpoint blood results correlated with clinical reports of neutropenia, highlighting the concern in combining MLN8237 with full dose taxane, but I predicted this would be less when combined with lower concentrations of paclitaxel. Therefore, I chose to use MLN8237 30 mg/kg for my combination studies with both paclitaxel and docetaxel.

Traditional combination studies would use the full normal single agent dose of the most established drug (here this would be taxanes) and then increase the dose of the newer agent (MLN8237). However, my *in vitro* work in Chapters 3 and 4 suggest that exploring a wider range of doses may allow synergy to be detected and reduce toxicity. Therefore in these studies, I aimed to achieve a similar anti-tumour effect between the combination and full dose taxane but with reduced toxicity.

6.5 MLN8237 and paclitaxel combination studies

6.5.1 Study to assess tolerability of MLN8237 and paclitaxel in combination

As paclitaxel 20 mg/kg was not tolerated, paclitaxel 6 mg/kg was used for these studies, with 2 mg/kg also assessed. Emerging data suggested that intermittent MLN8237 could be an effective strategy to reduce toxicity and hence the effect of reducing dosing from Days 1-5 per week to Days 1-3 per week was compared. For this tolerability study, three or four mice were randomised to four cycles of the treatments listed.

1. MLN8237 30 mg/kg once daily for five consecutive days and paclitaxel 6 mg/kg weekly
2. MLN8237 30 mg/kg once daily for three consecutive days and paclitaxel 6 mg/kg weekly
3. MLN8237 30 mg/kg once daily for five consecutive days and paclitaxel 2 mg/kg weekly

4. MLN8237 30 mg/kg once daily for three consecutive days and paclitaxel 2 mg/kg weekly
5. MLN8237 30 mg/kg once daily for five consecutive days
6. Paclitaxel 6 mg/kg weekly
7. Vehicle

Paclitaxel was dosed first followed by MLN8237 on the days when both treatments were given. Single agent paclitaxel 2 mg/kg was not repeated as it had previously been shown to be tolerable (6.4.1) and to minimise the numbers of mice required. For logistical reasons, the mice were divided into two cohorts, with mice in the first cohort killed approximately 20 hours after the last dose of MLN8237 and 96 hours after the last dose of paclitaxel of that cycle and mice in the second cohort killed approximately three hours after the last dose of MLN8237 and 72 hours after the last dose of paclitaxel of that cycle. As this could have had an effect on blood counts and PD markers, the cohort killed 20 hours after the last dose of MLN8237 are marked in blue on these graphs.

6.5.1.1 Tolerability of MLN8237 and paclitaxel combination

The mice appeared to tolerate the dosing well apart from one mouse in the 6mg/kg paclitaxel group which had a seizure after the first dose of paclitaxel but recovered within 30 minutes and remained on study without adverse effects after subsequent doses. Body weight remained stable as seen in Figure 6-21.

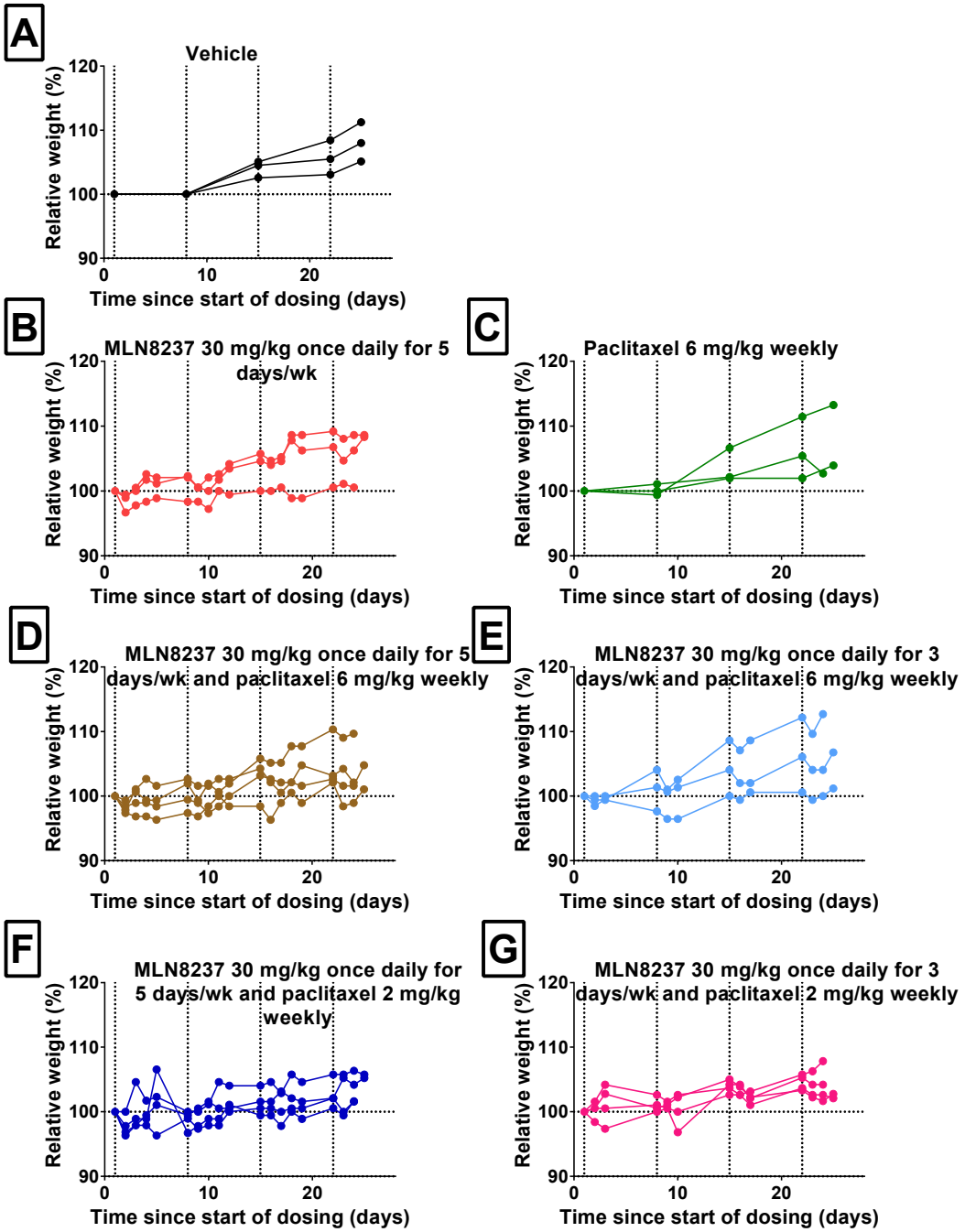

Figure 6-21: Percentage body weight relative to Day 1 of dosing over days since first dose for each individual mouse study assessing the tolerability of combinations of MLN8237 and paclitaxel in T24 xenografts.

Mice were dosed with four cycles of A. Vehicle B. MLN8237 30 mg/kg once daily for five days per week C. paclitaxel 6 mg/kg weekly D. MLN8237 30 mg/kg once daily for five days per week and paclitaxel 6 mg/kg weekly E. MLN8237 30 mg/kg once daily for three days per week and paclitaxel 6 mg/kg weekly F. MLN8237 30 mg/kg once daily for five days per week and paclitaxel 2 mg/kg weekly G. MLN8237 30 mg/kg once daily for three days per week and paclitaxel 6 mg/kg weekly. MLN8237 dosed by oral gavage and paclitaxel dosed intravenously weekly. Mice were weighed prior to each cycle, with vertical black dotted lines indicating the start of each cycle.

6.5.1.1.1 *Effect of MLN8237 and paclitaxel combination on endpoint blood tests*

The time since the last dose of MLN8237 and paclitaxel did not appear to affect the results, with no difference seen between the two cohorts (green dots 20 hours after last dose of MLN8237, black dots three hours after last dose of MLN8237) (Figure 6-22).

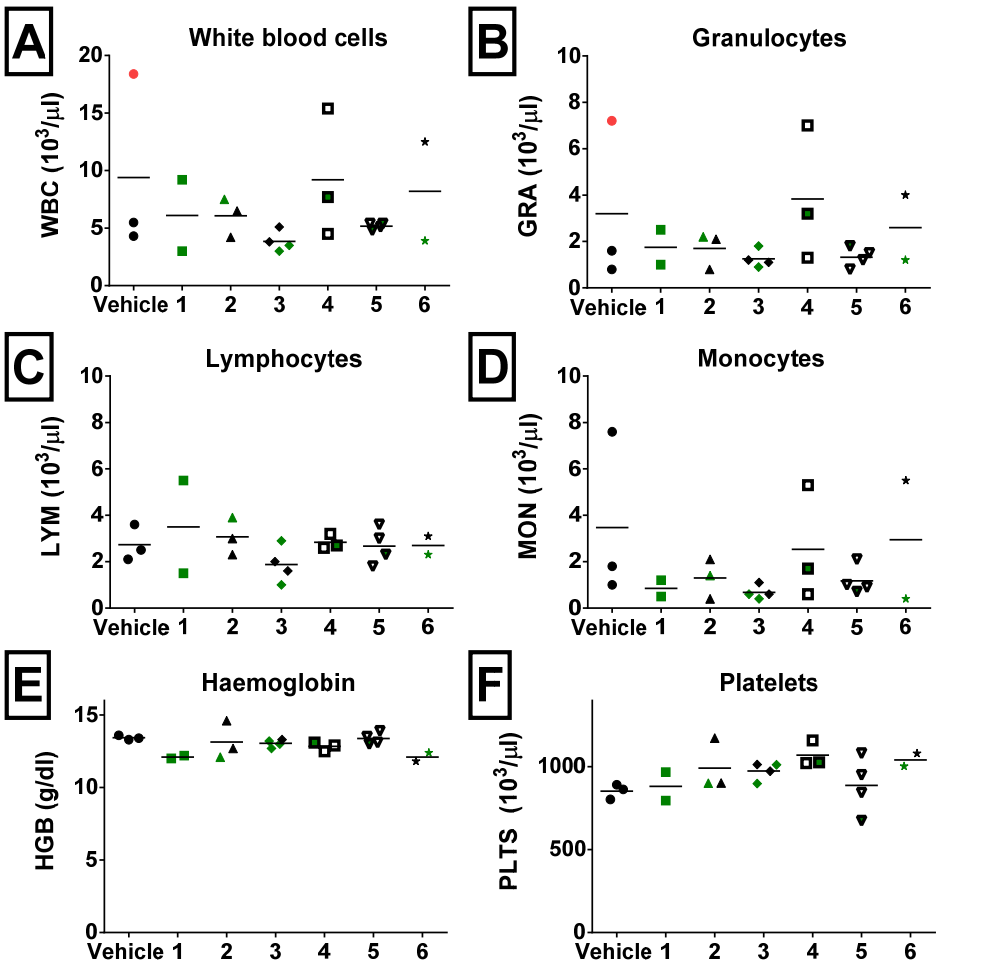

Treatment groups

Vehicle
1. MLN8237 30 mg/kg once daily for 5 days/wk
2. Paclitaxel 6 mg/kg weekly
3. MLN8237 30 mg/kg once daily for 5 days/wk and paclitaxel 6 mg/kg weekly
4. MLN8237 30 mg/kg once daily for 3 days/wk and paclitaxel 6 mg/kg weekly
5. MLN8237 30 mg/kg once daily for 5 days/wk and paclitaxel 2 mg/kg weekly
6. MLN8237 30 mg/kg once daily for 3 days/wk and paclitaxel 2 mg/kg weekly

Figure 6-22: Endpoint blood counts for study assessing the tolerability of combinations of MLN8237 and paclitaxel in T24 xenografts.
Mice were dosed with four cycles of treatments as detailed in Figure 6-21. Samples were taken on Day 24 three hours after last dose of MLN8237 and 72 hours after last dose of paclitaxel where applicable in samples shown with black dots and on Day 25 approximately twenty hours after last dose of MLN8237 and 96 hours after last dose of paclitaxel where applicable in samples shown with green dots. Parameters measured are A. total white blood cell count (WBC), B. granulocytes (gra), C. lymphocytes (lym), D. monocytes (mon), E. haemoglobin (HGB) and F. platelets (plts). One mouse in vehicle group had higher WBC count with increase granulocytes (marked with red dot). Due to technical issues with the blood samples, no full result was valid for three mice – two in the MLN8237 30 mg/kg once daily for three days and paclitaxel 2 mg/kg group and one in the MLN8237 30 mg/kg once daily for five days group and these were excluded. Statistical testing was performed using ordinary one way ANOVA with Dunnett's multiple comparison test comparing each treatment group to vehicle in GraphPad Prism.

There was one mouse in the vehicle group which had a higher WBC with increased granulocytes (marked in red in Figure 6-22 A), possibly due to occult infection. Analysis of the data with and without this outlier showed no significant differences

between the treatment groups for either overall WBC or the individual components. Haemoglobin and platelet counts were also similar across treatments.

These results suggest that the combinations appear to tolerable and did not cause a significantly greater reduction in granulocytes, which might have been expected, since both MLN8237 and paclitaxel can cause neutropenia as single agents.

6.5.1.1.2 *Effect of MLN8237 and paclitaxel combination on bone marrow*

As in the earlier MLN8237 efficacy study, the bone marrow was examined, with an opinion on a blinded series from Dr Penny Wright. In both groups of mice treated with the combination of MLN8237 30 mg/kg together with paclitaxel 6 mg/kg weekly, haemosiderin staining was seen, with more megakaryocytes, a "left shift" in the myeloid/erythroid cell ratio with few mature forms and more pronounced fat spaces indicative of reduced cellularity, compared to the single agents. In the combinations of MLN8237 30 mg/kg with paclitaxel 2 mg/kg, the bone marrow appeared very similar to single agent MLN8237 30 mg/kg. Dr Wright commented that the combination treatments did not show as much additional myelotoxicity as she might have expected over the single agent groups. Representative images highlighting these findings are shown in Figure 6-23.

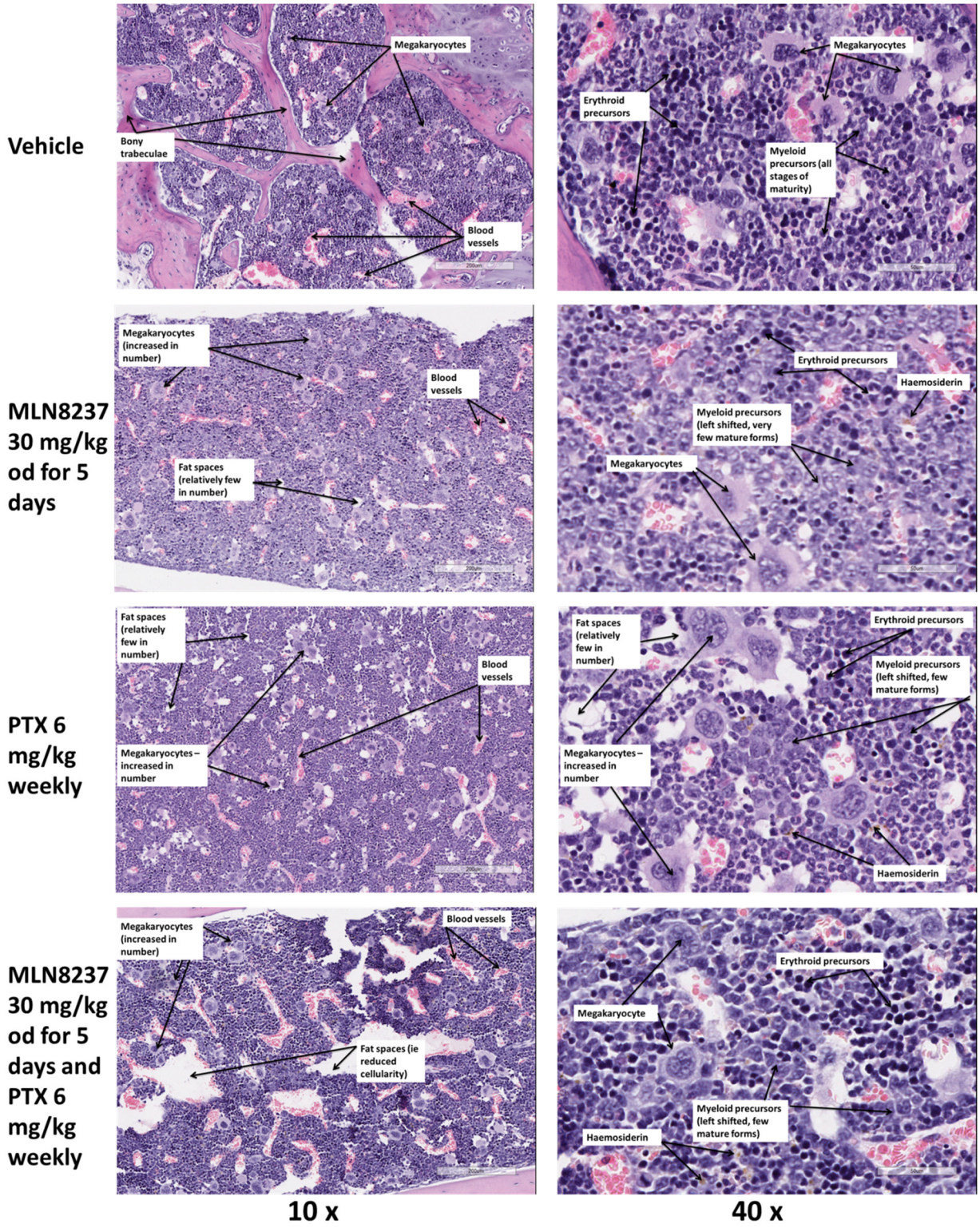

Figure 6-23: Representative images bone marrow images of femurs of mice in study assessing the tolerability of combinations of MLN8237 and paclitaxel in T24 xenografts.
Sample images are shown of bone marrow images from vehicle, MLN8237 30 mg/kg once daily for five days/week, paclitaxel 6 mg/kg weekly and the combination of MLN8237 30 mg/kg once daily for five days and paclitaxel 6 mg/kg weekly stained with H&E. Scale bars: left = 200 µm, right = 50 µm. Femurs from mice prepared and stained as described in 2.3.5.3. PTX=paclitaxel.

6.5.1.2 Effect of MLN8237 and paclitaxel combination on tumour growth

In this study, one of the three tumours did not grow in the vehicle group (Figure 6-24 A). With only three mice per group, this tolerance study was not designed to quantify tumour growth inhibition. However, there was an indication that all of the treatments may reduce tumour growth compared to the growth seen in the other two vehicle mice.

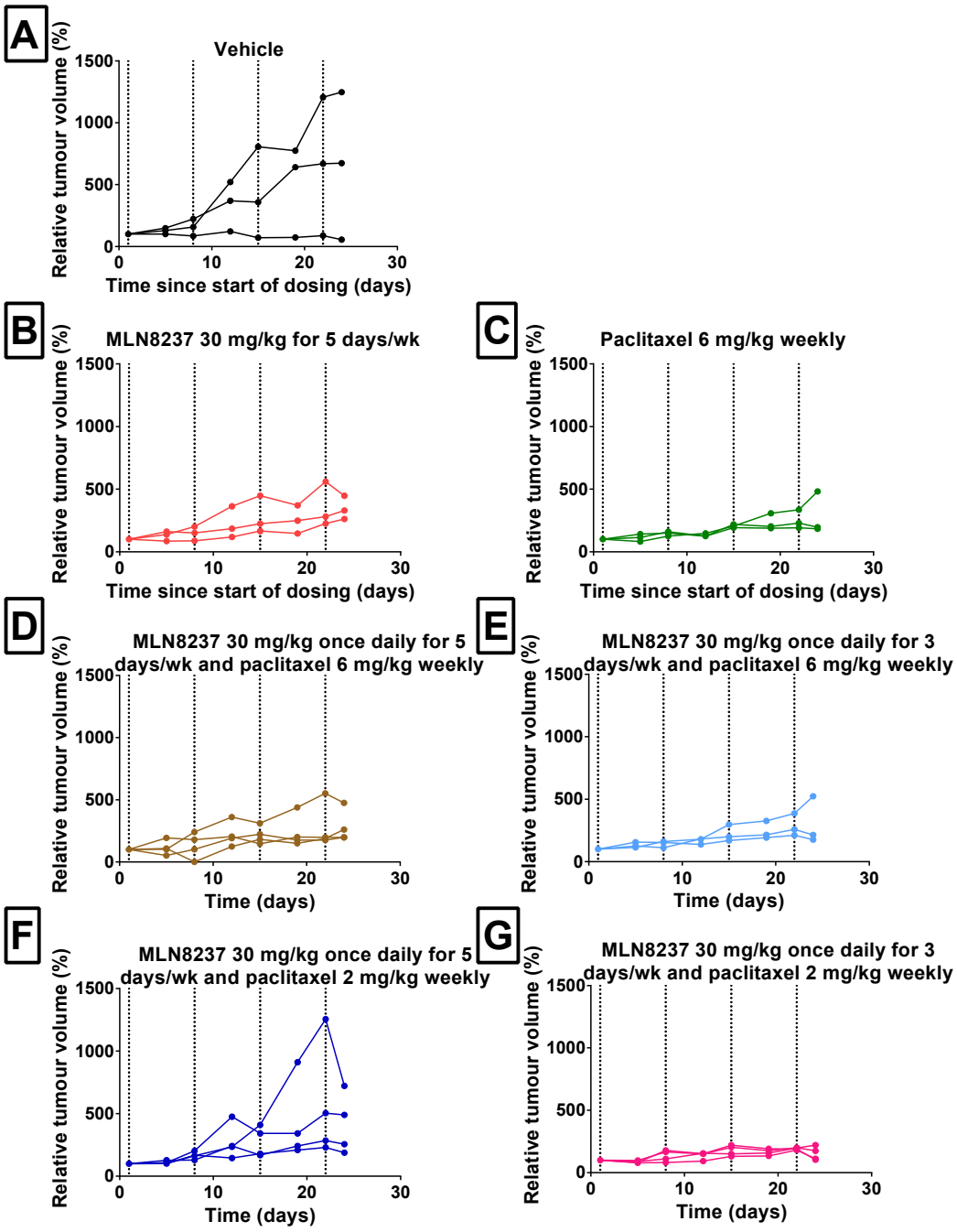

Figure 6-24: Tumour growth expressed as volume measured over time since start of dosing (days) in study assessing the tolerability of combinations of MLN8237 and paclitaxel in T24 xenografts. The individual mice tumour growth plots are shown for A. Vehicle B. MLN8237 30 mg/kg once daily for five days per week C. paclitaxel 6 mg/kg weekly D. MLN8237 30 mg/kg once daily for five days per week and paclitaxel 6 mg/kg weekly E. MLN8237 30 mg/kg once daily for three days per week and paclitaxel 6 mg/kg weekly F. MLN8237 30 mg/kg once daily for five days per week and paclitaxel 2 mg/kg weekly G. MLN8237 30 mg/kg once daily for three days per week and paclitaxel

2 mg/kg weekly. Mice were dosed with four cycles of treatments as detailed in Figure 6-21. Tumour volumes were measured prior to each dosing using calipers and weekly in vehicle group.

6.5.1.3 Effect of MLN8237 and paclitaxel combination on PD markers

When the tumour sections were stained for all the PD markers previously explored, there was no difference in the results depending on the time samples were collected, or across the treatment groups for any of these markers or percentage necrosis (Figure 6-25).

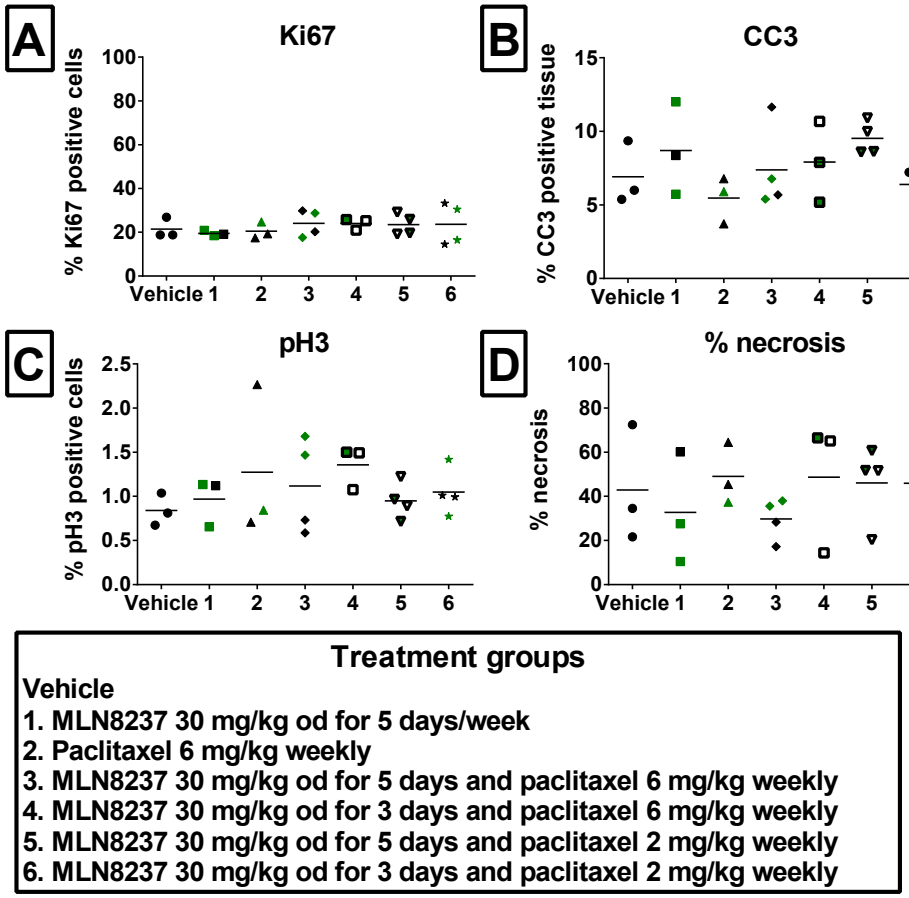

Figure 6-25: Pharmacodynamic markers measured at endpoint in study assessing the tolerability of combinations of MLN8237 and paclitaxel in T24 xenografts.
A. percentage positive cells for A. Ki67, B. percentage positive tissue for CC3, C. percentage positive cells pH3 after dosing with four cycles of treatments as detailed in Figure 6-21. D. shows percentage of necrosis for slides analysed in HALO™. Tumour samples were taken at the endpoint of the study, Day 24 three hours after last dose of MLN8237 and 72 hours after last dose of paclitaxel where applicable in samples shown with black dots and on Day 25 approximately twenty hours after last dose of MLN8237 and 96 hours after last dose of paclitaxel where applicable in samples shown with green dots. Slides analysed in HALO™ (as described in 2.3.5.1). Statistical testing was performed using ordinary one way ANOVA with Dunnett's multiple comparison test comparing each treatment group to vehicle in GraphPad Prism.

6.5.1.4 Summary of MLN8237 and paclitaxel tolerability study

In this study, all of the combinations tested appeared tolerable, with less effect on endpoint blood tests and bone marrow analysis than may have been anticipated. As there was no significant difference in tolerability between the dosing of MLN8237 for

Days 1-3 and Days 1-5, I decided to use Days 1-5 for the efficacy study to maximise MLN8237 exposure and to test both concentrations of paclitaxel.

6.5.2 Efficacy of MLN8237 and paclitaxel in combination

Mice were randomised to one of the following treatment groups (N = 10 per group):

1. MLN8237 30 mg/kg once daily for five days/week OG and vehicle iv
2. Vehicle OG and Paclitaxel 6 mg/kg iv weekly
3. Vehicle OG and Paclitaxel 2 mg/kg iv weekly
4. Combination of MLN8237 30 mg/kg once daily for five days/week and Paclitaxel 6 mg/kg iv weekly
5. Combination of MLN8237 30 mg/kg once daily for five days/week and Paclitaxel 2 mg/kg iv
6. Vehicle OG and vehicle IV weekly

Five full cycles of each treatment was delivered. Mice then received Days 1 and 2 of a sixth cycle and were killed on Day 39, 24 hours after the last dose of MLN8237 (groups 1, 4 and 5) and 48 hours after the last dose of paclitaxel (groups 2, 3, 4 and 5).

6.5.2.1 Tolerability of MLN8237 and paclitaxel combination

Two mice died in the restrainer tube, with no obvious reason –one prior to any injection in the vehicle group and one prior to the second dose of paclitaxel 2 mg/kg. Their data has been removed. All other mice remained well during the study with stable weights throughout in all groups (Figure 6-26). Given the tolerability of these combinations in 6.5.1, endpoint blood counts and bone marrows were not performed in this study.

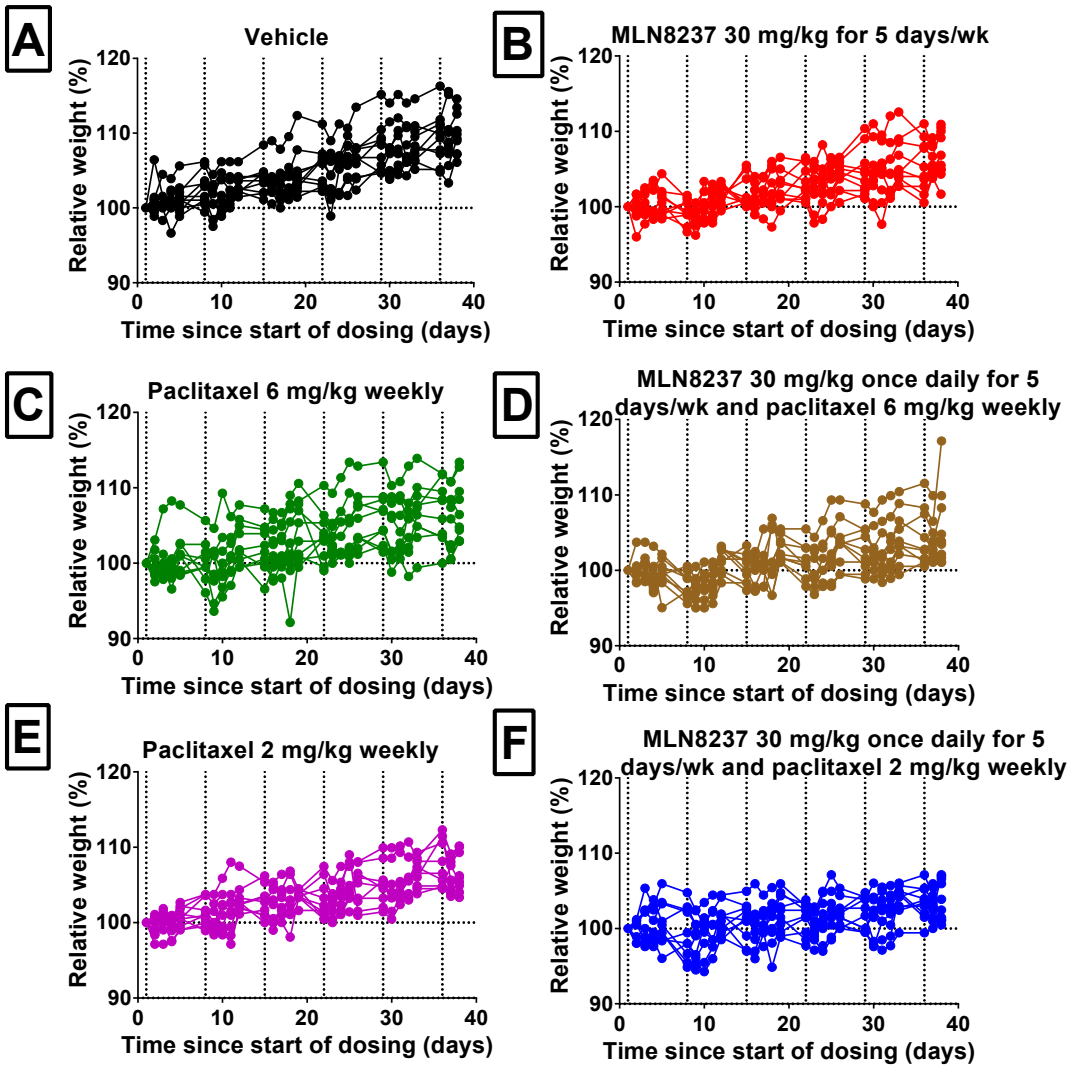

Figure 6-26: Percentage body weight relative to Day 1 of dosing over days since first dose for each individual mouse in study assessing the efficacy of combinations of MLN8237 and paclitaxel in T24 xenografts.

Percentage body weight relative to Day 1 of dosing over days since first dose for each individual mice dosed with five cycles of A. Vehicle B. MLN8237 30 mg/kg once daily for five days per week C. paclitaxel 6 mg/kg weekly D. MLN8237 30 mg/kg once daily for five days per week and paclitaxel 6 mg/kg weekly E. paclitaxel 2 mg/kg weekly F. MLN8237 30 mg/kg once daily for five days per week and paclitaxel 2 mg/kg. Mice were weighed prior to each cycle, with vertical black dotted lines indicating the start of each cycle. MLN8237 dosed daily by oral gavage for five consecutive days of a weekly cycle and paclitaxel dosed intravenously weekly.

6.5.2.2 Effect of MLN8237 and paclitaxel combination on tumour growth

6.5.2.2.1 *Growth curves*

Despite variable tumour growth, there was a significant difference for all the drug treatments compared to vehicle ($p<0.0001$ overall and for each group) (Figure 6-27). Whilst there were no significant differences between the treatment groups, the spider plots of individual tumours suggested that MLN8237 30 mg/kg once daily for five days and paclitaxel 6 mg/kg weekly (Figure 6-27 D) suppressed growth most consistently.

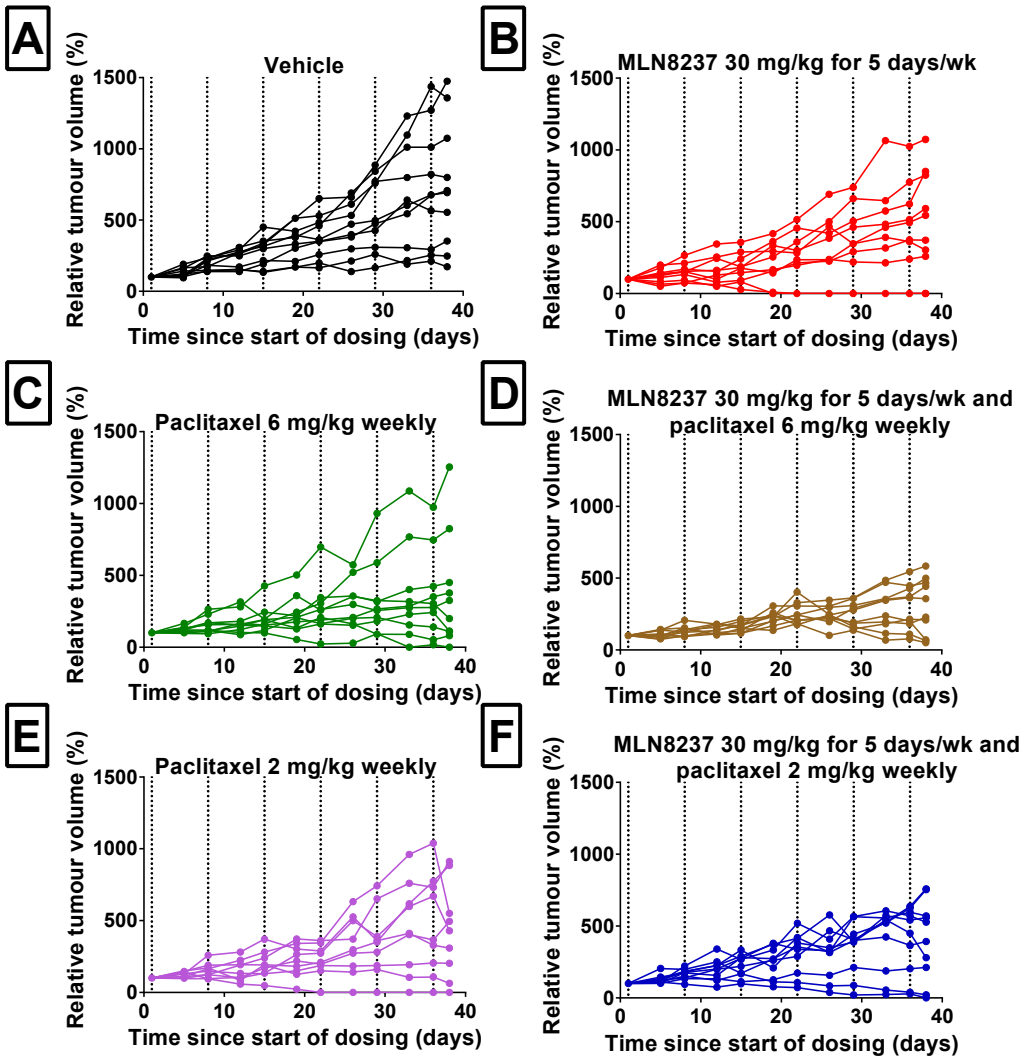

Figure 6-27: Tumour growth expressed as volume measured over time since start of dosing (days) in study assessing the efficacy of combinations of MLN8237 and paclitaxel in T24 xenografts.
The individual mice tumour growth plots are shown for A. Vehicle B. MLN8237 30 mg/kg once daily for five days per week C. paclitaxel 6 mg/kg weekly D. MLN8237 30 mg/kg once daily for five days per week and paclitaxel 6 mg/kg weekly E. paclitaxel 2 mg/kg weekly F. MLN8237 30 mg/kg once daily for five days per week and paclitaxel 2 mg/kg. Mice were dosed with five cycles of treatment as detailed in Figure 6-26. Tumour volumes were measured prior to each dosing using calipers and weekly in vehicle group. Statistical analysis was performed using two way ANOVA with Tukey's multiple comparison test to compare each of the treatments in GraphPad Prism.

6.5.2.2.2 *Waterfall plots*

When the change in tumour volume was compared to Day 1 of dosing (Figure 6-28), all the vehicle tumours showed PD. For the single agents, in the MLN8237 30 mg/kg group 2/10 had a CR, 8/10 PD, in the paclitaxel 6 mg/kg group, 1/10 CR, 3/10 SD, 6/10 PD, and in the paclitaxel 2 mg/kg cohort, there was 1/10 CR, 1/10 PR and 8/10 PD. With the combination of MLN8237 30 mg/kg and paclitaxel 6 mg/kg, there were 3/10 PR, 7/10 PD and in the MLN8237 30 mg/kg and paclitaxel 2 mg/kg group, there was 1/10 CR, 1/10 PR, 8/10 PD.

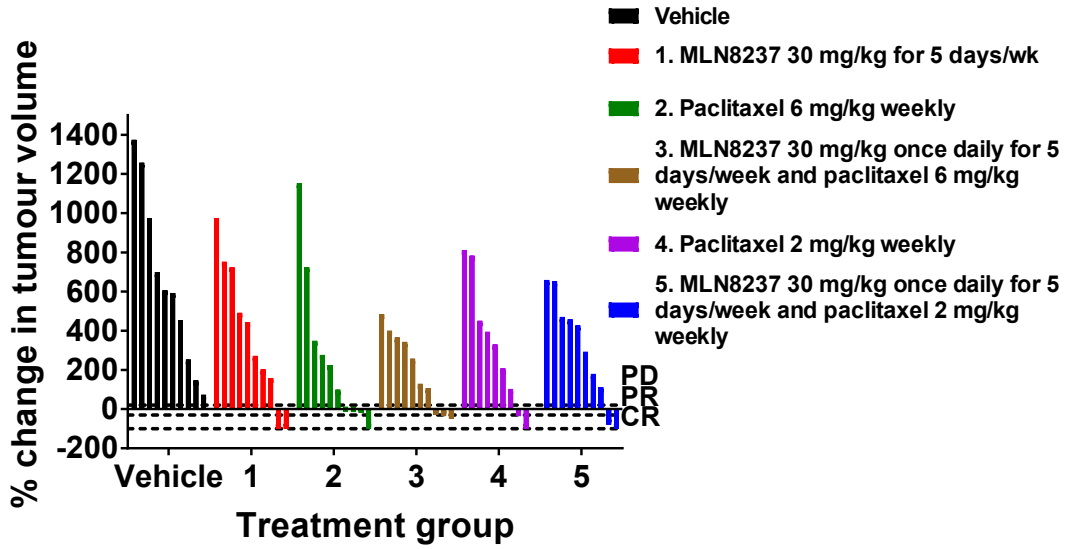

Figure 6-28: Waterfall plot of percentage change in tumour volume at endpoint compared to Day 1 of dosing in mice in MLN8237 and paclitaxel efficacy study.
Mice were dosed with five cycles of treatment as detailed in Figure 6-26. Tumour volumes were measured approximately using calipers. The black dotted lines indicate progressive disease (PD) with 20% increase in tumour volume, partial response (PR) with 30% decrease in tumour volume and complete response (CR) with complete regression of tumour.

Tumour inhibition compared to vehicle (calculated as in (261)) confirmed a treatment effect across all groups compared to vehicle. For the single agent groups it was 46% in the MLN8237 30 mg/kg group, 41% in the paclitaxel 6 mg/kg group and 33% in the paclitaxel 2 mg/kg group. Of the combinations, the combination with paclitaxel 6 mg/kg was more effective with 52% tumour inhibition compared to 40% in the paclitaxel 2 mg/kg combination.

6.5.2.3 Effect of MLN8237 and paclitaxel combination on PD markers

Similarly to the tolerability study, no significant differences were seen across the treatment groups for any of these markers, despite evidence of efficacy on tumour growth (Figure 6-29 A-C). These data are confounded by the fact that in the cases where there was a complete response to treatment, no tumour remained to analyse (two mice in group 1, and one mouse in groups 2, 3 and 4). The percentage of necrosis varied within all treatment groups (Figure 6-29 D).

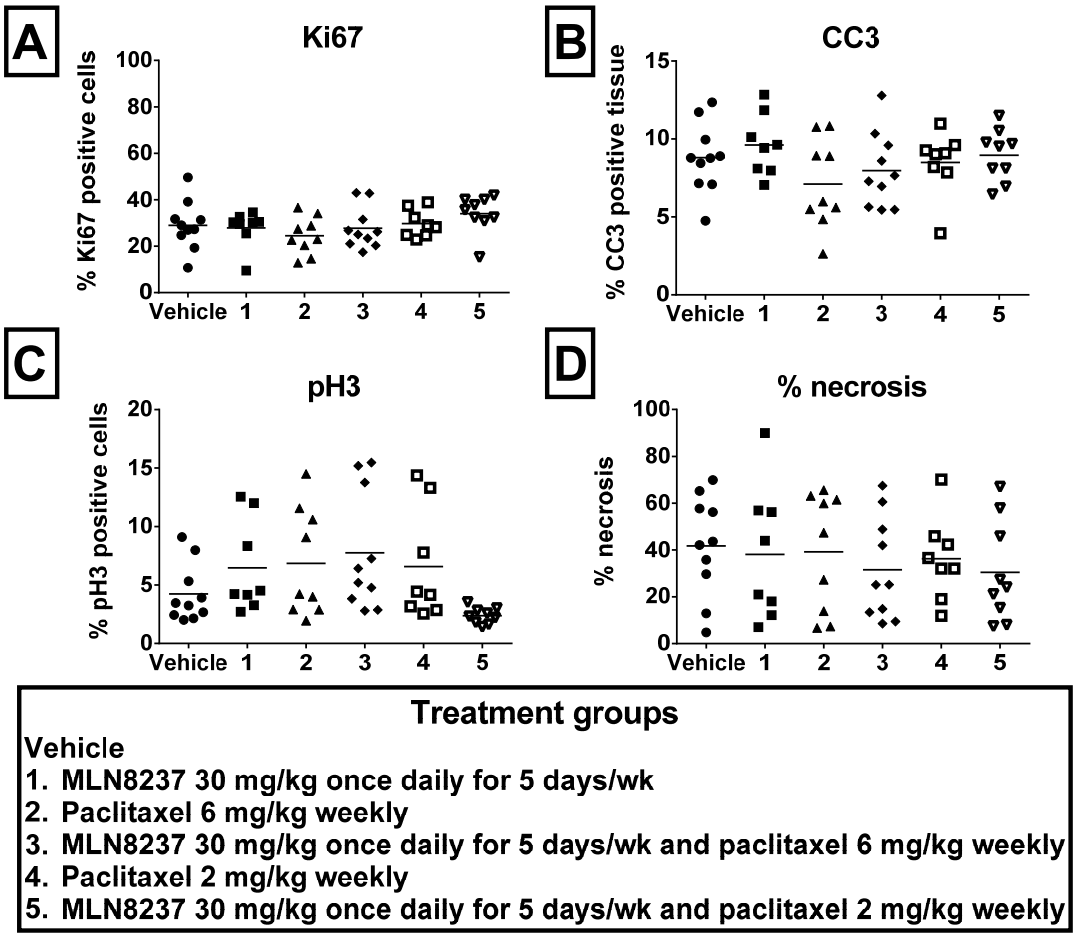

Figure 6-29: Pharmacodynamic markers measured at endpoint in study assessing the efficacy of combinations of MLN8237 and paclitaxel in T24 xenografts.
A. percentage positive cells for A. Ki67, B. percentage positive tissue for CC3, C. percentage positive cells pH3 after mice were dosed with five cycles of treatment as detailed in Figure 6-26 D. shows percentage of necrosis for slides analysed in HALO™. Tumour samples were taken at the endpoint of the study, Day 39- 24 hours after the last dose of MLN8237 (groups 1, 3 and 5) and 48 hours after the last dose of paclitaxel (groups 2, 3, 4 and 5). Slides analysed in HALO™ (as described in 2.3.5.1). Statistical testing performed using ordinary one way ANOVA with Dunnett's multiple comparison test comparing each treatment group to vehicle in GraphPad Prism.

Even in tumours with a PR to treatment, there was no clear relationship between any of the markers tested and tumour response. For example, in Figure 6-30 in one tumour with progressive disease (on the left) there was far more necrosis than the tumour where a partial response was seen (on the right). However, the percentage of positive cells/tissue for pH3, CC3 and Ki67 were very similar between the two tumours.

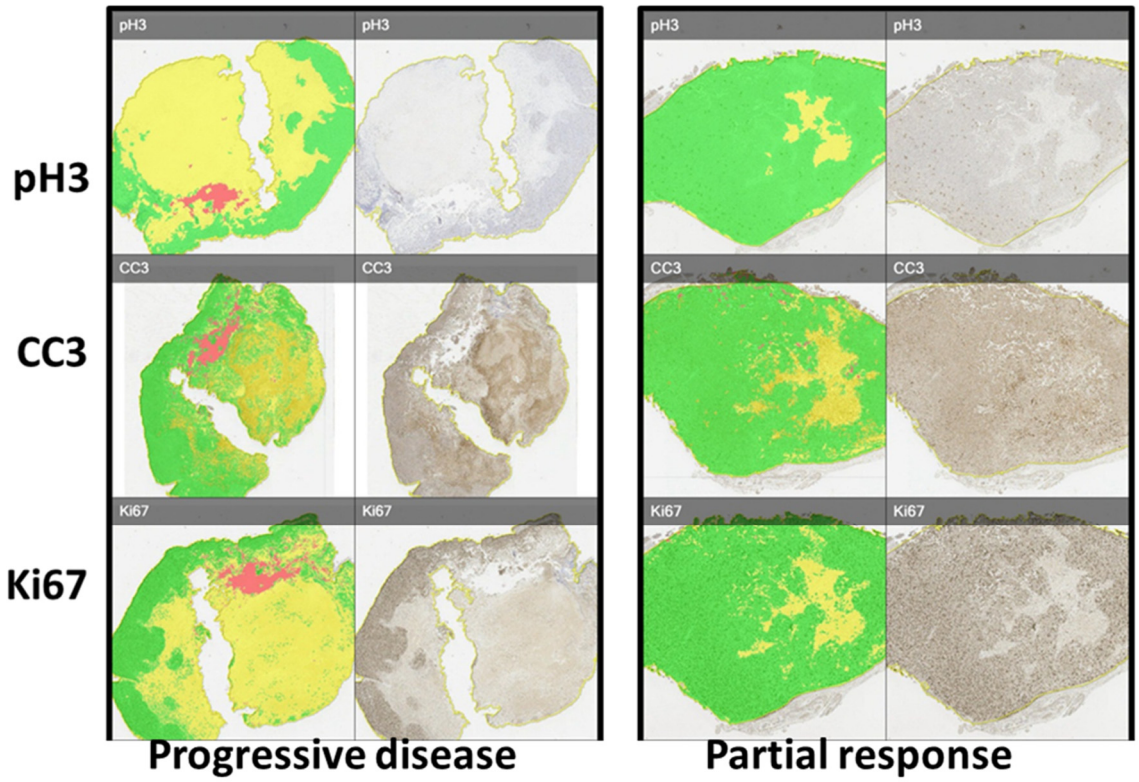

Figure 6-30: Representative images from HALO™ analysis of two different tumours, one with progressive disease and the other with a partial response with PD markers.
pH3, CC3 and Ki67 stains shown. For each marker, the left hand image shows the necrosis algorithm applied to the whole tumour (green – viable tumour, red- glass, yellow – necrosis) and the stained slide on the right.

6.5.3 Summary of MLN8237 and paclitaxel combination studies

In both the tolerability and efficacy studies, the combinations were well tolerated, with no significant changes in body weight or blood parameters and with the bone marrow analysis showing less additional myelotoxicity than might have been expected. Tumour growth was significantly reduced compared to vehicle in all treatment groups, particularly in the MLN8237 30 mg/kg and paclitaxel 6 mg/kg group, indicating this combination was both effective and well tolerated. However, there were no significant differences in PD markers between treatment groups and vehicles in either study, despite only analysing the non-necrotic areas.

As we were limited in our ability to compare full dose paclitaxel 20 mg/kg with other treatment groups due to hypersensitivity reactions, to attempt to prove equal efficacy between the combination of MLN8237 and a lower concentration of taxane compared to a full dose taxane, I therefore decided to also investigate the combination of MLN8237 and docetaxel, where hypersensitivity was not an issue.

6.6 MLN8237 and docetaxel combination studies

6.6.1 Assessment of tolerability of MLN8237 and docetaxel combination in non-tumour-bearing nude mice

T24 tumour growth inhibition had been seen in the single agent docetaxel 20 mg/kg study (Figure 6-11) and docetaxel has shown efficacy as a single agent in bladder cancer (262). To assess tolerability of the combination of MLN8237 30 mg/kg combined with docetaxel 20 mg/kg, I performed a study with twenty non tumour bearing mice comparing four treatment groups with five cycles of treatment administered. In the studies with paclitaxel, there had not been a significant difference seen in tumour growth inhibition between the groups treated with MLN8237 for three days or five days per week when in combination with lower concentrations of paclitaxel. Given that the maximum tolerated dose of docetaxel was being used, the MLN8237 30 mg/kg once daily for three days regimen was selected as it was predicted to reduce toxicity (283). The groups were:

1. MLN8237 30 mg/kg once daily for three days OG and vehicle IP
2. Docetaxel 20 mg/kg IP and vehicle OG weekly
3. MLN8237 30 mg/kg once daily for three days and docetaxel 20 mg/kg weekly
4. Vehicle OG and IP

6.6.1.1 Tolerability of MLN8237 and docetaxel combination

Many of the mice exhibited peritoneal guarding (sucking in the abdomen) approximately 15 minutes after IP docetaxel suggestive of some irritation but otherwise no adverse effects were seen. Body weights were stable across the groups during the study with no mice losing ≥10% of body weight (Figure 6-31).

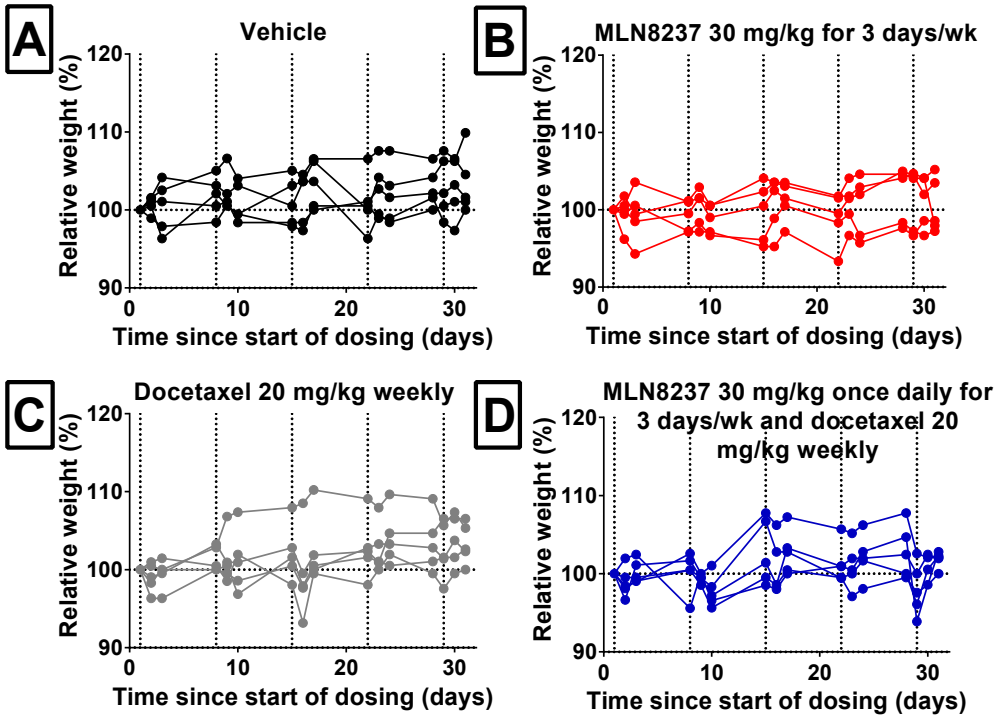

Figure 6-31: Percentage body weight relative to Day 1 of dosing over days since first dose for each mouse in study assessing the tolerability of combinations of MLN8237 and docetaxel in non-tumour bearing nude mice.
Percentage body weight for each mouse dosed with five cycles of A. Vehicle B. MLN8237 30 mg/kg once daily for three days per week C. Docetaxel 20 mg/kg weekly D. MLN8237 30 mg/kg once daily for three days and docetaxel 20 mg/kg weekly. Mice were weighed prior to each cycle, with vertical black dotted lines indicating the start of each cycle. MLN8237 dosed daily by oral gavage for three consecutive days of a weekly cycle and docetaxel dosed IP weekly.

6.6.1.1.1 *Effect of MLN8237 and docetaxel combination on endpoint blood counts*

In the previous studies, endpoint blood counts had been taken as a measure of tolerability. As I was particularly interested in how blood cell counts changed over time with repeated courses of treatment, a pilot feasibility study of interim blood tests was performed. The initial plan was to take bloods from the tail vein but when this was attempted on Day 22 (day of start of cycle 4), it proved challenging to get a sufficiently large drop of blood and several attempts were required. Therefore, for Day 26 (Day 5 of cycle 4, two days after the last MLN8237 dose or four days after the last docetaxel dose) the submandibular vein was used, which proved technically easier. Endpoint bloods were taken by cardiac puncture as in previous studies (day 31).

At day 22 (seven days after the cycle 3 docetaxel dose and four days after the last cycle 3 MLN8237 dose), the combination treatment did not appear to be more toxic then either of the single agents (Figure 6-32). Indeed the white cell count was higher than that seen in the single agents, with a mean of 8.0 x 10^3/µl compared to 5.4 x 10^3/µl in the vehicle group, although this was not significant. There was no significant difference across the groups in the WBC differential values, although both lymphocytes and

granulocytes were lower in the MLN8237 single agent group. There was variability in haemoglobin values, including some low readings, which may have been due to small sample volumes leading to issues with measurements as discussed. Platelet counts tended to be higher in the treatment groups, particularly in the combination, although some much lower values were seen (potentially due to platelet clumping rather than thrombocytopenia). This difference was statistically significant between vehicle and the combination group (mean of 310±190x10^3/µl in vehicle, 633±280x10^3/µl in combination, p=0.030).

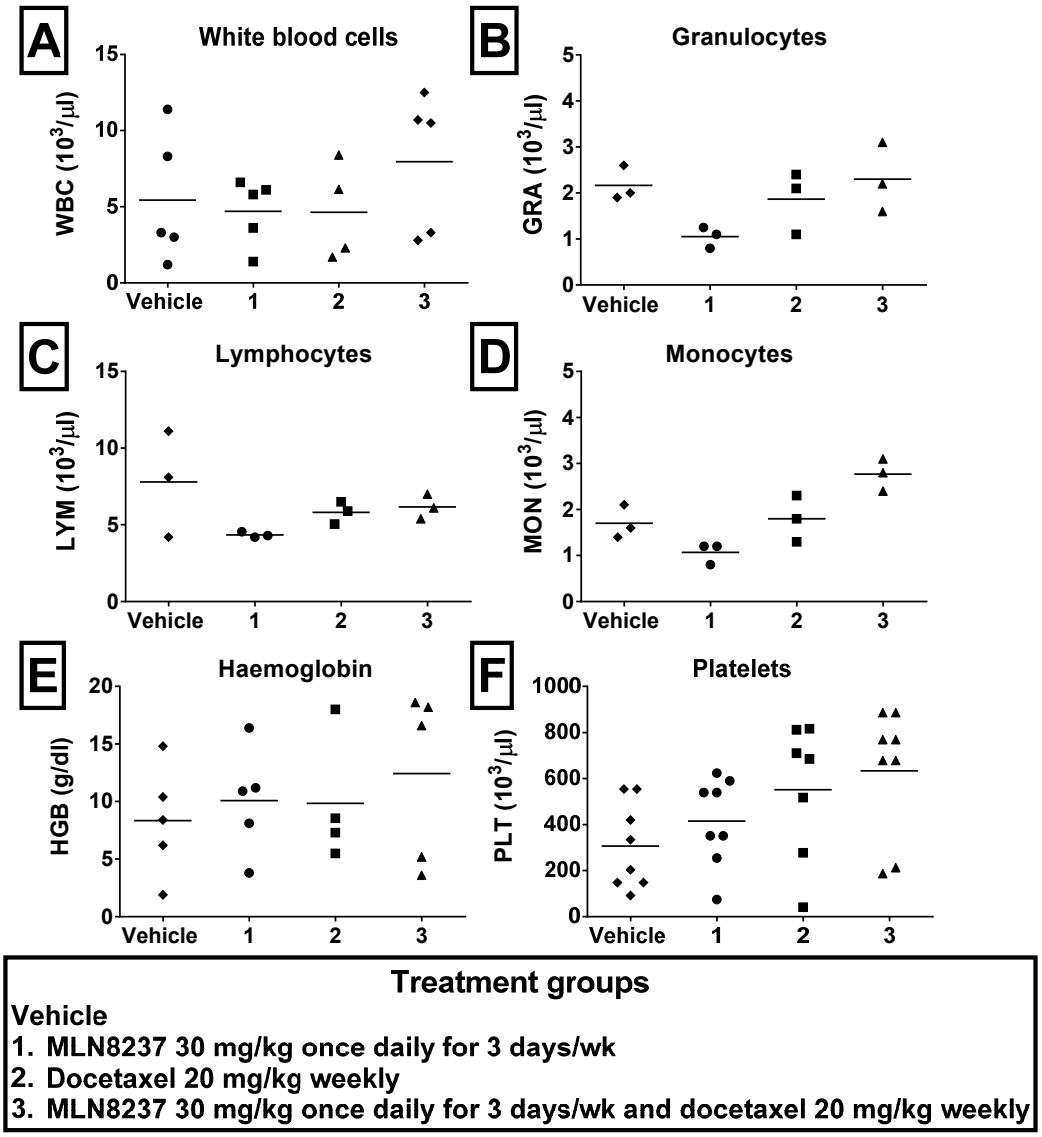

Figure 6-32: Day 22 blood counts for study assessing the tolerability of combination of MLN8237 and docetaxel in non tumour bearing nude mice.
Mice were dosed with five cycles of treatments as detailed in Figure 6-31. Samples were taken on Day 22 seven days after last dose of docetaxel and four days after last dose of MLN8237 where applicable. Parameters measured are A. total white blood cell count (WBC), B. granulocytes (gra), C. lymphocytes (lym), D. monocytes (mon), E. haemoglobin (HGB) and F. platelets (plts). Statistical testing performed using ordinary one way ANOVA with Dunnett's multiple comparison test comparing each treatment group to vehicle in GraphPad Prism.

On Day 26 (Day 5 of cycle 4, two days after the last MLN8237 dose or four days after the last docetaxel dose), there were no significant differences in any of the parameters between the groups (Figure 6-33). The platelet counts were higher in all groups compared to Day 22 bloods (For example 570±78 x 10^3/µl in vehicle), with the highest counts in the combination group, although this was not statistically significant.

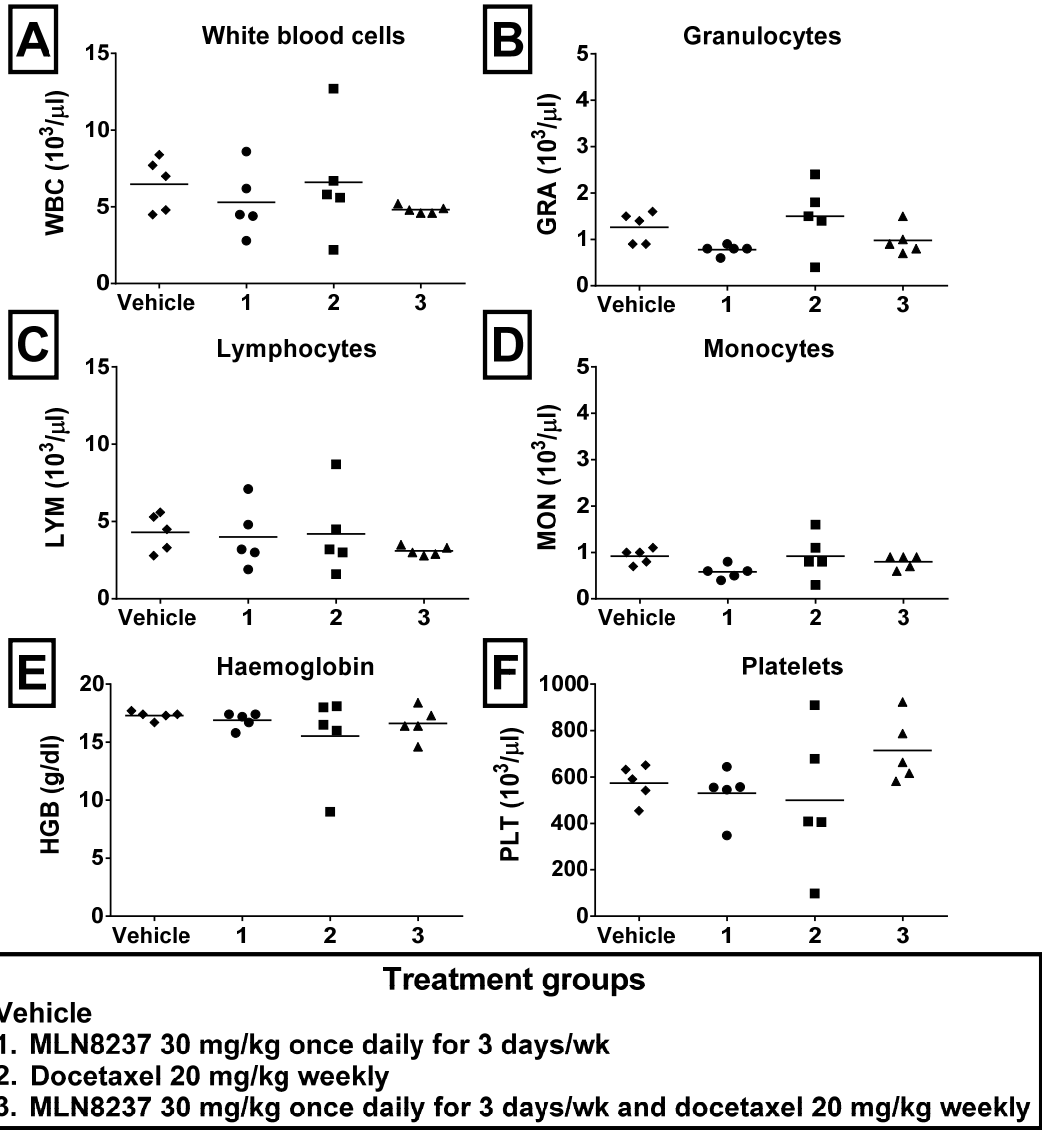

Figure 6-33: Day 26 blood counts for study assessing the tolerability of combination of MLN8237 and docetaxel in non tumour bearing nude mice.
Mice were dosed with five cycles of treatments as detailed in Figure 6-31. Samples were taken on Day 26 two days after last dose of MLN8237 and four days after last dose of docetaxel where applicable. Parameters measured are A. total white blood cell count (WBC), B. granulocytes (gra), C. lymphocytes (lym), D. monocytes (mon), E. haemoglobin (HGB) and F. platelets (plts). Statistical testing performed using ordinary one way ANOVA with Dunnett's multiple comparison test comparing each treatment group to vehicle in GraphPad Prism.

Finally endpoint blood counts were analysed as in previous studies (Figure 6-34). Here there were no significant differences between groups and the increased platelet count seen in the combination group at Days 22 and Day 26 was not seen.

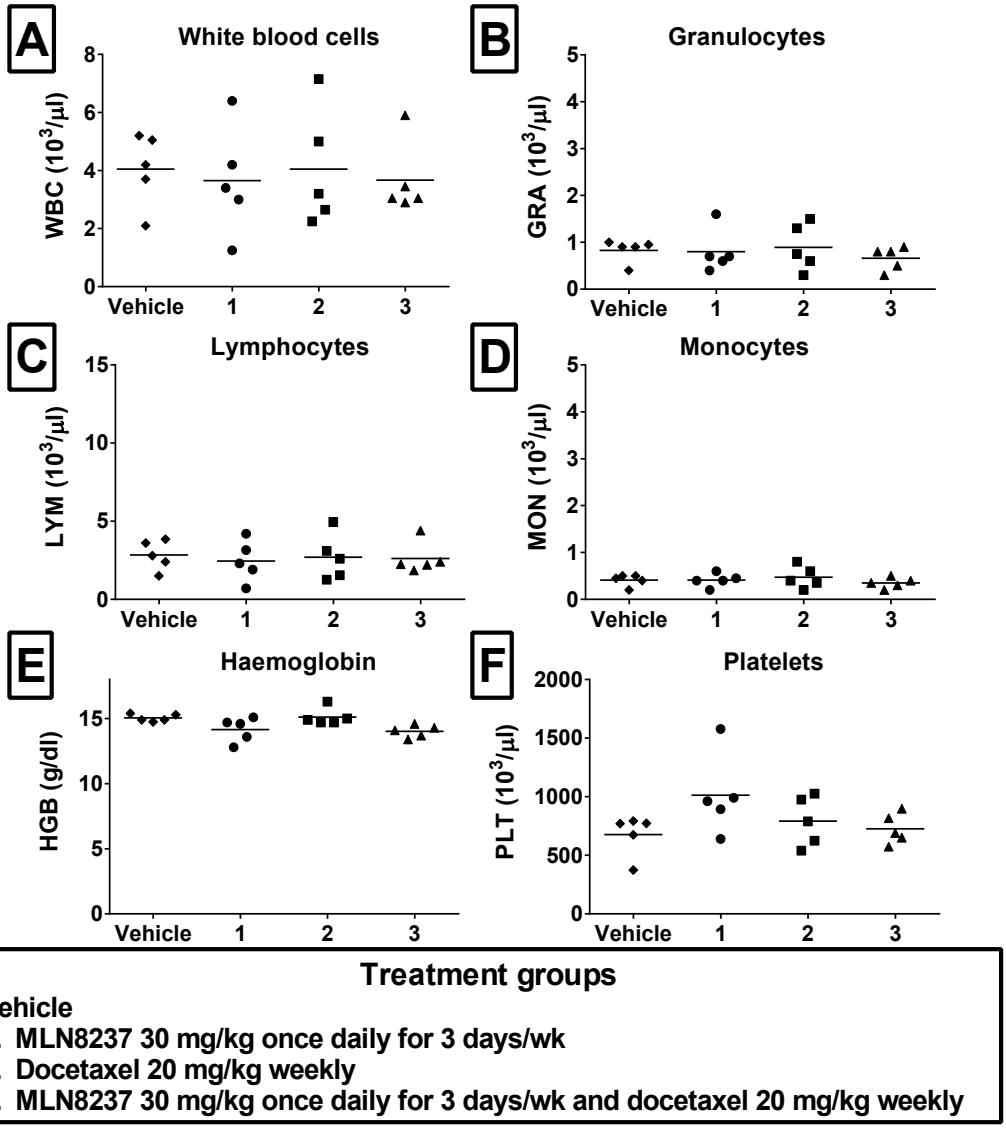

Figure 6-34: Endpoint blood counts for study assessing the tolerability of combination of MLN8237 and docetaxel in non tumour bearing nude mice.
Mice were dosed with five cycles of treatments as detailed in Figure 6-31. Samples were taken on Day 31, 24 hours after last dose of MLN8237 and four days after last dose of docetaxel where applicable. Parameters measured are A. total white blood cell count (WBC), B. granulocytes (gra), C. lymphocytes (lym), D. monocytes (mon), E. haemoglobin (HGB) and F. platelets (plts). Statistical testing performed using ordinary one way ANOVA with Dunnett's multiple comparison test comparing each treatment group to vehicle in GraphPad Prism.

In summary, the interim blood counts did not show a significant difference in WBC or granulocytes during treatment but did show an increase in platelet count (significant at Day 22). The combination of MLN8237 30 mg/kg with docetaxel 20 mg/kg was well tolerated and did not cause overt neutropenia.

6.6.1.1.2 *Effect of MLN8237 and docetaxel combination on bone marrow*

Review of the H&E slides showed reduced cellularity with more frequent fat spaces, particularly in the combination group and an increase in megakaryocytes in treated mice

(consistent with the raised platelet counts found in the interim blood tests) (Figure 6-35), similar findings to those described in Figure 6-23.

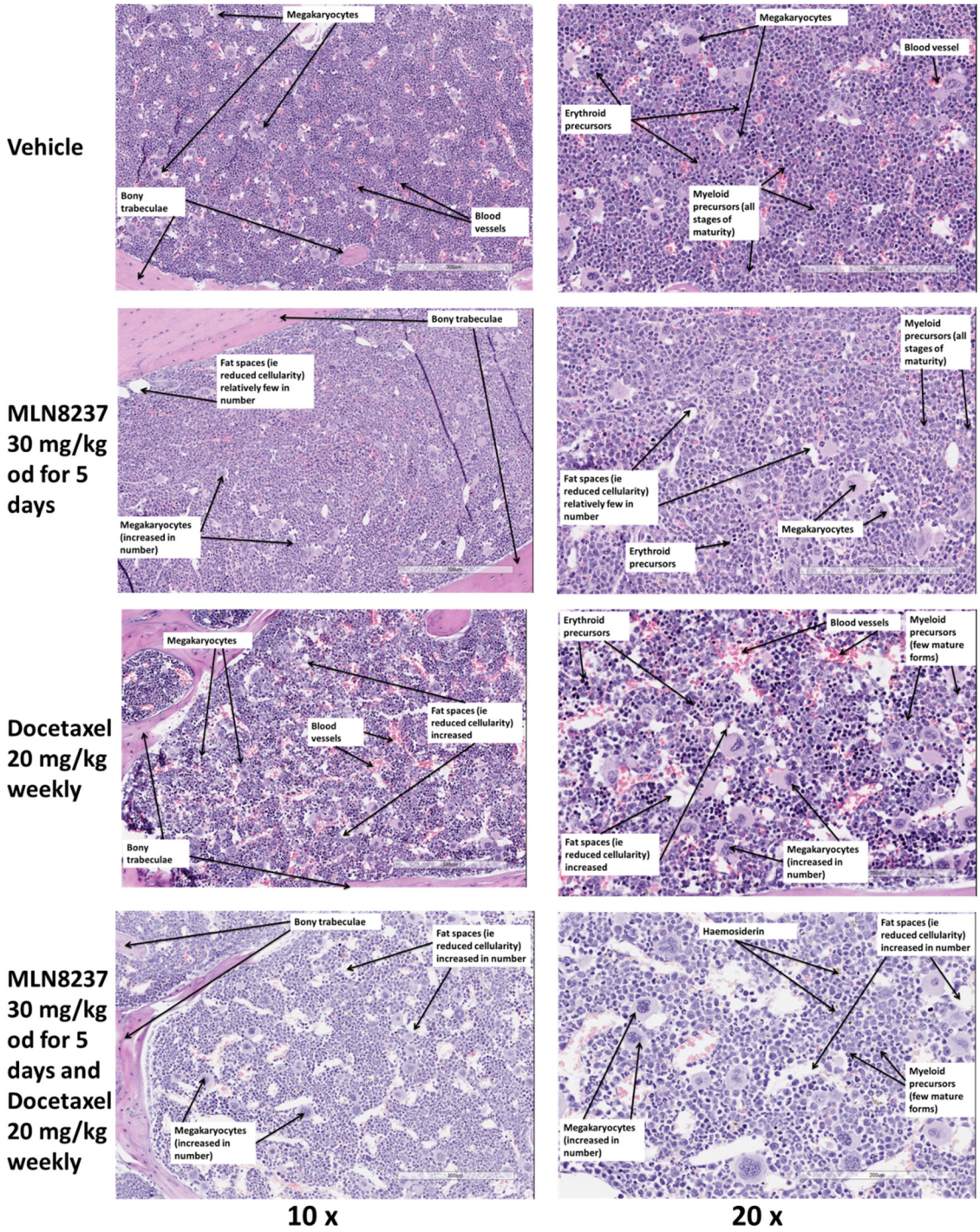

Figure 6-35 Representative images bone marrow images of femurs of mice in study assessing the tolerability of combinations of MLN8237 and docetaxel in T24 xenografts.
Sample images are shown of bone marrow images from vehicle, MLN8237 30 mg/kg once daily for five days/week, docetaxel 20 mg/kg weekly and the combination of MLN8237 30 mg/kg once daily for five days and docetaxel 20 mg/kg weekly stained with H&E. Scale bars: left = 300 µm, right = 100 µm. Femurs from mice prepared and stained as described in 2.3.5.3.

These samples were taken four days after the last dose of docetaxel and 24 hours after the last dose of MLN8237 where applicable so it is possible that the bone marrow may have shown a greater difference if taken straight after the docetaxel dosing. However,

these results appear to confirm the tolerability of the combination on the bone marrow, with its ability to compensate for the drug treatments.

6.6.1.1.3 *Pilot study of effect of MLN8237 and docetaxel combination on mouse CFU-GM assay*

As the MPO stain had not shown the differences in immature myeloid cells expected from manual review of the H&E slides in previous MLN8237 and paclitaxel studies (Figure 6-16), I decided to explore a further technique to assess the toxicity of the drug treatments on the bone marrow. The CFU-GM assay has been validated for use in fresh mouse femoral bone marrow cells (295) and was piloted in this study.

In contrast to our previous results with human bone marrow cells where fewer colonies had been seen than predicted with the manufacturer's recommended seeding (4.4), there were many CFU-GM colonies (range 224-1474) and it proved impossible to accurately count these manually (example images are shown in Figure 6-36 A). I therefore used GelCount™ to scan the dishes and developed an algorithm to identify colonies, which was manually checked. The MethoCult® medium selected is formulated to support optimal growth of granulocyte and macrophage progenitors (CFU-GM, CFU-M, CFU-G). However, due to the viscous nature of the media causing blurring of images, it proved difficult to use the GelCount™ images to distinguish different haematopoietic progenitors and therefore all types of colonies seen were counted. The analysis showed that there was no significant difference between the groups (Figure 6-36 B).

Therefore, this appears to again suggest that the combination of MLN8237 30 mg/kg once daily for three days and docetaxel 20 mg/kg weekly is no more myelotoxic than the single agent exposure, although this experiment would have to be repeated at a lower seeding density to confirm this.

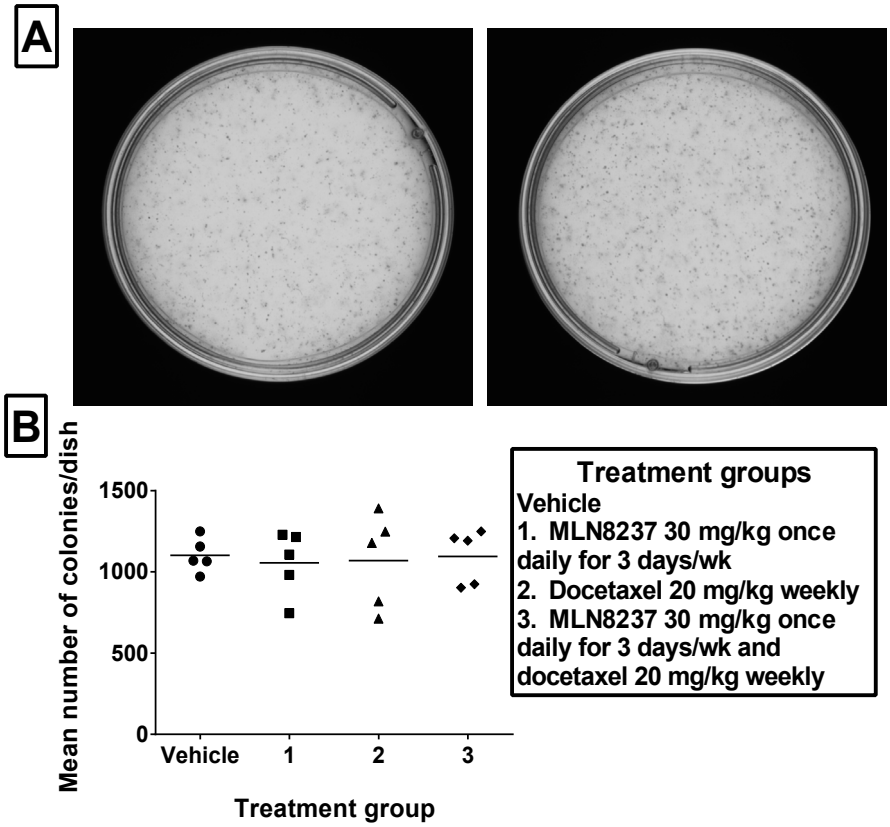

Figure 6-36: Results from mouse CFU-GM pilot in study assessing tolerability of MLN8237 and docetaxel
Following drug treatment with either vehicle, MLN8237 30 mg/kg once daily for three days, docetaxel 20 mg/kg weekly or the combination of both drugs, femurs of the mice were dissected. Bone marrow cells were flushed from these, counted and $2x10^5$ cells plated into MethoCult® GF M3534 medium, with three dishes per mouse femur. After twelve days, the resulting dishes were imaged using GelCount™. A. shows two representative images, showing the large number of colonies seen and B. shows the mean number of colonies seen for each treatment group.

6.6.2 Efficacy of MLN8237 and docetaxel combination in T24 xenografts

As the pilot study indicated that the combination of MLN8237 and docetaxel was tolerable, an efficacy study with ten mice per group was performed. Two dose levels of docetaxel were tested – the maximum dose of 20 mg/kg which had shown efficacy and the lower dose of 6 mg/kg to investigate whether this was effective when combined with MLN8237 (there had been little difference from vehicle in tumour growth in Figure 6-11). In this study mice were randomised to five cycles of the following treatment groups:

1. MLN8237 30mg/kg once daily for three days OG and vehicle IP
2. Docetaxel 20 mg/kg IP and vehicle OG weekly
3. MLN8237 30 mg/kg once daily for three days and docetaxel 20 mg/kg weekly
4. Docetaxel 6 mg/kg IP and vehicle OG weekly

5. MLN8237 30 mg/kg once daily for three days and docetaxel 6 mg/kg weekly
6. Vehicle OG and IP

6.6.2.1 Tolerability of MLN8237 and docetaxel combination

Despite the tolerability in non-tumour bearing mice, toxicity was seen within some of the groups in this study, largely towards the end of the five cycles of treatment. Weight loss was seen in some mice (Figure 6-37) with one mouse killed on day 31 in the docetaxel 20 mg/kg group and two in the combination MLN8237 30 mg/kg and docetaxel 20 mg/kg group (on days 30 and 31) because of weight loss >10%. One mouse in the MLN8237 30 mg/kg group also reached >10% weight loss on the final day of the study (day 32).

One mouse had an abnormal gait and was clinically dehydrated in the docetaxel 20 mg/kg group and was killed at Day 30. In the vehicle group, one mouse was killed on day 22 because a blood filled cyst connected to the tumour was impeding movement. Overtly impacted intestines were seen in six mice at necropsy, all of which had received docetaxel 20 mg/kg – four in the single agent group (with one killed on day 22 due to a swollen abdomen and three others killed on day 30 due to health concerns) and two found at endpoint necropsy in the combination of MLN8237 30 mg/kg with docetaxel 20 mg/kg. Splenomegaly was also seen in one mouse in MLN8237 30 mg/kg, one mouse in docetaxel 20 mg/kg, one in the combination of MLN8237 30 mg/kg and docetaxel 20 mg/kg and one in the vehicle group.

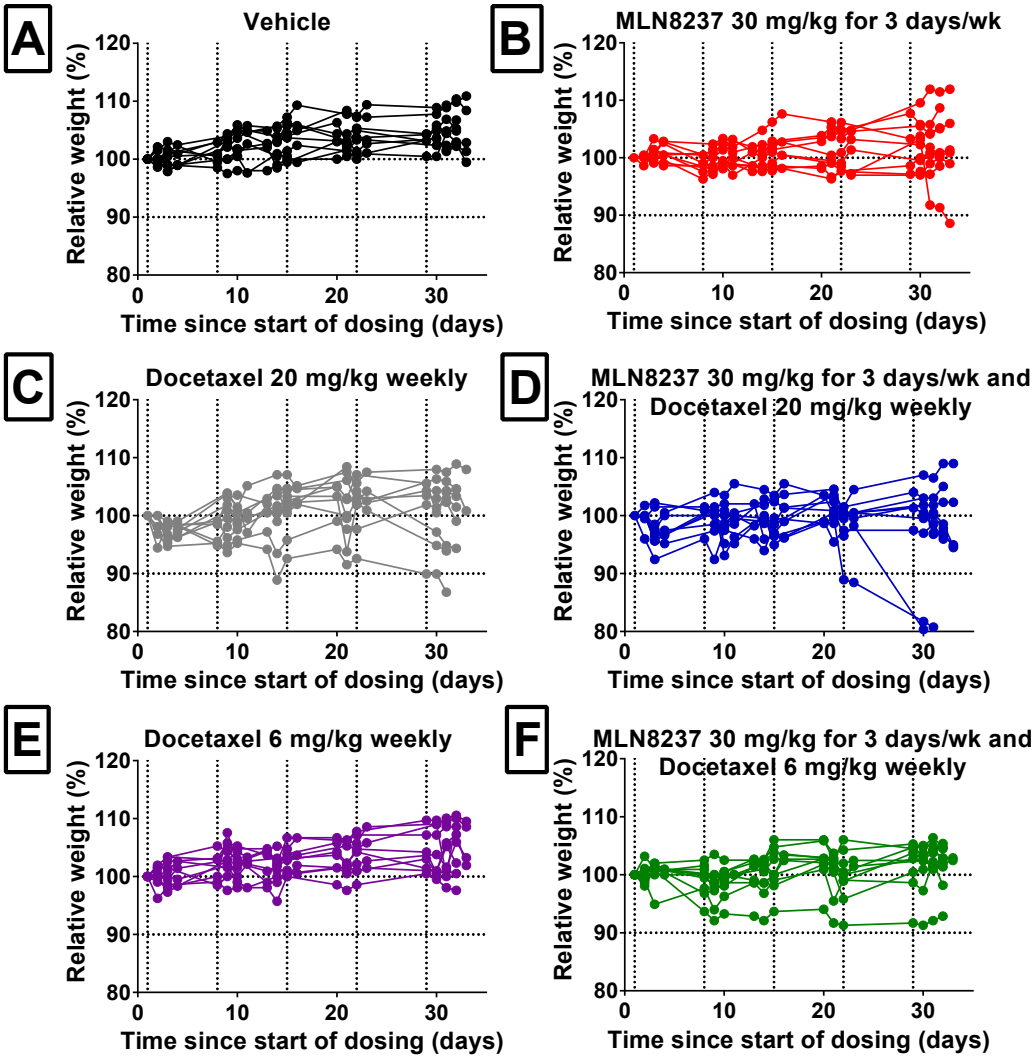

Figure 6-37: Percentage body weight relative to Day 1 of dosing over days since first dose for each individual mouse dosed in MLN8237 and docetaxel efficacy study.
Mice were treated with five cycles of A. Vehicle B. MLN8237 30 mg/kg once daily for three days per week C. Docetaxel 20 mg/kg weekly D. MLN8237 30 mg/kg once daily for three days/wk and docetaxel 20 mg/kg E. Docetaxel 6 mg/kg weekly F. MLN8237 30 mg/kg once daily for three days/wk and docetaxel 6 mg/kg. Mice were weighed prior to each cycle, with vertical black dotted lines indicating the start of each cycle. MLN8237 dosed daily by oral gavage for three consecutive days of a weekly cycle and docetaxel dosed IP weekly.

6.6.2.1.1 *Effect of MLN8237 and docetaxel combination on endpoint blood counts*

Two mice had very high WBC > 60 x10^3/µl (normal range reported by Charles River laboratories for these mice is 8.4 x10^3/µl (range 2.97 to 16 x10^3/µl), one in the docetaxel 20 mg/kg group and one in the vehicle group (Figure 6-38 A). In both cases, the profile consisted of a granulocytosis (approximately 75% of WBC). Both mice had splenomegaly at autopsy but stable weights throughout the study. Given that one of these was seen in a vehicle treated mouse, these results would be suggestive of a myeloproliferative disorder, extra-medullary haemopoiesis, infection or tumour burden rather than treatment related. An enlarged spleen was also seen in one mouse in the MLN8237 group accompanied by an increased WCC (21 x10^3/µl) and one mouse in the

combination of MLN8237 30 mg/kg and docetaxel 20 mg/kg) (normal WCC). Another mouse in the MLN8237 30 mg/kg group had an elevated white cell count, although no splenomegaly.

Due to these two outliers (marked in red in Figure 6-38 A), there were no significant differences in the white cell counts between groups, although if they were excluded (assuming an alternative pathological process was the cause), this difference was significant (Figure 6-38 B, p=0.0033). Across the groups, WBC were significantly reduced in both the combination with docetaxel 20 mg/kg (p=0.020) and the combination with docetaxel 6 mg/kg (p=0.012) compared with vehicle but there were no significant differences between the treatment groups. The granulocyte count appeared reduced overall in the MLN8237 30 mg/kg group and the two docetaxel combinations (Figure 6-38 C), although this effect was not significant even when the two very high granulocyte counts were excluded (Figure 6-38 D). There was a significant reduction in the lymphocyte count between the treatment groups compared to vehicle (p=0.0009, significant for the combination with docetaxel 20 mg/kg (p=0.0028) and with docetaxel 6 mg/kg (p=0.0028)).

There was a significant difference in haemoglobin between the treatment groups compared to vehicle (p=0.0090), although this is unlikely to be clinically significant given that the values across all groups remained within the normal range reported by Charles River laboratories (mean 15, range 13-18 g/dl). There was no significant difference in platelets.

Therefore, these results show a reduction in WCC and granulocytes in the docetaxel 20 mg/kg and combination groups, although there was not a significant difference when these groups were compared. These results are consistent with the reports from clinical studies and the bone marrow findings in the tolerability study.

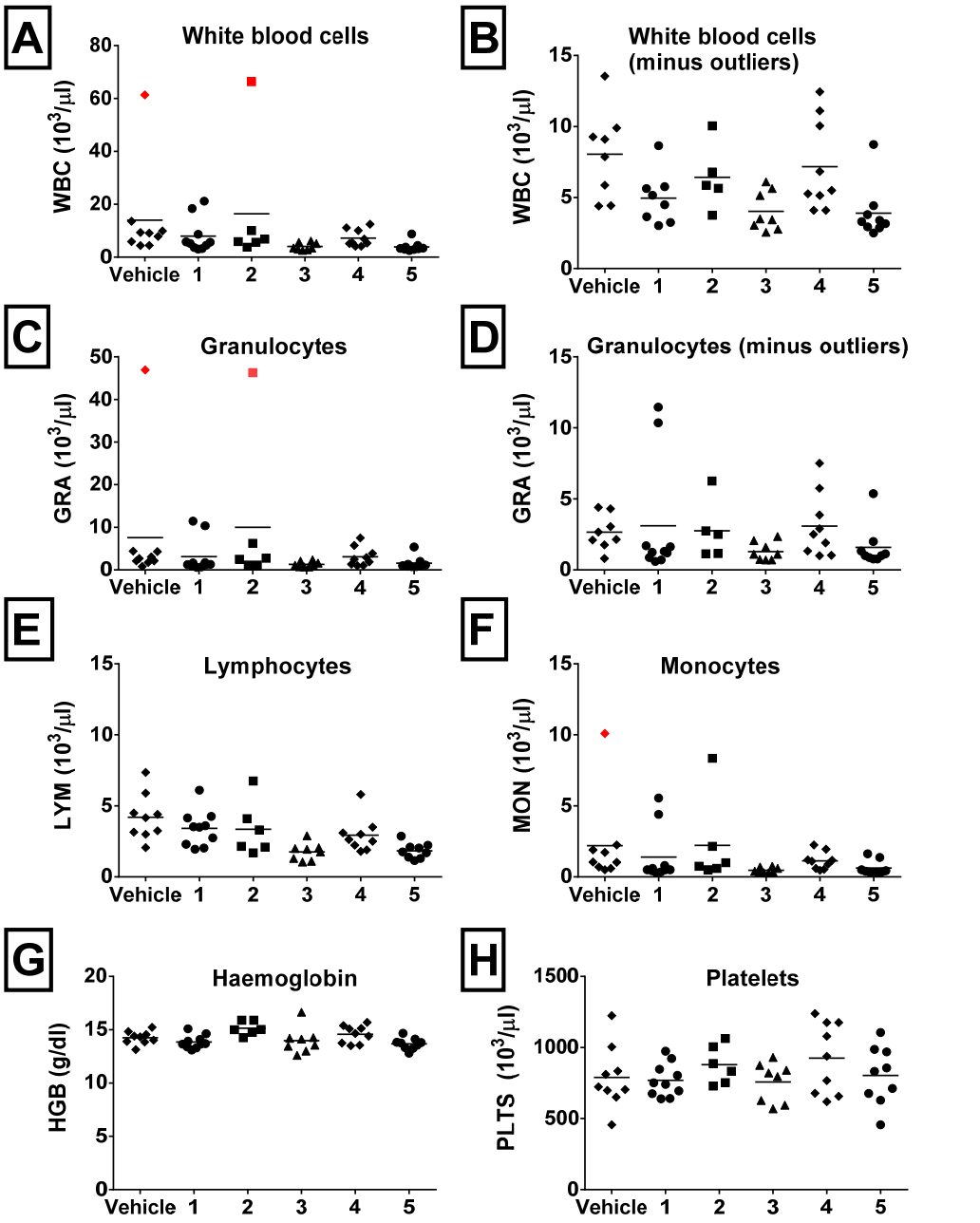

Figure 6-38: Endpoint blood counts for study assessing the efficacy of combination of MLN8237 and docetaxel in T24 xenografts.
Mice were dosed with five cycles of treatments as described in Figure 6-37. Samples were taken on Day 32, 24 hours after last dose of MLN8237 and four days after last dose of docetaxel where applicable. Parameters measured are A. total white blood cell count (WBC), B. WBC with two outliers marked in A in red excluded. C. granulocytes (gra), D. granulocytes with two outliers marked in B. in red excluded E. lymphocytes (lym), F. monocytes (mon), G. haemoglobin (HGB) and H. platelets (plts). Blood counts were not available for four of the mice killed early due to weight loss. Statistical testing performed using ordinary one way ANOVA with Tukey's multiple comparison test comparing each treatment group in GraphPad Prism.

6.6.2.2 Effect of MLN8237 and docetaxel combination on tumour growth

6.6.2.2.1 *Growth curves*

There was a significant difference between the treatment groups compared to vehicle ($p<0.00010$, Figure 6-39).

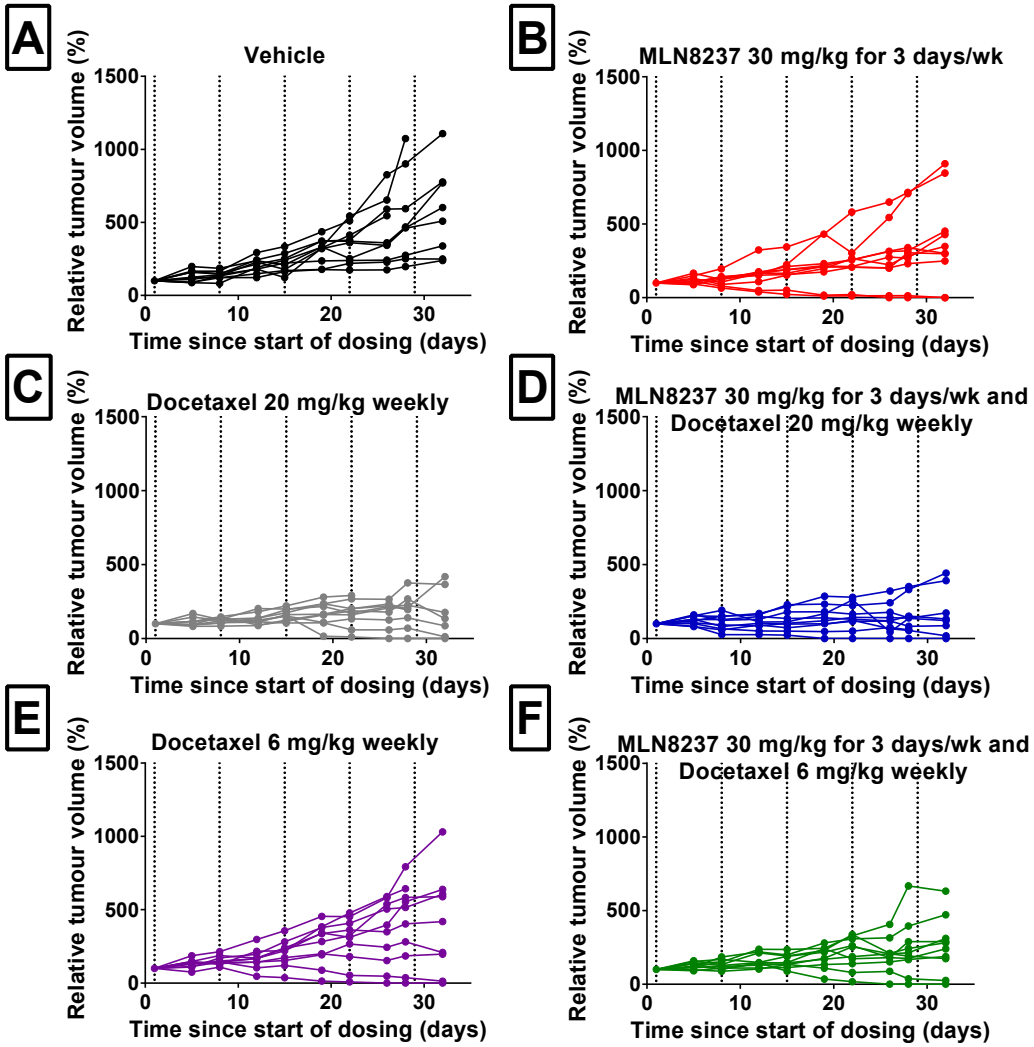

Figure 6-39: Tumour growth expressed as volume measured over time since start of dosing (days) in study assessing the efficacy of combinations of MLN8237 and docetaxel in T24 xenografts.
The individual mice tumour growth plots for mice treated with five cycles of A. Vehicle B. MLN8237 30 mg/kg once daily for three days per week C. Docetaxel 20 mg/kg weekly D. MLN8237 30 mg/kg once daily for three days/wk and docetaxel 20 mg/kg E. Docetaxel 6 mg/kg weekly F. MLN8237 30 mg/kg once daily for three days/wk and docetaxel 6 mg/kg. each group as labelled. Tumour volumes were measured prior to each dosing using using calipers and weekly in vehicle group. Statistical testing was performed using ordinary two way ANOVA with Tukey's multiple comparison test comparing each treatment group in GraphPad Prism.

When the individual groups were compared with vehicle, both MLN8237 30 mg/kg ($p=0.05$) and docetaxel 6 mg/kg ($p=0.89$) as single agents did not significantly reduce tumour growth compared to vehicle even though complete responses were seen in these groups whereas docetaxel 20 mg/kg and both of the combinations did ($p<0.00010$ for each). Docetaxel 20 mg/kg as a single agent and the combination of MLN8237 30 mg/kg and docetaxel 20 mg/kg appear the most effective from the plots in Figure 6-39,

but there was no significant difference between them (p=0.76). The difference between the combinations with either docetaxel 20 mg/kg or docetaxel 6 mg/kg was not significant (p=0.10), and there was not a statistically significant difference between docetaxel 20 mg/kg as a single agent and the combination of MLN8237 30 mg/kg and docetaxel 6 mg/kg. Therefore, despite no significant reduction in tumour growth with docetaxel 6 mg/kg or MLN8237 30 mg/kg as single agents, the effect of the combination with docetaxel 6 mg/kg was no different to either docetaxel 20 mg/kg as a single agent or the combination with docetaxel 20 mg/kg.

6.6.2.2.2 *Waterfall plot*

The waterfall graph (Figure 6-40) demonstrates that 10/10 vehicle tumours showed PD, the MLN8237 30 mg/kg group had 2/10 CR with 6/10 PD, the docetaxel 20 mg/kg group had 1/10 CR, 1/10 PR, 1/10 SD and 7/10 PD whilst the docetaxel 6 mg/kg group had 2/10 CR and 8/10 PD. In the combination with docetaxel 20 mg/kg, there was 1/10 CR, 2/10 PR, 1 SD and 6/10 PD and with the docetaxel 6 mg/kg combination there was 1/10 CR, 1/10 PR and 8/10 PD.

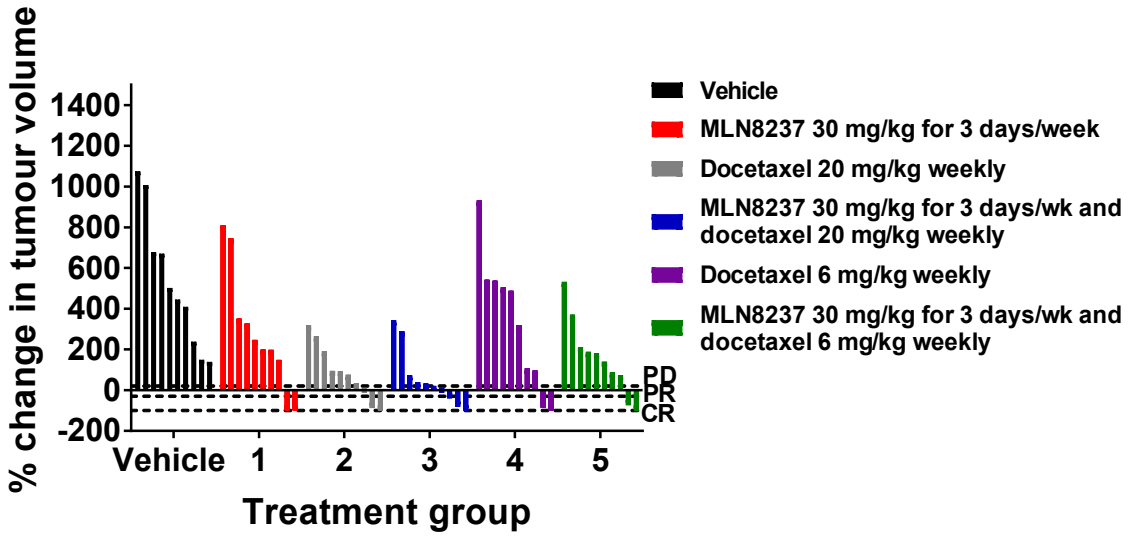

Figure 6-40: Waterfall plot of percentage change in tumour volume at endpoint compared to Day 1 of dosing in mice in MLN8237 and docetaxel efficacy study.
Mice were dosed with five cycles of treatments as described in Figure 6-37. Tumour volumes were measured approximately using calipers. The black dotted lines indicate progressive disease (PD) with 20% increase in tumour volume, partial response (PR) with 30% decrease in tumour volume and complete response (CR) with complete regression of tumour.

Tumour inhibition compared to vehicle (calculated as in (261)) confirmed a statistically different treatment effect across all groups compared to vehicle (p=0.013). For the single agent groups it was 32% in the MLN8237 30 mg/kg group, 80% in the docetaxel 20 mg/kg group and 26% in the docetaxel 6 mg/kg group. With the combinations, the

combination with docetaxel 20 mg/kg was most effective with 91 % tumour inhibition compared to 65 % in the docetaxel 6 mg/kg combination.

These results suggest that the addition of MLN8237 30 mg/kg to docetaxel 20 mg/kg does not significantly increase anti-tumour efficacy compared to docetaxel 20 mg/kg alone. Adding MLN8237 30 mg/kg to docetaxel 6 mg/kg appears more effective than docetaxel 6 mg/kg alone, although it does not equate to the effect of docetaxel 20 mg/kg as a single agent.

6.6.2.3 Effect of MLN8237 and docetaxel combination on PD markers

As in the MLN8237 and paclitaxel efficacy study, the variability between treatment groups meant that there were no significant differences in Ki67, pH3 or CC3, and no tumour remained to analyse in the tumours with a complete response (Figure 6-41).

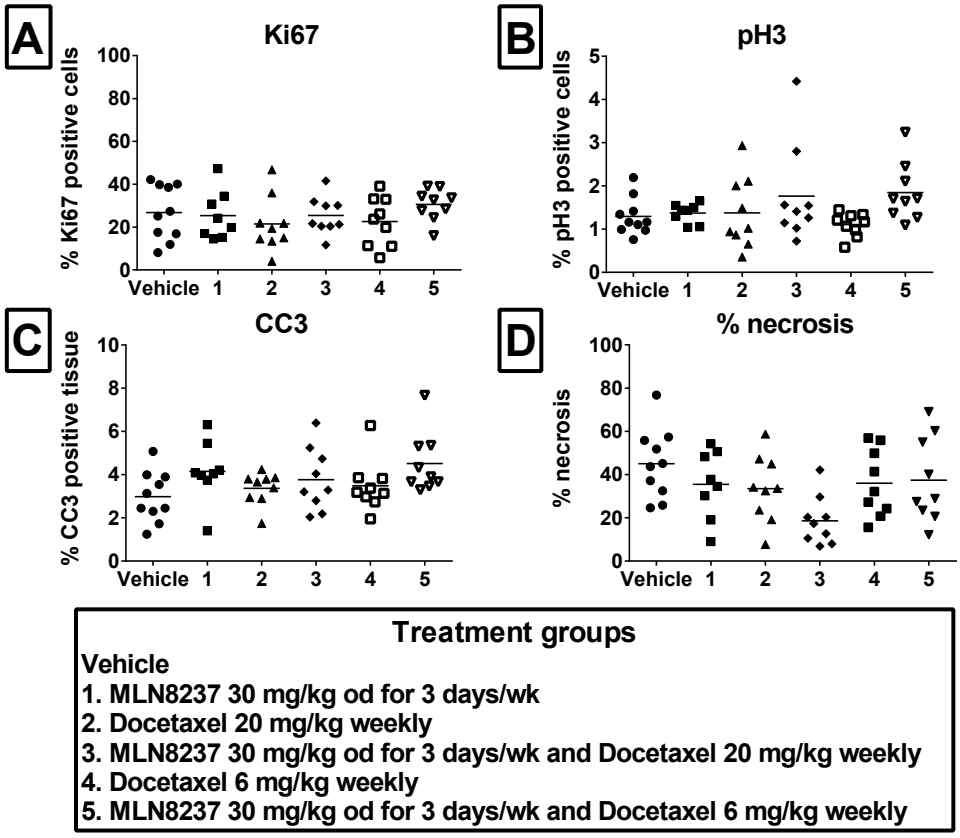

Figure 6-41: Pharmacodynamic markers measured at endpoint in MLN8237 and docetaxel efficacy study

Percentage positive cells for A. Ki67, B. percentage positive tissue for CC3, C. percentage positive cells pH3, after mice were dosed with five cycles of treatments as described in Figure 6-37. D. shows percentage of necrosis for slides analysed in HALO™. Tumour samples were taken at the endpoint of the study, day 32, 24 hours after the last dose of MLN8237 in cycle 5 or three days after the last dose of docetaxel where applicable). No tumour was available for mice where complete response seen – two mice in MLN8237 30 mg/kg group and one in each of other treatment groups. Slides analysed in HALO™ (as described in 2.3.5.1). Statistical testing performed using ordinary one way ANOVA with Dunnett's multiple comparison test comparing each treatment group to vehicle in GraphPad Prism.

However, the percentage of necrosis was significantly different (Figure 6-41 D, p=0.028) with less necrosis overall between treatment groups compared to vehicle. Whilst I might have assumed more necrosis would be present in tumours responding to drug treatment, in more rapidly growing T24 xenograft tumours, their size may have led to more necrosis as seen in Figure 6-30.

6.6.2.3.1 *Pilot studies of alternative PD biomarkers of effect of MLN8237 and docetaxel combination*

As has been seen across all of my *in vivo* studies, I have not been able to identify clear differences in proliferation as measured by Ki67, induction of apoptosis as measured by CC3 or AK-A inhibition as measured by pH3 in tumour sections. Therefore, in this study, I investigated two further alternative methods to assess response.

6.6.2.3.1.1 Analysis of endpoint skin biopsies

Although variability has been observed, skin biopsies have been reported as a useful pharmacodynamic marker of AK-A inhibition in clinical trials, detecting accumulation of mitotic cells within the basal epithelial layer using immunofluorescent staining for pH3 and MPM2. They have the advantage of being less invasive than repeated tumour biopsies and allowing changes during treatment to be assessed (204, 206, 296). As none of my *in vivo* studies above had shown pH3 to be a useful PD marker of AK-A inhibition when taken at study endpoint (partly due to the extent of variability between groups to identify clear trends), a pilot study was performed to assess Ki67 and pH3 in skin from the efficacy study endpoint (methods described in 2.3.5.2). As seen in Figure 6-42, there were no significant differences seen between groups, with very infrequent pH3 positive cells observed.

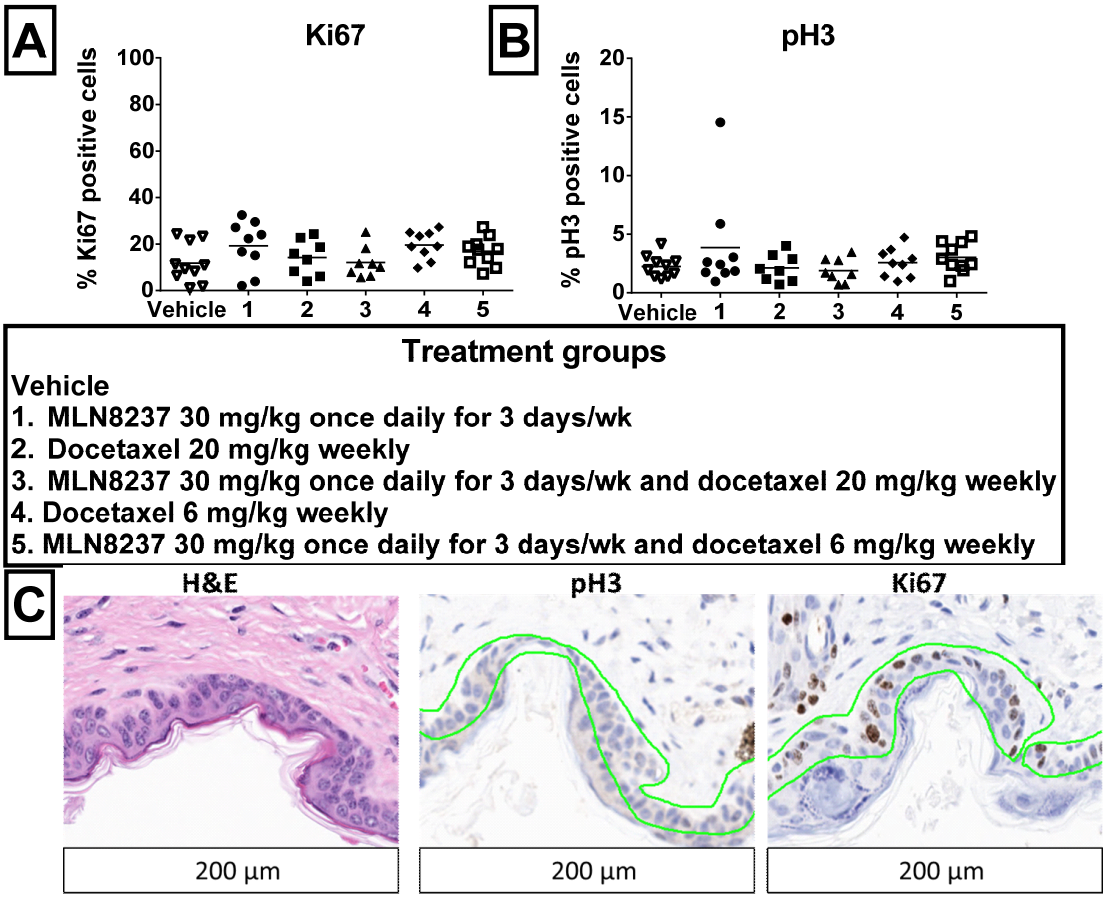

Figure 6-42: Analysis of skin samples of mice treated in efficacy study of MLN8237 and docetaxel. Pharmacodynamic markers measured at endpoint in study of MLN8237 and docetaxel with A. Ki67 B. pH3 in skin samples of mice after mice were dosed with five cycles of treatments as described in Figure 6-37. C. shows an example of an H&E slide and then the same area highlighted for analysis for pH3 and Ki67. Skin samples were taken from the back of each mouse at the endpoint of the study, day 32, 24 hours after the last dose of MLN8237 in cycle 5 or three days after the last dose of docetaxel where applicable). Slides were analysed using Aperio as described in 2.3.5.2.

However, these samples were taken at the study endpoint, day 32 (24 hours after the last dose of MLN8237 or three days after the last dose of docetaxel where applicable) study. At 24 hours, my MLN8237 single agent PK analysis (6.3.2.2) showed MLN8237 levels were around 1 µM at 24 hours, a level at which an increase in pH3 has previously been reported (205) but the peak in pH3 levels is likely to have been earlier when higher concentrations were seen around six hours. Therefore, this timepoint may well have been too late to identify changes between groups, as the most consistent results in the Phase 1 trials had been seen with samples taken six to eight hours post dose.

Whilst it might be technically possible to take small skin punch biopsies in mice during a course of treatment, there were concerns about wound healing and I have not found any studies which have used this methodology. Therefore, whilst skin biopsies have the potential to provide evidence of AK-A inhibition in clinical studies, it is difficult to translate these to the pre-clinical setting.

6.6.2.3.1.2 M30/M65 ELISA as marker of tumour cell apoptosis

One of the challenges in interpretation of the tumours across the studies has been the cystic areas within the tumours and the degree of necrosis. Although I have quantified the degree of necrosis and only applied the biomarkers to the non-necrotic areas, this has not shown consistent changes, which have correlated either with treatment response or treatment group. Using CC3 as a measure of apoptosis has not shown significant differences between treatment groups. An alternative strategy to tumour biopsies developed to demonstrate drug induced apoptosis is the M30/M65 assay (described in 2.3.8), where the ratio of M30:M65 can reflect the type of cell death, with a higher ratio in apoptosis (256). The assay has been used in pre-clinical studies with AZD1152 (an AK-B inhibitor) where a rise in M30 levels correlated with increased apoptosis seen on immunohistochemistry at three to five days after treatment and M65 plasma levels correlated with changes in tumour growth (256). In a clinical trial with AT9283 (an AKI used in my initial studies), increased M30 and M65 levels were observed during and following infusion of AT9283 (183).

Due to limited capacity on the kit, 26 plasma samples obtained at study endpoint (selected to represent each treatment group and to give examples of a range of responses from complete responses to progressive disease) were chosen for this pilot study. A highly significant correlation ($p<0.0001$) was seen between the final tumour volume and both M30 ($r=0.87$ (95% CI 0.73-0.94), Figure 6-43 A) and M65 ($r=0.84$ (95% CI 0.67-0.92), Figure 6-43 B). Many of the larger tumours with progressive disease showed regions of central necrosis (Figure 6-30). Given my choice of a range of samples from each group consisting of mixed responses, there were no clear trends in M30 (Figure 6-43 C) or M65 (Figure 6-43 D) across the treatment groups but surprisingly tumours with a complete response had a lower M30 value, whereas I might have expected these samples to show increased apoptosis. This may relate to the timing of endpoint sampling, and kinetics of apoptosis. A clear correlation was seen between M30 and M65 levels (Figure 6-43 E), with a correlation coefficient of 0.92 (95% CI 0.84-0.97, $p<0.0001$).

When the ratio of M30 to M65 were grouped by tumour response (Figure 6-43 F), there was a statistically significant difference between groups ($p<0.0001$), particularly when the tumours with a CR were compared to those with a PR ($p=0.0004$), SD ($p=0.0005$) or PD ($p<0.0001$). This ratio has been reported to show prognostic significance in predicting response to paclitaxel in non-small cell lung cancer (297).

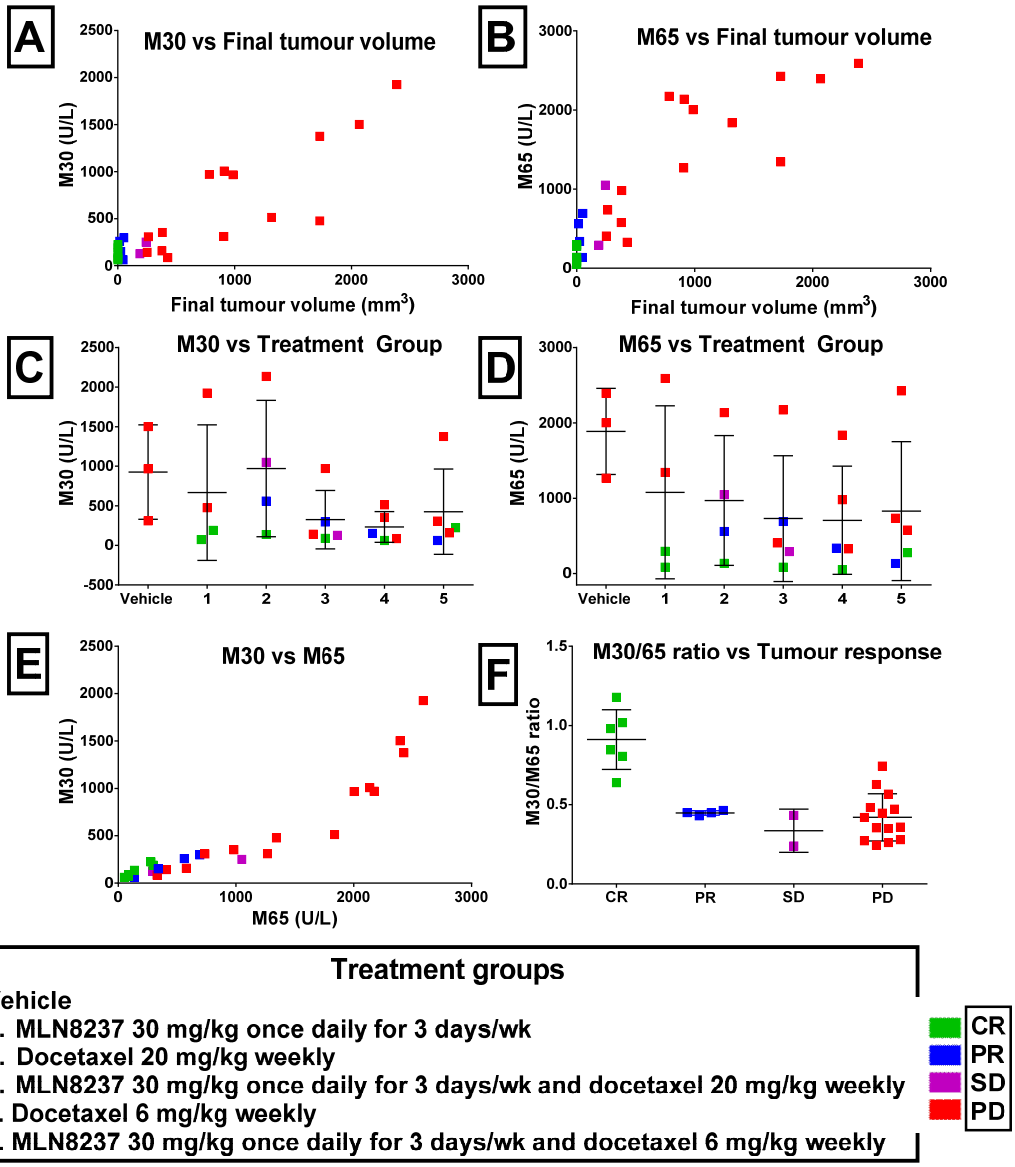

Figure 6-43: Assessment of M30 and M65 in MLN8237 and docetaxel efficacy study. Correlation between M30 (A) and M65 (B) values with final tumour volume and by treatment groups (M30 in C and M65 in D). E shows M30/M65 ratio and F. shows relationship between M30/M65 ratio and tumour response compared with tumour response. Plasma samples taken from a selection of mice treated with either vehicle, MLN8237 or docetaxel as single agents or in combination after five cycles of treatments as described in Figure 6-37. Plasma samples were taken at the endpoint of the study, day 32, 24 hours after the last dose of MLN8237 in cycle 5 or three days after the last dose of docetaxel where applicable) and analysed as described in 2.3.8. Tumour response to treatments are CR (complete response), PR (partial response), SD (stable disease) and PD (progressive disease). Statistical testing performed using GraphPad Prism to calculate Pearson correlation coefficients and ordinary one way ANOVA with Tukey's multiple comparison test used to compare each treatment group in F.

When the percentage of CC3 positive tissue (for apoptosis detection) was compared with the M30 value, there was no significant correlation between M30 values and CC3 positivity (Figure 6-44 A). Whilst others have shown rises in M30 are correlated with increased numbers of apoptotic cells seen at immunohistochemistry, these used a specific M30 CytoDEATH antibody (256, 257). However, there was a significant

correlation between the M65 level and the degree of necrosis seen in the tumours (r=0.612, p=0.0042) (Figure 6-44 B).

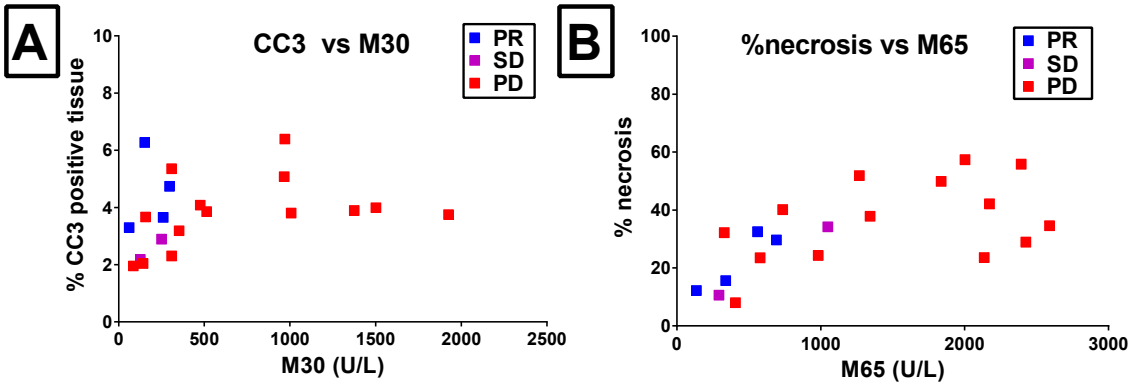

Figure 6-44: Comparison of M30 and M65 results with CC3 and percentage necrosis in MLN8237 and docetaxel efficacy study.
Correlation between A. CC3 positive staining vs M30 and B. % necrosis vs M65. Plasma samples taken from a selection of mice treated with either vehicle, MLN8237 or docetaxel as single agents or in combination after five cycles of treatments as described in Figure 6-37. Plasma samples were taken at the endpoint of the study, day 32, 24 hours after the last dose of MLN8237 in cycle 5 or three days after the last dose of docetaxel where applicable) and analysed as described in 2.3.8. Tumour response to treatments as labelled (PR=partial response, SD=stable disease, PD=progressive disease). Mice with complete response are excluded as no tumour remaining to analyse. Slides analysed in HALO™ for CC3 and percentage necrosis (as described in 2.3.5.1). Statistical testing performed using GraphPad Prism to calculate Pearson correlation coefficients.

In summary, this pilot study on a limited number of samples has shown that M30 and M65 can be measured in plasma. The results show significant correlation with final tumour volume and the M30 and M65 values in plasma at the endpoint. The M30/M65 ratio was significantly associated with tumour response. Although the CC3 IHC did not correlate with M30 results, there was a correlation between the percentage of necrosis seen and the M65 results.

6.6.3 Summary of MLN8237 and docetaxel combination studies

The combination of MLN8237 and docetaxel was tolerable in non-tumour bearing mice with stable weights on treatment. Blood tests, bone marrows and CFU-GM assays did not suggest significant additional toxicity between treatment groups compared to vehicle. In contrast, in the T24 xenograft mice in the efficacy study, toxicity was seen, largely in the mice receiving docetaxel 20 mg/kg either as a single agent or in combination.

In terms of tumour response, there was a significant difference between the treated mice compared to vehicle in all groups. However, the key outcome was that the anti-tumour effect of the combination of MLN8237 30 mg/kg for three days with docetaxel 6 mg/kg was not statistically different to that seen with docetaxel 20 mg/kg and was more

tolerable, as predicted by my *in vitro* CFU-GM studies (4.4). The M30/M65 assay also showed promise as a marker of response, with a higher M30/M65 ratio seen in tumours with a CR.

6.7 Summary of chapter

Having selected MLN8237 as the AK-A inhibitor of choice based on the PK profile of CYC3, the single agent PK studies for both MLN8237 and the taxanes showed target plasma and tumour concentrations were achieved. Whilst paclitaxel and docetaxel suppressed tumour growth as single agents at full dose, a significant reduction was also seen with paclitaxel 6 mg/kg, although there was little difference in tumour growth compared to vehicle with docetaxel 6 mg/kg. We were unable to compare the full dose paclitaxel 20 mg/kg and MLN8237 combination due to hypersensitivity reactions, but the combinations with both paclitaxel 6 mg/kg and 2 mg/kg were well tolerated and showed a significant reduction in tumour growth, particularly in the MLN8237 30 mg/kg and paclitaxel 6 mg/kg group.

As my hypothesis was that the combination of MLN8237 with lower concentrations of a taxane could produce a synergistic response which was similar to full dose taxane but with reduced toxicity, combination studies with docetaxel were performed. Although docetaxel 6 mg/kg did not show significant suppression of tumour growth, it did show efficacy when combined with MLN8237 30 mg/kg. Whilst the tumour inhibition rate was maximal with the docetaxel 20 mg/kg combination, this was at the expense of toxicity. There was not a statistically significant difference in tumour growth between either combination compared to docetaxel 20 mg/kg as a single agent and in addition, no significant difference between the combination with 20 mg/kg and that with 6 mg/kg.

Hence for both MLN8237 30 mg/kg in combination with paclitaxel 6 mg/kg or docetaxel 6 mg/kg, anti-tumour efficacy was seen with reduced toxicity, as predicted by my *in vitro* work. Following my *in vivo* studies, others have explored combination dose and schedule strategies with MLN8237 and taxanes in both the MDA-MB-231 and PHTX-02B breast cancer xenograft models. Combinations of MLN8237 with docetaxel 10 mg/kg (MTD docetaxel 15 mg/kg) or with paclitaxel 10 or 20 mg/kg (MTD for paclitaxel 30 mg/kg) led to either additive or synergistic anti-tumour activity, with tumour regression only seen in the combination (261). These results support my

conclusion that use of a concentration of taxane below the MTD together with MLN8237 can be an effective combination.

The lack of a relationship between the PD markers I tested and tumour responses was disappointing. In the Western blots in T24 cells with MLN8237 and paclitaxel, an increase in pH3 had been seen with MLN8237 as a single agent and with paclitaxel 30 nM consistent with mitotic arrest and I had also seen an increase in cPARP signal for the combination of MLN8237 50 nM and paclitaxel 2 nM and for paclitaxel 30 nM (Figure 3-26). Ki67 as a marker of proliferation was not significantly reduced in treatment groups compared to vehicle, CC3 did not show increased apoptosis in cases where tumours responded to treatment and pH3 did not show a significant rise consistent with AK-A inhibition. The study in breast cancer mouse models also found no marked change in mitotic index and only a small difference in CC3 in treated tumours (261). Potential reasons for the lack of differences seen could include the variability in tumour responses between groups, the degree of necrosis and also the timepoints at which mice were killed (although in the study of MLN8237 and paclitaxel, there was no difference in markers between mice killed at three hours after the last dose and 20 hours (Figure 6-25)).

Therefore, although my PK analysis with MLN8237 showed plasma concentrations in the range reported to cause AK-A inhibition in HCT-116 xenografts (Figure 6-5), I do not have any clear evidence that AK-A was successfully inhibited *in vivo* and there was only a modest anti-tumour effect of MLN8237 as a single agent. A number of publications investigating PD biomarkers of AK-A inhibition both in pre-clinical and clinical studies have also reported challenges in assessing the effects of AK-A inhibition The technique of most value uses immunofluorescent staining of tumours for α-tubulin and DNA and then imaging reconstruction to create 3D images to assess mitotic cells for chromosome alignment and spindle bipolarity, demonstrating an exposure related decrease in these markers at day 7 (296). Hence whilst an alternative approach could be to do further immunhistochemical staining for AK-A, exploration of this immunofluorescent technique shows the most potential.

Since we performed this study, one publication has investigated MLN8237 in T24 xenografts at MLN8237 30 mg/kg for five days a week for four weeks (121). A comparison of our results points to a difference in tumour behaviour. Although they only injected $1x10^6$ cells (compared to our $2x10^6$ T24 cells), they did this bilaterally and therefore appear to have assessed two tumours in each mouse, meaning that there were

only four mice in each group. Tumour growth in their control mice was so rapid that the mice had to be killed by day 15 due to tumour size, whereas the tumour doubling time observed in my studies was eight days (Figure 6-1). In their study, the tumours in the mice treated with MLN8237 30 mg/kg showed growth arrest, with no statistical difference in tumour size when compared between Day 1 and after four weeks of dosing. Whilst I did see some efficacy with single agent MLN8237 30 mg/kg with a tumour inhibition rate of 54%, tumour growth was still observed in the majority of mice. There are several potential explanations for this. As discussed in 6.2, there have been reports of subtypes of the T24 cell line which are more or less tumorigenic. Their line was sourced from ATCC with cells grown in RPMI-1640 media with 10% FBS whereas our cell line was obtained from CLS and grown in DMEM-F12/Ham with 5% FBS. We also genotyped our cell line to ensure that it matched the ATCC reference genotype as there have been particular issues with cell line contamination with T24 cells (298-300). Their sample size was small and if two tumours were assessed for each mouse, this could have also contributed to the lack of variability in their results. They also do not report how mice were randomised to the treatment groups. Differences between animal houses (including temperature, feed, microbiota) can also affect tumour growth, and lack of reproducibility in experiments has been reported frequently in recent years (301, 302).

They also harvested the tumours at the study endpoint and stained them with H&E, and analysed Ki67 and TUNEL, although using immunofluorescent techniques. They report that treated tumours showed decreased cellularity compared to tumours from control mice, as well as regions of cell death and fibrosis, but do not comment on the tumours being particularly cystic or necrotic, whereas this was a particular issue for our T24 xenograft studies. Tumours showed a 50% reduction in Ki67 positive cells (using fluorescent labelling) compared to control and TUNEL staining was 10-fold greater, whereas I saw no significant difference in Ki67 positive cells. Potential reasons for differences may include the different technology used, and their analysis technique. They calculated the percentage of positive cells in five visual fields per group, whereas I analysed staining across the whole tumour (excluding necrotic areas). The time point that they used to harvest after the last dose is not clear from their paper so this may have contributed to differences in results. It is also not stated whether they were blinded to treatment group when quantifying the biomarkers – all analysis in my studies was performed blinded to avoid bias.

Given the variability in T24 xenograft tumour growth even amongst the vehicle controls and the cystic nature of the tumours, together with the degree of necrosis seen, in hindsight the choice of a different bladder cancer model may have shown more consistent results within groups and therefore a greater magnitude of benefit, although despite this variation significant changes were seen. T24 xenografts have been used by others but alternative cell lines such as UM-UC-3 have also been successfully used in xenograft studies and performing pilot studies *in vivo* with UM-UC-3 or RT112 cells (which showed synergy *in* vitro) may have been worthwhile to see if more consistent tumour growth was seen. Given the known limitations of xenograft models (including their inability to recapitulate tumour microenvironment or to metastasise), there are now other animal models available such as genetically engineered mouse models which could be considered (303). One option considered was to perform studies in MIA-PaCa-2 xenografts, given that this was an established model in our institution. However, whilst *in vitro* work showed synergy with CYC3 and paclitaxel in MIA-PaCa-2 cells, synergy was not seen with MLN8237 and paclitaxel.

Although tolerability of the combinations was a concern, they were well tolerated apart from those with docetaxel 20 mg/kg where there was evidence of toxicity. Since these experiments, a PK-PD model modeling haematological toxicity with the combination of MLN8237 and docetaxel predicted that an intermittent schedule of MLN8237 dosing once daily three times a week concomitantly with weekly docetaxel (as used in my studies) (instead of daily MLN8237 dosing) would decrease the incidence of dose limiting neutropenia compared with a seven-day continuous schedule, whilst maintaining efficacy (283), consistent with my findings in blood tests, bone marrows, MPO staining and the pilot CFU-GM study. These findings were confirmed in an *in vivo* study which confirmed significant anti-tumour activity with this combination regimen compared to the single agents (261).

Therefore my results of improved tolerability with the combination of MLN8237 with lower concentrations of paclitaxel and docetaxel are consistent with those of others, using different xenograft models. As outlined in 1.7 and 1.8.3, a range of clinical trials have now been performed with AKI, both as single agents and in combination. In Chapter 7, I review this evidence, specifically assessing how pre-clinical data can guide clinical trial design with drug combinations.

7 TRANSLATION OF AK-A SPECIFIC INHIBITORS INTO CLINICAL TRIALS

7.1 Introduction

The work in previous chapters suggests that MLN8237 both as a single agent and in combination with either paclitaxel or docetaxel has potential efficacy. Reducing the dose of the taxanes in combination with MLN8237 may maintain efficacy but with reduced toxicity compared to higher doses of single agent taxanes. As part of this project, I planned to design a phase 1 clinical trial of the combination of an AKI and taxanes, using the results of my pre-clinical work to guide my dosing strategy. Since then, clinical trials have been published with AK-A inhibitors such as MLN8237, both as single agents (Table 1-3) and in combination (Table 1-5) with other drugs. In this chapter, I outline the principles of clinical trial designs, particularly for combination trials and review the clinical trials now published for the combination of MLN8237 and taxanes. I then present a clinical trial design for the combination of MLN8237 and paclitaxel (developed in conjunction with Dr Adrian Mander's group at MRC Biostatistics Unit Hub for Trials Methodology Research), before reviewing how PK and PD modelling could be used to aid clinical trial design and the potential of alternative clinical trial designs.

Contribution of others to this experimental work: The proposed trial protocol described in 7.4 was developed with Dr Adrian Mander's group at MRC Biostatistics Unit Hub for Trials Methodology Research, particularly with Dr Graham Wheeler.

7.2 Principles of Phase 1 clinical trials

Dose-escalation trials can be either rule- or model-based. Rule-based designs have set rules that allocate cohorts of patients to one of several pre-determined doses based on the DLT responses of the last cohort. The majority are "up-and-down" e.g. the 3+3 design (304, 305); here cohorts of three patients are assigned sequentially to increasing dose levels. If one DLT is observed in the first three patients, the cohort is expanded by a further three patients. Dose-escalation is stopped when at least two out of three or six patients experience a DLT. The design is simple and easy to implement since dose escalation and trial termination are governed by fixed rules. However, there are many issues with the 3+3 design, including slow dose-escalation, with many patients treated

at sub-therapeutic doses, and the design only considers the outcome of the last cohort to guide dose escalation (306-310).

Alternatively, model-based designs assume a dose-toxicity relationship, characterised by one or more parameters. As information accrues during the trial, this relationship is re-evaluated, with subsequent patients allocated to dose levels that best satisfy chosen decision criteria (e.g. the dose whose estimated probability of DLT is closest to the Target Probability of Toxicity (TPT)) (306). Many of the models proposed are Bayesian adaptive designs, where prior estimates/beliefs of DLT probabilities are elicited from experts familiar with the pre-clinical data (311-314) and can be combined with available historical data to generate prior probabilities of DLT for each agent. For example, in the Continual Reassessment Method (CRM) (315), the probability of a patient experiencing a DLT is dependent on a model chosen by the investigators, which requires the dose of the agent (or alternatively a "skeleton dose", often the prior probability of DLT at that dose (316)) and a single model parameter as inputs. Given a prior distribution for the parameter and previous patients' DLT responses, an updated distribution of the drug's dose-toxicity relationship is obtained and the next patient is given the dose with an estimated posterior probability of DLT closest to the TPT. This adaptive procedure continues for future patients, adjusting the relationship based on the accrued data, hence aiming to allow both a more accurate MTD estimate and safety assessment. Use of this prior information aids the dose-escalation decision-making process, meaning fewer patients may be required relative to a trial with no prior information.

The design of combination clinical trials is a particular challenge with guidelines emphasising the need for a strong scientific rationale, with pre-clinical evidence and the requirement to consider PK/PD and overlapping toxicities (317). Although prior knowledge of individual drug's toxicity is usually available, this may be of limited use when two agents are combined, as there are multiple potential RP2D combinations in a two-dimensional dose-toxicity surface, which may have the same probability of DLT. Figure 7-1 illustrates this with the RP2D contour showing all the possible dose combinations of Drug A and Drug B with a probability of DLT of 0.3.

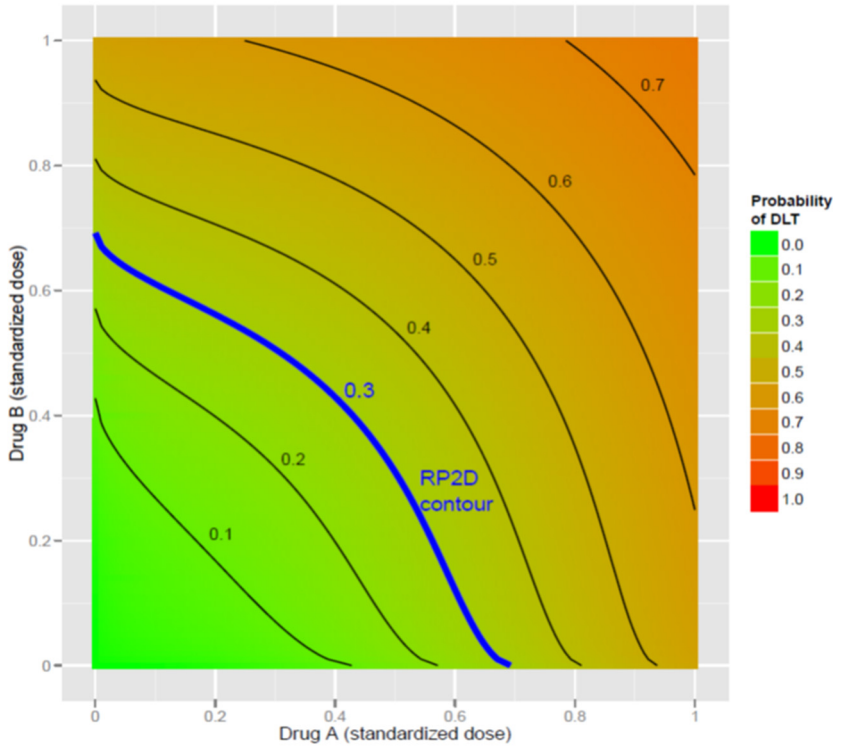

Figure 7-1: Example of a 2D dose surface formed by Drug A and Drug B.
The RP2D contour is shown for a target probability of toxicity of 0.3 (bold line) and is the line of all the dose combinations that have a probability of DLT equal to 0.3. Adapted from (318).

At present the majority of combination trials fix the level of one drug either at its single agent RP2D or at a dose close to this (normally the drug with most prior information, Drug A here). The novel agent is then escalated with the initial aim of reaching its single agent RP2D dose, typically using the single-agent 3+3 design and hence only a limited number of dose levels are explored (Figure 7-2) – referred to as the "standard method" in this chapter. This is based on the assumption that if the agents to be administered in combination have different mechanisms of action or non-overlapping toxicities, reaching the RP2D of each single agent would be the optimal drug combination (306). It also assumes that the optimal dose of Drug A is known, even when used in combination with another agent.

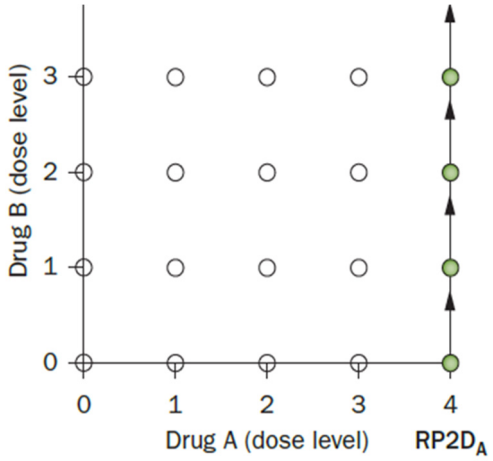

Figure 7-2: Example of dose escalation studies.
Standard method of dose escalation, with drug A fixed at its RP2D when administered alone (RP2D$_A$). Adapted from (318).

Any reductions in either agent's dose due to tolerability are regarded as compromises, with decisions made based on multiple factors, including ethical, regulatory, safety, and scientific concerns. A problem with this approach is that the full dose single agent may already cause significant toxicity and hence assessing the tolerability of an additional and presumably toxic drug is challenging, a particular concern here with the known overlapping toxicity of neutropenia with both taxanes and MLN8237. Unless a PD readout is available, the occurrence of DLT may halt dose escalation of the second drug and lead to suboptimal target inhibition, such as occurred in the trial of MLN8237 and docetaxel (242). By not fully exploring the surface of interactions within the two-dimensional plane, a trial may overlook the most efficacious dose combinations, or dose combinations with reduced toxicity (319).

With respect to toxicity, any of the dose combinations upon the RP2D contour could be taken forward into phase 2 testing. Currently the majority of trials choose not to evaluate multiple doses/schedules due to practical concerns regarding time, cost and the additional patient numbers required together with the pragmatic view that one dose/schedule is preferred. However, it may be that more than one RP2D combination is equally effective at target inhibition, and these could then be compared in a randomised phase 2 trial for efficacy.

Adopting this "standard method" based on toxicity alone is a particular challenge with the small numbers of patients typically seen within a dose cohort and with oncology patients who are often heavily pre-treated, and hence may be more susceptible to additional toxicity. A review of phase 1 oncology combination trials showed that 88% of trials used the "standard method", only approximately one third of potential

combinations were considered and the DLT rate at the RP2D was 6%, well below the target rate of 33% (320).

7.3 Summary of MLN8237 and taxanes clinical trials

Before discussing my proposed clinial trial design, I firstly review the studies now published with MLN8237 in combination with both docetaxel and paclitaxel, with a focus on trial design and DLT.

7.3.1 Paclitaxel

A combination study with MLN8237 and paclitaxel enrolled 49 patients with ovarian or breast cancer with paclitaxel given on days 1,8 and 15 and MLN8237 given on Days 1-3, 8-10, 15-17 of a 28 day cycle (241, 321). The design fixed the dose of paclitaxel at 80 mg/m^2 (full single agent dose), and dose escalated MLN8237 from 10 mg bd, a conventional approach to dual-agent trials. At dose level 2 (MLN8237 20 mg bd), two patients suffered DLT (Grade 4 diarrhoea and Grade 3 stomatitis) and a protocol amendment was required to reduce the paclitaxel to 60 mg/m^2. Two separate MTDs were identified – MLN8237 10 mg bd with paclitaxel 80 mg/m^2 and MLN8237 40 mg bd with paclitaxel 60 mg/m^2, with neutropenia the DLT, but biologically active concentrations of MLN8237 were not achieved with the MLN8237 10 mg dose. Hence the RP2D was MLN8237 40 mg bd Days 1-3, 8-10, 15-17 with paclitaxel 60 mg/m^2 Days 1, 8 and 15 of a 28 day cycle, a dose reduction of both agents compared to single agent schedules.

Two randomised phase 2 studies have now reported their interim analysis, comparing this combination against standard dose single agent paclitaxel 80 mg/m^2. In a study of 142 patients with ovarian, fallopian tube or primary peritoneal cancer, the median PFS (measured by RECIST and CA-125 criteria) was significantly longer with the combination at 7.6 versus 4.6 months (HR 0.55; 80% CI 0.40, 0.77; p=0.021) (239). However, increased toxicity was reported with the combination, with 14% vs 1% discontinuing treatment due to toxicity. Drug related AE ≥Grade 3 were seen in 85% vs 20% of patients, including neutropenia (64% vs 9%), and febrile neutropenia (14% vs 0%). However, less peripheral neuropathy was seen in the combination compared to single agent paclitaxel (8% vs 19%) and they state that the toxicities were largely manageable.

In a study of 178 patients with small cell lung cancer, the combination was again more effective with median PFS of 101 days vs 66 days (HR 0.72; 95% CI 0.52, 1.0; p=0.038) and a disease control rate of 58% versus 46% (250). Similar increased toxicity was seen with the combination (drug related AE ≥ Grade 3 of 67% compared to 25% and trial discontinuation in 15% vs 6%), with neutropenia in 49% (grade not specified in report). Despite the increased toxicity seen, the improvements in PFS lend some support to the activity of the combination compared to single agent paclitaxel.

7.3.2 Nab-paclitaxel

An alternative formulation of paclitaxel is nab-paclitaxel (nanoparticle albumin bound paclitaxel). In an ongoing phase 1 study, nab-paclitaxel 100 mg/m^2 (full single agent dose) given weekly Days 1, 8 and 15 was combined with escalating doses of MLN8237 from 20 mg bd given Days 1-3, 8-10, 15-17 of a 28 day cycle (17 patients). The most frequent drug related AE (all grade/grade 3-4) were nausea (65%/6%) and neutropenia (61%/18%). Two of three patients experienced DLT with the combination of MLN8237 50 mg bd and nab-paclitaxel 100 mg/m^2 (grade 4 neutropenia; febrile neutropenia) with the MTD established as MLN8237 40 mg bd with nab-paclitaxel at full dose. In the dose expansion cohort (16 patients), patients with advanced pancreatic or high grade neuroendocrine cancer were enrolled and at the time of report, twenty patients were evaluable with one partial response and nine with stable disease after two cycles (243), suggesting the combination may be effective. It is notable that with nab-paclitaxel, it was possible to maintain the full single agent dose, consistent with reports of its reduced toxicity compared to paclitaxel (322).

7.3.3 Docetaxel

A trial investigating the combination of MLN8237 with docetaxel recruited 41 patients (242). As with paclitaxel, the aim was to maintain the taxane at its standard dose (docetaxel 75 mg/m^2 on Day 1) with dose escalation of MLN8237 from 10 mg bd but using the original MLN8237 single agent regimen (Days 1-7 of a 21 day cycle). In the first two dose levels, single DLTs were observed and in the third cohort (MLN8237 30 mg bd), two of five patients had a DLT with Grade 3 stomatitis and grade 4 neutropenia. The number of days of MLN8237 was reduced from seven to five days but two out of the three patients developed febrile neutropenia (Grade 3 and Grade 4). A decision was then made to reduce the dose of docetaxel to 60 mg/m^2 with MLN8237 30 mg bd for seven days but both patients had Grade 4 febrile neutropenia. A cohort with

MLN8237 for five days and docetaxel 60 mg/m^2 was closed early because the investigators were concerned that the single agent docetaxel dose was too low for patient benefit, despite the fact that docetaxel 60 mg/m^2 has previously been shown to be effective (323). Instead prophylactic GCSF support was added, but despite this two of the four patients had DLT with MLN8237 40 mg bd and docetaxel 75 mg/m^2; Grade 3 stomatitis and Grade 4 febrile neutropenia. They report an overall response rate of 29%, with seven PR, including one in bladder cancer with MLN8237 30 mg bd for five days and docetaxel 60 mg/m^2.

The RP2D was recommended as MLN8237 20 mg bd for seven days with docetaxel 75 mg/m^2 because GCSF was not required. Although there was one PR and six SD in the nine patients treated at the RP2D with assessable disease, the PR and three of the SD were in metastatic castrate refractory prostate cancer where no previous taxane therapy was permitted. Although the authors speculate MLN8237 20 mg could still have an additive or synergistic effect, the anti-tumour responses in this combination are likely to have been largely due to docetaxel 75 mg/m^2 as a single agent.

7.3.4 Summary of results from clinical trials

The single agent MLN8237 DLT is myelosuppression, with high rates of Grade 3 or 4 neutropenia. Whilst in most cases this was reversible and therefore the majority of trials have not used prophylactic GCSF, in the combination trials with overlapping toxicities it proved more problematic. The amended intermittent scheduling of MLN8237 was predicted to lower the risk of myelosuppression but unplanned dose modifications to paclitaxel were required. Despite this additional toxicity, improved PFS was seen in Phase 2 trials with the RP2D combination, compared to full dose single agent paclitaxel and with lower incidence of neuropathy, indicating that the combination may provide clinical benefit. Interestingly it was possible to maintain nab-paclitaxel at full dose with MLN8237 40 mg bd. Due to the investigators' concerns about using lower doses of docetaxel, their recommended RP2D combination is unlikely to have given additional benefit over single agent full dose docetaxel alone. None of these trials planned to investigate lower concentrations of taxanes and all used the "standard method". In contrast, I proposed using a model-based approach to attempt to fully explore the RP2D contour and reduce toxicity with lower doses of paclitaxel.

7.4 Proposed trial protocol for the combination of MLN8237 and paclitaxel

7.4.1 Starting doses of MLN8237 and paclitaxel

My *in vivo* work demonstrated that paclitaxel 2 mg/kg and 6 mg/kg (human equivalent dose approximately 6 mg/m^2 and 18 mg/m^2 (calculated as per (324)) were tolerable and showed anti-tumour efficacy in combination with MLN8237 (6.5). Hence the starting dose of paclitaxel for my trial design was 10 mg/m^2 administered on Days 1, 8 and 15 of a 28 day cycle (1/8 of the standard single agent dosage). The expected maximum dose of paclitaxel was 40 mg/m^2, since my work suggested that aiming to achieve the full weekly dose of paclitaxel would lead to additional toxicity, could prevent dose escalation of MLN8237 and may not provide the synergy desired. The maximum tolerated dose in man for MLN8237 as a single agent is 50 mg bd for seven days of a 21 day cycle (204, 206). In mice MLN8237 15 mg/kg and MLN8237 30 mg/kg (human equivalent dose approximately 25 mg bd and 45 mg bd) had shown an effect on tumour growth, without a significant difference in response between the two dose levels (6.4.2.2). I selected a starting dose of MLN8237 10 mg bd with the same dosing schedule due to the potential for unknown PK/PD interactions with the combination.

7.4.2 Trial design

Having considered the potential advantages of different trial designs, a model-based design was proposed to allow the identification of the MTD combination, utilising toxicity data and following a modified CRM approach (325, 326). Information was available for single agent paclitaxel, particularly for the risk of neutropenia, the most likely predicted overlapping toxicity. Dr Graham Wheeler used a random intercept, random slope model (327) to combine the data and obtain a prior for this risk, which was incorporated into the modelling. However, we did not have any detailed toxicity information available at the start for the combination other than a vague prior. Therefore, there was an initial rule-based start-up, before the full dose escalation commenced with a minimum of three patients/cohort (Figure 7-3). Although initial admissable combinations are shown, the model could allocate to any combinations along the contour (providing the TPT was ≤0.3). As the data from each patient became available at the end of cycle 1, the accumulated toxicity data would be used to update the model (as described in 7.2) and recommend dose escalation (if the toxicity of the current dose level is acceptable) or de-escalation (if the current dose level is too toxic)

to neighbouring dose levels with the dose level for the next patient estimated to be closest to the TPT of 0.3. Intermediate dose levels could be selected or further splitting of the dose into eight hourly (t.d.s.) or six hourly (q.d.s.) dosing could be considered depending on the emerging safety information and/or PK and PD data. Hence my proposed design would have explored a wider range of combinations to that seen in the published clinical trials.

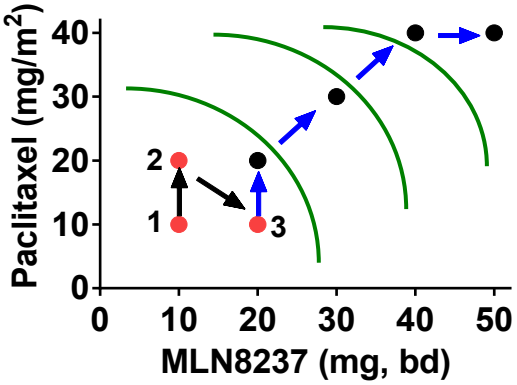

Figure 7-3: Admissable dose levels for proposed MLN8237 and paclitaxel clinical trial.
Initial rule based start up phase with three cohorts (red dots and black arrows) before dose escalation (black dots for initial admissable levels with blue arrows). Green curved lines show how any combinations along the contour could be explored.

An important consideration when attempting to translate promising pre-clinical work into novel therapeutic strategies is the use of biomarkers to demonstrate target effect and identify appropriate patient populations. My protocol included detailed PK studies to assess the PK of MLN8237 and paclitaxel when given in combination and characterise the effect of concomitant administration of the PK of both drugs. I proposed mandatory tumour biopsies pre-trial entry and following seven days of dosing, with the assessment of mitotic cells within tumours for misaligned chromosomes and the absence of properly formed bipolar mitotic spindles hoped to be of greater utility than methods I had trialed in my *in vivo* studies.

7.5 Use of pharmacodynamic and pharmacokinetic data

Increasingly modelling has been used to incorporate both PK and PD data and these can be useful with drug combinations, with the ability to investigate the optimal sequencing of these drugs (328). Models have been created for MLN8237 both as a single agent and in combination, but the extent to which this has been used to influence clinical trial design varies.

7.5.1 Single agent MLN8237 PK, PD and efficacy models

A model created by Yang *et al.* which incorporated PK, PD (mitotic index in tumour samples) and efficacy (tumour growth inhibition) data from xenograft studies revealed that optimal PD effects were seen with a MLN8237 plasma concentration ≥1 μM for at least 8-12 hours and estimated an oral dose in man of 103 mg od or 62 mg bd, close to the eventual single agent RP2D of 50 mg bd (329). Despite this, the starting dose for Phase 1 trials was 5 mg/day, with the dose doubled in successive cohorts until two or more patients experienced a grade 2 drug-related toxicity, or one patient experienced a grade ≥3 DLT which did not occur until 110 mg od (204). Analysis of the Phase 1 trials showed very similar PK to that predicted with steady-state average plasma concentration of 2.7 μM at the RP2D of 50 mg bd, with PD effects on the mitotic index seen at this dose. This demonstrates the challenge in translating modelling data into the clinic for first in human studies as many patients were treated at doses well below those anticipated to have any clinical effect.

Using data from several single agent studies, further PK and PD analysis demonstrated a significant steady-state PD effect at the MLN8237 MTD of 50 mg bd, with predicted decreases in chromosome alignment of 75% (68-80%) and spindle bipolarity of 62% (55-70%) (330). Whilst there was a low probability of DLT at the RP2D (7%, consistent with the 10% observed), modelling showed that dose modifications to either 40 mg bd or 30 mg bd reduced the expected DLT probability (to 2% at 30 mg bd) whilst still showing tumour PD effects (50-60% decrease in chromosome alignment and spindle bipolarity), meaning that the dose modification to MLN8237 to 40 mg bd seen in the MLN8237 and paclitaxel trials would still be predicted to be effective. This work provides useful information about toxicity profiles and inputs for combination studies, although additional factors need to be considered for these, including the potential for overlapping toxicities and drug-drug interactions.

7.5.2 Models for combination of MLN8237 and taxanes

Whilst there was interest in combining MLN8237 and taxanes, there was particular concern about the risk of neutropenia. Hence a PK-absolute neutrophil count model was created by Le *et al.* for the combination of MLN8237 and docetaxel, using *in vivo* data (283). An intermittent schedule of MLN8237 (three days on, four days off twice daily) gave a predicted incidence of Grade 4 neutropenia in humans of 1.4% compared to 17% when dosed twice daily for seven days (fixed total dose of 700 mg/cycle). When

combined with a single dose of docetaxel 75 mg/m^2, this rose to 72% for the intermittent dosing compared to 91% with the seven day continuous regimen, indicating that this was a preferable option, although still with high predicted rates of neutropenia, consistent with the actual issues seen in the Phase 1 combination trial.

Building on this work, a model was created by Huck *et al.* using pre-clinical anti-tumour data to predict the most effective combination of MLN8237 and paclitaxel, creating an exposure-efficacy surface plot and an isobologram where the effect of each combination could be assessed (261). Using pre-clinical anti-tumour efficacy and the results of the phase 1 trial of the combination of MLN8237 and paclitaxel (241), they demonstrated that similar efficacy was seen for both paclitaxel single agent 60 or 80 mg/m^2, supportive of other trials which have shown anti-tumour effects with paclitaxel 60 mg/m^2 (331). The addition of increasing doses of MLN8237 from 10 mg up to 50 mg bd would lead to increased efficacy. Their plot suggests that reducing the dose of paclitaxel to 60 mg/m^2 could still allow increased efficacy compared to single agent paclitaxel 80 mg/m^2. They state that as no patients were dosed with paclitaxel at a lower dose than this, modelling of this scenario was not possible, although extrapolation could have been used. Given synergy in their *in vivo* work with paclitaxel doses as low as 5 mg/kg, further reductions in paclitaxel could well still provide synergy in combination with MLN8237.

7.6 Alternative clinical trial designs

In the era of molecularly targeted agents, the focus is shifting towards using clinical trials to identify the optimal biological dose rather than the MTD. This requires changes in trial design with a focus on efficacy rather than toxicity alone, and increasingly biomarker driven clinical trials (332, 333). This may require trials to incorporate emerging results of PD endpoints whether toxicity, biological or efficacy-related to identify one or more doses/schedules for further evaluation. All the Phase 1 studies with MLN8237 used a standard rule based 3+3 design, both in single agent and combination studies. In this section, the potential to improve upon this, particularly with adaptive designs is reviewed in the Phase 1 setting (reviews which discuss adaptive designs for all phases of clinical trials including Phase 2 biomarker adaptive designs include (334-336)). I co-wrote a review of adaptive designs for dual-agent phase 1 dose escalation studies, covering this topic in detail (318) (Appendix 2).

7.6.1 Alternative dual-agent clinical trial designs

Rather than adopting the standard approach of fixing the dose of one drug and dose-escalating the other (Figure 7-2 A), different designs can be used. Rule-based strategies for dose escalation include 1) alternate escalation of the agents in the series of dose levels; 2) simultaneous escalation of both agents; and 3) performing two trials using the standard method, holding different agents constant for each trial. Although these aim to improve upon the standard method, several limitations remain and the probabilities of DLT associated with the selected RP2D combinations may be well below – or indeed above – values deemed acceptable (310). Hence model-based adaptive designs are attractive. Because of the lack of prior information, many use an initial rule based start-up stage to obtain preliminary data that can be fed into the statistical model (as proposed in my MLN8237 and paclitaxel design), followed by a second stage, implementing the model, modified CRM in this case. Entirely model-based two-stage dual-agent dose-escalation designs do exist when information about both drugs as single agents is available (for example (325)).

7.6.2 Phase 1 combination trial designs assessing toxicity and efficacy

The standard indicator of efficacy has been tumour shrinkage identified on imaging, normally measured at periodic intervals well after cycle 1 toxicity assessments. As eligible patients in oncology trials generally have advanced refractory disease and progress after only a few cycles, efficacy data has not been widely incorporated into decisions about dose escalation, with toxicity endpoints alone used to define RP2Ds in the majority of phase 1 trials (306, 337). However, with targeted agents this hypothesis may be invalid both because such agents may be cytostatic and not lead to tumor shrinkage, and because surrogate measures such as target inhibition or PK endpoints can be used with results available to researchers rapidly. Certainly in the trials of MLN8237 comment was made that response often occurred in cycles three or four (210), potentially because adequate cell divisions in the presence of drug are required for disease stabilization.

In this context, an ideal model would recommend RP2D based on both toxicity and efficacy (338, 339). This should minimise toxicity which may occur with off-target effects at higher concentrations of the drug (306, 340). A range of designs have been proposed to achieve this. Several two-step designs initially consider the toxicity of dose combinations (achieved using either 3+3 or CRM designs), followed by assessing

efficacy of a subset of dose combinations chosen from the first stage (341, 342). Entirely model based designs which can distinguish between the probabilities of toxicity and efficacy have shown utility in clinical trials (343, 344). More complex models include one where surrogate measures of efficacy (such as real time PD data) can be used until confirmatory efficacy data is obtained from for example imaging, allowing improved dose selection and shorter trial duration (345).

7.7 Summary of chapter

This chapter highlights the importance of clinical trial design in translating promising pre-clinical work into clinical trials, particularly with drug combinations. Whilst the "standard method" has identified a RP2D combination for MLN8237 and paclitaxel, toxicity has been an issue, largely myelosuppression, emphasising the importance of my work investigating this in the pre-clinical setting. The longer PFS with the combination of MLN8237 and paclitaxel in the phase 2 trials suggest that the combination may have value, but the increased myelotoxicity was problematic. By considering lower doses of paclitaxel as proposed in my trial design, this toxicity may have been reduced but with similar efficacy.

The PK and PD modelling studies show their potential value in predicting efficacious doses both in single agent studies and in combinations. Using *in vivo* studies, generating such exposure-efficacy correlations can allow multiple combinations to be assessed by a model. Combining these with safety data could ensure prioritisation of dosing schedules which are most likely to be both safe and effective. It is not clear how much of these data were available at the time the clinical trials were designed, particularly the Phase 1 combination studies. For example, in the combination study with MLN8237 and docetaxel the investigators struggled to maintain dosing of either drug using a seven day continuous MLN8237 dosing regime and ultimately chose to prioritise maintaining docetaxel dose over MLN8237 dose escalation (242). However, use of intermittent MLN8237 and dose reducing docetaxel is likely to have been equally effective, but with reduced toxicity, based on the work modelling neutropenia for the combination of MLN8237 and docetaxel (283) and the translational work with MLN8237 and paclitaxel (261).

The use of model-based designs when assessing drug combinations provides a framework to incorporate additional data - both prior and accrued – into dosing and schedule decisions that rule-based designs (particularly the "standard method") often

lack. With these adaptations, more information per patient is provided and the chances of placing patients on doses or schedules that are dangerously toxic are reduced (346, 347). Concurrently, the extra information provided can lead to more accurate estimation of the RP2D contour (348) and – in trials concerned with efficacy endpoints also – more accurate estimation of the therapeutic window. However, their implementation in clinical practice is still infrequent, partly due to the relative novelty of these designs, the need for the presence and input of statistical experts together with concerns about support from regulatory agencies (339, 349, 350). By escalating both agents and exploring the dose-combination surface, more patients may be required but this would allow the efficacy-toxicity trade-off of both agents to be better evaluated.

8 *DISCUSSION*

I have demonstrated that the combination of specific AK-A inhibitors with low concentrations of paclitaxel (GI_{20}) are synergistic in T24, RT112 and UM-UC-3 cell lines. Initial studies were performed with a novel AK-A inhibitor, CYC3, and these finding were confirmed using the more clinically relevant MLN8237. The use of response-surface modelling allowed a range of concentration-combinations to be studied and identified maximal synergy with concentrations of paclitaxel which had little effect as single agents (GI_{20} to GI_{40}). These results are consistent with the reports of synergy between AK-A specific inhibitors and taxanes in other cancer cell lines that emerged during my studies. In one of these publications, MLN8237 was evaluated in similar bladder cell lines in combination with paclitaxel. Those studies also suggested that exposure to MLN8237 followed by paclitaxel led to maximal synergy. However, in my studies, I show that that simultaneous exposure to MLN8237 and paclitaxel is the optimal schedule, which is a more convenient regimen to administer clinically. My scheduling findings are similar to those of others both *in vitro* and *in vivo* evaluating the combination of MLN8237 and taxanes (261).

Assessment of synergy is crucial in evaluating new drug combinations, with most studies using either the Loewe additivity model or Bliss independence model, although both have limitations (227). In my work, I used the Bliss independence model because it could be used on any data set, regardless of the shape of the single-agent dose-response curves and several of the AKI did not show the typical dose-response relationship as single agents required to use the Loewe model. However, the Bliss model assumes that both drugs act independently and therefore given that both AKI and taxanes target mitosis, albeit in different ways, there is a potential issue in my use of this model. Alternative ways of assessing combinations are required and remain in development, including a model developed by Dr Giovanni Di Veroli in our group called “Synergy, Antagonism or Neutrality Estimation” (unpublished).

I chose to use a bladder cancer cell line panel selected to represent a range of grades and stages of the disease and with different mutations (Table 3-5). It is notable that the cell lines where synergy was seen with the combination of MLN8237 and paclitaxel (T24, UM-UC-3 and RT112) all had p53 mutations, known to be a marker of a more aggressive tumour type (105). However, it is difficult to fully capture the clinical heterogeneity of cancer, particularly when metastatic, from cell lines alone. Recent

publications with more comprehensive molecular characterisation of tumours has suggested bladder cancers can be divided into luminal and basal subtypes, with aggressive tumours and AK-A over-expression seen in the basal subtype (107, 122). The status of all the cell lines in my panel has not been reported but UM-UC-3 is described as basal and T24 as mixed luminal/basal. Therefore, with this new knowledge, it may have been particularly beneficial to assess the combination in basal subtype bladder cancer cell lines.

With the combination of MLN8237 and paclitaxel, a differential response was seen between cancer cell lines (T24) and non-cancer cell lines (ARPE-19), as simply additive and even antagonistic effects were seen with the combination of an AK-A inhibitor and paclitaxel in ARPE-19 cells. A similar phenomenon has been identified clinically, when paclitaxel and carboplatin are combined, leading to less thrombocytopenia than would have been predicted (351). Identifying such differences between cancer and non-cancer cells was a major driver to the design of my combination studies and the development of the software that was used to analyse the combination data (252). Live cell imaging was used to provide new insights into the mechanistic differences between ARPE-19 cells and T24 cells. More cells remained viable after exposure to the combination of MLN8237 50 nM and paclitaxel 2 nM in ARPE-19 cells compared to T24 cells, with the potential for more ARPE-19 cells to recover after exposure, compared to a higher concentration of single agent paclitaxel.

Advances in technology since I performed my experimental work have shown the increasing promise of time-lapse live cell imaging in assessing the individual fate of cells. Performing the analysis manually was very time consuming and meant that only a limited number of cells could be studied. Automation to analyse more cells would be very beneficial and I worked together with Dr Joana Grah to develop a workflow which can detect and track mitotic cells, allowing time in mitosis to be assessed and avoiding the need for fluorescent markers. Initial experiments showed promising results assessing the fate of T24 cells treated with different drugs and the tools have now been published (Appendix 3, (352)). In addition, my colleague Dr Siang Boon Koh was involved in developing an alternative live cell imaging technique which uses fluoresence-ubiquination based cell cycle reporters to analyse cells exposed to drugs, which would again have been of interest to use in my work (353).

Using the CFU-GM assay, more colonies survived with the combinations of MLN8237 and paclitaxel 1-3 nM than MLN8237 as a single agent and they were less myelotoxic

than higher paclitaxel concentrations as a single agent. This was also the case in studies that we have already published, assessing CYC3 in combination with paclitaxel in this assay ((258) Appendix 1). The indication that the combination may be less myelotoxic than higher concentrations of paclitaxel as a single agent is encouraging, particularly as neutropenia has been shown to be the dose limiting toxicity in the clinical trials performed to date.

In my studies, AK-A expression in cell lines (measured by total AK-A Western blotting) did not correlate with the degree of growth inhibition associated with exposure to single agent AK-A inhibitors. However, in the HeLa AK-A inducible cell line, at clinically relevant degrees of AK-A over-expression, a modest reduction in sensitivity to paclitaxel, and less growth inhibition was observed with the combination of MLN8237 and paclitaxel. These differences were small and certainly contrast with the report that AK-A over-expression leads to substantial taxane resistance (2). Therefore, AK-A expression in tumours may not be a useful biomarker for patient selection in clinical trials of AKI. Supporting this conclusion, subsequent clinical trials with MLN8237 have not been able to show a correlation between baseline tumour AK-A expression levels and anti-tumour response (210).

Based on my *in vitro* data, I hypothesised that the combination of MLN8237 with lower doses of a taxane could provide a synergistic response which was similar to full dose (MTD) taxane, but with reduced toxicity. Therefore, I proceeded to evaluate the combination of MLN8237 with a taxane in T24 xenograft experiments. With paclitaxel 20 mg/kg iv (reported MTD), hypersensitivity reactions were seen with weekly dosing and therefore combination studies directly comparing paclitaxel 20 mg/kg with combinations of MLN8237 and paclitaxel were not possible. However, the combinations of MLN8237 30 mg/kg (OG) once daily for five days/week with paclitaxel weekly (iv) at either 2 mg/kg or 6 mg/kg were well tolerated and showed a significant reduction in tumour growth.

It was possible to deliver docetaxel at its reported MTD (20 mg/kg weekly iv), allowing this to be compared against combinations of MLN8237 and docetaxel. Whilst maximal tumour inhibition was seen with docetaxel 20 mg/kg either as a single agent or in combination with MLN8237 30 mg/kg, toxicity was seen with weight loss and incidences of overtly impacted intestines. I was able to demonstrate that there was no statistically significant difference in tumour growth inhibition when MLN8237 30 mg/kg (OG) once daily for three days a week was combined with weekly 6 mg/kg

docetaxel (IP), compared to weekly docetaxel 20 mg/kg (IP) as a single agent and that this combination was tolerable. Indeed, other studies have also concluded that doses of taxanes below the MTD together with MLN8237 demonstrate additive or synergistic anti-tumour activity using different xenograft models (261). Hence my results for both MLN8237 30 mg/kg dosed intermittently in combination with paclitaxel 6 mg/kg or docetaxel 6 mg/kg weekly were encouraging, suggesting that clinical trials should explore sub-"standard of care" dosages of taxanes, in combination with MLN8237 to potentially maximise therapeutic benefit, whilst minimising toxicity.

As discussed in Chapter 6, there were issues with the use of the T24 xenograft model, particularly significant variability in tumour growth even in vehicle controls. Given the synergy seen in UM-UC-3 cell lines and with the additional knowledge that it is a basal subtype cell line, it would have been helpful to perform pilot studies *in vivo* with this cell line as this may have been a better model to test the drug combinations. In addition, it would have been interesting to compare the results with paclitaxel and docetaxel with the alternative taxane nab-paclitaxel, both *in vitro* and *in vivo* based on the interim report of the Phase 1 trial where it proved possible to maintain full single agent dose in combination with MLN8237 40 mg bd (243).

Clinical trial design is critical when translating promising pre-clinical work into clinical trials, particularly with drug combinations. Whilst Phase 1 clinical trials did identify a RP2D combination for MLN8237 and paclitaxel, toxicity has been an issue in Phase 2 trials, largely myelosuppression. Notably the randomised Phase 2 trials revealed that PFS was longer for the RP2D combination compared to paclitaxel 80 mg/m^2, but with additional toxicity. A protocol which explores the combination effect surface more fully may have allow a greater range of synergistic combinations to be identified. It is possible that if the trial designs had considered combinations with lower doses of paclitaxel, to more fully explore the dose surface (as proposed in our trial design), similar anti-tumour efficacy may have been seen with reduced toxicity. Whilst the majority of current combination trial designs may provide reassurance that patients are at least receiving one drug at its full dose and hence gaining potential benefit from enrolling in the trial, modelling has shown that the dose of paclitaxel and MLN8237 could be adjusted whilst maintaining a predicted anti-tumour effect.

Whilst 23 studies remain active using MLN8237 (alisertib) in combination with a range of drugs, including one comparing paclitaxel alone compared to MLN8237 and paclitaxel (clinicaltrials.gov, accessed 21 December 2017), MLN8237 no longer forms

part of Takeda Oncology's development pipeline. AK-A appeared a relevant therapeutic target, with evidence of over-expression in many cancers, its important interactions with p53 and BRCA1 and with promising *in vitro* and *in vivo* results with AK-A specific inhibitors in multiple cancer types. Whilst AKI were once described as potential "shining lights on the therapeutic horizon" (354), overall they have shown disappointing results as single agents in solid tumours, although they have shown more promise in haematological malignancies. It has been proposed that tumour heterogenity and the low proliferative index in solid tumours, with a doubling time usually exceeding 100 days, compared to 3 to 6 days for many xenografts (355) may account for this. In a recent publication, when the mitotic index was compared between patient samples from bladder tumours and T24 cells, the mitotic index was eight fold higher in the cell line (276). Therefore, a large proportion of the tumour may not be affected by exposure to the drug during any one cycle of therapy, consistent with the observation that responses to MLN8237 were seen after cycles three or four (210).

Identifying patients who may benefit from treatment with AKI is crucial. Tumour AK-A expression alone has not proved useful in predicting response to AKI. Two recent publications have assessed two functional single nucelotide polymorphisms in AURKA. In the Phase 2 MLN8237 study in bladder cancer, targeted gene sequencing showed a longer PFS in carriers of the minor allele A of rs2273535 in AURKA than in patients who were homozygous for the major allele T, although the significance of this is not clear given the small numbers in this pilot study (356). Another publication combining the data from two of the larger phase 2 studies (391 patients in total) showed that amongst patients treated with MLN8237, those with a single nucleotide polymorphism at codon 57 in AURKA (VV alleles) had a significantly longer PFS than those with VI or II alleles (357). Further work is required to see if AURKA genotype could prove a useful biomarker for patient selection.

To enhance the effect of AK-A inhibition, focus has turned to increasing understanding of the multiple interactions AK-A has with other critical signalling pathways. Examples include the role AK-A plays in DNA-damage response with a recent pre-clinical study reporting synergy with combined AK-A and CHEK-1 inhibition, which enhanced the response of ovarian cancer cells to docetaxel (358), and the interaction between AURKA and KRAS (359). There has been renewed interest in AK-A as a drug target, since its interactions with MYC in cancers such as neuroblastoma and small cell lung

cancer has been identified and it has proved possible to disrupt the protein-protein interaction with AK-A inhibitors (360, 361).

Conclusions

My original hypothesis was that the combination of an AK-A inhibitor and a taxane could provide a therapeutic option for patients with metastatic bladder cancer. My *in vitro* and *in vivo* studies have suggested that using combinations of AK-A inhibitors with taxanes at concentrations below the GI_{50} and hence lower doses may show anti-tumour efficacy with reduced toxicity compared to full dose taxanes. Published clinical trials have struggled to translate similar findings into a new treatment approach for patients. I suggest that to fully define the efficacy and tolerability of the combination, a combination phase 1 trial design which prospectively explored full dose combination-surface, as proposed in my trial design, would have been more efficient and effective. However, given the toxicity seen with MLN8237 as a single agent in patients with metastatic bladder cancer and with new treatment options such as immunotherapy now available, exploring the combination in an unselected patient population is no longer appropriate. Instead research needs to focus on better identifying patients most likely to respond to AK-A inhibitors, either potentially with a taxane or most probably with a molecularly targeted agent. To identify true synergistic activity with regards to efficacy and potentially simultaneously less-toxic combinations, the flexibility of adaptive designs should be used more frequently in the development of promising new drug combinations.

9 *REFERENCES*

1. Dancey JE, Chen HX. Strategies for optimizing combinations of molecularly targeted anticancer agents. Nat Rev Drug Discov. 2006;5(8):649-59. Epub 2006/08/03.
2. Anand S, Penrhyn-Lowe S, Venkitaraman AR. AURORA-A amplification overrides the mitotic spindle assembly checkpoint, inducing resistance to Taxol. Cancer cell. 2003;3(1):51-62. Epub 2003/02/01.
3. Iyer DR, Rhind N. The Intra-S Checkpoint Responses to DNA Damage. Genes. 2017;8(2). Epub 2017/02/22.
4. Hanahan D, Weinberg RA. Hallmarks of cancer: the next generation. Cell. 2011;144(5):646-74. Epub 2011/03/08.
5. Bucher N, Britten CD. G2 checkpoint abrogation and checkpoint kinase-1 targeting in the treatment of cancer. British journal of cancer. 2008;98(3):523-8. Epub 2008/01/31.
6. Musacchio A, Salmon ED. The spindle-assembly checkpoint in space and time. Nature reviews Molecular cell biology. 2007;8(5):379-93. Epub 2007/04/12.
7. Lara-Gonzalez P, Westhorpe FG, Taylor SS. The spindle assembly checkpoint. Current biology : CB. 2012;22(22):R966-80. Epub 2012/11/24.
8. Carmena M, Ruchaud S, Earnshaw WC. Making the Auroras glow: regulation of Aurora A and B kinase function by interacting proteins. Current opinion in cell biology. 2009;21(6):796-805. Epub 2009/10/20.
9. Meraldi P, Honda R, Nigg EA. Aurora kinases link chromosome segregation and cell division to cancer susceptibility. Current opinion in genetics & development. 2004;14(1):29-36. Epub 2004/04/28.
10. Barr AR, Gergely F. Aurora-A: the maker and breaker of spindle poles. Journal of cell science. 2007;120(Pt 17):2987-96. Epub 2007/08/24.
11. Kimura M, Kotani S, Hattori T, Sumi N, Yoshioka T, Todokoro K, et al. Cell cycle-dependent expression and spindle pole localization of a novel human protein kinase, Aik, related to Aurora of Drosophila and yeast Ipl1. The Journal of biological chemistry. 1997;272(21):13766-71. Epub 1997/05/23.
12. Crosio C, Fimia GM, Loury R, Kimura M, Okano Y, Zhou H, et al. Mitotic phosphorylation of histone H3: spatio-temporal regulation by mammalian Aurora kinases. Molecular and cellular biology. 2002;22(3):874-85. Epub 2002/01/11.
13. Goto H, Yasui Y, Nigg EA, Inagaki M. Aurora-B phosphorylates Histone H3 at serine28 with regard to the mitotic chromosome condensation. Genes to cells : devoted to molecular & cellular mechanisms. 2002;7(1):11-7. Epub 2002/02/22.
14. Sasai K, Katayama H, Stenoien DL, Fujii S, Honda R, Kimura M, et al. Aurora-C kinase is a novel chromosomal passenger protein that can complement Aurora-B kinase function in mitotic cells. Cell motility and the cytoskeleton. 2004;59(4):249-63. Epub 2004/10/23.
15. Khan J, Ezan F, Cremet JY, Fautrel A, Gilot D, Lambert M, et al. Overexpression of active Aurora-C kinase results in cell transformation and tumour formation. PloS one. 2011;6(10):e26512. Epub 2011/11/03.
16. Inamdar KV, O'Brien S, Sen S, Keating M, Nguyen MH, Wang X, et al. Aurora-A kinase nuclear expression in chronic lymphocytic leukemia. Modern pathology : an official journal of the United States and Canadian Academy of Pathology, Inc. 2008;21(12):1428-35. Epub 2008/10/22.
17. Zhang J, Li B, Yang Q, Zhang P, Wang H. Prognostic value of Aurora kinase A (AURKA) expression among solid tumor patients: a systematic review and meta-analysis. Japanese journal of clinical oncology. 2015;45(7):629-36. Epub 2015/04/23.

18. Tang W, Qiu H, Ding H, Sun B, Wang L, Yin J, et al. Association between the STK15 F31I polymorphism and cancer susceptibility: a meta-analysis involving 43,626 subjects. PloS one. 2013;8(12):e82790. Epub 2013/12/19.
19. Bruyere F, Corcoran NM, Berdjis N, Namdarian B, Pedersen J, Ockrim J, et al. Aurora kinase B is an independent protective factor in superficial bladder tumours with a dysfunctional G1 checkpoint. BJU international. 2008;102(2):247-52. Epub 2008/03/18.
20. Bufo P, Sanguedolce F, Tortorella S, Cormio L, Carrieri G, Pannone G. Expression of mitotic kinases phospho-aurora A and aurora B correlates with clinical and pathological parameters in bladder neoplasms. Histol Histopathol.25(11):1371-7. Epub 2010/09/25.
21. Comperat E, Bieche I, Dargere D, Laurendeau I, Vieillefond A, Benoit G, et al. Gene expression study of Aurora-A reveals implication during bladder carcinogenesis and increasing values in invasive urothelial cancer. Urology. 2008;72(4):873-7. Epub 2008/05/20.
22. Comperat E, Camparo P, Haus R, Chartier-Kastler E, Radenen B, Richard F, et al. Aurora-A/STK-15 is a predictive factor for recurrent behaviour in non-invasive bladder carcinoma: a study of 128 cases of non-invasive neoplasms. Virchows Archiv : an international journal of pathology. 2007;450(4):419-24. Epub 2007/03/03.
23. Fraizer GC, Diaz MF, Lee IL, Grossman HB, Sen S. Aurora-A/STK15/BTAK enhances chromosomal instability in bladder cancer cells. International journal of oncology. 2004;25(6):1631-9. Epub 2004/11/18.
24. Sen S, Zhou H, Zhang RD, Yoon DS, Vakar-Lopez F, Ito S, et al. Amplification/overexpression of a mitotic kinase gene in human bladder cancer. Journal of the National Cancer Institute. 2002;94(17):1320-9. Epub 2002/09/05.
25. Tseng YS, Tzeng CC, Huang CY, Chen PH, Chiu AW, Hsu PY, et al. Aurora-A overexpression associates with Ha-ras codon-12 mutation and blackfoot disease endemic area in bladder cancer. Cancer letters. 2006;241(1):93-101. Epub 2005/12/13.
26. Araki K, Nozaki K, Ueba T, Tatsuka M, Hashimoto N. High expression of Aurora-B/Aurora and Ipll-like midbody-associated protein (AIM-1) in astrocytomas. Journal of neuro-oncology. 2004;67(1-2):53-64. Epub 2004/04/10.
27. Reichardt W, Jung V, Brunner C, Klein A, Wemmert S, Romeike BF, et al. The putative serine/threonine kinase gene STK15 on chromosome 20q13.2 is amplified in human gliomas. Oncology reports. 2003;10(5):1275-9. Epub 2003/07/29.
28. Samaras V, Stamatelli A, Samaras E, Arnaoutoglou C, Arnaoutoglou M, Stergiou I, et al. Comparative immunohistochemical analysis of aurora-A and aurora-B expression in human glioblastomas. Associations with proliferative activity and clinicopathological features. Pathology, research and practice. 2009;205(11):765-73. Epub 2009/07/21.
29. Sun LB, Fu SL, Luo YN, Chen H, Li WC, Ge PF. [Expression of Aurora-B in human glioma tissue and its significance]. Nan fang yi ke da xue xue bao = Journal of Southern Medical University. 2009;29(1):47-9. Epub 2009/02/17.
30. Zeng WF, Navaratne K, Prayson RA, Weil RJ. Aurora B expression correlates with aggressive behaviour in glioblastoma multiforme. Journal of clinical pathology. 2007;60(2):218-21. Epub 2007/02/01.
31. Miyoshi Y, Iwao K, Egawa C, Noguchi S. Association of centrosomal kinase STK15/BTAK mRNA expression with chromosomal instability in human breast cancers. International journal of cancer Journal international du cancer. 2001;92(3):370-3. Epub 2001/04/06.
32. Hoque A, Carter J, Xia W, Hung MC, Sahin AA, Sen S, et al. Loss of aurora A/STK15/BTAK overexpression correlates with transition of in situ to invasive ductal

carcinoma of the breast. Cancer epidemiology, biomarkers & prevention : a publication of the American Association for Cancer Research, cosponsored by the American Society of Preventive Oncology. 2003;12(12):1518-22. Epub 2003/12/25.
33. Royce ME, Xia W, Sahin AA, Katayama H, Johnston DA, Hortobagyi G, et al. STK15/Aurora-A expression in primary breast tumors is correlated with nuclear grade but not with prognosis. Cancer. 2004;100(1):12-9. Epub 2003/12/24.
34. Bodvarsdottir SK, Hilmarsdottir H, Birgisdottir V, Steinarsdottir M, Jonasson JG, Eyfjord JE. Aurora-A amplification associated with BRCA2 mutation in breast tumours. Cancer letters. 2007;248(1):96-102. Epub 2006/07/25.
35. Cox DG, Hankinson SE, Hunter DJ. Polymorphisms of the AURKA (STK15/Aurora Kinase) Gene and Breast Cancer Risk (United States). Cancer causes & control : CCC. 2006;17(1):81-3. Epub 2006/01/18.
36. Das K, Lorena PD, Ng LK, Shen L, Lim D, Siow WY, et al. Aurora-A expression, hormone receptor status and clinical outcome in hormone related cancers. Pathology.42(6):540-6. Epub 2010/09/22.
37. Jiang W, Watkins G, Douglas-Jones A, Mansel R. Expression of Aurora-B and Aurora-C in human breast cancer is linked to tumour grade and differentiation. AACR Meeting Abstracts. 2007;2007(1_Annual_Meeting):5080-.
38. Xia LP, Zhou FF, Yang MT, Liu Q. [Roles of Aurora-A in tumorigenesis and prognosis of breast cancer]. Ai zheng = Aizheng = Chinese journal of cancer. 2009;28(6):668-72. Epub 2009/07/29.
39. Tchatchou S, Wirtenberger M, Hemminki K, Sutter C, Meindl A, Wappenschmidt B, et al. Aurora kinases A and B and familial breast cancer risk. Cancer letters. 2007;247(2):266-72. Epub 2006/06/10.
40. Staff S, Isola J, Jumppanen M, Tanner M. Aurora-A gene is frequently amplified in basal-like breast cancer. Oncology reports.23(2):307-12. Epub 2010/01/01.
41. Lo YL, Yu JC, Chen ST, Yang HC, Fann CS, Mau YC, et al. Breast cancer risk associated with genotypic polymorphism of the mitosis-regulating gene Aurora-A/STK15/BTAK. International journal of cancer Journal international du cancer. 2005;115(2):276-83. Epub 2005/02/03.
42. Vidarsdottir L, Bodvarsdottir S, Ogmundsdottir H, Eyfjord J. Targeting Aurora kinases in BRCA2-mutated breast cell lines. AACR Meeting Abstracts. 2008;2008(1_Annual_Meeting):2395-.
43. Tanaka T, Kimura M, Matsunaga K, Fukada D, Mori H, Okano Y. Centrosomal kinase AIK1 is overexpressed in invasive ductal carcinoma of the breast. Cancer research. 1999;59(9):2041-4. Epub 1999/05/08.
44. Guo XG, Zheng L, Feng WB, Xia Y. The AURKA gene rs2273535 polymorphism contributes to breast carcinoma risk - meta-analysis of eleven studies. Asian Pacific journal of cancer prevention : APJCP. 2014;15(16):6709-14. Epub 2014/08/30.
45. Ali HR, Dawson SJ, Blows FM, Provenzano E, Pharoah PD, Caldas C. Aurora kinase A outperforms Ki67 as a prognostic marker in ER-positive breast cancer. British journal of cancer. 2012;106(11):1798-806. Epub 2012/04/28.
46. Saxena M, Singh S, Negi MP, Srivastava AK, Trivedi R, Singh U, et al. Expression profiling of G2/M phase regulatory proteins in normal, premalignant and malignant uterine cervix and their correlation with survival of patients. Journal of cancer research and therapeutics. 2010;6(2):167-71. Epub 2010/07/14.
47. Twu NF, Yuan CC, Yen MS, Lai CR, Chao KC, Wang PH, et al. Expression of Aurora kinase A and B in normal and malignant cervical tissue: high Aurora A kinase expression in squamous cervical cancer. European journal of obstetrics, gynecology, and reproductive biology. 2009;142(1):57-63. Epub 2008/12/09.

48. Baba Y, Nosho K, Shima K, Irahara N, Kure S, Toyoda S, et al. Aurora-A expression is independently associated with chromosomal instability in colorectal cancer. Neoplasia. 2009;11(5):418-25. Epub 2009/05/05.
49. Bischoff JR, Anderson L, Zhu Y, Mossie K, Ng L, Souza B, et al. A homologue of Drosophila aurora kinase is oncogenic and amplified in human colorectal cancers. The EMBO journal. 1998;17(11):3052-65. Epub 1998/06/26.
50. Cammareri P, Scopelliti A, Todaro M, Eterno V, Francescangeli F, Moyer MP, et al. Aurora-a is essential for the tumorigenic capacity and chemoresistance of colorectal cancer stem cells. Cancer research.70(11):4655-65. Epub 2010/05/13.
51. Lam AK, Ong K, Ho YH. Aurora kinase expression in colorectal adenocarcinoma: correlations with clinicopathological features, p16 expression, and telomerase activity. Human pathology. 2008;39(4):599-604. Epub 2008/02/21.
52. Casorzo L, Dell'Aglio C, Sarotto I, Risio M. Aurora kinase A gene copy number is associated with the malignant transformation of colorectal adenomas but not with the serrated neoplasia progression. Human pathology. 2015;46(3):411-8. Epub 2015/01/19.
53. Kurai M, Shiozawa T, Shih HC, Miyamoto T, Feng YZ, Kashima H, et al. Expression of Aurora kinases A and B in normal, hyperplastic, and malignant human endometrium: Aurora B as a predictor for poor prognosis in endometrial carcinoma. Human pathology. 2005;36(12):1281-8. Epub 2005/11/29.
54. Li P, Zhou Q, Ren L, Xiao L. Clinical implication of the expression of Aurora B in normal endometrium and endometrial carcinoma. J Huazhong Univ Sci Technolog Med Sci. 2008;28(3):337-9. Epub 2008/06/20.
55. Enjoji M, Iida S, Sugita H, Ishikawa T, Uetake H, Inokuchi M, et al. BubR1 and AURKB overexpression are associated with a favorable prognosis in gastric cancer. Mol Med Report. 2009;2(4):589-96. Epub 2009/07/01.
56. Fang Z, Xiong Y, Li J, Liu L, Li M, Zhang C, et al. Copy-number increase of AURKA in gastric cancers in a Chinese population: a correlation with tumor progression. Medical oncology. Epub 2010/06/30.
57. Ju H, Cho H, Kim YS, Kim WH, Ihm C, Noh SM, et al. Functional polymorphism 57Val>Ile of aurora kinase A associated with increased risk of gastric cancer progression. Cancer letters. 2006;242(2):273-9. Epub 2006/01/18.
58. Kamada K, Yamada Y, Hirao T, Fujimoto H, Takahama Y, Ueno M, et al. Amplification/overexpression of Aurora-A in human gastric carcinoma: potential role in differentiated type gastric carcinogenesis. Oncology reports. 2004;12(3):593-9. Epub 2004/08/04.
59. Sakakura C, Hagiwara A, Yasuoka R, Fujita Y, Nakanishi M, Masuda K, et al. Tumour-amplified kinase BTAK is amplified and overexpressed in gastric cancers with possible involvement in aneuploid formation. British journal of cancer. 2001;84(6):824-31. Epub 2001/03/22.
60. Han H, Von Hoff DD. Aurora sheds light on head and neck squamous cell carcinoma. Clinical cancer research : an official journal of the American Association for Cancer Research. 2006;12(17):5003-4. Epub 2006/09/05.
61. Reiter R, Gais P, Jutting U, Steuer-Vogt MK, Pickhard A, Bink K, et al. Aurora kinase A messenger RNA overexpression is correlated with tumor progression and shortened survival in head and neck squamous cell carcinoma. Clinical cancer research : an official journal of the American Association for Cancer Research. 2006;12(17):5136-41. Epub 2006/09/05.
62. Li FC, Li YH, Zhao X, Kang N, Fu WN, Xu ZM, et al. [Deletion of p15 and p16 genes and overexpression of STK15 gene in human laryngeal squamous cell carcinoma]. Zhonghua yi xue za zhi. 2003;83(4):316-9. Epub 2003/06/19.

63. Aihara A, Tanaka S, Yasen M, Matsumura S, Mitsunori Y, Murakata A, et al. The selective Aurora B kinase inhibitor AZD1152 as a novel treatment for hepatocellular carcinoma. Journal of hepatology. 2010;52(1):63-71. Epub 2009/11/17.
64. Jeng Y-M, Sr. Overexpression and amplification of Aurora-A in hepatocellular carcinoma. AACR Meeting Abstracts. 2004;2004(1):603-.
65. Lin Z-Z, Jeng Y-M, Hsu H-C, Cheng A-L. Validating Aurora B as a potential therapeutic target for human hepatocellular carcinoma. AACR Meeting Abstracts. 2007;2007(3_Molecular_Targets_Meeting):B216-.
66. Tanaka S, Aihara A, Yasen M, Mogushi K, Taira K, Kudo A, et al. Aurora kinase B is a novel target for treatment of hepatocellular carcinoma. AACR Meeting Abstracts. 2008;2008(1_Annual_Meeting):4467-.
67. Tanaka S, Arii S, Yasen M, Mogushi K, Su NT, Zhao C, et al. Aurora kinase B is a predictive factor for the aggressive recurrence of hepatocellular carcinoma after curative hepatectomy. The British journal of surgery. 2008;95(5):611-9. Epub 2008/03/04.
68. Gu J, Gong Y, Huang M, Lu C, Spitz MR, Wu X. Polymorphisms of STK15 (Aurora-A) gene and lung cancer risk in Caucasians. Carcinogenesis. 2007;28(2):350-5. Epub 2006/08/24.
69. Hayama S, Daigo Y, Yamabuki T, Hirata D, Kato T, Miyamoto M, et al. Phosphorylation and activation of cell division cycle associated 8 by aurora kinase B plays a significant role in human lung carcinogenesis. Cancer research. 2007;67(9):4113-22. Epub 2007/05/08.
70. Huang M, Gu J, Balmain A, Gong Y, Lu C, Wang Y, et al. STK15 polymorphisms and lung cancer risk. AACR Meeting Abstracts. 2005;2005(1):767-a-.
71. Ogawa E, Takenaka K, Katakura H, Adachi M, Otake Y, Toda Y, et al. Perimembrane Aurora-A expression is a significant prognostic factor in correlation with proliferative activity in non-small-cell lung cancer (NSCLC). Annals of surgical oncology. 2008;15(2):547-54. Epub 2007/11/29.
72. Vischioni B, Oudejans JJ, Vos W, Rodriguez JA, Giaccone G. Frequent overexpression of aurora B kinase, a novel drug target, in non-small cell lung carcinoma patients. Molecular cancer therapeutics. 2006;5(11):2905-13. Epub 2006/11/24.
73. Wang WR, Yang SS, Lin JX, Zeng ZY, Liu DM, Liu HT. [Expression of Aurora-B in non-small cell lung cancer and its clinical significance]. Nan fang yi ke da xue xue bao = Journal of Southern Medical University. 2009;29(9):1853-6. Epub 2009/09/26.
74. Zou LJ, Li GQ, Gong LL, Wang Y, Jin W, Zhao JY, et al. [Expression of aurora-A kinase in human lung cancer cell lines PG, A549, and NCI-H460]. Ai zheng = Aizheng = Chinese journal of cancer. 2005;24(7):792-5. Epub 2005/07/12.
75. Smith SL, Bowers NL, Betticher DC, Gautschi O, Ratschiller D, Hoban PR, et al. Overexpression of aurora B kinase (AURKB) in primary non-small cell lung carcinoma is frequent, generally driven from one allele, and correlates with the level of genetic instability. British journal of cancer. 2005;93(6):719-29. Epub 2005/10/14.
76. Xu HT, Ma L, Qi FJ, Liu Y, Yu JH, Dai SD, et al. Expression of serine threonine kinase 15 is associated with poor differentiation in lung squamous cell carcinoma and adenocarcinoma. Pathol Int. 2006;56(7):375-80. Epub 2006/06/24.
77. Berger W, Pirker C, Spiegel-Kreinecker S, Sutterluty H, Gsur A, Elbling L, et al. The mitotic kinase Aurora-A as a promising therapy target in human malignant melanoma. AACR Meeting Abstracts. 2006;2006(1):710-b-.
78. Agnese V, Cabibi D, Calcara D, Terrasi M, Pantuso G, Fiorentino E, et al. Aurora-A overexpression as an early marker of reflux-related columnar mucosa and

Barrett's oesophagus. Annals of oncology : official journal of the European Society for Medical Oncology / ESMO. 2007;18 Suppl 6:vi110-5. Epub 2007/09/27.
79. Rugge M, Fassan M, Zaninotto G, Pizzi M, Giacomelli L, Battaglia G, et al. Aurora kinase A in Barrett's carcinogenesis. Human pathology. 2010;41(10):1380-6. Epub 2010/07/27.
80. Tong T, Zhong Y, Kong J, Dong L, Song Y, Fu M, et al. Overexpression of Aurora-A contributes to malignant development of human esophageal squamous cell carcinoma. Clinical cancer research : an official journal of the American Association for Cancer Research. 2004;10(21):7304-10. Epub 2004/11/10.
81. Yang SB, Zhou XB, Zhu HX, Quan LP, Bai JF, He J, et al. Amplification and overexpression of Aurora-A in esophageal squamous cell carcinoma. Oncology reports. 2007;17(5):1083-8. Epub 2007/03/29.
82. Kimura MT, Mori T, Conroy J, Nowak NJ, Satomi S, Tamai K, et al. Two functional coding single nucleotide polymorphisms in STK15 (Aurora-A) coordinately increase esophageal cancer risk. Cancer research. 2005;65(9):3548-54. Epub 2005/05/04.
83. Tamotsu K, Okumura H, Uchikado Y, Kita Y, Sasaki K, Omoto I, et al. Correlation of Aurora-A expression with the effect of chemoradiation therapy on esophageal squamous cell carcinoma. BMC cancer. 2015;15:323. Epub 2015/05/01.
84. Chen YJ, Chen CM, Twu NF, Yen MS, Lai CR, Wu HH, et al. Overexpression of Aurora B is associated with poor prognosis in epithelial ovarian cancer patients. Virchows Archiv : an international journal of pathology. 2009;455(5):431-40. Epub 2009/10/20.
85. Chung CM, Man C, Jin Y, Jin C, Guan XY, Wang Q, et al. Amplification and overexpression of aurora kinase A (AURKA) in immortalized human ovarian epithelial (HOSE) cells. Molecular carcinogenesis. 2005;43(3):165-74. Epub 2005/05/10.
86. Gritsko TM, Coppola D, Paciga JE, Yang L, Sun M, Shelley SA, et al. Activation and overexpression of centrosome kinase BTAK/Aurora-A in human ovarian cancer. Clinical cancer research : an official journal of the American Association for Cancer Research. 2003;9(4):1420-6. Epub 2003/04/10.
87. Lassmann S, Shen Y, Jutting U, Whiele P, Walch A, Gitsch G, et al. [Aurora-a is a predictive marker for stage III epithelial ovarian cancers]. Verh Dtsch Ges Pathol. 2007;91:225-32. Epub 2008/03/05. Aurora-a ist ein pradiktiver Marker fur Ovarialkarzinome des Stadiums III.
88. Landen CN, Immaneni A, Deavers MT, Thornton A, Celestino J, Thanker PH, et al. Overexpression of the centrosomal protein aurora-A kinase is associated with poor prognosis in epithelial ovarian cancer patients. ASCO Meeting Abstracts. 2005;23(16_suppl):5039.
89. Lassus H, Staff S, Leminen A, Isola J, Butzow R. Aurora-A overexpression and aneuploidy predict poor outcome in serous ovarian carcinoma. Gynecologic oncology. 2011;120(1):11-7. Epub 2010/10/13.
90. Zheng L, Song A, Ruan Y, Chen L, Liu D, Li X, et al. Genetic polymorphisms in AURKA, BRCA1, CCNE1 and CDK2 are associated with ovarian cancer susceptibility among Chinese Han women. Cancer epidemiology. 2013;37(5):639-46. Epub 2013/06/22.
91. Rojanala S, Han H, Munoz RM, Browne W, Nagle R, Von Hoff DD, et al. The mitotic serine threonine kinase, Aurora-2, is a potential target for drug development in human pancreatic cancer. Molecular cancer therapeutics. 2004;3(4):451-7. Epub 2004/04/14.
92. Li D, Zhu J, Firozi PF, Abbruzzese JL, Evans DB, Cleary K, et al. Overexpression of oncogenic STK15/BTAK/Aurora A kinase in human pancreatic

cancer. Clinical cancer research : an official journal of the American Association for Cancer Research. 2003;9(3):991-7. Epub 2003/03/13.
93. Chieffi P, Cozzolino L, Kisslinger A, Libertini S, Staibano S, Mansueto G, et al. Aurora B expression directly correlates with prostate cancer malignancy and influence prostate cell proliferation. Prostate. 2006;66(3):326-33. Epub 2005/11/04.
94. Buschhorn HM, Klein RR, Chambers SM, Hardy MC, Green S, Bearss D, et al. Aurora-A over-expression in high-grade PIN lesions and prostate cancer. Prostate. 2005;64(4):341-6. Epub 2005/03/09.
95. Furukawa J, Miyake H, Takenaka A, Hara I, Fujisawa M. Persistent expression of Aurora-A after neoadjuvant hormonal therapy as a predictor of a poor clinical outcome in patients undergoing radical prostatectomy for prostate cancer. BJU international. 2007;100(2):310-4. Epub 2007/05/22.
96. Ehara H, Yokoi S, Tamaki M, Nishino Y, Takahashi Y, Deguchi T, et al. Expression of mitotic Aurora/Ipl1p-related kinases in renal cell carcinomas: an immunohistochemical study. Urol Res. 2003;31(6):382-6. Epub 2003/09/19.
97. Kurahashi T, Miyake H, Hara I, Fujisawa M. Significance of Aurora-A expression in renal cell carcinoma. Urologic oncology. 2007;25(2):128-33. Epub 2007/03/14.
98. Xu J, Li H, Wang B, Xu Y, Yang J, Zhang X, et al. VHL inactivation induces HEF1 and Aurora kinase A. Journal of the American Society of Nephrology : JASN. 2010;21(12):2041-6. Epub 2010/09/25.
99. Sorrentino R, Libertini S, Pallante PL, Troncone G, Palombini L, Bavetsias V, et al. Aurora B overexpression associates with the thyroid carcinoma undifferentiated phenotype and is required for thyroid carcinoma cell proliferation. J Clin Endocrinol Metab. 2005;90(2):928-35. Epub 2004/11/25.
100. Ulisse S, Delcros JG, Baldini E, Toller M, Curcio F, Giacomelli L, et al. Expression of Aurora kinases in human thyroid carcinoma cell lines and tissues. International journal of cancer Journal international du cancer. 2006;119(2):275-82. Epub 2006/02/16.
101. Humme D, Haider A, Mobs M, Mitsui H, Suarez-Farinas M, Ohmatsu H, et al. Aurora Kinase A Is Upregulated in Cutaneous T-Cell Lymphoma and Represents a Potential Therapeutic Target. The Journal of investigative dermatology. 2015;135(9):2292-300. Epub 2015/04/08.
102. Kanagal-Shamanna R, Lehman NL, O'Donnell JP, Lim MS, Schultz DS, Chitale DA, et al. Differential expression of aurora-A kinase in T-cell lymphomas. Modern pathology : an official journal of the United States and Canadian Academy of Pathology, Inc. 2013;26(5):640-7. Epub 2013/02/16.
103. UK CR. Bladder Cancer Statistics. 2014 [cited 2017 11 June]; Available from: http://www.cancerresearchuk.org/health-professional/cancer-statistics/statistics-by-cancer-type/bladder-cancer#heading-Zero.
104. Cote RJ, Datar RH. Therapeutic approaches to bladder cancer: identifying targets and mechanisms. Critical reviews in oncology/hematology. 2003;46 Suppl:S67-83. Epub 2003/07/10.
105. Spruck CH, 3rd, Ohneseit PF, Gonzalez-Zulueta M, Esrig D, Miyao N, Tsai YC, et al. Two molecular pathways to transitional cell carcinoma of the bladder. Cancer research. 1994;54(3):784-8. Epub 1994/02/01.
106. Florl AR, Schulz WA. Chromosomal instability in bladder cancer. Archives of toxicology. 2008;82(3):173-82. Epub 2008/02/07.
107. Cancer Genome Atlas Research N. Comprehensive molecular characterization of urothelial bladder carcinoma. Nature. 2014;507(7492):315-22. Epub 2014/01/31.

108. von der Maase H, Hansen SW, Roberts JT, Dogliotti L, Oliver T, Moore MJ, et al. Gemcitabine and cisplatin versus methotrexate, vinblastine, doxorubicin, and cisplatin in advanced or metastatic bladder cancer: results of a large, randomized, multinational, multicenter, phase III study. Journal of clinical oncology : official journal of the American Society of Clinical Oncology. 2000;18(17):3068-77. Epub 2000/09/23.
109. Sonpavde G, Sternberg CN, Rosenberg JE, Hahn NM, Galsky MD, Vogelzang NJ. Second-line systemic therapy and emerging drugs for metastatic transitional-cell carcinoma of the urothelium. The Lancet Oncology. 2010;11(9):861-70. Epub 2010/06/12.
110. Bellmunt J, Powles T, Vogelzang NJ. A review on the evolution of PD-1/PD-L1 immunotherapy for bladder cancer: The future is now. Cancer treatment reviews. 2017;54:58-67. Epub 2017/02/20.
111. Strefford JC, Lillington DM, Steggall M, Lane TM, Nouri AM, Young BD, et al. Novel chromosome findings in bladder cancer cell lines detected with multiplex fluorescence in situ hybridization. Cancer Genet Cytogenet. 2002;135(2):139-46. Epub 2002/07/20.
112. Richter J, Beffa L, Wagner U, Schraml P, Gasser TC, Moch H, et al. Patterns of chromosomal imbalances in advanced urinary bladder cancer detected by comparative genomic hybridization. The American journal of pathology. 1998;153(5):1615-21. Epub 1998/11/12.
113. Veerakumarasivam A, Goldstein LD, Saeb-Parsy K, Scott HE, Warren A, Thorne NP, et al. AURKA overexpression accompanies dysregulation of DNA-damage response genes in invasive urothelial cell carcinoma. Cell cycle. 2008;7(22):3525-33. Epub 2008/11/13.
114. Park HS, Park WS, Bondaruk J, Tanaka N, Katayama H, Lee S, et al. Quantitation of Aurora kinase A gene copy number in urine sediments and bladder cancer detection. Journal of the National Cancer Institute. 2008;100(19):1401-11. Epub 2008/09/25.
115. Veerakumarasivam A, Scott HE, Chin SF, Warren A, Wallard MJ, Grimmer D, et al. High-resolution array-based comparative genomic hybridization of bladder cancers identifies mouse double minute 4 (MDM4) as an amplification target exclusive of MDM2 and TP53. Clinical cancer research : an official journal of the American Association for Cancer Research. 2008;14(9):2527-34. Epub 2008/05/03.
116. Katayama H, Sasai K, Kawai H, Yuan ZM, Bondaruk J, Suzuki F, et al. Phosphorylation by aurora kinase A induces Mdm2-mediated destabilization and inhibition of p53. Nature genetics. 2004;36(1):55-62. Epub 2004/01/01.
117. Mhawech-Fauceglia P, Fischer G, Beck A, Cheney RT, Herrmann FR. Raf1, Aurora-A/STK15 and E-cadherin biomarkers expression in patients with pTa/pT1 urothelial bladder carcinoma; a retrospective TMA study of 246 patients with long-term follow-up. European journal of surgical oncology : the journal of the European Society of Surgical Oncology and the British Association of Surgical Oncology. 2006;32(4):439-44. Epub 2006/03/07.
118. Lei Y, Yan S, Ming-De L, Na L, Rui-Fa H. Prognostic significance of Aurora-A expression in human bladder cancer. Acta Histochem. Epub 2010/07/06.
119. Akao J, Matsuyama H, Yamamoto Y, Sasaki K, Naito K. Chromosome 20q13.2 gain may predict intravesical recurrence after nephroureterectomy in upper urinary tract urothelial tumors. Clinical cancer research : an official journal of the American Association for Cancer Research. 2006;12(23):7004-8. Epub 2006/12/06.
120. Santarius T, Shipley J, Brewer D, Stratton MR, Cooper CS. A census of amplified and overexpressed human cancer genes. Nature reviews Cancer. 2010;10(1):59-64. Epub 2009/12/24.

121. Zhou N, Singh K, Mir MC, Parker Y, Lindner D, Dreicer R, et al. The investigational Aurora kinase A inhibitor MLN8237 induces defects in cell viability and cell-cycle progression in malignant bladder cancer cells in vitro and in vivo. Clinical cancer research : an official journal of the American Association for Cancer Research. 2013;19(7):1717-28. Epub 2013/02/14.
122. Mobley A, Zhang S, Bondaruk J, Wang Y, Majewski T, Caraway NP, et al. Aurora Kinase A is a Biomarker for Bladder Cancer Detection and Contributes to its Aggressive Behavior. Scientific reports. 2017;7:40714. Epub 2017/01/20.
123. Zhou H, Kuang J, Zhong L, Kuo WL, Gray JW, Sahin A, et al. Tumour amplified kinase STK15/BTAK induces centrosome amplification, aneuploidy and transformation. Nature genetics. 1998;20(2):189-93. Epub 1998/10/15.
124. Zhang D, Hirota T, Marumoto T, Shimizu M, Kunitoku N, Sasayama T, et al. Cre-loxP-controlled periodic Aurora-A overexpression induces mitotic abnormalities and hyperplasia in mammary glands of mouse models. Oncogene. 2004;23(54):8720-30. Epub 2004/10/14.
125. Liu Q, Kaneko S, Yang L, Feldman RI, Nicosia SV, Chen J, et al. Aurora-A abrogation of p53 DNA binding and transactivation activity by phosphorylation of serine 215. The Journal of biological chemistry. 2004;279(50):52175-82. Epub 2004/10/08.
126. Hsueh KW, Fu SL, Chang CB, Chang YL, Lin CH. A novel Aurora-A-mediated phosphorylation of p53 inhibits its interaction with MDM2. Biochimica et biophysica acta. 2013;1834(2):508-15. Epub 2012/12/04.
127. Wu CC, Yang TY, Yu CT, Phan L, Ivan C, Sood AK, et al. p53 negatively regulates Aurora A via both transcriptional and posttranslational regulation. Cell cycle. 2012;11(18):3433-42. Epub 2012/08/17.
128. Chen SS, Chang PC, Cheng YW, Tang FM, Lin YS. Suppression of the STK15 oncogenic activity requires a transactivation-independent p53 function. The EMBO journal. 2002;21(17):4491-9. Epub 2002/08/29.
129. Katayama H, Wang J, Treekitkarnmongkol W, Kawai H, Sasai K, Zhang H, et al. Aurora kinase-A inactivates DNA damage-induced apoptosis and spindle assembly checkpoint response functions of p73. Cancer cell. 2012;21(2):196-211. Epub 2012/02/22.
130. Cheok CF, Kua N, Kaldis P, Lane DP. Combination of nutlin-3 and VX-680 selectively targets p53 mutant cells with reversible effects on cells expressing wild-type p53. Cell death and differentiation. 2010;17(9):1486-500. Epub 2010/03/06.
131. Dar AA, Belkhiri A, Ecsedy J, Zaika A, El-Rifai W. Aurora kinase A inhibition leads to p73-dependent apoptosis in p53-deficient cancer cells. Cancer research. 2008;68(21):8998-9004. Epub 2008/11/01.
132. Diamond JR, Eckhardt SG, Tan AC, Newton TP, Selby HM, Brunkow KL, et al. Predictive biomarkers of sensitivity to the aurora and angiogenic kinase inhibitor ENMD-2076 in preclinical breast cancer models. Clinical cancer research : an official journal of the American Association for Cancer Research. 2013;19(1):291-303. Epub 2012/11/09.
133. Ouchi M, Fujiuchi N, Sasai K, Katayama H, Minamishima YA, Ongusaha PP, et al. BRCA1 phosphorylation by Aurora-A in the regulation of G2 to M transition. The Journal of biological chemistry. 2004;279(19):19643-8. Epub 2004/03/03.
134. Yang G, Chang B, Yang F, Guo X, Cai KQ, Xiao XS, et al. Aurora kinase A promotes ovarian tumorigenesis through dysregulation of the cell cycle and suppression of BRCA2. Clinical cancer research : an official journal of the American Association for Cancer Research. 2010;16(12):3171-81. Epub 2010/04/29.

135. Tatsuka M, Sato S, Kitajima S, Suto S, Kawai H, Miyauchi M, et al. Overexpression of Aurora-A potentiates HRAS-mediated oncogenic transformation and is implicated in oral carcinogenesis. Oncogene. 2005;24(6):1122-7. Epub 2004/12/14.
136. Hadj-Slimane R, Pamonsinlapatham P, Herbeuval JP, Garbay C, Lepelletier Y, Raynaud F. RasV12 induces Survivin/AuroraB pathway conferring tumor cell apoptosis resistance. Cellular signalling.22(8):1214-21. Epub 2010/04/07.
137. Wu JC, Chen TY, Yu CT, Tsai SJ, Hsu JM, Tang MJ, et al. Identification of V23RalA-Ser194 as a critical mediator for Aurora-A-induced cellular motility and transformation by small pool expression screening. The Journal of biological chemistry. 2005;280(10):9013-22. Epub 2005/01/08.
138. Bee C, Moshnikova A, Mellor CD, Molloy JE, Koryakina Y, Stieglitz B, et al. Growth and tumor suppressor NORE1A is a regulatory node between Ras signaling and microtubule nucleation. The Journal of biological chemistry.285(21):16258-66. Epub 2010/03/27.
139. den Hollander J, Rimpi S, Doherty JR, Rudelius M, Buck A, Hoellein A, et al. Aurora kinases A and B are up-regulated by Myc and are essential for maintenance of the malignant state. Blood.116(9):1498-505. Epub 2010/06/04.
140. Yang S, He S, Zhou X, Liu M, Zhu H, Wang Y, et al. Suppression of Aurora-A Oncogenic Potential by c-Myc Downregulation. Experimental & molecular medicine. Epub 2010/10/05.
141. Nikonova AS, Astsaturov I, Serebriiskii IG, Dunbrack RL, Jr., Golemis EA. Aurora A kinase (AURKA) in normal and pathological cell division. Cellular and molecular life sciences : CMLS. 2013;70(4):661-87. Epub 2012/08/07.
142. Gascoigne KE, Taylor SS. Cancer cells display profound intra- and interline variation following prolonged exposure to antimitotic drugs. Cancer cell. 2008;14(2):111-22. Epub 2008/07/29.
143. Brito DA, Rieder CL. Mitotic checkpoint slippage in humans occurs via cyclin B destruction in the presence of an active checkpoint. Current biology : CB. 2006;16(12):1194-200. Epub 2006/06/20.
144. Topham CH, Taylor SS. Mitosis and apoptosis: how is the balance set? Current opinion in cell biology. 2013;25(6):780-5. Epub 2013/07/31.
145. Eichhorn JM, Sakurikar N, Alford SE, Chu R, Chambers TC. Critical role of anti-apoptotic Bcl-2 protein phosphorylation in mitotic death. Cell death & disease. 2013;4:e834. Epub 2013/10/05.
146. Sloss O, Topham C, Diez M, Taylor S. Mcl-1 dynamics influence mitotic slippage and death in mitosis. Oncotarget. 2016;7(5):5176-92. Epub 2016/01/16.
147. Topham C, Tighe A, Ly P, Bennett A, Sloss O, Nelson L, et al. MYC Is a Major Determinant of Mitotic Cell Fate. Cancer cell. 2015;28(1):129-40. Epub 2015/07/16.
148. Bennett A, Sloss O, Topham C, Nelson L, Tighe A, Taylor SS. Inhibition of Bcl-xL sensitizes cells to mitotic blockers, but not mitotic drivers. Open biology. 2016;6(8). Epub 2016/08/12.
149. Rowinsky EK, Chaudhry V, Cornblath DR, Donehower RC. Neurotoxicity of Taxol. Journal of the National Cancer Institute Monographs. 1993(15):107-15. Epub 1993/01/01.
150. Girdler F, Gascoigne KE, Eyers PA, Hartmuth S, Crafter C, Foote KM, et al. Validating Aurora B as an anti-cancer drug target. Journal of cell science. 2006;119(Pt 17):3664-75. Epub 2006/08/17.
151. Hauf S, Cole RW, LaTerra S, Zimmer C, Schnapp G, Walter R, et al. The small molecule Hesperadin reveals a role for Aurora B in correcting kinetochore-microtubule attachment and in maintaining the spindle assembly checkpoint. The Journal of cell biology. 2003;161(2):281-94. Epub 2003/04/23.

152. Yang H, Burke T, Dempsey J, Diaz B, Collins E, Toth J, et al. Mitotic requirement for aurora A kinase is bypassed in the absence of aurora B kinase. FEBS letters. 2005;579(16):3385-91. Epub 2005/06/01.
153. Hilton JF, Shapiro GI. Aurora kinase inhibition as an anticancer strategy. Journal of clinical oncology : official journal of the American Society of Clinical Oncology. 2014;32(1):57-9. Epub 2013/09/18.
154. Meraldi P, Honda R, Nigg EA. Aurora-A overexpression reveals tetraploidization as a major route to centrosome amplification in p53-/- cells. The EMBO journal. 2002;21(4):483-92. Epub 2002/02/16.
155. Blagosklonny MV, Darzynkiewicz Z. Cyclotherapy: protection of normal cells and unshielding of cancer cells. Cell cycle. 2002;1(6):375-82. Epub 2003/01/28.
156. Brown CJ, Cheok CF, Verma CS, Lane DP. Reactivation of p53: from peptides to small molecules. Trends in pharmacological sciences.32(1):53-62. Epub 2010/12/15.
157. Girdler F, Sessa F, Patercoli S, Villa F, Musacchio A, Taylor S. Molecular basis of drug resistance in aurora kinases. Chemistry & biology. 2008;15(6):552-62. Epub 2008/06/19.
158. Cochran AG. Aurora A: target invalidated? Chemistry & biology. 2008;15(6):525-6. Epub 2008/06/19.
159. Warner SL, Munoz RM, Stafford P, Koller E, Hurley LH, Von Hoff DD, et al. Comparing Aurora A and Aurora B as molecular targets for growth inhibition of pancreatic cancer cells. Molecular cancer therapeutics. 2006;5(10):2450-8. Epub 2006/10/17.
160. Pollard JR, Mortimore M. Discovery and development of aurora kinase inhibitors as anticancer agents. Journal of medicinal chemistry. 2009;52(9):2629-51. Epub 2009/03/27.
161. Boss DS, Beijnen JH, Schellens JH. Clinical experience with aurora kinase inhibitors: a review. The oncologist. 2009;14(8):780-93. Epub 2009/08/18.
162. Kollareddy M, Zheleva D, Dzubak P, Brahmkshatriya PS, Lepsik M, Hajduch M. Aurora kinase inhibitors: progress towards the clinic. Investigational new drugs. 2012;30(6):2411-32. Epub 2012/02/22.
163. Marugan C, Torres R, Lallena MJ. Phenotypic Screening Approaches to Develop Aurora Kinase Inhibitors: Drug Discovery Perspectives. Frontiers in oncology. 2015;5:299. Epub 2016/01/19.
164. Liu G, Abraham S, Tran L, Vickers TD, Xu S, Hadd MJ, et al. Discovery of highly potent and selective pan-Aurora kinase inhibitors with enhanced in vivo antitumor therapeutic index. Journal of medicinal chemistry. 2012;55(7):3250-60. Epub 2012/03/03.
165. Carry JC, Clerc F, Minoux H, Schio L, Mauger J, Nair A, et al. SAR156497, an exquisitely selective inhibitor of aurora kinases. Journal of medicinal chemistry. 2015;58(1):362-75. Epub 2014/11/05.
166. Bouloc N, Large JM, Kosmopoulou M, Sun C, Faisal A, Matteucci M, et al. Structure-based design of imidazo[1,2-a]pyrazine derivatives as selective inhibitors of Aurora-A kinase in cells. Bioorganic & medicinal chemistry letters. 2010;20(20):5988-93. Epub 2010/09/14.
167. Kilchmann F, Marcaida MJ, Kotak S, Schick T, Boss SD, Awale M, et al. Discovery of a Selective Aurora A Kinase Inhibitor by Virtual Screening. Journal of medicinal chemistry. 2016;59(15):7188-211. Epub 2016/07/09.
168. Xie H, Lee MH, Zhu F, Reddy K, Peng C, Li Y, et al. Identification of an Aurora kinase inhibitor specific for the Aurora B isoform. Cancer research. 2013;73(2):716-24. Epub 2012/11/03.

169. Le Brazidec JY, Pasis A, Tam B, Boykin C, Black C, Wang D, et al. Synthesis, SAR and biological evaluation of 1,6-disubstituted-1H-pyrazolo[3,4-d]pyrimidines as dual inhibitors of Aurora kinases and CDK1. Bioorganic & medicinal chemistry letters. 2012;22(5):2070-4. Epub 2012/02/14.
170. Arai R, Tsuda M, Watanabe T, Ose T, Obuse C, Maenaka K, et al. Simultaneous inhibition of Src and Aurora kinases by SU6656 induces therapeutic synergy in human synovial sarcoma growth, invasion and angiogenesis in vivo. European journal of cancer. 2012;48(15):2417-30. Epub 2012/01/17.
171. Dar AA, Goff LW, Majid S, Berlin J, El-Rifai W. Aurora kinase inhibitors--rising stars in cancer therapeutics? Molecular cancer therapeutics. 2010;9(2):268-78. Epub 2010/02/04.
172. Babb JS, & Rogatko, A. Bayesian Methods for Phase I Cancer Clinical Trials. In: Gellar NL, editor. Advances in Clinical Trial Biostatistics: CRC Press; 2003.
173. Choudary I, Barr PM, Friedberg J. Recent advances in the development of Aurora kinases inhibitors in hematological malignancies. Therapeutic advances in hematology. 2015;6(6):282-94. Epub 2015/12/02.
174. Hay AE, Murugesan A, DiPasquale AM, Kouroukis T, Sandhu I, Kukreti V, et al. A phase II study of AT9283, an aurora kinase inhibitor, in patients with relapsed or refractory multiple myeloma: NCIC clinical trials group IND.191. Leukemia & lymphoma. 2016;57(6):1463-6.
175. Kantarjian HM, Schuster MW, Jain N, Advani A, Jabbour E, Gamelin E, et al. A phase 1 study of AMG 900, an orally administered pan-aurora kinase inhibitor, in adult patients with acute myeloid leukemia. American journal of hematology. 2017;92(7):660-7.
176. O'Connor O, Leonard EJ, Benaim E. Phase III study of investigational MLN8237 (alisertib) versus investigator's choice in patients (pts) with relapsed/refractory (rel/ref) peripheral T-cell lymphoma (PTCL). Journal of Clinical Oncology. 2012;30(15_suppl):TPS8110-TPS.
177. Pharmaceuticals T. Takeda announces termination of alisertib Phase 3 trial in relapsed or refractory peripheral T cell lymphoma. 2015 [cited 2017]; Available from: https://www.takeda.com/newsroom/newsreleases/2015/takeda-announces-termination-of-alisertib-phase-3-trial-in-relapsed-or-refractory-peripheral-t-cell-lymphoma/.
178. Necchi A, Lo Vullo S, Mariani L, Raggi D, Giannatempo P, Calareso G, et al. An open-label, single-arm, phase 2 study of the Aurora kinase A inhibitor alisertib in patients with advanced urothelial cancer. Investigational new drugs. 2016;34(2):236-42. Epub 2016/02/14.
179. Fletcher GC, Brokx RD, Denny TA, Hembrough TA, Plum SM, Fogler WE, et al. ENMD-2076 is an orally active kinase inhibitor with antiangiogenic and antiproliferative mechanisms of action. Molecular cancer therapeutics. 2011;10(1):126-37. Epub 2010/12/24.
180. Carducci MA, Shaheen MF, Paller CJ, Bauman JE, Azad NS, Shubhakar P, et al. First-in-human study of AMG 900, an oral pan-Aurora kinase inhibitor, in adult patients (pts) with advanced solid tumors. Journal of Clinical Oncology. 2012;30(15_suppl):3009-.
181. Shaheen M, Markman B, Carducci M, Hurvitz S, Mahadevan D, Kotasek D, et al. Abstract CT045: Phase 1, open-label, first-in-human study of AMG 900, an orally administered pan-aurora kinase inhibitor, in adult patients (pts) with advanced solid tumors. Cancer research. 2016;76(14 Supplement):CT045-CT.
182. Payton M, Bush TL, Chung G, Ziegler B, Eden P, McElroy P, et al. Preclinical evaluation of AMG 900, a novel potent and highly selective pan-aurora kinase inhibitor

with activity in taxane-resistant tumor cell lines. Cancer research. 2010;70(23):9846-54. Epub 2010/10/12.
183. Arkenau HT, Plummer R, Molife LR, Olmos D, Yap TA, Squires M, et al. A phase I dose escalation study of AT9283, a small molecule inhibitor of aurora kinases, in patients with advanced solid malignancies. Annals of oncology : official journal of the European Society for Medical Oncology / ESMO. 2012;23(5):1307-13. Epub 2011/10/22.
184. Howard S, Berdini V, Boulstridge JA, Carr MG, Cross DM, Curry J, et al. Fragment-based discovery of the pyrazol-4-yl urea (AT9283), a multitargeted kinase inhibitor with potent aurora kinase activity. Journal of medicinal chemistry. 2009;52(2):379-88. Epub 2009/01/16.
185. Dent SF, Gelmon KA, Chi KN, Jonker DJ, Wainman N, Capier CA, et al. NCIC CTG IND.181: phase I study of AT9283 given as a weekly 24 hour infusion in advanced malignancies. Investigational new drugs. 2013;31(6):1522-9. Epub 2013/09/28.
186. Steeghs N, Eskens FA, Gelderblom H, Verweij J, Nortier JW, Ouwerkerk J, et al. Phase I pharmacokinetic and pharmacodynamic study of the aurora kinase inhibitor danusertib in patients with advanced or metastatic solid tumors. Journal of clinical oncology : official journal of the American Society of Clinical Oncology. 2009;27(30):5094-101. Epub 2009/09/23.
187. Carpinelli P, Ceruti R, Giorgini ML, Cappella P, Gianellini L, Croci V, et al. PHA-739358, a potent inhibitor of Aurora kinases with a selective target inhibition profile relevant to cancer. Molecular cancer therapeutics. 2007;6(12 Pt 1):3158-68. Epub 2007/12/20.
188. Cohen RB, Jones SF, Aggarwal C, von Mehren M, Cheng J, Spigel DR, et al. A phase I dose-escalation study of danusertib (PHA-739358) administered as a 24-hour infusion with and without granulocyte colony-stimulating factor in a 14-day cycle in patients with advanced solid tumors. Clinical cancer research : an official journal of the American Association for Cancer Research. 2009;15(21):6694-701. Epub 2009/10/15.
189. Schoffski P, Besse B, Gauler T, de Jonge MJ, Scambia G, Santoro A, et al. Efficacy and safety of biweekly i.v. administrations of the Aurora kinase inhibitor danusertib hydrochloride in independent cohorts of patients with advanced or metastatic breast, ovarian, colorectal, pancreatic, small-cell and non-small-cell lung cancer: a multi-tumour, multi-institutional phase II study. Annals of oncology : official journal of the European Society for Medical Oncology / ESMO. 2015;26(3):598-607. Epub 2014/12/10.
190. Meulenbeld HJ, Bleuse JP, Vinci EM, Raymond E, Vitali G, Santoro A, et al. Randomized phase II study of danusertib in patients with metastatic castration-resistant prostate cancer after docetaxel failure. BJU international. 2013;111(1):44-52. Epub 2012/08/30.
191. Mita M, Gordon M, Rejeb N, Gianella-Borradori A, Jego V, Mita A, et al. A phase l study of three different dosing schedules of the oral aurora kinase inhibitor MSC1992371A in patients with solid tumors. Targeted oncology. 2014;9(3):215-24. Epub 2013/07/09.
192. McLaughlin J, Markovtsov V, Li H, Wong S, Gelman M, Zhu Y, et al. Preclinical characterization of Aurora kinase inhibitor R763/AS703569 identified through an image-based phenotypic screen. Journal of cancer research and clinical oncology. 2010;136(1):99-113. Epub 2009/07/18.
193. Schoffski P, Jones SF, Dumez H, Infante JR, Van Mieghem E, Fowst C, et al. Phase I, open-label, multicentre, dose-escalation, pharmacokinetic and

pharmacodynamic trial of the oral aurora kinase inhibitor PF-03814735 in advanced solid tumours. European journal of cancer. 2011;47(15):2256-64. Epub 2011/08/20.
194. Jani JP, Arcari J, Bernardo V, Bhattacharya SK, Briere D, Cohen BD, et al. PF-03814735, an orally bioavailable small molecule aurora kinase inhibitor for cancer therapy. Molecular cancer therapeutics. 2010;9(4):883-94. Epub 2010/04/01.
195. Robert F, Verschraegen C, Hurwitz H, Uronis H, Advani R, Chen A, et al. A phase I trial of sns-314, a novel and selective pan-aurora kinase inhibitor, in advanced solid tumor patients. ASCO Meeting Abstracts. 2009;27(15S):2536.
196. VanderPorten EC, Taverna P, Hogan JN, Ballinger MD, Flanagan WM, Fucini RV. The Aurora kinase inhibitor SNS-314 shows broad therapeutic potential with chemotherapeutics and synergy with microtubule-targeted agents in a colon carcinoma model. Molecular cancer therapeutics. 2009;8(4):930-9. Epub 2009/04/18.
197. Traynor AM, Hewitt M, Liu G, Flaherty KT, Clark J, Freedman SJ, et al. Phase I dose escalation study of MK-0457, a novel Aurora kinase inhibitor, in adult patients with advanced solid tumors. Cancer chemotherapy and pharmacology. 2011;67(2):305-14. Epub 2010/04/14.
198. Cheetham GM, Charlton PA, Golec JM, Pollard JR. Structural basis for potent inhibition of the Aurora kinases and a T315I multi-drug resistant mutant form of Abl kinase by VX-680. Cancer letters. 2007;251(2):323-9. Epub 2007/01/24.
199. Diamond JR, Bastos BR, Hansen RJ, Gustafson DL, Eckhardt SG, Kwak EL, et al. Phase I safety, pharmacokinetic, and pharmacodynamic study of ENMD-2076, a novel angiogenic and Aurora kinase inhibitor, in patients with advanced solid tumors. Clinical cancer research : an official journal of the American Association for Cancer Research. 2011;17(4):849-60. Epub 2010/12/07.
200. Matulonis UA, Lee J, Lasonde B, Tew WP, Yehwalashet A, Matei D, et al. ENMD-2076, an oral inhibitor of angiogenic and proliferation kinases, has activity in recurrent, platinum resistant ovarian cancer. European journal of cancer. 2013;49(1):121-31. Epub 2012/08/28.
201. Dees EC, Infante JR, Cohen RB, O'Neil BH, Jones S, von Mehren M, et al. Phase 1 study of MLN8054, a selective inhibitor of Aurora A kinase in patients with advanced solid tumors. Cancer chemotherapy and pharmacology. 2011;67(4):945-54. Epub 2010/07/08.
202. Huck JJ, Zhang M, McDonald A, Bowman D, Hoar KM, Stringer B, et al. MLN8054, an inhibitor of Aurora A kinase, induces senescence in human tumor cells both in vitro and in vivo. Molecular cancer research : MCR. 2010;8(3):373-84. Epub 2010/03/04.
203. Macarulla T, Cervantes A, Elez E, Rodriguez-Braun E, Baselga J, Rosello S, et al. Phase I study of the selective Aurora A kinase inhibitor MLN8054 in patients with advanced solid tumors: safety, pharmacokinetics, and pharmacodynamics. Molecular cancer therapeutics. 2010;9(10):2844-52. Epub 2010/08/21.
204. Dees EC, Cohen RB, von Mehren M, Stinchcombe TE, Liu H, Venkatakrishnan K, et al. Phase I study of aurora A kinase inhibitor MLN8237 in advanced solid tumors: safety, pharmacokinetics, pharmacodynamics, and bioavailability of two oral formulations. Clinical cancer research : an official journal of the American Association for Cancer Research. 2012;18(17):4775-84. Epub 2012/07/07.
205. Manfredi MG, Ecsedy JA, Chakravarty A, Silverman L, Zhang M, Hoar KM, et al. Characterization of Alisertib (MLN8237), an investigational small-molecule inhibitor of aurora A kinase using novel in vivo pharmacodynamic assays. Clinical cancer research : an official journal of the American Association for Cancer Research. 2011;17(24):7614-24. Epub 2011/10/22.

206. Cervantes A, Elez E, Roda D, Ecsedy J, Macarulla T, Venkatakrishnan K, et al. Phase I pharmacokinetic/pharmacodynamic study of MLN8237, an investigational, oral, selective aurora a kinase inhibitor, in patients with advanced solid tumors. Clinical cancer research : an official journal of the American Association for Cancer Research. 2012;18(17):4764-74. Epub 2012/07/04.
207. Kelly KR, Shea TC, Goy A, Berdeja JG, Reeder CB, McDonagh KT, et al. Phase I study of MLN8237--investigational Aurora A kinase inhibitor--in relapsed/refractory multiple myeloma, non-Hodgkin lymphoma and chronic lymphocytic leukemia. Investigational new drugs. 2014;32(3):489-99. Epub 2013/12/20.
208. Falchook G, Kurzrock R, Gouw L, Hong D, McGregor KA, Zhou X, et al. Investigational Aurora A kinase inhibitor alisertib (MLN8237) as an enteric-coated tablet formulation in non-hematologic malignancies: phase 1 dose-escalation study. Investigational new drugs. 2014;32(6):1181-7. Epub 2014/06/01.
209. Venkatakrishnan K, Kim TM, Lin CC, Thye LS, Chng WJ, Ma B, et al. Phase 1 study of the investigational Aurora A kinase inhibitor alisertib (MLN8237) in East Asian cancer patients: pharmacokinetics and recommended phase 2 dose. Investigational new drugs. 2015;33(4):942-53. Epub 2015/06/19.
210. Matulonis UA, Sharma S, Ghamande S, Gordon MS, Del Prete SA, Ray-Coquard I, et al. Phase II study of MLN8237 (alisertib), an investigational Aurora A kinase inhibitor, in patients with platinum-resistant or -refractory epithelial ovarian, fallopian tube, or primary peritoneal carcinoma. Gynecologic oncology. 2012;127(1):63-9. Epub 2012/07/10.
211. Melichar B, Adenis A, Lockhart AC, Bennouna J, Dees EC, Kayaleh O, et al. Safety and activity of alisertib, an investigational aurora kinase A inhibitor, in patients with breast cancer, small-cell lung cancer, non-small-cell lung cancer, head and neck squamous-cell carcinoma, and gastro-oesophageal adenocarcinoma: a five-arm phase 2 study. The Lancet Oncology. 2015;16(4):395-405. Epub 2015/03/03.
212. Dickson MA, Mahoney MR, Tap WD, D'Angelo SP, Keohan ML, Van Tine BA, et al. Phase II study of MLN8237 (Alisertib) in advanced/metastatic sarcoma. Annals of oncology : official journal of the European Society for Medical Oncology / ESMO. 2016;27(10):1855-60. Epub 2016/08/10.
213. Hyman DM, Sill MW, Lankes HA, Piekarz R, Shahin MS, Ridgway MR, et al. A phase 2 study of alisertib (MLN8237) in recurrent or persistent uterine leiomyosarcoma: An NRG Oncology/Gynecologic Oncology Group study 0231D. Gynecologic oncology. 2017;144(1):96-100. Epub 2017/01/18.
214. Friedberg JW, Mahadevan D, Cebula E, Persky D, Lossos I, Agarwal AB, et al. Phase II study of alisertib, a selective Aurora A kinase inhibitor, in relapsed and refractory aggressive B- and T-cell non-Hodgkin lymphomas. Journal of clinical oncology : official journal of the American Society of Clinical Oncology. 2014;32(1):44-50. Epub 2013/09/18.
215. Barr PM, Li H, Spier C, Mahadevan D, LeBlanc M, Ul Haq M, et al. Phase II Intergroup Trial of Alisertib in Relapsed and Refractory Peripheral T-Cell Lymphoma and Transformed Mycosis Fungoides: SWOG 1108. Journal of clinical oncology : official journal of the American Society of Clinical Oncology. 2015;33(21):2399-404. Epub 2015/06/17.
216. Amin M, Minton SE, LoRusso PM, Krishnamurthi SS, Pickett CA, Lunceford J, et al. A phase I study of MK-5108, an oral aurora a kinase inhibitor, administered both as monotherapy and in combination with docetaxel, in patients with advanced or refractory solid tumors. Investigational new drugs. 2016;34(1):84-95. Epub 2015/12/02.

217. Shimomura T, Hasako S, Nakatsuru Y, Mita T, Ichikawa K, Kodera T, et al. MK-5108, a highly selective Aurora-A kinase inhibitor, shows antitumor activity alone and in combination with docetaxel. Molecular cancer therapeutics. 2010;9(1):157-66. Epub 2010/01/08.
218. Boss DS, Witteveen PO, van der Sar J, Lolkema MP, Voest EE, Stockman PK, et al. Clinical evaluation of AZD1152, an i.v. inhibitor of Aurora B kinase, in patients with solid malignant tumors. Annals of oncology : official journal of the European Society for Medical Oncology / ESMO. 2011;22(2):431-7. Epub 2010/10/07.
219. Mortlock AA, Foote KM, Heron NM, Jung FH, Pasquet G, Lohmann JJ, et al. Discovery, synthesis, and in vivo activity of a new class of pyrazoloquinazolines as selective inhibitors of aurora B kinase. Journal of medicinal chemistry. 2007;50(9):2213-24. Epub 2007/03/22.
220. Mross K, Richly H, Frost A, Scharr D, Nokay B, Graeser R, et al. A phase I study of BI 811283, an Aurora B kinase inhibitor, in patients with advanced solid tumors. Cancer chemotherapy and pharmacology. 2016;78(2):405-17. Epub 2016/06/29.
221. Tontsch-Grunt U, Gürtler U, Zahn SK, Boehmelt G, Jarvis M, Adolf GR, et al. Abstract 1080: Molecular and cellular pharmacology of BI 811283, a potent inhibitor of Aurora B kinase. Cancer research. 2010;70(8 Supplement):1080-.
222. Dittrich C, Fridrik MA, Koenigsberg R, Lee C, Goeldner RG, Hilbert J, et al. A phase 1 dose escalation study of BI 831266, an inhibitor of Aurora kinase B, in patients with advanced solid tumors. Investigational new drugs. 2015;33(2):409-22. Epub 2014/12/23.
223. McNeish I, Anthoney A, Loadman P, Berney D, Joel S, Halford SER, et al. A phase I pharmacokinetic (PK) and pharmacodynamic (PD) study of the selective aurora kinase inhibitor GSK1070916A. Journal of Clinical Oncology. 2013;31(15_suppl):2525-.
224. Groten JP, Feron VJ, Suhnel J. Toxicology of simple and complex mixtures. Trends in pharmacological sciences. 2001;22(6):316-22. Epub 2001/06/08.
225. Chou TC, Talalay P. Quantitative analysis of dose-effect relationships: the combined effects of multiple drugs or enzyme inhibitors. Advances in enzyme regulation. 1984;22:27-55. Epub 1984/01/01.
226. Jonker DM, Visser SA, van der Graaf PH, Voskuyl RA, Danhof M. Towards a mechanism-based analysis of pharmacodynamic drug-drug interactions in vivo. Pharmacol Ther. 2005;106(1):1-18. Epub 2005/03/23.
227. Greco WR, Bravo G, Parsons JC. The search for synergy: a critical review from a response surface perspective. Pharmacol Rev. 1995;47(2):331-85. Epub 1995/06/01.
228. Jiang Y, Zhang Y, Lees E, Seghezzi W. AuroraA overexpression overrides the mitotic spindle checkpoint triggered by nocodazole, a microtubule destabilizer. Oncogene. 2003;22(51):8293-301. Epub 2003/11/14.
229. Yang H, He L, Kruk P, Nicosia SV, Cheng JQ. Aurora-A induces cell survival and chemoresistance by activation of Akt through a p53-dependent manner in ovarian cancer cells. International journal of cancer Journal international du cancer. 2006;119(10):2304-12. Epub 2006/08/09.
230. Hata T, Furukawa T, Sunamura M, Egawa S, Motoi F, Ohmura N, et al. RNA interference targeting aurora kinase a suppresses tumor growth and enhances the taxane chemosensitivity in human pancreatic cancer cells. Cancer research. 2005;65(7):2899-905. Epub 2005/04/05.
231. Qi W, Cooke LS, Liu X, Rimsza L, Roe DJ, Manziolli A, et al. Aurora inhibitor MLN8237 in combination with docetaxel enhances apoptosis and anti-tumor activity in mantle cell lymphoma. Biochemical pharmacology. 2011;81(7):881-90. Epub 2011/02/05.

232. Sehdev V, Katsha A, Ecsedy J, Zaika A, Belkhiri A, El-Rifai W. The combination of alisertib, an investigational Aurora kinase A inhibitor, and docetaxel promotes cell death and reduces tumor growth in preclinical cell models of upper gastrointestinal adenocarcinomas. Cancer. 2013;119(4):904-14. Epub 2012/09/14.
233. Wysong DR, Chakravarty A, Hoar K, Ecsedy JA. The inhibition of Aurora A abrogates the mitotic delay induced by microtubule perturbing agents. Cell cycle. 2009;8(6):876-88. Epub 2009/02/18.
234. Lin YG, Immaneni A, Merritt WM, Mangala LS, Kim SW, Shahzad MM, et al. Targeting aurora kinase with MK-0457 inhibits ovarian cancer growth. Clinical cancer research : an official journal of the American Association for Cancer Research. 2008;14(17):5437-46. Epub 2008/09/04.
235. Bush TL, Payton M, Heller S, Chung G, Hanestad K, Rottman JB, et al. AMG 900, a small-molecule inhibitor of aurora kinases, potentiates the activity of microtubule-targeting agents in human metastatic breast cancer models. Molecular cancer therapeutics. 2013;12(11):2356-66. Epub 2013/08/31.
236. Scharer CD, Laycock N, Osunkoya AO, Logani S, McDonald JF, Benigno BB, et al. Aurora kinase inhibitors synergize with paclitaxel to induce apoptosis in ovarian cancer cells. Journal of translational medicine. 2008;6:79. Epub 2008/12/17.
237. Bekier ME, Fischbach R, Lee J, Taylor WR. Length of mitotic arrest induced by microtubule-stabilizing drugs determines cell death after mitotic exit. Molecular cancer therapeutics. 2009;8(6):1646-54. Epub 2009/06/11.
238. Olszanski AJ, Middleton MR, Bahleda R, Heist RS, Rangachari L, Zhou X, et al. A phase Ib study of investigational pan-RAF kinase inhibitor MLN2480 plus investigational TORC1/2 inhibitor MLN0128, investigational Aurora A kinase inhibitor alisertib (MLN8237), or paclitaxel in patients (pts) with advanced solid tumors. Journal of Clinical Oncology. 2015;33(15_suppl):TPS2609-TPS.
239. Coleman R, Roszak, A., Behbakht, K., Ray-Coquard, I.L., Matulonis, U., Liu, H., Schusterbauer, C. and Ullmann, C.D. 876O Randomized phase 2 study of investigational, selective aurora A kinase inhibitor alisertib (MLN8237) with weekly paclitaxel vs paclitaxel alone in patients (pts) with recurrent ovarian cancer (OC). Annals of Oncology. 2014;25 (suppl 4):iv305.
240. Raymond E, Alexandre J, Faivre S, Goldwasser F, Besse-Hammer T, Gianella-Borradori A, et al. A phase I schedule dependency study of the aurora kinase inhibitor MSC1992371A in combination with gemcitabine in patients with solid tumors. Investigational new drugs. 2014;32(1):94-103. Epub 2013/03/30.
241. Falchook GS, Goff BA, Kurzrock R, Gray HJ, Martin LP, Coleman RL, et al. Phase I/II study of weekly paclitaxel with or without MLN8237 (alisertib), an investigational aurora A kinase inhibitor, in patients with recurrent epithelial ovarian, fallopian tube, or primary peritoneal cancer (OC), or breast cancer (BrC): Phase I results. Journal of Clinical Oncology. 2012;30:5021.
242. Graff JN, Higano CS, Hahn NM, Taylor MH, Zhang B, Zhou X, et al. Open label, multicenter, phase 1 study of alisertib (MLN8237), an aurora A kinase inhibitor, with docetaxel in patients with solid tumors. Cancer. 2016;122(16):2524-33. Epub 2016/05/19.
243. Lim K-H, Lockhart AC, Waqar SN, Govindan R, Morgensztern D, Picus J, et al. Phase I study combining MLN8237 with nab-paclitaxel in patients with advanced solid malignancies. Journal of Clinical Oncology. 2017;35(15_suppl):2553-.
244. Semrad T, Kelly K, Gandara D, Riess J, Li T, Yu A, et al. P1.06Phase I study of the combination of alisertib (MLN8237) and gemcitabine in advanced solid tumors. Annals of Oncology. 2015;26(suppl_2):ii17-ii.

245. Lin J, Patel SA, Sama AR, Hoffman-Censits JH, Kennedy B, Kilpatrick D, et al. A Phase I/II Study of the Investigational Drug Alisertib in Combination With Abiraterone and Prednisone for Patients With Metastatic Castration-Resistant Prostate Cancer Progressing on Abiraterone. The oncologist. 2016;21(11):1296-7e. Epub 2017/02/09.
246. DuBois SG, Marachelian A, Fox E, Kudgus RA, Reid JM, Groshen S, et al. Phase I Study of the Aurora A Kinase Inhibitor Alisertib in Combination With Irinotecan and Temozolomide for Patients With Relapsed or Refractory Neuroblastoma: A NANT (New Approaches to Neuroblastoma Therapy) Trial. Journal of clinical oncology : official journal of the American Society of Clinical Oncology. 2016;34(12):1368-75. Epub 2016/02/18.
247. Goff LW, Azad NS, Stein S, Whisenant J, Vaishampayan UN, Hochster HS, et al. Phase I study combining the aurora kinase A (AURKA) inhibitor alisertib (Ali) with mFOLFOX in gastrointestinal (GI) cancer. Journal of Clinical Oncology. 2017;35(15_suppl):2593-.
248. Shah HA, Christian S, Ahmed B, Chowdhery RA, Venepalli NK, Danciu OC, et al. STM-01: Phase I EffTox study of aurora A kinase inhibitor alisertib (MLN8237) given in combination with selective VEGFR inhibitor pazopanib for therapy of solid tumors. Journal of Clinical Oncology. 2016;34(15_suppl):2587-.
249. Godwin JL, Mehra R, Litwin S, Olszanski AJ, Bauman JR, Borghaei H. A phase I/II study of MLN-8237 (alisertib), an oral aurora kinase inhibitor, in combination with erlotinib in patients with recurrent or metastatic EGFR wild-type non-small cell lung cancer. Journal of Clinical Oncology. 2016;34(15_suppl):e20588-e.
250. Owonikoko TK, Nackaerts K, Csoszi T, Ostoros G, Baik C, Mark Z, et al. Randomized phase 2 study of investigational aurora A kinase (AAK) inhibitor alisertib (MLN8237) + paclitaxel (P) vs placebo + P as second line therapy for small-cell lung cancer (SCLC). Annals of Oncology. 2016;27(suppl_6):1423O-O.
251. Vichai V, Kirtikara K. Sulforhodamine B colorimetric assay for cytotoxicity screening. Nature protocols. 2006;1(3):1112-6. Epub 2007/04/05.
252. Di Veroli GY, Fornari C, Wang D, Mollard S, Bramhall JL, Richards FM, et al. Combenefit: an interactive platform for the analysis and visualization of drug combinations. Bioinformatics. 2016;32(18):2866-8. Epub 2016/05/07.253. Tighe A, Johnson VL, Taylor SS. Truncating APC mutations have dominant effects on proliferation, spindle checkpoint control, survival and chromosome stability. Journal of cell science. 2004;117(Pt 26):6339-53. Epub 2004/11/25.
254. Workman P, Aboagye EO, Balkwill F, Balmain A, Bruder G, Chaplin DJ, et al. Guidelines for the welfare and use of animals in cancer research. British journal of cancer. 2010;102(11):1555-77. Epub 2010/05/27.
255. Suresh K. An overview of randomization techniques: An unbiased assessment of outcome in clinical research. Journal of human reproductive sciences. 2011;4(1):8-11. Epub 2011/07/21.
256. Cummings J, Hodgkinson C, Odedra R, Sini P, Heaton SP, Mundt KE, et al. Preclinical evaluation of M30 and M65 ELISAs as biomarkers of drug induced tumor cell death and antitumor activity. Molecular cancer therapeutics. 2008;7(3):455-63. Epub 2008/03/19.
257. Olofsson MH, Cummings J, Fayad W, Brnjic S, Herrmann R, Berndtsson M, et al. Specific demonstration of drug-induced tumour cell apoptosis in human xenografts models using a plasma biomarker. Cancer biomarkers : section A of Disease markers. 2009;5(3):117-25. Epub 2009/05/02.
258. Lin Y, Richards FM, Krippendorff BF, Bramhall JL, Harrington JA, Bapiro TE, et al. Paclitaxel and CYC3, an aurora kinase A inhibitor, synergise in pancreatic cancer

cells but not bone marrow precursor cells. British journal of cancer. 2012;107(10):1692-701. Epub 2012/10/06.
259. Knowles MA, Hurst CD. Molecular biology of bladder cancer: new insights into pathogenesis and clinical diversity. Nature reviews Cancer. 2015;15(1):25-41. Epub 2014/12/24.
260. Forbes SA, Bindal N, Bamford S, Cole C, Kok CY, Beare D, et al. COSMIC: mining complete cancer genomes in the Catalogue of Somatic Mutations in Cancer. Nucleic acids research. 2011;39(Database issue):D945-50. Epub 2010/10/19.
261. Huck JJ, Zhang M, Mettetal J, Chakravarty A, Venkatakrishnan K, Zhou X, et al. Translational exposure-efficacy modeling to optimize the dose and schedule of taxanes combined with the investigational Aurora A kinase inhibitor MLN8237 (alisertib). Molecular cancer therapeutics. 2014;13(9):2170-83. Epub 2014/07/02.
262. Albany C, Sonpavde G. Docetaxel for the treatment of bladder cancer. Expert opinion on investigational drugs. 2015;24(12):1657-64. Epub 2015/11/05.
263. Chinn DC, Holland WS, Mack PC. Anticancer activity of the Aurora A kinase inhibitor MK-5108 in non-small-cell lung cancer (NSCLC) in vitro as monotherapy and in combination with chemotherapies. Journal of cancer research and clinical oncology. 2014;140(7):1137-49. Epub 2014/04/24.
264. Gizatullin F, Yao Y, Kung V, Harding MW, Loda M, Shapiro GI. The Aurora kinase inhibitor VX-680 induces endoreduplication and apoptosis preferentially in cells with compromised p53-dependent postmitotic checkpoint function. Cancer research. 2006;66(15):7668-77. Epub 2006/08/04.
265. Kalous O, Conklin D, Desai AJ, Dering J, Goldstein J, Ginther C, et al. AMG 900, pan-Aurora kinase inhibitor, preferentially inhibits the proliferation of breast cancer cell lines with dysfunctional p53. Breast cancer research and treatment. 2013;141(3):397-408. Epub 2013/10/05.
266. Kaestner P, Stolz A, Bastians H. Determinants for the efficiency of anticancer drugs targeting either Aurora-A or Aurora-B kinases in human colon carcinoma cells. Molecular cancer therapeutics. 2009;8(7):2046-56. Epub 2009/07/09.
267. Petitjean A, Mathe E, Kato S, Ishioka C, Tavtigian SV, Hainaut P, et al. Impact of mutant p53 functional properties on TP53 mutation patterns and tumor phenotype: lessons from recent developments in the IARC TP53 database. Human mutation. 2007;28(6):622-9. Epub 2007/02/22.
268. Shi J, Orth JD, Mitchison T. Cell type variation in responses to antimitotic drugs that target microtubules and kinesin-5. Cancer research. 2008;68(9):3269-76. Epub 2008/05/03.
269. Brito DA, Rieder CL. The ability to survive mitosis in the presence of microtubule poisons differs significantly between human nontransformed (RPE-1) and cancer (U2OS, HeLa) cells. Cell motility and the cytoskeleton. 2009;66(8):437-47. Epub 2008/09/16.
270. Orth JD, Tang Y, Shi J, Loy CT, Amendt C, Wilm C, et al. Quantitative live imaging of cancer and normal cells treated with Kinesin-5 inhibitors indicates significant differences in phenotypic responses and cell fate. Molecular cancer therapeutics. 2008;7(11):3480-9. Epub 2008/11/01.
271. Parent-Massin D. Relevance of clonogenic assays in hematotoxicology. Cell biology and toxicology. 2001;17(2):87-94. Epub 2001/08/14.
272. Pessina A, Albella B, Bayo M, Bueren J, Brantom P, Casati S, et al. In vitro tests for haematotoxicity: prediction of drug-induced myelosuppression by the CFU-GM assay. Alternatives to laboratory animals : ATLA. 2002;30 Suppl 2:75-9. Epub 2003/01/07.

273. Nichols WW, Murphy DG, Cristofalo VJ, Toji LH, Greene AE, Dwight SA. Characterization of a new human diploid cell strain, IMR-90. Science. 1977;196(4285):60-3. Epub 1977/04/01.
274. Dunn KC, Aotaki-Keen AE, Putkey FR, Hjelmeland LM. ARPE-19, a human retinal pigment epithelial cell line with differentiated properties. Experimental eye research. 1996;62(2):155-69. Epub 1996/02/01.
275. Brito DA, Yang Z, Rieder CL. Microtubules do not promote mitotic slippage when the spindle assembly checkpoint cannot be satisfied. The Journal of cell biology. 2008;182(4):623-9. Epub 2008/08/20.
276. Mittal K, Choi DH, Ogden A, Donthamsetty S, Melton BD, Gupta MV, et al. Amplified centrosomes and mitotic index display poor concordance between patient tumors and cultured cancer cells. Scientific reports. 2017;7:43984. Epub 2017/03/09.
277. Kurtzberg LS, Roth SD, Bagley RG, Rouleau C, Yao M, Crawford JL, et al. Bone marrow CFU-GM and human tumor xenograft efficacy of three tubulin binding agents. Cancer chemotherapy and pharmacology. 2009;64(5):1029-38. Epub 2009/03/12.
278. Pessina A, Albella B, Bayo M, Bueren J, Brantom P, Casati S, et al. Application of the CFU-GM assay to predict acute drug-induced neutropenia: an international blind trial to validate a prediction model for the maximum tolerated dose (MTD) of myelosuppressive xenobiotics. Toxicological sciences : an official journal of the Society of Toxicology. 2003;75(2):355-67. Epub 2003/07/29.
279. Alge CS, Hauck SM, Priglinger SG, Kampik A, Ueffing M. Differential protein profiling of primary versus immortalized human RPE cells identifies expression patterns associated with cytoskeletal remodeling and cell survival. Journal of proteome research. 2006;5(4):862-78. Epub 2006/04/11.
280. Haglund C, Aleskog A, Nygren P, Gullbo J, Hoglund M, Wickstrom M, et al. In vitro evaluation of clinical activity and toxicity of anticancer drugs using tumor cells from patients and cells representing normal tissues. Cancer chemotherapy and pharmacology. 2012;69(3):697-707. Epub 2011/10/11.
281. Liu F, Huang J, Ning B, Liu Z, Chen S, Zhao W. Drug Discovery via Human-Derived Stem Cell Organoids. Frontiers in pharmacology. 2016;7:334. Epub 2016/10/08.
282. Friberg LE, Henningsson A, Maas H, Nguyen L, Karlsson MO. Model of chemotherapy-induced myelosuppression with parameter consistency across drugs. Journal of clinical oncology : official journal of the American Society of Clinical Oncology. 2002;20(24):4713-21. Epub 2002/12/19.
283. Le K YL, Manfredi M, Ecsedy J, Silverman L, Cardoza K, et al. Evaluation of optimal dosing regimens for investigational drug MLN8237, an Aurora A kinase inhibitor, in combination with docetaxel through pharmacokinetic-pharmacodynamic (PK-PD)modeling of hematological toxicity. Clinical Pharmacology & Therapeutics. 2011;89:S58-S9.
284. Marshall CJ, Franks LM, Carbonell AW. Markers of neoplastic transformation in epithelial cell lines derived from human carcinomas. Journal of the National Cancer Institute. 1977;58(6):1743-51. Epub 1977/06/01.
285. Flatow U, Rabson AB, Rabson AS. Tumorigenicity of T24 urinary bladder carcinoma cell sublines. International journal of cancer Journal international du cancer. 1987;40(2):240-5. Epub 1987/08/15.
286. Gorgun G, Calabrese E, Hideshima T, Ecsedy J, Perrone G, Mani M, et al. A novel Aurora-A kinase inhibitor MLN8237 induces cytotoxicity and cell-cycle arrest in multiple myeloma. Blood. 2010;115(25):5202-13. Epub 2010/04/13.

287. Sparreboom A, van Tellingen O, Nooijen WJ, Beijnen JH. Tissue distribution, metabolism and excretion of paclitaxel in mice. Anti-cancer drugs. 1996;7(1):78-86. Epub 1996/01/01.
288. Jordan MA, Toso RJ, Thrower D, Wilson L. Mechanism of mitotic block and inhibition of cell proliferation by taxol at low concentrations. Proceedings of the National Academy of Sciences of the United States of America. 1993;90(20):9552-6. Epub 1993/10/15.
289. Yvon AM, Wadsworth P, Jordan MA. Taxol suppresses dynamics of individual microtubules in living human tumor cells. Molecular biology of the cell. 1999;10(4):947-59. Epub 1999/04/10.
290. Zasadil LM, Andersen KA, Yeum D, Rocque GB, Wilke LG, Tevaarwerk AJ, et al. Cytotoxicity of paclitaxel in breast cancer is due to chromosome missegregation on multipolar spindles. Science translational medicine. 2014;6(229):229ra43. Epub 2014/03/29.
291. Donehower RC, Rowinsky EK, Grochow LB, Longnecker SM, Ettinger DS. Phase I trial of taxol in patients with advanced cancer. Cancer treatment reports. 1987;71(12):1171-7. Epub 1987/12/01.
292. Baird RD, Tan DS, Kaye SB. Weekly paclitaxel in the treatment of recurrent ovarian cancer. Nature reviews Clinical oncology. 2010;7(10):575-82. Epub 2010/08/05.
293. Pinkus GS, Pinkus JL. Myeloperoxidase: a specific marker for myeloid cells in paraffin sections. Modern pathology : an official journal of the United States and Canadian Academy of Pathology, Inc. 1991;4(6):733-41. Epub 1991/11/01.
294. Eisenhauer EA, Therasse P, Bogaerts J, Schwartz LH, Sargent D, Ford R, et al. New response evaluation criteria in solid tumours: revised RECIST guideline (version 1.1). European journal of cancer. 2009;45(2):228-47. Epub 2008/12/23.
295. Pessina A, Albella B, Bueren J, Brantom P, Casati S, Gribaldo L, et al. Prevalidation of a model for predicting acute neutropenia by colony forming unit granulocyte/macrophage (CFU-GM) assay. Toxicology in vitro : an international journal published in association with BIBRA. 2001;15(6):729-40. Epub 2001/11/08.
296. Chakravarty A, Shinde V, Tabernero J, Cervantes A, Cohen RB, Dees EC, et al. Phase I assessment of new mechanism-based pharmacodynamic biomarkers for MLN8054, a small-molecule inhibitor of Aurora A kinase. Cancer research. 2011;71(3):675-85. Epub 2010/12/15.
297. Chu T, Jiang L, Ying W, Han B. M30/M65 ratio predicts the outcome of paclitaxel chemotherapy for NSCLC. Clinical & translational oncology : official publication of the Federation of Spanish Oncology Societies and of the National Cancer Institute of Mexico. 2017;19(3):326-31. Epub 2016/07/30.
298. Capes-Davis A, Theodosopoulos G, Atkin I, Drexler HG, Kohara A, MacLeod RA, et al. Check your cultures! A list of cross-contaminated or misidentified cell lines. International journal of cancer Journal international du cancer. 2010;127(1):1-8. Epub 2010/02/10.
299. American Type Culture Collection Standards Development Organization Workgroup ASN. Cell line misidentification: the beginning of the end. Nature reviews Cancer. 2010;10(6):441-8. Epub 2010/05/08.
300. Johnen G, Rozynek P, von der Gathen Y, Bryk O, Zdrenka R, Johannes C, et al. Cross-contamination of a UROtsa stock with T24 cells--molecular comparison of different cell lines and stocks. PloS one. 2013;8(5):e64139. Epub 2013/05/22.
301. Landis SC, Amara SG, Asadullah K, Austin CP, Blumenstein R, Bradley EW, et al. A call for transparent reporting to optimize the predictive value of preclinical research. Nature. 2012;490(7419):187-91. Epub 2012/10/13.

302. Macleod MR, Lawson McLean A, Kyriakopoulou A, Serghiou S, de Wilde A, Sherratt N, et al. Risk of Bias in Reports of In Vivo Research: A Focus for Improvement. PLoS biology. 2015;13(10):e1002273. Epub 2015/10/16.
303. John BA, Said N. Insights from animal models of bladder cancer: recent advances, challenges, and opportunities. Oncotarget. 2017;8(34):57766-81. Epub 2017/09/17.
304. Carter S. Study design principles for the clinical evaluation of new drugs as developed by the chemotherapy programme of the National Cancer Institute. Staquet M, editor. Mount Kisco, NY: Futura Publishing Co.; 1973.
305. Storer BE. Design and analysis of phase I clinical trials. Biometrics. 1989;45(3):925-37. Epub 1989/09/01.
306. Le Tourneau C, Lee JJ, Siu LL. Dose escalation methods in phase I cancer clinical trials. Journal of the National Cancer Institute. 2009;101(10):708-20. Epub 2009/05/14.
307. Kang S-H, Ahn CW. An Investigation of the Traditional Algorithm-Based Designs for Phase 1 Cancer Clinical Trials. Drug Information Journal. 2002;36(4):865-73.
308. Iasonos A, Gounder M, Spriggs DR, Gerecitano JF, Hyman DM, Zohar S, et al. The Impact of Non-Drug-Related Toxicities on the Estimation of the Maximum Tolerated Dose in Phase I Trials. Clinical cancer research : an official journal of the American Association for Cancer Research. 2012. Epub 2012/07/25.
309. O'Quigley J, Zohar S. Experimental designs for phase I and phase I/II dose-finding studies. British journal of cancer. 2006;94(5):609-13. Epub 2006/01/26.
310. Braun TM, Alonzo TA. Beyond the 3+3 method: expanded algorithms for dose-escalation in Phase I oncology trials of two agents. Clinical trials. 2011;8(3):247-59. Epub 2011/07/07.
311. Flournoy N. A Clinical Experiment in Bone Marrow Transplantation: Estimating a Percentage Point of a Quantal Response Curve. In: Gatsonis C, . Hodges, J.S., Kass, R.E., & Singpurwalla, N.D., editor. Case Studies in Bayesian Statistics: Springer-Verlag; 1993.
312. Legedza AT, Ibrahim JG. Heterogeneity in phase I clinical trials: prior elicitation and computation using the continual reassessment method. Statistics in medicine. 2001;20(6):867-82. Epub 2001/03/17.
313. Speigelhalter DJ, Abrams, K.R. and Myles, J.P. Bayesian Approaches to Clinical Trials and Health-Care Evaluation: John Wiley & Sons; 2004.
314. Rosenberger WF, Canfield GC, Perevozskaya I, Haines LM, Hausner P. Development of Interactive Software for Bayesian Optimal Phase 1 Clinical Trial Design. Drug Information Journal. 2005;39(1):89-98.
315. O'Quigley J, Pepe M, Fisher L. Continual reassessment method: a practical design for phase 1 clinical trials in cancer. Biometrics. 1990;46(1):33-48. Epub 1990/03/01.
316. Iasonos A, O'Quigley J. Interplay of priors and skeletons in two-stage continual reassessment method. Statistics in medicine. 2012;31(30):4321-36. Epub 2012/08/16.
317. Paller CJ, Bradbury PA, Ivy SP, Seymour L, LoRusso PM, Baker L, et al. Design of phase I combination trials: recommendations of the Clinical Trial Design Task Force of the NCI Investigational Drug Steering Committee. Clinical cancer research : an official journal of the American Association for Cancer Research. 2014;20(16):4210-7. Epub 2014/08/16.
318. Harrington JA, Wheeler GM, Sweeting MJ, Mander AP, Jodrell DI. Adaptive designs for dual-agent phase I dose-escalation studies. Nature reviews Clinical oncology. 2013;10(5):277-88. Epub 2013/03/20.

319. Gasparini M, Bailey S, Neuenschwander B. Bayesian dose finding in oncology for drug combinations by copula regression. Journal of the Royal Statistical Society Series C-Applied Statistics. 2010;59:543-4.
320. Riviere MK, Le Tourneau C, Paoletti X, Dubois F, Zohar S. Designs of drug-combination phase I trials in oncology: a systematic review of the literature. Annals of oncology : official journal of the European Society for Medical Oncology / ESMO. 2015;26(4):669-74. Epub 2014/11/19.
321. Falchook GS, Bastida CC, Kurzrock R. Aurora Kinase Inhibitors in Oncology Clinical Trials: Current State of the Progress. Seminars in oncology. 2015;42(6):832-48. Epub 2015/11/29.
322. Gradishar WJ, Tjulandin S, Davidson N, Shaw H, Desai N, Bhar P, et al. Phase III trial of nanoparticle albumin-bound paclitaxel compared with polyethylated castor oil-based paclitaxel in women with breast cancer. Journal of clinical oncology : official journal of the American Society of Clinical Oncology. 2005;23(31):7794-803. Epub 2005/09/21.
323. Ando M, Watanabe T, Nagata K, Narabayashi M, Adachi I, Katsumata N. Efficacy of docetaxel 60 mg/m2 in patients with metastatic breast cancer according to the status of anthracycline resistance. Journal of clinical oncology : official journal of the American Society of Clinical Oncology. 2001;19(2):336-42. Epub 2001/02/24.
324. Nair AB, Jacob S. A simple practice guide for dose conversion between animals and human. Journal of Basic and Clinical Pharmacy. 2016;7(2):27-31.
325. Thall PF, Millikan RE, Mueller P, Lee SJ. Dose-finding with two agents in Phase I oncology trials. Biometrics. 2003;59(3):487-96. Epub 2003/11/07.
326. Paoletti X, Baron B, Schoffski P, Fumoleau P, Lacombe D, Marreaud S, et al. Using the continual reassessment method: lessons learned from an EORTC phase I dose finding study. European journal of cancer. 2006;42(10):1362-8. Epub 2006/06/03.
327. Higgins JPT, Thompson SG, Spiegelhalter DJ. A re-evaluation of random-effects meta-analysis. Journal of the Royal Statistical Society Series A, (Statistics in Society). 2009;172(1):137-59.
328. Jackson RC. Pharmacodynamic modelling of biomarker data in oncology. ISRN pharmacology. 2012;2012:590626. Epub 2012/04/24.
329. Yang JJ, Li Y, Chakravarty A, Lu C, Xia CQ, Chen S, et al. Preclinical drug metabolism and pharmacokinetics, and prediction of human pharmacokinetics and efficacious dose of the investigational Aurora A kinase inhibitor alisertib (MLN8237). Drug metabolism letters. 2014;7(2):96-104. Epub 2014/02/04.
330. Venkatakrishnan K, Zhou X, Ecsedy J, Mould DR, Liu H, Danaee H, et al. Dose selection for the investigational anticancer agent alisertib (MLN8237): Pharmacokinetics, pharmacodynamics, and exposure-safety relationships. Journal of clinical pharmacology. 2014. Epub 2014/10/11.
331. Rose PG, Smrekar M, Fusco N. A phase II trial of weekly paclitaxel and every 3 weeks of carboplatin in potentially platinum-sensitive ovarian and peritoneal carcinoma. Gynecologic oncology. 2005;96(2):296-300. Epub 2005/01/22.
332. Mathijssen RH, Sparreboom A, Verweij J. Determining the optimal dose in the development of anticancer agents. Nature reviews Clinical oncology. 2014;11(5):272-81. Epub 2014/03/26.
333. Yap TA, Sandhu SK, Workman P, de Bono JS. Envisioning the future of early anticancer drug development. Nature reviews Cancer. 2010;10(7):514-23. Epub 2010/06/11.
334. Chow SC. Adaptive clinical trial design. Annual review of medicine. 2014;65:405-15. Epub 2014/01/16.

335. Zang Y, Lee JJ. Adaptive clinical trial designs in oncology. Chinese clinical oncology. 2014;3(4). Epub 2015/03/27.
336. Ananthakrishnan R, Menon S. Design of oncology clinical trials: a review. Critical reviews in oncology/hematology. 2013;88(1):144-53. Epub 2013/04/30.
337. Parulekar WR, Eisenhauer EA. Phase I trial design for solid tumor studies of targeted, non-cytotoxic agents: theory and practice. Journal of the National Cancer Institute. 2004;96(13):990-7. Epub 2004/07/09.
338. Fox E, Curt GA, Balis FM. Clinical trial design for target-based therapy. The oncologist. 2002;7(5):401-9. Epub 2002/10/29.
339. Mandrekar SJ, Qin R, Sargent DJ. Model-based phase I designs incorporating toxicity and efficacy for single and dual agent drug combinations: methods and challenges. Statistics in medicine. 2010;29(10):1077-83. Epub 2010/04/27.
340. Rodon J, Perez J, Kurzrock R. Combining Targeted Therapies: Practical Issues to Consider at the Bench and Bedside. The oncologist. 2010;15(1):37-50.
341. Huang X, Biswas S, Oki Y, Issa JP, Berry DA. A parallel phase I/II clinical trial design for combination therapies. Biometrics. 2007;63(2):429-36. Epub 2007/08/11.
342. Hoering A, Mitchell A, LeBlanc M, Crowley J. Early phase trial design for assessing several dose levels for toxicity and efficacy for targeted agents. Clinical trials. 2013;10(3):422-9. Epub 2013/03/27.
343. Mandrekar SJ, Cui Y, Sargent DJ. An adaptive phase I design for identifying a biologically optimal dose for dual agent drug combinations. Statistics in medicine. 2007;26(11):2317-30. Epub 2006/10/04.
344. Whitehead J, Thygesen H, Whitehead A. Bayesian procedures for phase I/II clinical trials investigating the safety and efficacy of drug combinations. Statistics in medicine. 2011;30(16):1952-70. Epub 2011/05/19.
345. Asakawa T, Hamada C. A pragmatic dose-finding approach using short-term surrogate efficacy outcomes to evaluate binary efficacy and toxicity outcomes in phase I cancer clinical trials. Pharm Stat. 2013;12(5):315-27. Epub 2013/09/11.
346. Lee SM, Cheng B, Cheung YK. Continual reassessment method with multiple toxicity constraints. Biostatistics. 2011;12(2):386-98. Epub 2010/09/30.
347. Van Meter EM, Garrett-Mayer E, Bandyopadhyay D. Proportional odds model for dose-finding clinical trial designs with ordinal toxicity grading. Statistics in medicine. 2011;30(17):2070-80. Epub 2011/02/24.
348. Lee SM, Hershman DL, Martin P, Leonard JP, Cheung YK. Toxicity burden score: a novel approach to summarize multiple toxic effects. Annals of oncology : official journal of the European Society for Medical Oncology / ESMO. 2012;23(2):537-41. Epub 2011/05/04.
349. Thall PF. Bayesian Models and Decision Algorithms for Complex Early Phase Clinical Trials. Stat Sci. 2010;25(2):227-44. Epub 2011/02/15.
350. Bailey S, Neuenschwander B, Laird G, Branson M. A Bayesian case study in oncology Phase I combination dose-finding using logistic regression with covariates. J Biopharm Stat. 2009;19(3):469-84. Epub 2009/04/23.
351. Xiong X, Sui M, Fan W, Kraft AS. Cell cycle dependent antagonistic interactions between paclitaxel and carboplatin in combination therapy. Cancer biology & therapy. 2007;6(7):1067-73. Epub 2007/06/15.
352. Grah JS, Harrington JA, Koh SB, Pike JA, Schreiner A, Burger M, et al. Mathematical imaging methods for mitosis analysis in live-cell phase contrast microscopy. Methods. 2017;115:91-9. Epub 2017/02/13.
353. Koh SB, Mascalchi P, Rodriguez E, Lin Y, Jodrell DI, Richards FM, et al. A quantitative FastFUCCI assay defines cell cycle dynamics at a single-cell level. Journal of cell science. 2017;130(2):512-20. Epub 2016/11/27.

354. Andrews PD. Aurora kinases: shining lights on the therapeutic horizon? Oncogene. 2005;24(32):5005-15. Epub 2005/07/29.
355. Komlodi-Pasztor E, Sackett DL, Fojo AT. Inhibitors targeting mitosis: tales of how great drugs against a promising target were brought down by a flawed rationale. Clin Cancer Res. 2012;18(1):51-63. Epub 2012/01/05.
356. Necchi A, Pintarelli G, Raggi D, Giannatempo P, Colombo F. Association of an aurora kinase a (AURKA) gene polymorphism with progression-free survival in patients with advanced urothelial carcinoma treated with the selective aurora kinase a inhibitor alisertib. Investigational new drugs. 2017;35(4):524-8. Epub 2017/02/06.
357. Niu H, Shin H, Gao F, Zhang J, Bahamon B, Danaee H, et al. Aurora A Functional Single Nucleotide Polymorphism (SNP) Correlates With Clinical Outcome in Patients With Advanced Solid Tumors Treated With Alisertib, an Investigational Aurora A Kinase Inhibitor. EBioMedicine. 2017;25:50-7. Epub 2017/11/11.
358. Alcaraz-Sanabria A, Nieto-Jimenez C, Corrales-Sanchez V, Serrano-Oviedo L, Andres-Pretel F, Montero JC, et al. Synthetic Lethality Interaction Between Aurora Kinases and CHEK1 Inhibitors in Ovarian Cancer. Molecular cancer therapeutics. 2017;16(11):2552-62. Epub 2017/08/30.
359. Dos Santos EO, Carneiro-Lobo TC, Aoki MN, Levantini E, Basseres DS. Aurora kinase targeting in lung cancer reduces KRAS-induced transformation. Molecular cancer. 2016;15:12. Epub 2016/02/05.
360. Brockmann M, Poon E, Berry T, Carstensen A, Deubzer HE, Rycak L, et al. Small molecule inhibitors of aurora-a induce proteasomal degradation of N-myc in childhood neuroblastoma. Cancer cell. 2013;24(1):75-89. Epub 2013/06/25.
361. Mollaoglu G, Guthrie MR, Bohm S, Bragelmann J, Can I, Ballieu PM, et al. MYC Drives Progression of Small Cell Lung Cancer to a Variant Neuroendocrine Subtype with Vulnerability to Aurora Kinase Inhibition. Cancer cell. 2017;31(2):270-85. Epub 2017/01/17

10 *APPENDICES*